Development of a novel test rig for the evaluation of aircraft fuel tank sealants

Mark N. Hooper (2007)

Development of a novel test rig for the evaluation of aircraft fuel tank sealants

Mark Nicholas Hooper

A thesis submitted in partial fulfilment of the requirement of Oxford Brookes University for the degree of Doctor of Philosophy

December 2007

DO NOT SCAN

fig 2.1 - page 16

fig 2.3 - page 18

fig 2.5 – page 21

fig 2.6 – page 22

fig 2.7 – page 23

fig 2.8 – page 24

fig 2.10 – page 26

fig 3.2 – page 43

fig 3.3 – page 44

fig – 7.2 + 7.3 – page 120

fig 8.11 – page 158

Appendix 1-4

PAGE NUMBERING AS ORIGINAL

Dedicated to the memory of my Father, Terry

ABSTRACT

Leaks from aircraft fuel tanks have always represented a problem for aircraft manufacturers, airline operators and maintenance crews. The integral fuel tanks within aircraft structures are typically located within the wings and they rely upon sealant materials to prevent leakage past joints and fasteners. However, the wing is designed as a structural member first and as a fuel tank second and there exist many potential leak paths for the fuel from these complex, highly loaded structures. Fuel leaks result in direct loss of fuel which may be dangerous, cause a loss in revenue due to aircraft being withdrawn from service and be difficult and expensive to repair. On top of this there are important health and safety issues involved in the repair of fuel tanks, for example, the Royal Australian Air Force's, F-111 Deseal Reseal Programme 1979 to 2000, where it was found that a significant number of RAAF personnel involved in the Deseal Reseal Programme were suffering from a variety of health problems.

Current approaches to fuel tank sealant evaluation embrace immersion in a range of different fluids at different temperatures, of both bulk sealant samples and sealed joints. However, nearly all such tests are of a "static" nature and yet it is acknowledged that joint movement leads to leaks. Thus the missing component of testing is movement coupled with the other key variables. The aircraft industry has been searching for a relatively simple test method that can be used to evaluate sealed joint systems using realistic combinations of materials, joint geometries, imposed stresses and environmental conditions. The aim of this project was to do exactly this.

A practical but realistic dynamic test, the Model Sealed System (MSS), was designed, made and evaluated. This unique mechanism consists of an axial stress machine into which fatigue, high and low temperatures and pressures can be programmed for automatic operation. A novel circular lap joint lies at the heart of the MSS in which test sealant is sandwiched between the circular coupons that are then assembled with aerospace fasteners and sealed. This joint configuration is representative of a wing skin butt-strap joint in a real aircraft.

The MSS is easy to run, it accurately simulates real world dynamics and conditioning, and it provides results to qualify sealants in a more realistic manner than current testing methods provide. The MSS enables evaluation and comparative testing of sealant systems when used for interfay, fillet and overcoat applications. The information provided is complementary to that obtained from conventional small scale coupon testing; it is not seen as a substitute. Further work is required to refine the test variables and further data are required to provide confidence in the utility of the MSS.

Development of the MSS was undertaken with the support of Airbus UK to ensure that the design, materials and all other variables met with the overall requirements of a commercial aircraft manufacturer. Airbus UK have a duplicate MSS of their own, installed by the author, from which they can obtain patterns of data for different combinations of materials and experimental variables.

ACKNOWLEDGEMENTS

I should like to express my thanks to everyone that has helped me in this project. To my director of studies, Professor Allan Hutchinson, and my project supervisors, Dr. James Broughton and Dr. Tim Lee, for their support and patience throughout the project. Special thanks must go to Tony Attwood for his enthusiastic and invaluable help in fabricating the parts for the Model Sealed System.

Thanks must also go to Dr Mike Taylor, Colin West and David Sutton of Airbus UK for their help throughout the project and Philip Duke, from QinetiQ, in the initial stages.

I would also like to thank my family, especially my Mother, for always encouraging me in everything I decided to do and for their support throughout. Special mention must also be made of my nephew Sam, who is sadly no longer with us, for making me realise that life really is too short to waste.

My love and special thanks must go to my lovely wife to be, Lucy, for putting up with me during the good and bad times with her unending support and for just being lovely Lucy.

Finally, I would like to dedicate this thesis to my late Father, who inspired within me an interest in all things mechanical, who sadly died during the project but is, as always, never far my from thoughts.

CONTENTS

Appendices

Appendix 1: Model Fuel Tank specifications

Appendix 2: Airbus Industrie Test Method (AITM) and the International Standards Organisation (ISO) utilised in ensuring that the sealant meets Airbus UK's technical specifications.

Appendix 3: Current test procedures for evaluating seals and sealants

Appendix 4: The product data sheet for the Julabo FP90-SL Ultra Low Refrigerated Circulator

Appendix 5: A copy of an email sent in 2004, reproduced with the kind permission of Bill Keller

Appendix 6: The results of sealant tests carried out in the Joining Technology Research Centre (JTRC) at Oxford Brookes University in 2006.

Appendix 7: Calculation of Stresses from Measured Strains

Appendix 8: The results of the Finite Element Analysis carried out at Oxford Brookes University

Appendix 9: The final drawings of some of the Pressure Pot's major components.

Appendix 10: The progress statement to Airbus UK illustrating how the test program was altered to encourage a leak in coupon set number 02-06

Figures

Tables

Nomenclature

This following is a list of symbols used in this report:

F	Force (N)
τ	Shear Stress (MPa)
A	Bond Area (mm^2)
° C	Degrees Celsius
MSS	Model Sealed Structure
DMTA	Dynamic Mechanical Thermal Analysis
T_g	Glass Transition Temperature (°C)
E	Young's Modulus (Pa)
DSC	Differential Scanning Calorimetry
Hz	Hertz
δ	Phase lag between applied stress & strain response (°)
$\hat{\sigma}$	Maximum Stress (Pa)
$\hat{\varepsilon}$	Maximum Strain
FEA	Finite Element Analysis
M	Metre
μm	Micron
RH	Relative Humidity

1 Introduction

1.1. Background

Aircraft fuel tanks represent a constant source of problems for aircraft designers and users. The integrity of sealed joints in the integral fuel tanks of civil and military aircraft has important operational, cost, safety and ecological implications. Integral fuel tanks within aircraft structures are typically located within the wings. Traditionally, aircraft integral fuel tanks are designed from a structural point of view first and as a fuel tank second. The skin of the wing is attached to the internal structure of the wing and the joints between the internal structure and the skin have to be sealed to prevent leakage of fuel. The highly loaded structures on a modern aircraft are designed and built with the use of machined parts that, if sealed correctly, perform both as a load bearing structural member and as an integral fuel tank. Unfortunately, within the wings of a modern aircraft there exist innumerable potential leak paths for the fuel ranging from those between interfaying surfaces, those from skin joints, those from conduits (housing electric cables), pipes and hoses (for fuel, hydraulic and de-icing fluids), and those from the fasteners themselves. To these may be added the effects of flight stress fatigue, temperature, contaminants (water, de-icer fluid and microbiological attack), the fuel itself, and practical application failures on initial assembly and at subsequent repairs. It can therefore be appreciated that the potential for leaks is enormous. The life of an aircraft can be 30 + years with no significant operational leaks, so that to promote a leak in a test rig that is reproducible, and accurately simulate the real world dynamics of an aircraft integral tank, is a challenge.

In a single typical wing of a commercial aircraft it is likely that there is about 100kg of sealant material. This is applied and has to stick to primed, coated, etched and anodised aluminium in current aircraft. In some military aircraft (and future civil aircraft) the relevant surfaces will be epoxy-matrix fibre-reinforced plastics. A sealed joint system, therefore, comprises the sealant, primer coating(s) and the parent skin material (**Figs. 1.1, 1.2 and 1.3**).

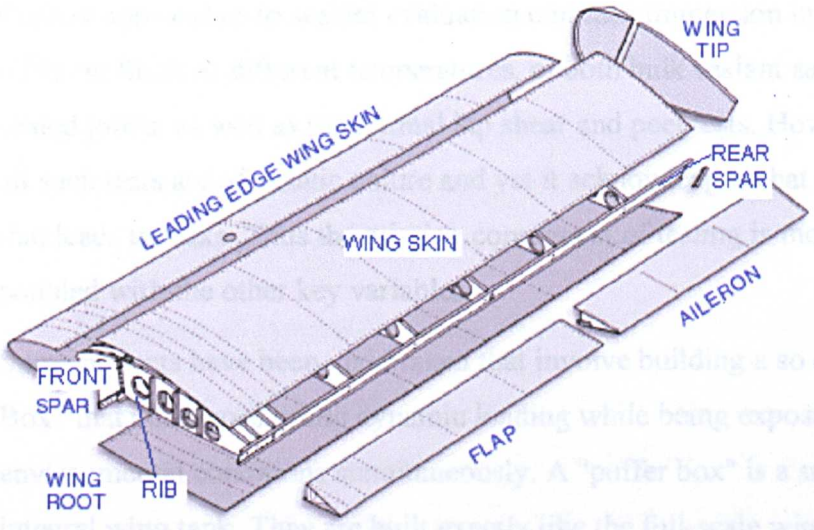

Figure 1.1 External wing components

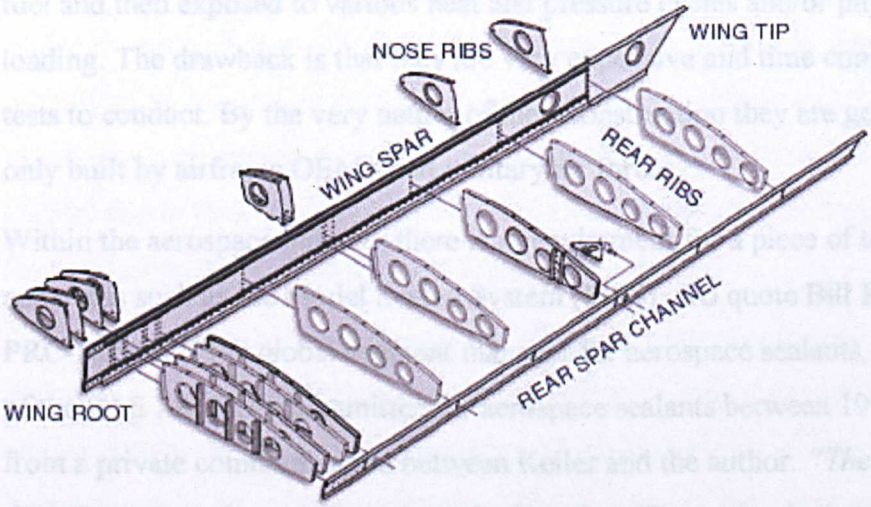

Figure 1.2 Internal wing components

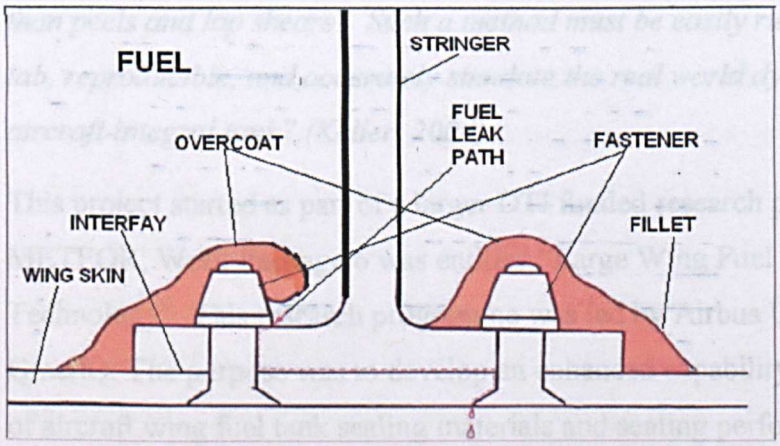

Figure 1.3 A cross section through the wingskin and stringer. This shows a potential leak path if only overcoat and fillet sealant is used with no interfay sealant.

Current approaches to sealant evaluation embrace immersion in a range of different fluids at different temperatures, of both bulk sealant samples and sealed joints, as well as the normal lap shear and peel tests. However, nearly all such tests are of a static nature and yet it acknowledged that it is movement that leads to leaks. Thus the missing component of testing is movement coupled with the other key variables.

Some projects have been undertaken that involve building a so called "Puffer Box" that undergoes cyclic dynamic loading while being exposed to several environmental conditions simultaneously. A "puffer box" is a small-scale integral wing tank. They are built exactly like the full-scale wing with interfay, sealed stringers, ribs, and sealed fasteners. When assembled it is filled with fuel and then exposed to various heat and pressure cycles and/or physical loading. The drawback is that they are very expensive and time consuming tests to conduct. By the very nature of their construction they are generally only built by airframe OEM's and military air forces.

Within the aerospace industry there is a requirement for a piece of test apparatus such as the Model Sealed System (MSS). To quote Bill Keller of PRC-DeSoto (PPG global segment manager for aerospace sealants, Secretary of the SAE AMS G-9 committee for aerospace sealants between 1997-2004) from a private communication between Keller and the author. *"The "Holy Grail" question that our Industry is looking for: Can a simple test method be developed that is less cumbersome than a "puffer box", but more real world than peels and lap shears? Such a method must be easily run in a materials lab, reproducible, and accurately simulate the real world dynamics of an aircraft integral tank" (Keller, 2004).*

This project started as part of a larger DTI funded research programme called METEOR; Work Package 6 was entitled "Large Wing Fuel Tank Technology". This research programme was led by Airbus UK and involved QinetiQ. The purpose was to develop an enhanced capability for the evaluation of aircraft wing fuel tank sealing materials and sealing performance for in-service aircraft. The involvement of Oxford Brookes University (OBU) started in October 2001 and ran until the end of 2003 (Phase 1). At the beginning of 2003, Phase 2 of the project began with Airbus (UK) deciding to fund OBU's

research exclusively. It was decided that the test rig be referred to as the Model Sealed System (MSS).

The full-scale structural features of a commercial aircraft wing define the fatigue loading spectrum. These stresses were established separately for a single aisle aircraft by (Buller (2002)(a)).

1.2. Purpose of research work and inherent considerations

Integral fuel tank sealing methods currently employed by the major aerospace companies are faying surface and fillet sealing with the wet installation and over-coating of fasteners **(Fig. 1.3)**. The most common sealing materials are those based on polysulfide compounds, which have been used by the aircraft industry for over 50 years. When polysulfide materials are applied carefully within the manufacturing process requirements of the aircraft constructor, they provide a reliable sealing method against fuel leakage. However, in-service experience with sealing integral fuel tanks has been far from satisfactory. This may be due to the possible influence of combined dynamic and environmental factors on sealant performance and sealant degradation.

A key concept for the future evaluation of sealant materials for commercial aircraft is to expose realistic sealed joint systems to typical dynamic and environmental parameters representative of actual flight conditions. The development of a facility to undertake the full range of test parameters for the evaluation of sealants for current and future aircraft is an essential requirement of a research programme.

There are several factors that became the driving force behind this research project. The first is that evaluation and comparative tests on new experimental sealants can be carried out early in their development when only a small sample of the test sealant may be available for testing. From this, data can be provided that can be used in life prediction techniques using accelerated testing. Secondly, preliminary screening of sealants for new aircraft can be accomplished using the MSS, thereby allowing a reliable selection of the optimum sealant and/or sealing system for the aircraft. Thirdly, maintenance and operational cost can also be reduced since field use conditions can be

simulated, thereby reducing the need for costly and time consuming flight tests.

Factors that should be considered and addressed as the cause of leaks in fuel tanks are:

- Are the substrates and fasteners compatible?
- Are the sealants used in the joint compatible with each other?
- Are the joints complex or simple to seal?
- What are the procedures for applying the sealant and are they correct?
- Is the correct sealant used?
- What surface preparation is used and is this adequate?
- Are the test conditions and methods (temperature, pressure, fatigue etc) adequate?
- The design of the joint itself (tolerances, corrosion and assembly stress).

1.3. Seals and fuel tanks

The preferred sealant used is a two-part, manganese-dioxide cured, liquid polysulfide. The polysulfide sealants theoretical function is understood (Meyer (1982), Lee (1999), Panek and Cook (1991)) along with the degradation mechanisms in service (Healey (1996)) and the durability of aluminium sealed joints (Comyn, Day and Shaw (1997)). The sealant also has to meet very stringent standards and specifications set down by Airbus UK Ltd, in the Airbus Industries Materials Standards (AIMS) documents and the military specification of the United States Department of Defence (Military Specification, MIL-S-8802F, December 1997). This covers the specification and application of the sealant, the preparation of the aluminium surface and the manufacture of the structures themselves.

A report published by the Advisory Group for Aerospace Research and Development (AGARD-R-771, 1989), points out that fuel tank leaks, generally, share the following contributing factors:

- The design of integral fuel tanks makes sealing difficult (new and repair), with many complex joints.
- Surface preparation and priming is difficult.
- Application of coating primers and sealant during initial assembly and subsequent repair is difficult to achieve consistently.

A review of recommendations from AGARD-R-771 can be summarised thus:

- Existing leak problems could be avoided if structural testing to certify fuel tank integrity had been performed in the development phase of the aircraft design (Sheridan (1989), Dawson (1989)).
- Fuel tank testing should be done using realistic combinations of both flight loading and other environmental factors such as temperature, humidity and pressure (Richardson (1989)).
- The ageing of the sealant systems as a result of chemical interaction with hydrocarbon fuels must be duplicated during testing to provide valid performance information during the expected service life of the fuel tank (Richardson (1989)).
- This ageing can only be accomplished by combining environmental exposures with the use of actual fuel in the test structure (Richardson (1989)).
- Improve sealing system materials with respect to ease of application, sealant properties and durability (Sheridan (1989), Dawson (1989)).
- Provide better training for staff responsible for the application of the sealant to integral fuel tanks at the initial stage and during subsequent repair (Dawson (1989)).

In 1977 the United States Air Force Wright-Patterson Aeronautical Laboratories (AFWAL) supervised a programme of research to evaluate experimental sealant materials against dynamic and environmental criteria. This led to Mallory and Elmer (1978) developing the Wright-Patterson Bench "Dynamic" Apparatus. The programme led to the assigned investigators testing sealant materials (but not a combination of all the components in the joint, for example, the sealant, the aluminium substrate and/or the fasteners)

under integrated conditions of dynamic loading and environmental parameters of fuel, pressure and temperature, that were representative of a typical aircraft flight spectrum. A key issue explored was the durability of a fillet seal on a joint subjected to cyclic loading.

The first two-year period of the research programme was terminated prematurely due to the poor reliability of the bench facility and heat distortion of the cup and disc test coupons. However, regardless of the shortcomings of the experimental facility, the feasibility of dynamic testing in conjunction with environmental parameters had been demonstrated.

1.4. Aims and objectives

The overall aim of the current research was to design, develop, fabricate and evaluate a novel sealant test rig, or Model Sealed System (MSS).The objectives were:

- To define the requirements for a novel test procedure that could be used to realistically evaluate sealed joint systems
- To develop and optimise a test coupon configuration and use Finite Element Analysis (FEA) to confirm and refine the results
- To design and develop the apparatus and control system for a novel test rig
- To undertake a limited parametric experimental programme to establish the limits of the dynamic loading and environmental conditioning to which the sealed joints can be subjected before failure of the sealant occurs.

1.5. Research strategy

There is a sealant and aircraft industry requirement for a simple test method that is less cumbersome than a "puffer box", but more realistic than the use of "static" testing of bulk specimens and joints. The fundamental aim of the research was to design, fabricate and develop a mechanism to achieve this requirement. A flow diagram of the research strategy is shown in Fig.1.4 and the details of the work are expanded in Table 1.1.

The main test parameters were identified, discussed and agreed with the METEOR project team partners during the first year of the research project (2001-2002). A copy of these can be found in **Appendix 1**.

The next step was to review previous work in the research area and carry out a literature review. This showed that there is a fundamental requirement within the aerospace industry for a systematic investigation of sealed joints in wings in order to understand the causes of failure, to provide improved methods of testing for predicting the performance of sealed systems and as a method for screening a variety of sealants. It confirmed that there is a requirement for a sealant test rig and that to date only Mallory and Elmer (1978) **(Section 1.3),** had managed to develop a workable machine to evaluate fuel tank sealants dynamically.

Several concept ideas were drawn up, investigated and after discussion amongst the project partners a shortlist of viable concepts was investigated further (Hooper et al, (2003)). Once a decision had been made on the chosen concept, the coupon configuration and size had to be determined.

Initial investigations using analytical calculations to try to predict the stresses in the chosen test configuration produced unsatisfactory results. The main problem was that this method does not allow for the stress concentrations caused by the ring of fasteners holding the two coupons together (the modelled wing butt plate – skin joint) similar to **Fig.6.2.** Initial investigations using FEA also produced unsatisfactory results in the timescale allowed for in the project.

It was decided to pursue an experimental approach to the problem. This involved designing and fabricating a prototype test rig, bonding strain gauges to the coupons and applying static loads to the rig to open and close the joint. From this it was determined that the measured stresses experienced by the Airbus A318 (Buller (2002) (a)) could be achieved in the laboratory.

The next phase of the project involved fitting the coupon set into a fatigue machine, attaching strain gauges and, with the use of aerospace fasteners, the coupon set was subjected to the loads and frequency defined in the project's test parameters **(Section 5.2).** This was carried out to check that the loads were not excessive or unrealistic, consequently causing premature damage to the

coupons and /or the fasteners. Further predictions of the stresses in the coupons were undertaken during this phase.

The coupons were next mounted in a Pressure Pot **(Section 6.2)** and the environmental parameters of fuel, pressure and temperature, representative of a typical aircraft flight spectrum, were developed and modified along with the control system and the methods used to apply these parameters. This was an involved and complex part of the project that was undertaken during 2003-2005. The precise details of the control and data acquisition system were developed during this time, together with refining the test protocols and defining the appropriate test regimes.

Data were collected for the performance of different coupon configurations and environmental conditions.

A limited investigation into which fluids (jet fuel, water and saline solution) the sealant comes into contact with was undertaken using standard small-scale specimens in several different types of tests. The bulk properties of the sealant (Young's modulus, ultimate tensile strength, T_g etc.) were determined before and after immersion in jet fuel, water and saline solution over different time periods (14, 28 and 56 days).

In order to provide confidence in the new procedure, the performance patterns from the MSS trials were compared with the bulk sealant data obtained from conventional testing. These comparisons are provided in Chapter 8.

Chapter	Phase	Task	Deliverables
2, 3 and 5	1	Project definition	Define the project requirements, test parameters and materials (sealants used, fasteners, temperatures, pressures, stresses, fatigue loads and frequency etc.)
5	1	Conceptual designs	Box beam, Scab patches, Vacuum bag and aluminium sheet, Flange and tube, Fastener and pressurised tube.
5	1	Mark 1. First prototype	**Development of Mechanics** Dimensions, materials, the test coupons axial loads(static and dynamic). Load application(axial and/or torsion). FEA optimisation of test coupon dimensions.
9	2	Mark 1. Application of temperature, pressure and fatigue	Control systems, pumping systems, leak detection, test cycles, fatigue test programme heating and cooling.
7	2	Mark 2. Integrated control system	Modifications, Fuel circulation, operating principles, control systems, fatigue testing.
7	2	Mark 3. Environmental and dynamic control system	Test loads, conditioning data acquisition and control.
8	2	Mark 3. results of testing	Selection of joint/coupon type, Sealants, data trends, Comparison with conventional test methods.

Table 1.1 Research strategy

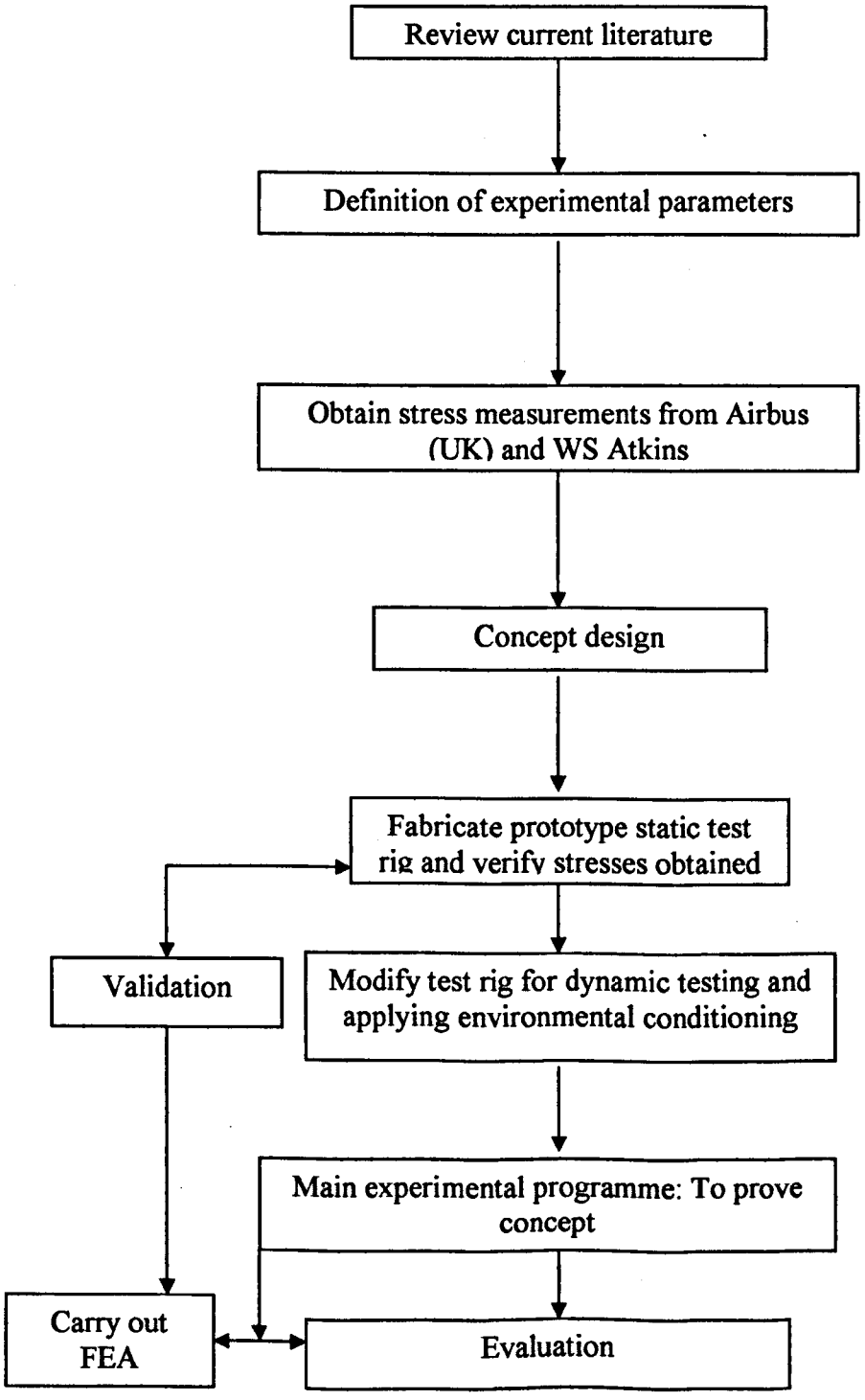

Figure 1.4 Flow diagram of research strategy

2 Review of aircraft wing design and construction, and integral fuel tank technology

The purpose of this chapter is to consider the aircraft operational skin stresses, pressures, temperature and loadings that are relevant to the experimental inputs for the Model Sealed System (MSS).

2.1. General wing design considerations

2.1.1. Structural principles

The wings have to incorporate aerodynamic shapes for long range flights up to near supersonic speeds, serve as fuel tanks and support the engine structures. They must withstand the effects of inclement weather (rain, hail and lightning strikes) and must be serviceable for at least 20 years (or longer) with the minimum of maintenance.

Structural integrity is a major factor in aircraft design and construction. An aircraft structure in flight is subjected to many, and different, stresses due to the varying loads that may be imposed. The problem is trying to anticipate the possible stresses that the structure will have to endure, and to build it sufficiently robustly to withstand these. This problem is complicated by the fact that an aircraft structure must obviously be light as well as strong. Current production passenger aircraft are constructed of various materials, the primary one being aluminium alloys. Rivets, bolts, screws and adhesives are used to hold the sheet metal in place.

Modern aircraft structures are designed using a semi-monocoque concept and a skin- stringer construction supported by spars and ribs below the surfaces. Semi-monocoque structures are thin shell structures where longitudinal stiffening members and transverse frames resist bending, compressive and torsional loads, whilst supporting the outer surface or skin of the shell without buckling. The basic functions are to transmit and resist the applied loads, to provide an aerodynamic shape and to protect passengers, payload, systems etc. from the environmental conditions encountered in flight. A comprehensive review of airframe design is given by (Niu, (1988)).

2.1.2. Types of structural stress

The structure of an aircraft is required to support two distinct classes of load:

- Ground loads; including all loads during movement or transportation on the ground such as taxiing and landing loads, towing and hoisting loads
- Air loads; comprising loads imposed in the structure during flight by manoeuvres and gusts.

The two classes of loads can be further divided into surface forces e.g. aerodynamic and hydrostatic pressure, and body forces which act over the volume of the structure and are the produced by gravitational and inertial effects. These loads will result in stresses being experienced by the aircraft's structure.

Limit loads are the maximum loads anticipated on the airframe during its life and the airframe should be capable of supporting these loads without permanent deformation (Niu, (1988)).

Ultimate loads are the load at which complete failure occurs. The ultimate load is normally related to the Limit load by the following formula:

Ultimate load = Limit load X Factor of Safety

In general, the factor of safety is 1.5 (Niu, (1988)).

The five basic structural loadings to which aircraft are subject are:

- Tension
- Compression
- Torsion
- Shear
- Bending

While there are many other ways to describe the actual stresses which an aircraft undergoes in normal (or abnormal) operation, they are special arrangements of these basic ones.

Tension is the stress acting against another force that is trying to pull something apart. For example, while in straight and level flight the engine

power is pulling the aircraft forward. The wings, tail section and fuselage, however, resist that movement because of the airflow around them. The result is a stretching effect on the airframe. A tension member is inherently stable. However, an important point to remember with tension members is that failure implies severance of the structure, normally with catastrophic results unless alternative load paths are provided.

Compression is a squeezing or crushing force that tries to make parts smaller. Anti-compression design resists an inward or crushing force applied to a piece or assembly. Aircraft wings are subjected to compression stresses. Again, an ideal member in pure compression is stable. However, since the ideal is never achieved in practice all compression members must be designed with consideration of instability. Extra material is therefore required relative to that necessary to take the simple direct load in compression. There are three forms of compression instability:

- Overall, which is a simple strut failure (Euler buckling)
- Local, where a flange or other part of the local cross section buckled in a short distance
- Torsion, where the whole section twists, but it is frequently difficult to distinguish this from local instability.

Euler buckling relates to the critical column load which would produce buckling. A member in compression *buckles*, that is, moves laterally and shortens under a load it can no longer support. With any smaller load, the column would remain straight and support it. It must be remembered that a compression member is often capable of transmitting some load after initial buckling has occurred. With any larger load, the least disturbance would cause the column to bend sideways with an indefinitely large displacement; that is, it would buckle. This means that any buckling merely encourages further buckling, explaining why such failure can be catastrophic.

Torsion is a twisting force. Because aluminium is used almost exclusively for the outside and inside fabrication of parts and covering of the airframe, its tensile strength under torsion is very important. The torsional strength of a material is its ability to resist torque (a twisting force). The airframe is

subjected to variable torsional stresses during turns and other manoeuvres. As are the wings when flaps are used in flight.

Shear tends to slide one piece of material over another. In an aircraft fuselage, the aluminium skin panels are riveted to one another. Shear forces try to make the rivets fail under flight loads; therefore, selection of rivets with adequate shear resistance is critical. Bolts and other fasteners are often loaded in shear, even though this is not necessarily desirable. An example of this is the bolts that fasten the wing to the spar or carry-through structure. Although other forces may also be present, shear forces try to break the bolt in two. Generally, shear strength is less than tensile or compressive strength in a particular material.

Bending is a combination of two forces, compression and tension. During bending stress, the material on the inside of the bend is compressed and the outside material is stretched in tension. An example of this is the G-loading an aircraft structure experiences during manoeuvring. During an abrupt pull-up, the aircraft's wing spars, wing skin and fuselage undergo positive loading and the upper surfaces are subject to compression, while the lower wing skin experiences tension loads.

There is another factor to be taken into account when considering the strength of an aircraft's structure that has already been mentioned. If a load on a structure is applied and released repeatedly, or alternates between tension and compression damage can be generated due to fatigue crack growth. Such structures will fail under fluctuating loads at much lower values of stress than their normal static failure stress. Atmospheric turbulence, and variable cabin pressures are two of the fluctuating loads that can cause fatigue damage in an aircraft. On the ground the wing is supported on the undercarriage and experiences tensile stresses in its upper surfaces and, conversely, compressive forces on its lower surfaces. In flight these stresses are reversed as aerodynamic lift supports the wing. Landing and taxiing on imperfect surfaces causes stress fluctuations. Engine pylons are also subjected to fatigue loading from variations in thrust during take off and landing, and inertia loads caused by lateral gusts on the aircraft as a whole cause fatigue as well.

2.1.3. Wing construction

Wing construction is basically the same in all types of aircraft. To maintain its all-important aerodynamic shape, a wing must be designed and built to hold its shape even under extreme stress. Basically, the wing is a framework composed chiefly of spars, ribs, and stringers (**Fig. 2.1**). Spars are the main members of the wing. They extend lengthwise along the wing (crosswise to the fuselage). The entire load carried by the wing is ultimately taken by the spars. In flight, the force of the air acts against the skin. From the skin, this force is transmitted to the ribs and then to the spars.

Figure 2.1 An early wood and fabric wing structure (Allstar network (2004) (top) and a multi-spar box structure and detail of a metallic rib (Niu, 1988) (bottom).

Most wing structures have two spars, the front spar and the rear spar. The front spar is found near the leading edge while the rear spar is located about two-thirds of the distance towards the trailing edge.

The ribs are the parts of a wing which support the covering and provide the aerofoil shape. These ribs are called forming ribs. Their primary purpose is to provide shape. Some may have an additional purpose of bearing flight stress, and these are called compression ribs. The ribs are formed and have flanges around their edges to enable the skin and spar webs to be fastened to them. Cut-outs around their edges allow the spanwise stringers to go through them. Stringers are first machined and then formed to shape and connect the wing skin panels to the rib/spar structure by the use of fasteners and the aforementioned flanges. They also give stiffness and form to the skin as they run longitudinally from root to wing tip.

The strongest wing structure is the full cantilever which is attached directly to the fuselage, via the carry-through structure, and does not have any type of external, stress-bearing structures. **(Fig. 2.2 and 2.3)**.

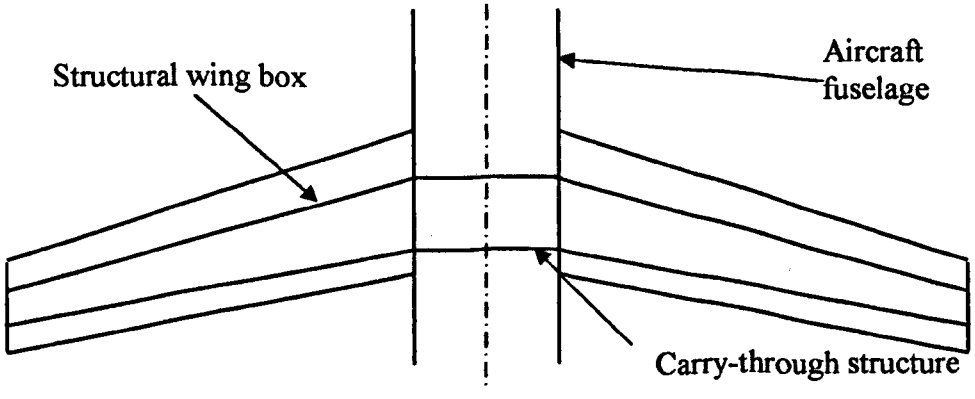

Figure 2.2 Wing carry-through structure.

2.1.4. Aerodynamic principles

Obviously, the lifting air loads (lift force) on an aircraft wing have to be as great as the weight in order to support the airplane in flight **(Fig.2.3).**

Figure 2.3 Aircraft weight and lifting air loads (Niu (1988)). Showing the full cantilever design.

The following text provides a very brief and basic explanation of aerodynamics as it applies to aircraft. This will help explain where the forces that act upon the various components in the wings are derived and from these, the five basic structural stresses **(Section 2.1.2)** to which aircraft are subjected come from. Most aerodynamic principles relate to the two basic aerodynamic forces: lift and drag.

Drag

Drag is an aerodynamic force that resists the forward motion of an object. The shape of the object influences the amount of drag. Objects shaped to produce as little drag as possible are called streamlined or aerodynamically clean.

Three types of drag, friction drag, form or pressure drag, and induced drag act on all moving objects but induced drag only affect objects with lift.

When a moving fluid, such as air, comes into contact with a curved surface it will try to follow that surface. This tendency of fluids to follow a curved surface is known as the Coanda effect (Coanda, 1930) and the cause is viscosity, the resistance to flow of a fluid. The viscosity of air is very small but it is enough for the air molecules to want to stick to the surface of the aircraft. Next to the surface there is no measurable relative motion. Individual molecules do not actually physically stick but move randomly, with an average

velocity component parallel to the surface of zero. The relative velocity of the airflow increases rapidly with distance away from a surface, and only a thin layer is slowed down by the presence of the surface. This can be illustrated by the fact that a thin film of dust can, and usually does, exist on the blades of a rotating fan. Because the fluid near the surface has a change in velocity, the fluid flow is bent towards the surface and unless the bend is too tight, the fluid will follow the surface. This volume of air around the wing that appears to be partially stuck to the wing is called the "boundary layer".

Friction drag (laminar and turbulent boundary layers)

The molecules of air in the boundary layer move in either orderly paths parallel to the surface (laminar) or irregular paths (turbulent). A turbulent flow increases friction drag (Anderson and Eberhardt, 2001).

Near the leading edge the air flows smoothly with no turbulence, and appears to behave rather like a stack of flat sheets (laminae) sliding over each other with friction, the outer ones moving faster than the inner ones. Therefore the boundary layer is laminar at the front of an object. As the air flow moves over the object there is a sudden change (transition) to a turbulent flow in which random flow is superimposed on the average flow. To keep frictional drag to a minimum it is desirable to delay this change from laminar to turbulent flow for as long as possible. This can be achieved by making the surface of the object as smooth as possible, called streamlined or aerodynamically clean. The important difference between the flow mechanisms in the two layers is that in the laminar type, the influence of the surface is transmitted outward mainly by a process of molecular impacts, whereas in the turbulent type the influence is spread by turbulent mixing.

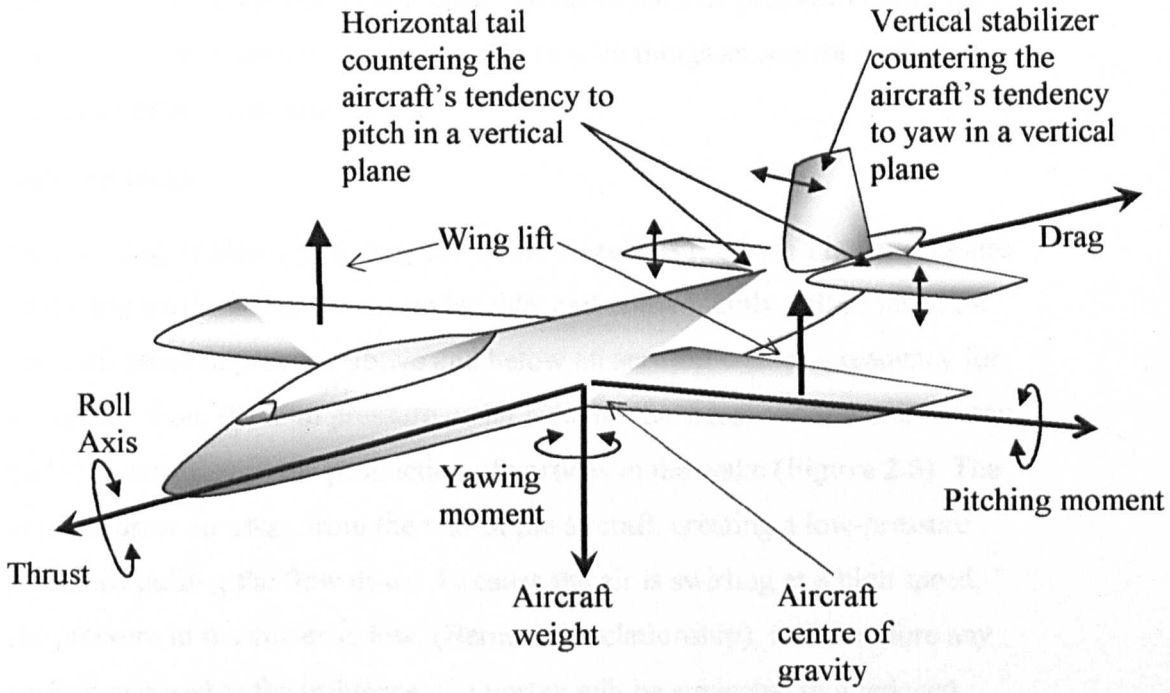

Figure 2.4 Principal aerodynamics forces on an aircraft during flight.

Pressure or Form drag

At the front of the aerofoil (wing), where the relative air speed is brought to zero, the flow separates to go either under or over the wing. The air then accelerates to the widest part of the wing and as the airflow reaches the rear of the wing it slows down again and converges. Without the influence of viscosity and with no sharp corners the streamlines would close up neatly behind the wing and from the Bernoulli relationship (Bernoulli discovered that as the velocity of a fluid increases, its pressure decreases) the pressure distribution would be equal. Consequently, there will be no drag. In reality because of the effects of viscosity the airflow will separate towards the rear of the wing and there will be a resultant wake of slower moving air. In this airflow the stream line pattern and pressure distribution are no longer symmetrical. The pressure over the rear portion of the shape is on average lower than the front and there will therefore be a net rearward drag force **(Fig.2.4).** This is known as Pressure or Form drag. This type of drag produces swirling eddies of air that takes energy from the object and slows it down. One simple way to reduce profile drag is to ensure that the aerofoil has a sharp trailing edge, so that the streamlines come smoothly off the upper and lower

surfaces, without leaving a blunt edge behind which low pressures exist. There is usually some additional form drag due to such things as control surface gaps, and other extraneous items.

Induced Drag

Induced drag is also called drag due to lift. Aerofoils produce a lower pressure on the top surfaces than on the under side, and consequently will produce lift. The difference in pressure above and below an aerofoil creates a tendency for air to flow from the high pressure under side, up the sides, and towards the top surfaces, resulting in the production of vortices in the wake **(Figure 2.5)**. The vortices draw air away from the rear of the aircraft, creating a low-pressure area, thus pulling the flow down. Because the air is swirling at a high speed, the pressure in the vortex is low, (Bernoulli's relationship), and therefore any surface exposed to the influence of a vortex will be subjected to a reduced pressure with the resultant increased drag.

Figure 2.5 Vortices drawn from the rear of the aircraft (University of Adelaide (2005)

Lift

Lift is an aerodynamic force produced by the motion of an aerofoil through the air and acts at a right angle to the direction of motion **(Fig.2.4).**

A typical aerofoil has a rounded leading (front) edge and a sharp trailing (rear) edge. As the flow of air approaches the leading edge, it splits to go around the

aerofoil. To produce lift, the flows along the upper surface and the lower surface must be unsymmetrical. An unsymmetrical flow can be created by the curved shape of the aerofoil, called the camber **(Fig.2.6)**. Such a flow also occurs when the aerofoil meets the air at an angle (angle of attack, this is discussed later). Furthermore, the two flows must merge smoothly as they leave the trailing edge (see Pressure or form drag), known as the Kutta condition, named after the German mathematician (1902). This in combination with the unsymmetrical flow of air, produces a faster flow along the upper surface, thus reducing the air pressure on that surface **(Fig.2.6).** This difference in pressure results from a difference in the speed of the air flowing along the two surfaces, obeying the principle discovered by Bernoulli as previously mentioned. As a result of this, the aerofoil, is lifted into the air.

Figure 2.6 Cross section of an aerofoil (Anderson and Eberhardt. 2001).

This explanation doesn't cover all of the factors involved in flight. This description focuses on the shape of the wing and does not address such important phenomena as power, the dependence of lift on the angle of attack of the wing and, to a lesser extent, even inverted flight. An example of an aircraft where other factors to enable flight are involved is the Lockheed F-104 Starfighter **(Fig.2.7)** of the 1950's where its small wing area, very powerful engine and needle-nose earned it the nickname of "Missile with a man in it".

Figure 2.7 Lockheed F104 Starfighter (Ferriere (2006)).

Most jet fighters of the period (and to this day) used a swept-wing or delta-wing. This configuration allowed a reasonable balance between aerodynamic performance, lift, and internal space for fuel and equipment. Lockheed determined that the most efficient shape for high-speed, supersonic flight was a very small, straight, mid-mounted, trapezoidal wing. The wing was extremely thin, with a thickness-to-chord ratio of only 3.36% and its aspect ratio was 2.45 **(Figs.2.7 and 2.10).** The thinness of the wings meant that fuel tanks and landing gear had to be contained in the fuselage. So it can be seen that though the earlier explanation of lift does apply to the F-104 this was not the only explanation for its ability to fly. The following physical description is based primarily on *Newton's laws* and is useful for understanding flight in its entirety. This, simplified, version omits the mathematics involved but just relates to first principles.

If *Newton's First Law of Motion* is applied to the aerofoil which states: *"A body at rest will remain at rest, or a body in motion will continue in straight-line motion unless subjected to an external applied force"*, it can be seen that as the aerofoil travels through the air, if one sees a bend in the flow of air, or if air originally at rest is accelerated into motion, there must be a force acting on it. If one were to also apply *Newton's Third Law of Motion* to the aerofoil, which states *"That for every action there is an equal and opposite reaction"*, it can be seen that the fluid must impart an equal and opposite force on the object (aerofoil) which causes the fluid to bend. From this it can be surmised that as the aerofoil deflects air downward (action) the reaction to this motion forces the aerofoil upward producing lift. If the two figures (**Fig.2.8**) are compared the one on the left shows the air (streamlines) flowing over and under the wing

leaving the wing the same as it appeared at the front of the wing. As there is no action on the air there can't be any lift (reaction) present. The lower figure shows the air passing over the wing and being deflected down. The deflected air stream is the action and lift is the reaction.

Figure 2.8 Airflow over an aerofoil. (Anderson and Eberhardt. 2001).

As the wing moves through the air it must change something in the air to achieve lift. *Newton's Second Law of Motion* states that *"The relationship between an object's mass* ***m****, its acceleration* ***a****, and the applied force* ***F*** *is* ***F = ma***". This implies that for more lift (force) the wing can either divert more air (mass) or increase its downward or vertical velocity (acceleration). From this statement two things can be surmised that contribute to achieve greater lift. The first is that an increase in the angle of attack will increase the vertical velocity and secondly, for the same angle of attack an increase in the speed of the aerofoil will increase the vertical velocity. Both the increase in the speed and the increase of the angle of attack increase the vertical velocity that gives the wing lift.

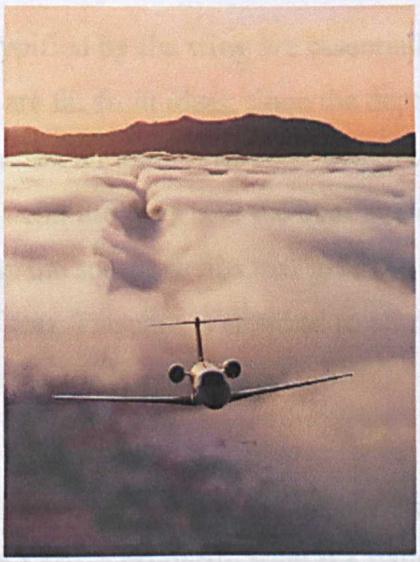

Figure 2.9 Downwash and wing vortices in the fog. (Photographer Paul Bowen, courtesy of Cessna Aircraft, Co.)

Figure 2.9 illustrates the effect of the air being diverted down from a wing. The wing must generate lift from the airflow over it to support the aircraft in flight. The amount of lift required depends on how the aircraft is flying or manoeuvring. For straight and level flight, the total lift produced must be equal to the weight of the aircraft. To take off and climb, the required lift must be developed at a low airspeed. For highly manoeuvrable aircraft where it's a requirement for the aircraft to fly in very tight turns, the wing must produce lift equal to maybe as much as eight times the aircraft weight. For landing, the slowest possible forward speed is required, and enough lift must be produced to support the aircraft at these low speeds. For example, the amount of air (air weighs approx 1.18 kilogram/cubic metre at sea level) that has to be diverted down at relatively low speed to allow a Boeing 747 weighing 363 tonnes to take off, or land gently, is huge (Anderson and Eberhardt, 2001).

The wing's angle of attack only works efficiently between certain angles. Air cannot flow smoothly over the wing if the angle becomes too steep. Instead, the air stream suddenly breaks up into eddies on top of the wing and the airflow becomes turbulent and the airflow becomes separated. This decreases the lift dangerously and consequently the plane will lose altitude quickly. This condition is called a stall. Planes fly at an angle ranging from 3 degrees to 15 degrees. A plane will stall if the angle becomes larger than 15 to 20 degrees.

2.1.5. Design parameters

The flying surfaces as typified by the wing are essentially cantilever beams **(Fig.2.3)**. As such they are far from ideal, since the depth is not very large. Cantilever wings must resist all loads with their own internal structure. The aircraft weight tends to bend the wing and the bending load is carried primarily by the spars. Attached to the spars are ribs that give the aerodynamic shape to the wing **(Figs.1.1 and 1.2)**. The skin is attached to all the structural members and carries part of the wing loads and stresses.

In addition to acting as a beam to resist spanwise loads, the wing must also carry considerable torsion loads and provide sufficient stiffness to prevent excessive twist. This load arises primarily from the flaps and control surfaces. A reduction in the thickness/chord ratio (the ratio between the thickness of a wing section and the chord, which is the distance between the leading and

trailing edge) is critical since the bending strength is proportional to this dimension.

The aspect ratio of a wing is defined to be the square of the span divided by the wing area. This ratio is a measure of how long and slender a wing is from tip to tip. A reduced aspect ratio thus reduces both bending moment and twist and this is structurally advantageous **(Fig.2.10).** An example of a high aspect ratio wing would be the U2 spy plane, the B-52 bomber and most gliders. An example of a low aspect ratio wing would be the Lockheed Starfighter, the Hawker Harrier or the Russian Mig 21.

Figure 2.10 Examples of wing aspect ratio (Florit, 2001)

During flight, stresses are transmitted first to the wing skin, then to the ribs, and finally to the spars. Spars also must carry loads distributed by the fuselage, landing gear and any nacelles (terminology for any part that is joined to the structure of the wing, such as the engines and pylons). As has been mentioned previously, most aircraft use the area between the spars as a fuel tank. The mass of the fuel acts in the opposite direction to wing lift, thus reducing wing-bending moment and, hence, stress.

The amount and disposition of the fuel weight in the wing is particularly important as it can provide bending relief during flight. Placing fuel as far

outboard as possible and using fuel from the most outboard tanks last would appear to provide the optimum arrangement for wing bending during flight (Niu (1988)).

However, if one considers the large inertia effects of the fuel and the resultant bending of the wing in a downward direction in the event of a hard landing, for example, to avoid aquaplaning on a wet runway, this arrangement of the fuel is not necessarily the best solution and can cause undue stresses on the wing structure to occur. From this it can be seen how important fuel management during flight is.

Fuel in an aircraft is redistributed in the tank fuel for several reasons besides bending relief. Fuel tapped from the engine high pressure fuel line cools the engine oil. This, in turn, heats the fuel and from this a recirculation system returns part of the heated fuel to the wing tanks to prevent frosting.

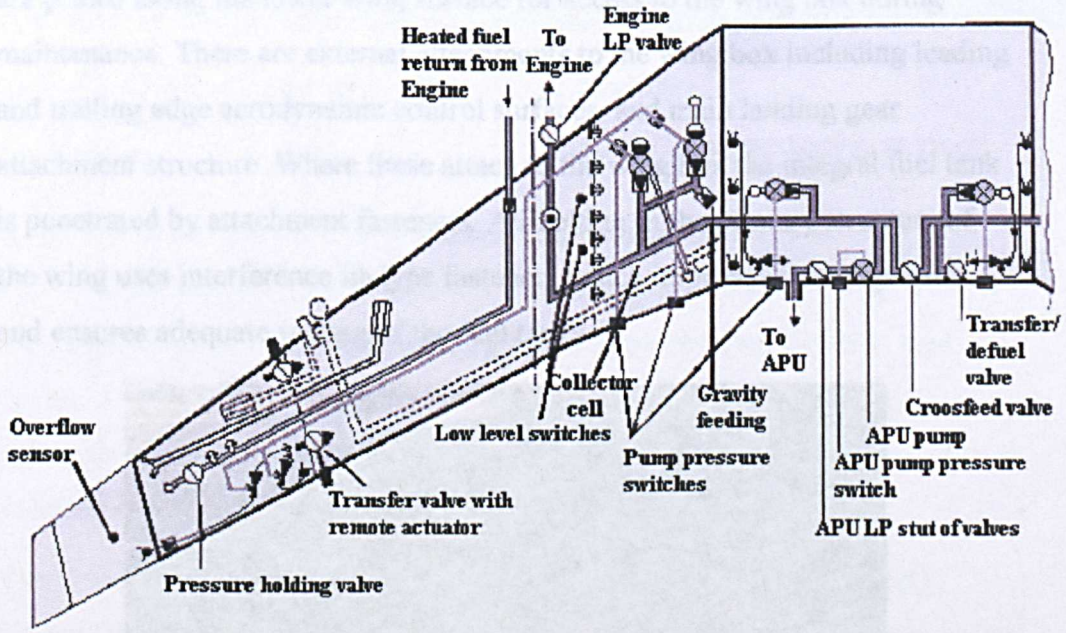

Figure 2.11 Figure Schematic of fuel system, transfer, scavenge & recirculation Courtesy of Airbus (Adams, 2004).

The fuel system also allows for ventilation and surge (**Fig 2.11**). The fuel venting system prevents over stressing of the tank structure by maintaining near ambient air pressure between tanks during re-fuelling and fuel use, engine consumption, fuel tank transfer and also during climb and descent. Each fuel tank is vented through vent lines into a surge tank.

2.2. Integral fuel tank technology

2.2.1. Principles

The wing structure is an integrally machined design comprising a main load carrying box structure made up of upper and lower skins, front and rear spars. The upper and lower skins consist of machined plates stiffened by internal spanwise stringers. There are spanwise butt joints in the upper and lower skins formed by a butt-strap and stringer combination (**Figs. 2.12 and 2.13**). The fuel tank is integral with the wing box structure. Each wing tank is divided into cells by sealed ribs. The ribs act as baffles to stop the fuel surging during manoeuvres which would make the aircraft unstable and difficult to control (**Figs.1.1,1.2 and 1.3**). A surge tank is formed in the outer section of the wing in which fuel is collected if discharged from the tank vent system. The tanks are sealed and internally treated against corrosion. Removable access panels are placed along the lower wing surface for access to the wing box during maintenance. There are external attachments to the wing box including leading and trailing edge aerodynamic control surfaces, and main landing gear attachment structure. Where these attach to the wing box the integral fuel tank is penetrated by attachment fasteners. All bolting in the primary structure of the wing uses interference fit-type fasteners which improves the fatigue life and ensures adequate sealing of the fuel tanks.

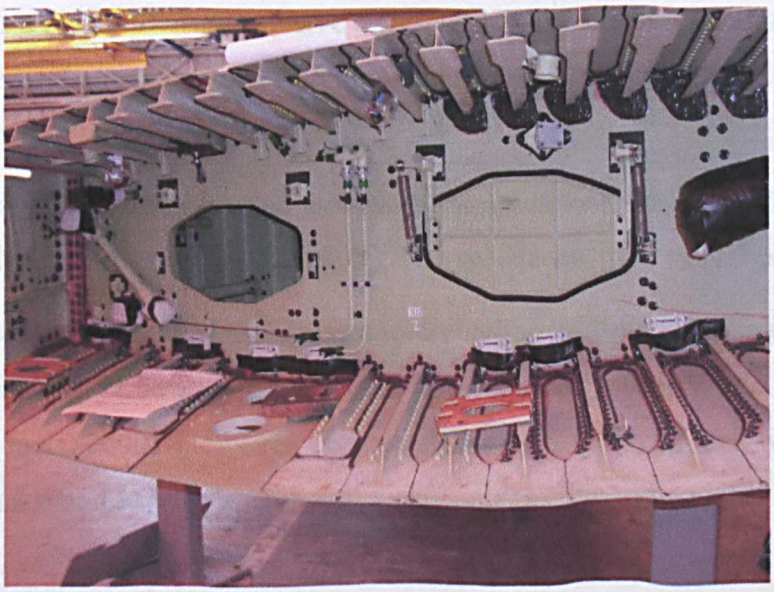

Figure 2.12 The inner components of an Airbus wing, showing the ribs, stringers, skin and the removable access panels.

The joint integrity must be maintained from the static load condition through to the dynamic condition of temperature and pressure cycling and aircraft flexure in flight. For example, a 30 metre wing can flex vertically 5 metres under operating conditions (Meyer (1982)). The temperature range can vary from – 41°C (A340-600, 40000-42000ft, Mach 0.83) to approximately 50°C (USAF transport) (Buller (2002)).

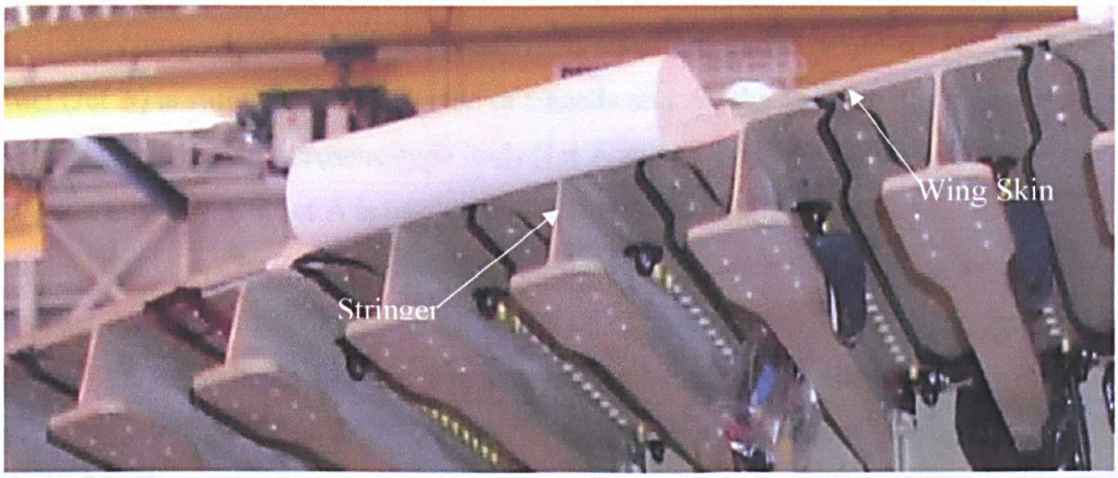

Figure 2.13 Detail of the wing skin /stringer assembly.

2.2.2. Fuel

In the 1940s, the turbine or jet engine emerged and gradually took over from piston driven engines. The principal difference between piston and jet engines is that combustion is intermittent in a piston engine and continuous in a jet engine. As a result, the engines have different fuel combustion quality requirements. In piston engines, combustion timing is critical to good performance.

The fuel used in the first aircraft turbine engines was kerosene (paraffin) because the engines were thought to be relatively insensitive to fuel properties.

"Wide-cut" fuel, which essentially is a hydrocarbon mixture spanning the petrol and kerosene boiling ranges, was used extensively after World War II (Chevron fuels, 2000). However, compared to a kerosene-type fuel, wide-cut jet fuel was found to have operational disadvantages due to its higher volatility:

- Evaporation losses greater at high altitudes
- Greater risk of fire during handling on the ground

- Less survivable crashes of planes fuelled with wide-cut fuel.

In the 1970's Military operators, especially the US Air Force, began a reversion back to kerosene type fuels and they have essentially completed the process of converting from wide-cut (JP-4) to kerosene-type (JP-8) fuels. (JP-8 is the fuel used in the Model Sealed System).

When the commercial jet industry was developing in the 1950s, kerosene-type fuel was chosen as having the best combinations of properties. Wide-cut jet fuel (Jet B) is still used in some parts of Canada and Alaska because it is suited to cold climates, but kerosene-type fuels (Jet A and Jet A-1) predominate in the rest of the world. Jet A is used in the United States while most of the rest of the world uses Jet A-1. The important difference between the two fuels is that Jet A-1 has a lower maximum freezing point than Jet A (Jet A: – 40°C, Jet A-1:–47°C). The lower freezing point makes Jet A-1 more suitable for long international flights, especially on polar routes during the winter (Chevron fuels, 2000).

2.2.3. Operational parameters

A combination of structural loading, fuel inertia, tank pressures, thermal and chemical effects influence the structural integrity of the fuel tanks (Richardson, 1989). There are some conditions that are common to all aircraft types and these can be summarised as:

Ground loads

- Taxi
- Take off
- Landing

Flight

- Manoeuvring loads
- Gust loads
- Fuel inertia

Thermal effects

- Pressure changes
- Rapid temperature changes
- High solar heating (highest recorded 58°C in Libya, September 13th1922) or low ground temperatures(lowest recorded -68°C in USSR on 5th and 7th February 1892)(US Dept. of Defence, 1997)
- Low flight temperatures (-55°C for a C-130(Hercules) transport, down to -87°C for an F-16 fighter)(Richardson, 1989)

Chemical effects

- Fuel
- Water
- Humidity
- De-icing fluids
- Hydraulic oils
- Microbiological contamination
- Corrosion
- Airframe ageing.

2.3. Summary

Main stresses

The structure of an aircraft is required to support two distinct classes of load:

- Ground loads
- Air loads

These two classes of loads can be further divided into surface forces e.g. aerodynamic and hydrostatic pressure, and body forces which act over the volume of the structure and are the produced by gravitational and inertial effects. The important wing skin stresses are transient in nature, with extremes caused by a combination of flight and gust loads.

Pressures

Metal fuel tanks are required to withstand an internal test pressure of 3.5psi (0.24bar) (Niu, 1988).

Temperature changes

The temperatures can range from –87°C to +58 °C.

Airframe construction

Aircraft structures are designed using a semi-monocoque concept and a skin-stringer construction supported by spars and ribs below the surfaces. The basic functions are to transmit and resist the applied loads, to provide an aerodynamic shape and to protect passengers, payload, systems etc. from the environmental conditions encountered in flight. Current production passenger aircraft are constructed primarily from aluminium alloys. Rivets, bolts, screws and adhesives are used to hold the sheet metal in place.

Joints

The types of joint and their general locations within the integral fuel tank are covered in **Chapter 4, Sealants**.

Sealed areas

The fuel tank is integral with the wing box structure. The upper and lower skins consist of machined plates stiffened by internal spanwise stringers. There are spanwise butt joints in the upper and lower skins formed by a butt-strap and stringer combination (**Figs. 2.12 and 2.13**). The upper and lower skins form the top and bottom of the fuel tank. Each wing tank is then divided into cells by the sealed ribs. The ribs act as baffles to stop the fuel surging and act as the ends of the tanks. The joints between the ribs, spars etc. and skin are sealed to prevent fuel leakage. The number of parts in the wing-box walls and floors should be kept to a minimum. If there are fewer parts then there are fewer joints and seams to potentially leak.

3 Materials and assembly methods used in aircraft wings

This chapter considers all of the materials and assembly methods used in current metallic airframes. This allows an appropriate selection of materials, surface treatments, thicknesses, fasteners, and sealant materials to be derived for the design of the Model Sealed System (MSS).

3.1. Materials

3.1.1. General requirements

An aircraft structure should be designed to meet a number of conflicting requirements, the main ones being (Nui,1988):

- Low weight
- Acceptable material and manufacturing costs
- Adequate strength to meet expected loads, with a suitable safety factor
- Adequate stiffness so that distortions are kept to an acceptable level
- Good in service properties such as fatigue and corrosion resistance, together with tolerance of expected temperatures and other atmospheric conditions.

The choice of materials used in aircraft manufacture emphasizes not only strength/weight ratio but also (Nui,1988):

- Fracture toughness
- Crack propagation rate
- Notch sensitivity
- Stress corrosion resistance.

These physical requirements are illustrated in **Figure 3.1.**

The stresses a particular part must withstand are carefully calculated. Strict compliance with the regulations applicable to the category of aircraft being designed is mandatory. Every part used in the aircraft, whether it be a stringer, former, bulkhead, or any attaching hardware must meet safety criteria, not

only for the certification period, but for the expected life of the airframe under design conditions of use. Some airframe parts such as wing spars require high strength. Others, such as cowlings, while not requiring as much strength, still must be capable of withstanding some loading and stress, as well as contributing to an aerodynamically clean design.

Component parts must be made of carefully selected materials because of their importance in maintaining integrity of the aircraft under expected stress and loading. The same holds true for fasteners such as bolts and rivets. It is essential that these parts do not fail or weaken with exposure to stress and weather elements. Corrosion must also be considered. A fitting made of one metal cannot be secured to the structure with a bolt or fastener made of another metal without measures being taken to prevent dissimilar metal corrosion. Over a period of time dissimilar metal corrosion can result in a weakening of the assembly to the extent that the assembly is rendered unsafe.

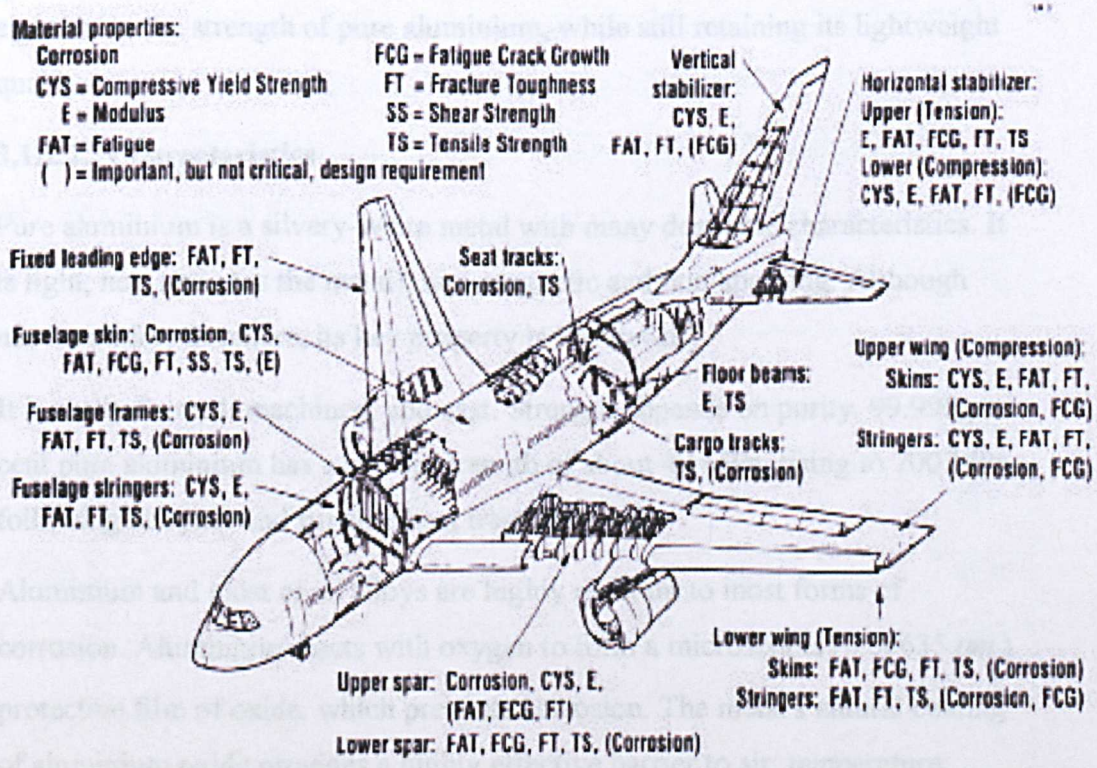

Figure 3.1 The required material properties used in aircraft construction. (Robson (2002)).

3.1.2. Aluminium

3.1.2.1. General

Aluminium with its combination of lightness, strength and workability makes it the ideal material for mass-produced commercial aircraft. Aluminium is the primary aircraft material, comprising about 80 per cent of a typical aircraft's unladen weight. For example, the standard Boeing 747 jumbo jet contains approx. 75,000kg of aluminium.

Today the main material used in the construction of aircraft is aluminium alloy, in which pure aluminium is mixed with other metals to improve its strength and other properties. A typical alloy used in aircraft structures may be 4% copper, 0.5% silicon, 0.5% magnesium, a little manganese, iron and chromium and the remainder; more than 90%, will be aluminium itself. Mixing aluminium with these very small quantities of other metals has an enormous effect on its strength. The strength of the structural alloys is six to eight times the strength of pure aluminium, while still retaining its lightweight quality.

3.1.2.2. Characteristics

Pure aluminium is a silvery-white metal with many desirable characteristics. It is light, non-toxic (as the metal), non-magnetic and non-sparking. Although not found free in nature, its key property is low density.

It is easily formed, machined, and cast. Strength depends on purity. 99.996 per cent pure aluminium has a tensile strength of about 49 MPa, rising to 700 MPa following alloying and suitable heat treatment.

Aluminium and most of its alloys are highly resistant to most forms of corrosion. Aluminium reacts with oxygen to form a microscopic (0.00635 μm) protective film of oxide, which prevents corrosion. The metal's natural coating of aluminium oxide provides a highly effective barrier to air, temperature, moisture and chemical attack. In fact, aluminium resists corrosion so well that some airlines do not paint their planes, saving several hundred kgs of weight, thus saving fuel, reducing emissions and increasing the aircraft's payload.

The composition of alloys are regulated by an internationally agreed classification system or nomenclature for wrought alloys and by various domestic nomenclature schemes for the casting alloys.

The wrought scheme is shown in **Table 3.1.** Each registered alloy is described by a four digit number, with a further letter and number indicating the temper, or condition of the alloy. For example, 6082-T6 is a medium strength grade based on the aluminium-magnesium-silicon family, in the fully heat-treated condition.

1XXX	Aluminium of 99% minimum purity
2XXX	Aluminium-copper alloys
3XXX	Aluminium-manganese alloys
4XXX	Aluminium-silicon alloys
5XXX	Aluminium-magnesium alloys
6XXX	Aluminium-magnesium-silicon alloys
7XXX	Aluminium-zinc-magnesium alloys
8XXX	Miscellaneous alloys, e.g. aluminium-lithium alloys

Table 3.1 The classification table for aluminium alloys. (The International Aluminium Institute (2000)).

Density / Specific Gravity (g/cm^3)	2.78
Melting Point (°C)	502
Tensile Strength, Yield (MPa)	345
Tensile Strength, Ultimate (MPa)	485
Modulus of Elasticity (GPa)	72.4
Poisson's Ratio	0.33
Shear Strength (MPa)	280
Hardness, (Brinell)	120
Coefficient of linear thermal expansion @20°C($\left(\mu m/m\right)/°C$)	23.2

Table 3.2 Physical Properties of Aluminium.2024 T3. (MatWeb.com (2002)).

Alloys fall into two main groups. In the first group of work-hardening alloys, strength is achieved by the amount of "cold work" applied to the alloy, e.g. by rolling. In the second group of heat-treatable or precipitation hardening alloys, the strength and properties are achieved by heat treatments of varying complexity. The rolling process changes the characteristics of the metal, making it more brittle and less ductile. Aluminium can also be extruded by heating it to around 500°C and pushing it through a die at great pressure to form intricate shapes and sections. The metal can also be forged by hammering to make stress-bearing parts for aircraft.

Some typical properties of aluminium 2024 T3 used in the outer test coupon of the MSS are summarised in **Table 3.2**. It must be remembered that these properties can be very significantly altered with the addition of small amounts of alloying materials.

3.1.2.3. Alloy cladding

In this process, a composite billet is made of the base metal with a coating. As the metal is reduced in thickness by rolling or drawing, the thickness of the base and coating are reduced proportionally. A typical application of this process is the cladding of aluminium alloy with corrosion resistant, but weaker, high purity aluminium.

The choice of a cladding alloy for a given core product has to meet several goals:

- A cladding alloy has to provide intrinsic resistance to corrosion. Uniform and pitting corrosion are allowed provided that the attack does not penetrate through the cladding.

- The cladding alloy must protect the core cathodically, playing the role of a sacrificial anode. In other words, the corrosion potential must be lower (at least by 50mV) for the cladding (anodic) than for the core (cathodic).

- The potential gap between core and cladding must not be too high because, in the event that core and cladding are both exposed to corrosive environments (machining, chemical milling, sheet edge, scratches etc.), the cladding must protect the core cathodically without dissolving too rapidly (otherwise, the

cathodic protection of the core will disappear too quickly). A potential gap of less than 100mV is recommended.

- The cladding must not contain elements that cannot be recycled in the core.

The influence of chemical elements in solid solution on the corrosion potential of aluminium alloys is well known (Hunsicker (1987)). Briefly, zinc and magnesium are anodic (lower the potential) whereas copper, silicon and manganese are cathodic (increase the potential).

3.1.3. Titanium fasteners

3.1.3.1. General

The combination of high strength and low density results in exceptionally favourable strength-to-weight ratios for titanium-based alloys. Titanium plays a critical role in weight reduction of highly-stressed parts, especially the fuselages and wings. The most important properties titanium offers are high fatigue strength and fracture toughness. Titanium typically comprises 9% by weight of commercial airframes. This percentage is not forecast to diminish even with increasing use of carbon fibre composites. In fact, usage is increasing steadily, replacing high strength steels and aluminium.

Alloyed with aluminium and vanadium, titanium is used in aircraft for firewalls, outer skin, landing-gear components, hydraulic tubing, and engine supports. The compressor blades, disks, and housing of jet engines are also made of titanium. A commercial jet transport uses between 3500 and 12000 kg of the metal. A supersonic transport uses much more, between 14000 to 45000 kg of titanium. A typical alloy would comprise 90% titanium, 6% aluminium and 4% vanadium, by weight (6AL-4V).

3.1.3.2. Characteristics

The densities of titanium-based alloys range between 4.43 gm/cm^3 and 4.85 gm/cm^3. Yield strengths range from 172 MPa for commercially pure Grade 1, to above 1380 MPa for heat-treated alloys. These properties for titanium based alloys are superior to almost all other metals.

Aircraft grade titanium has a tensile strength of up to approximately 1100 MPa and a Brinell hardness value of approximately 350. Some typical properties of

the titanium alloy (6AL-4V)used in the fasteners are summarised in **Table 3.3.** The advantages of titanium include:

- Low coefficient of linear thermal expansion. Titanium possesses a coefficient of expansion which is significantly less than ferrous alloys. This property also allows titanium to be much more compatible with ceramic or glass materials than most metals.

- Non-magnetic. Titanium is virtually non-magnetic, making it ideal for applications where electro- magnetic interference must be minimized.

- Excellent fire resistance, even at very high temperatures.

Density / Specific Gravity (g/cm^3)	4.43
Melting Point (°C)	Max. 1660
Tensile Strength, Yield (MPa)	880
Tensile Strength, Ultimate (MPa)	950
Modulus of Elasticity (GPa)	113.8
Poisson's Ratio	0.342
Shear Strength (MPa)	550
Hardness, (Brinell)	334
coefficient of linear thermal expansion @ 20°C $\left(\left(\mu m/m\right)/°C\right)$	8.6

Table 3.3 Physical Properties of Titanium 6AL-4V. (MatWeb.com (2002)).

3.2. Typical assembly details

3.2.1. General

The wings of fixed wing aircraft generally consist of spars, ribs, stringers and skin. The spars comprise thin aluminium alloy webs and flanges, the latter being extruded or machined and are bolted or riveted to the web. The ribs are formed and have flanges around their edges to enable them to be fastened to

the skin and spar webs; cut-outs around their edges allow the spanwise stringers access. Holes are cut in the ribs at positions of low stress for lightness and to allow for conduits for control runs, fuel and electrical systems (Buller, 2002).

Wing skins are frequently machined integrally with stringers from solid billets of aluminium alloy, as are the wing ribs. This integral method of construction has the advantage of combining a high grade of surface finish, free from irregularities, with a more efficient use of material since skin thickness can be easily tapered to coincide with the spanwise decrease in bending stresses (Floyd, 1958).

The skin is fastened to the rib flanges and longitudinal stiffeners (butt-strap and stringers). An aerodynamic requirement means that the forward edge of the wing is as smooth as possible to delay transition from laminar to turbulent airflow. This means that the fasteners used are countersunk.

3.2.2. Fasteners and hole preparation

3.2.2.1. Fasteners

Some particular aspects concerning the fasteners and drilled holes, especially in the region of the fuel tanks, are:

- How the holes fasteners are located
- The hole diameter tolerance
- Hole perpendicularity
- Surface roughness of the hole
- Eccentricity of the countersink
- Chamfering of the hole
- The maximum distance between holes
- The material the fasteners are manufactured from
- The preparation of the fasteners before fitting, for example, degreasing, applying lubricant and sealant

- The manner in which the fasteners are tightened which can also affect the integrity of the structure greatly.

There are two main types of bolted joint designs. In one method the bolted joint does not have a designed clamp load but relies on the shear strength of the bolt shaft. This may include clevis linkages, joints that can move, and joints that rely on a locking mechanism (like lock washers, thread adhesives, and lock nuts) but this type of joint did not apply in this project. In the other type of bolted joint, the bolt is tightened to a calculated torque, producing a clamp load. The joint is designed such that the clamp load is never overcome by the forces acting on the joint (and therefore the joined parts see no relative motion). This is the method by which aircraft wings are fabricated and, consequently, the test coupons too.

When a cap screw or bolt is tightened it is stretched, and the parts that are captured are compressed. The result is a spring-like assembly. The outcomes of this type of joint design are:

- Greater preloads in bolted joints reduce the fatigue loading on the bolted components

- As long as the external loads on a joint do not approach the clamping load the bolt and component surfaces remain in contact preventing the bolt coming loose (no locking mechanisms required).

Another important point is the use of proper grip length. Standard design practice is to choose a grip length such that the threads are never in shear.

3.2.2.2. Torque setting

Engineered joints require the torque to be accurately set. The clamp load produced during tightening is about 75% of the fastener's proof load. Over tightening will damage threads and stretch the bolt, impairing the joint's strength.

If the clamped part is plated, or lubricated (or both), the torque can be reduced by 15–25% to achieve the same clamp load. There are specialty coatings that allow for a reduction of 50% in torque (compared to non-plated, non-lubricated hardware) to achieve the designed clamp load.

Unfortunately, torquing the bolt is notoriously inaccurate. Even with a calibrated torque wrench large errors are caused by dirt, surface finish, lubrication, etc. The turn of the nut method is more accurate, but requires additional calculations and tests for each application.

3.2.2.3. Locking methods

There are many locking methods to ensure that the nut does not loosen during use due to vibrations. These range from the use of locknuts, where the principle is to bind or "wedge" the nut thread to the bolt thread, to the "Nylok" pellet, where an undersize ring of Nylon in the nut projects from the threads and when the mating threads engage, compression creates a counterforce that results in locking contact. Alternatively, a variety of shakeproof washers and locking adhesives (for example, Loctite), locking wires, plates and split pins can be used as well. Most of the above require the addition of an extra component to the system which in turn increases the weight and one of the main issues with aircraft design is weight reduction. The deformed-thread locknut (**Fig 3.2**) is the common method used in the aerospace industry and was the method used on the test coupons. Its advantages are:

- The temperature range is limited only by the parent metal, its plating or both
- The nut can be reused a number of times
- The overall weight increase of the nut/bolt assembly is negligible.

Figure 3.2 Deformed thread locknut (NASA, 1990).

3.2.3. Hole preparation

The manner in which the hole for the fastener is formed is critical. As the fasteners are interference fit the holes have to adhere to certain standards to ensure that the diameters, finish and underhead radius of the hole are within the agreed parameters.

The hole is first marked out to the drawing requirements using a soft pencil with, preferably, a template. A pilot drill is used prior to final drilling to size. The hole is then finished with a reamer and its dimensions are checked with a "GoNoGo" gauge. This achieves two things, firstly the reamer ensures that the hole is circular and that the surface finish in the hole complies with the standards required. Secondly, the "GoNoGo" checks that the dimensions are within close tolerances to ensure that the fastener is an interference fit but not so tight as to stress the surrounding material unduly. If the fastener fit in the holes is too loose, the loads will not be spread evenly amongst the fasteners, causing certain fasteners to carry excessive loads. This will eventually damage the fastener and can cause the hole to elongate which in turn can cause cracking to occur.

Figure 3.3 Underhead radius (Modified from NASA. 1990).

Beneath the head of the fastener where the shank meets the head there is a small radius **(Fig.3.3).** This reduces the stress concentration at this point on the fastener. Unfortunately, if the hole is not modified, the hole will be distorted when the fastener is installed and may result in the fastener not seating completely (**Fig. 3.4**). Stress cracks may then occur and a potential leak path instigated. A corner radius has to be machined into the hole to eradicate this (**Fig. 3.5**).

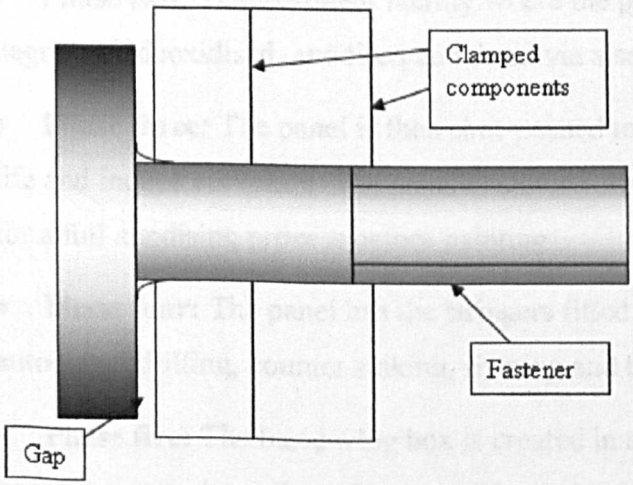

Figure 3.4 Gap caused by underhead radius

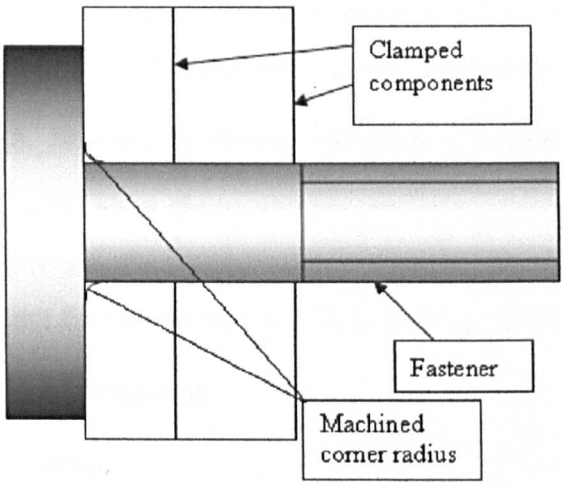

Figure 3.5 With corner radius machined

3.2.4. Machine and assembly operations

To use Airbus structures as an example, there are six main phases in the production of the wing assembly (Birch, 2001):

- **Phase one:** The machining of solid aluminium-alloy billets into skin panels takes place on a long-bed milling machine (41m in length).

- **Phase two:** The treatment facility where the panel is cleaned and degreased, deoxidised, anodised and dried via a series of tanks.

- **Phase three:** The panel is then shot-peened to enhance the panels fatigue life and induce curvature. The panel is then returned to the treatment facility for a full anodising process before painting.

- **Phase four:** The panel has the stringers fitted through a process of automated drilling, counter sinking, riveting and bolting.

- **Phase five:** The basic wing box is created in the assembly jigs. The major components such as ribs and spars are loaded into the wings in a set sequence. The wing skins, with stringers attached, are progressively located and drilled before returning to the jig where all the elements are fitted together.

- **Phase six:** Single aisle wings are fully equipped with control surfaces, electrical, hydraulic and fuel systems. Long range aircraft wings are fitted with leading and trailing edges plus fuel and hydraulic systems.

3.2.5. Surface treatment, priming and sealing operations

The aluminium sheets and components used in the construction of the wing require a surface preparation before they are assembled using the polysulfide sealant for the interfay and fillet sealing (Airbus UK). The basic procedure is:

- Alloy cladding
- Peening
- Pickling
- Anodising
- Painting
- Adhesion primer application
- Sealant application.

Before any of the following are carried out the component is thoroughly cleaned to remove any dirt or grease that is on the surface.

3.2.5.1. Alloy cladding

As mentioned previously, a composite billet is made of the base metal with a coating. As the metal is reduced in thickness by rolling or drawing, the thickness of the base and coating are reduced proportionally. A typical application of this process is the cladding of aluminium alloy with corrosion resistant, but weaker, high purity aluminium.

3.2.5.2. Peening

Fatigue failure results from tension stresses that initiate cracks and cause them to grow. Shot peening is an effective method of increasing stress life because the compressive stresses generated by the peening process must first be overcome before the surface can go into tension. The surface is also slightly hardened and strengthened by work hardening (Campbell, 2001).

Shot peening is a cold working method of improving fatigue resistance by setting up compressive residual stresses in its surface. This is achieved by blasting or impacting the surface of the metal by a torrent of small shots at high velocity. The materials used for the shot can be of a variety of materials, for example, glass, alumina or iron/steel. The sizes range from 0.2mm to 1.4mm, depending on the thickness of the section. The shots produce small indentations on the surface causing a slight plastic flow of the surface of the metal to a depth of a few hundredths of a millimetre. The stretching of the outer surface layer is resisted by the lower layers, which tend to return the outer layer to its original configuration. This produces an outer layer experiencing compressive stress while the lower layers tend to be in tension.

3.2.5.3. Pickling

Pickling is a process of chemical abrasion/etching which prepares surfaces for good paint adhesion. The process involves a system of dip tanks containing a variety of acids ranging from sulphuric, chromic, and nitric acids in different solutions that chemically clean the surface ready for painting or anodising.

3.2.5.4. Anodising

Aluminium and its alloys rely upon the formation of a "self healing", homogenous, transparent oxide film on the surface of the metal to prevent corrosion. The process of anodising artificially builds up a thick, adherent layer of aluminium oxide that is resistant to atmospheric corrosion both for interior and exterior purposes even when subjected to the pollution of urban environments.

The fatigue properties of aluminium alloys can be severely reduced by anodic coatings, generally the thicker the coating the greater the reduction in the metals' fatigue properties. Chromic and sulphuric acid are used to anodise aluminium sheet. Of the two processes, chromic acid gives the thinner coating compared to the sulphuric acid process. Another disadvantage with the sulphuric acid process is that it is unsuitable for use on items containing riveted and lap or folded joints where there is a risk that the electrolyte can be trapped. Consequently, because of these points, chromic acid is the preferred process used in aircraft manufacture. Within Airbus UK, Phosphoric Acid

Anodising (PAA) may be applied as an alternative to chromic acid anodising for specific repairs as a pre-treatment of aluminium alloys for paint application and structural bonding (Airbus UK (1996)).

Components to be anodised are first cleaned and degreased by the use of chemical solvents, after which they are etched, wire brushed or polished depending on the surface texture required. The aluminium is then made an anode of an electrolytic cell and a direct current is passed through it. The electrolyte is a dilute acid selected according to the finish required. Finally, the surface is sealed, using boiling water, to improve the corrosion resistance of the coating and to minimise the absorptive properties.

3.2.5.5. Painting

Painting involves the application of predominantly organic coatings to a work piece for protective and/or decorative purposes. It is applied in various forms, including dry powder, solvent-diluted formulations and water-borne formulations. Various methods of application are used, the most common being spray painting and electrostatic deposition . Spray painting is a process by which paint is placed into a pressurized cup or pot and is atomized into a spray pattern when it is released from the vessel and forced through an orifice.

3.2.5.6. Adhesion primer

Primers are required whenever a sealant does not adhere sufficiently well to a surface. There are two types of primer, a monomolecular film and a film format. The preferred thickness of the primer film is 20 ± 5 microns. Film-forming primers actually form a film across the surface. These primers may be a combination of phenolic resins, epoxy resins, polyester resins, and silanes, in solution prepared at approximately 25% solids content to obtain good wetting and also to lay down a reasonable film thickness. These primers dry within 15 minutes, otherwise the silane will become inactive as a result of moisture in the air. Most sealant manufacturers have several standard primers to cover a wide variety of surfaces.

3.2.5.7. Sealant

For a sealant to be effective in performing its function it must possess some essential characteristics: flexibility and fatigue resistance; physical strength;

chemical and environmental resistance, and; adhesion to all substrates to which the sealant is applied. Sealants are not designed as load bearing materials and so will not contribute to the structural properties of a joint. Any given sealant may be required to resist the passage of heat, light, sound, water, odour, dust, etc. and in this specific application, the passage of aviation fuel. Sealants must also be capable of compensating for any change in size or shape of the gap in the joint to which they are sealing due to thermal gradients, moisture and movement, including vibration and creep.

Materials used for sealing of integral fuel tanks are required to perform under harsh operating conditions. The sealants are exposed to a range of stresses- wide temperature range varying from -50°C to +55°C, fuel tank refuelling and manoeuvre pressures and contaminants such as water. Under these conditions the sealant must provide adequate physical and mechanical properties, as well as adhesion over the service life of the aircraft

The sealant must be able to perform these functions, whilst, at the same time, it must have acceptable appearance, durability, economic production and maintenance cost. **(See Chapter 4, Sealants and sealant testing).**

4 Sealants and sealant testing

This chapter considers the geometrical and material considerations that govern a typical sealed joint in a wingbox integral fuel tank. The purpose of the review is to arrive at the requirements for a test procedure that is realistic.

4.1. Introduction

One definition of a sealant is "A material that isolates one environment from another". For a sealant to be effective in performing its function it must possess some essential characteristics: flexibility and fatigue resistance; physical strength, chemical and environmental resistance, and adhesion to all substrates to which the sealant is applied. Of these characteristics, adhesion is most important as a material will lose its ability to "Seal" the moment that adhesion is lost. There is no such thing as the "Perfect Sealant" since no one sealant can possess all of the desirable properties for all applications.

Aircraft manufacturers currently use polysulfide based sealants which are resistant to aviation fuels and are therefore useful for sealing fuel tanks. The principal application areas are shown in a typical skin butt-strap joint in **Figure 4.1**

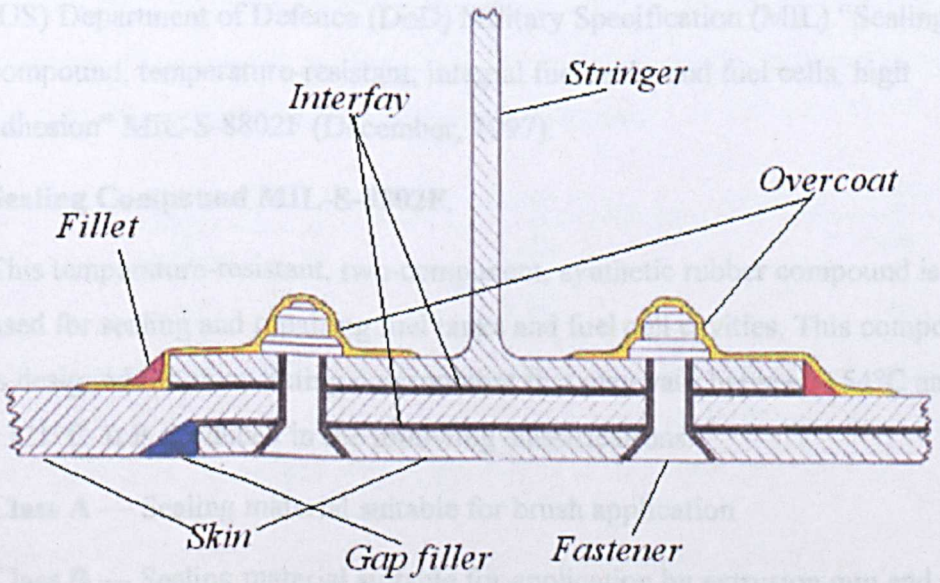

Figure 4.1 Sealant application used in aircraft integral fuel tanks (Taylor, (2004))

• **Interfay Sealing** – Sealing is applied by applying sealant thinly to the whole surface area of both faces of the parts to be assembled. Nominal thickness of the sealant is 0.2mm.

• **Joint Edge Sealing** – The sealant is applied as a fillet bead etc.

• **Overcoat** – A layer of sealant is applied over rivet or bolt heads and nuts etc.

Sealant selection and the joint design must be developed in unison. In selecting the proper sealant for a specific application, consideration must be given to such characteristics as modulus, cure time, application parameters, adhesion, weatherability, chemical resistance and suitability of the sealant to "seal" the chosen sealed medium (gas, fluid etc.).

The sealants utilised in integral fuel tanks must attain certain specifications and standards. The general specifications of all sealants used in Airbus aircraft are listed in Airbus Industrie Material Specification (AIMS) 04-05-000 (November, 1995), with the specific specifications for sealants used in fuel tanks in AIMS 04-05-002 (September, 2000). Some of the Airbus Industrie Test Methods (AITMs) and the International Standards Organisation (ISO) tests that the sealant has to pass at various stages are listed in **Appendix 2.**

These standards are very similar to the requirements defined in United States (US) Department of Defence (DoD) Military Specification (MIL) "Sealing compound, temperature-resistant, integral fuel tanks and fuel cells, high adhesion" MIL-S-8802F (December, 1997).

Sealing Compound MIL-S-8802F.

This temperature-resistant, two-component, synthetic rubber compound is used for sealing and repairing fuel tanks and fuel cell cavities. This compound is designed for an operating environment that may vary between –54°C and +121°C. It is produced in the following classifications:

Class A — Sealing material suitable for brush application

Class B — Sealing material suitable for application by extrusion gun and spatula

Class C — Sealing material suitable for faying surface sealing

4.2. Basics of sealant joint design

The design of a sealing system involves more than merely choosing a material with the right physical and chemical properties. The following considerations are also essential to obtain optimal joint performance:

- Joint design
- Type and nature of the substrates
- Application, curing, and performance characteristics of the sealant.

The calculated movement in the joint will primarily determine the selection of the joint configuration and its geometry. The sealant and joint design must be able to accommodate all expected movements of the joint under all expected service conditions. The following factors must be considered:

- The anticipated temperature and humidity at the time of forming the joint
- Any additional joint opening that will occur during the process of applying and curing the sealant
- The extremes of expected service temperatures.

4.2.1. Common lap joints

Various lap joint designs are shown in **Figure 4.2.** Lap joints can be sealed effectively by sandwich sealing where the sealant is applied between mating surfaces that are secured with mechanical fasteners.

(a) (b) (c)

Sealant sandwiched between plates and bolted, riveted or spot welded (a). Sealed with a bead (b). Tape can be used if there is enough overlap (c).

Figure 4.2 Various lap joint configurations (Thompson, (1990))

Some sealant materials are capable of being welded through with spot welding equipment to achieve mechanical fastening. These were developed primarily for the automobile industry where the sound deadening

characteristics of an elastomeric sealant were desired, but the production time meant that there was inadequate time for the sealant to cure. Thus, by spot welding through the sealant, the substrates could be held together while the sealant set. Lap joints can also be sealed by applying a bead of sealant to the edges of a joint.

4.2.2. Seam joints

Figure 4.3 shows various seam joint designs where the substrates cannot be overlapped. Seam joints that are applied to hold in a fluid, such as on storage tanks, should be sealed from the inside so that the seal is augmented by the fluid pressure. Outside sealants are not recommended because the force of the fluid pressure will be working to cleave the sealant from the substrate.

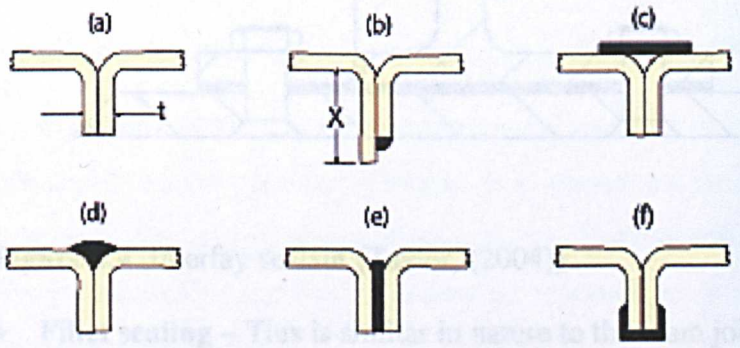

Figure 4.3 Various seam sealing joints. Edge (a) is not thick enough to support bead. Lap joint (b) provides receptacle for sealant. Seams can be insider sealed by tape (c), putty (d), or sandwich sealed with putty or anaerobic (e), tape can also be used on the outside of seam (f). (Thompson, (1990))

4.2.3. Sealant joints used in aircraft integral fuel tanks

Figure 4.1 shows the common types of joint used in fuel tanks. There are, however, a couple of other types and methods that are not featured in **Section 4.2.** These are:

- **Interfay sealing** - The method of sealing faying surfaces is the same as the old wood ships using pine tar between planks (mating surfaces) so that there were no leaks. Also it kept the water from being trapped between structure and rotting (corroding) the wood at the faying (contacting) surfaces.

When a jointing compound has not been deployed in the assembly, fretting can result. Fretting corrosion refers to corrosion damage at the contact surfaces.

Damage can occur at the interface of two highly loaded surfaces which are not designed to move against each other **(Fig.4.4).** The most common type of fretting is caused by vibration. The protective film on the metal surfaces is removed by the rubbing action and exposes fresh, active metal to the corrosive action of the atmosphere.

Interestingly, the concept of using interfay sealant in aircraft construction was driven in the first instance by the need to address fretting and corrosion issues as opposed to achieving fluid sealing. Unfortunately, bare aluminium 2024 can corrode in hours.

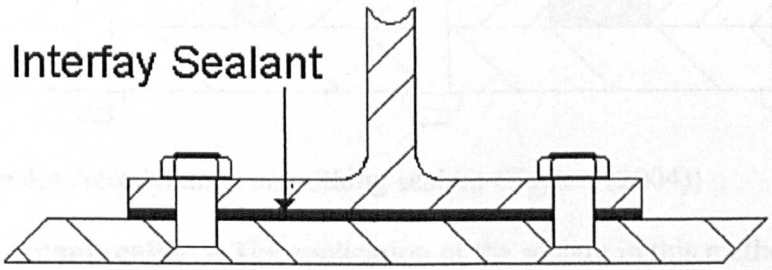

Figure 4.4 Interfay sealant (Taylor, (2004))

- **Fillet sealing** – This is similar in nature to the seam joint **(Section 4.2.2).**

When the components are assembled using interfay sealant, there may be areas where the sealant has been displaced by the pressure exerted by the fasteners. To augment the interfay sealant a fillet sealant is applied to the edge of the joint. In the integral fuel tank this may be the primary sealant and when repairs to fuel tank leaks are carried out this is how the sealant is usually applied **(Fig 4.5).**

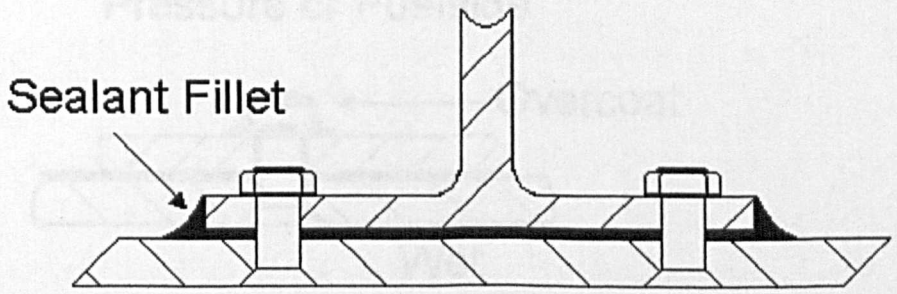

Figure 4.5 Fillet sealant (Taylor, (2004))

- **Aerodynamic smoothing sealant** – This is used to keep the surface of the aircraft smooth and streamlined **(Fig. 4.6).** If the surface of the aircraft, especially near the leading edge of the wings, can be kept as streamlined as possible the transition from laminar to turbulent airflow can be delayed. This in turn reduces the frictional drag experienced by the aircraft (see **Section 2.1.4. Aerodynamic principles).**

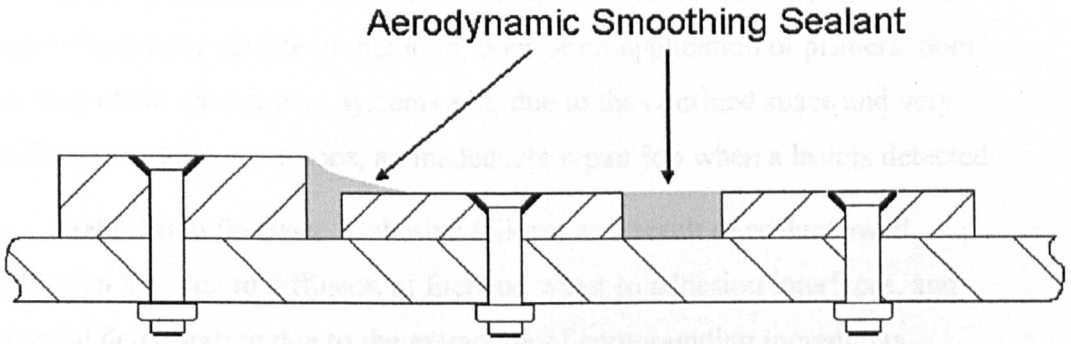

Figure 4.6 Aerodynamic smoothing sealant (Taylor, (2004))

- **Overcoat sealing** – The application of the sealant in this method can be compared to applying paint. The part to be sealed is cleaned and a **Class A** type sealant is applied with a brush to the component, usually a fastener, to ensure that fluids cannot migrate down the threads or along any small surface imperfections present.

- **Wet assembly** – When one end of a fastener or rivet is to come into contact with the sealed medium (fuel), the fasteners or rivet is assembled using the wet sealant(i.e. prior to cure). This ensures that the sealant will fill any imperfections along the fastener length, thread or under the head thus stopping the fuel from finding a leak path **(Fig.4.7).**

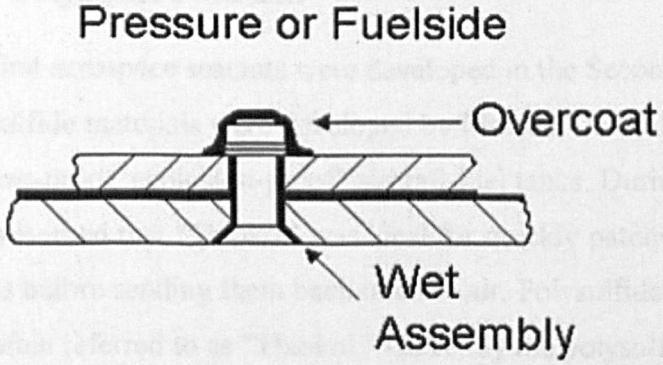

Figure 4.7 Overcoat and wet assembly sealant (Taylor, (2004))

4.2.4. Causes of sealant failure in integral fuel tanks

It can be appreciated that the adhesive and cohesive properties of aircraft sealant /primer systems and the surfaces to be sealed are influenced by factors such as temperature, fuel contamination and fatigue cycling. The principal causes of failure can be summarised as (Hutchinson, 2000):

- **Application related failures**. Although difficult to identify, failures can result from poor surface preparation, poor or no application of primers, poor mixing of two component systems and, due to the confined space and very difficult working conditions, an inadequate repair job when a leak is detected.

- **Fuel related failures**. Cohesive failures as a result of sealant swell, adhesion loss due to diffusion of fuel and water to adhesion interfaces, and general deterioration due to the extraction of compounding ingredients (resulting in hardening) and biodegradation (often leading to softening).

- **Temperature related failures**. At very low temperatures the sealant may stiffen, leading to cracking or loss of adhesion. At very high temperatures, degradation of the sealing system may result in an initial softening and eventual hardening of the sealant.

- **Fatigue related failures**. The joints in fuel tanks are subjected to high and low frequency movements. How the sealing system responds to such movements will depend on the materials and the joint design. High frequency flexing for example will lead to flex cracking. Low frequency movements resulting from the differential expansion and contraction of sealing system and substrates impose stresses, which can lead to loss of adhesion and/or tearing.

4.3. Polysulfide sealant

The first aerospace sealants were developed in the Second World War. These polysulfide materials were developed by Morton Thiokol for the manufacture of "leak-proof, explosion-proof" aircraft fuel tanks. During the war, aircraft crews learned that "Thiokol" was ideal for quickly patching bullet holes in planes before sending them back into the air. Polysulfide adhesive sealant is still often referred to as "Thiokol." Currently the polysulfide polymers used in

all polysulfide adhesive sealants are manufactured in Germany, Japan and the Russian Federation (Lee, 1999).

The first aerospace sealants were two- part products based on liquid polysulfide (LP's) polymer cured with lead peroxide. During the 1950's dichromate-cured sealants were used and the late 1960's saw the introduction of manganese-cured sealants. The latest developments have been in epoxy-cured polythioether sealants, which came on the market in the late 1980's.

The Thiokol –based sealants used in aerospace applications are still mainly two component systems which, on mixing, cure by chemical reaction. Basically, the polysulfide polymer in the base component reacts with an oxidising agent (for example manganese dioxide) in the curative component. Sometimes the two components are pre-mixed and then stored at very low temperature to stop the reaction. Only at the time of application is the mixed sealant brought to room temperature, applied to the joint, with the cure commencing simultaneously. The sealant will cure within a few hours, but the sealant's full physical properties may take several days to develop.

Polysulfides will adhere to metal, glass, fibreglass, wood, or any combination of these. The polysulfides are not resistant to high temperatures, but are all impervious to fuel and solvent deterioration. This makes them suitable for refrigeration equipment, fuel tanks, and fuel systems.

4.3.1. Advantages and disadvantages of polysulfide sealants

Some of the key properties in the cured, polysulfide sealant, are listed below.

Advantages:

- Good resistance to swell in aviation fuels
- Fair resistance to hydraulic fluids
- Good adhesion (in tension, sheer and peel) to aluminium, anodised aluminium, titanium, other metals and composites (primers and surface treatments may be used for optimum adhesion and durability of adhesion)
- Low permeation to fuel vapour, water vapour and air (good barrier properties)

- Good low temperature flexibility (-50°C and lower)
- Good heat resistance (100°C continuous, 150°C intermittent for manganese dioxide cure)
- Good elasticity, reasonable strength (in the presence of fuels), good resilience
- Good adhesion of new sealant to old sealant (i.e. in repair)
- Good application properties, rheology control (gunnability, toolability)

Limitations:

- Water and antifreeze absorption, leading to swell and a drop in properties, in particular, tear resistance
- Absorption of water and antifreeze weakens adhesion
- Attack by mercaptans in the fuel leads to reversion of the sealant (severe softening)
- Attack by bacteria leads to reversion
- High Specific Gravity (SG).

4.3.2. Structure of aliphatic polysulfide polymers

Polysulfide liquid polymers are easily made. The typical reaction is designated as follows (Panek and Cook (1991)):

$$n ClC_2H_4OCH_2O\ C_2H_4Cl + nNa_2S_{2.25} \longrightarrow$$

$$HS\ (C_2H_4OCH_2OC_2\ H_4SS_{2.25})\ n \text{ —— } C_2H_4OCH_2O\ C_2H_4SH + nNaCl$$

Dichloroethylformal is added to a solution of sodium polysulfide plus emulsifying agents, and a high molecular weight polysulfide latex is formed. After the latex is washed, splitting salts of sodium sulfhydrate and sodium sulfite are added to reduce the molecular weight and make the liquid polymers. The mixture is then acidified, coagulated, and washed clean. The amount of sodium sulfhydrate determines the final molecular weight of the polymer. The number of repeating units (in the polymer structure above) indicates the molecular weight of the polymer. The use of small amounts of the cross-linking agent trichloropropane added during manufacture introduces

trifunctionality, which is desired to improve compression set resistance. The level of cross-linking agent also determines the modulus and other elastomeric characterisations of the cured sealant.

The cure mechanism is the oxidisation of the mercaptan groups (-SH) using a metallic salt as follows:

$$2HSRSH + MO_2 \longrightarrow RSSR + H_2O + MO$$

The type of oxide or dioxide used in the cure mechanism greatly affects the final properties. The use of various inorganic chromates gives cured sealants with greater heat resistance, better resistance to jet fuel, better compression set resistance, and very little heat ageing weight loss when compared to lead dioxide. For these reasons chromates became the standard curing agents for fuel tank sealants. In more recent times, they have been largely replaced by manganese dioxide, following concerns over the toxic nature of chromate.

4.3.3. Compounding for fuel resistance

Aircraft sealants using either the manganese or the chromate cure and carbon black for reinforcement produce tough sealants with excellent physical properties, higher hardness, good recovery, and a high resistance to jet fuel at 180° C (Lee, (1999)).

Base Component

- **Polymer** 55% - 65% by weight for optimum fuel and chemical resistance and low temperature flexibility
- **Fillers** (e.g. calcium carbonate, carbon black,), for reinforcement (tear resistance, tensile strength), modulus control, rheology.
- **Plasticisers** (e.g. phthalate esters), for control of modulus, rheology
- **Adhesion Promoters** (e.g. phenolic resins, silanes), polysulfide polymers have no inherent adhesion capability
- **Thixotropes** (e.g. silicas, castor oil derivatives), for control of gunnability and slump
- **Solvents** (e.g. MEK, toluene), viscosity control, brushability, sprayability
- **Pigments** (e.g. metal oxides, carbon black)

Cure Paste

- **Oxidising agent** (dichromates, peroxides, hydroperoxides). Manganese dioxide gives a good balance of open time, cure rate, and cured properties (elasticity, heat resistance).

- **Accelerator** (TMTD, TMG) - to control open time and cure rate. (Sometimes put into the base component)

- **Plasticiser** (phthalate esters) as a dispersion medium for the inorganic oxide curing agent

It's important to note that because the reaction between polysulfide (organic) and the oxidising agent (inorganic) is heterogeneous, it is necessary to use an excess of the curative in order to facilitate a fast and complete conversion of the mercaptan groups.

This means that a precise ratio of base compound to cure paste is not essential (i.e. there is some 'forgiveness' or latitude in the mix ratio. This is not the case for wholly organic systems, where it is essential to use the precise mix ratio. e.g. polyurethanes). The presence of curing agent residues in the cured sealant encourages water absorption which can be a problem (Lee, (1999)).

4.3.4. Typical properties

Liquid polysulfide sealants posses viscosities ranging from 2 to 1800 Pa.s (Pascal second) at 25°C (Mayer, (1992)) depending on the type, for example:

Sprayable application = 2 - 15 Pa.s

Class A (Brush application) = **10 – 40 Pa.s**

Class C (Sealing material suitable for faying surface sealing) =**100 – 150 Pa.s**

Class B (Application by extrusion gun and spatula) = **600 – 1800 Pa.s**

Class B sealant needs to be extruded relatively easily but must also be able to hang from a vertical or overhead substrate without sagging.

The glass transition temperature (T_g) ranges from -20°C to around -59°C whilst the upper service temperature can be as high as 177°C (Meyer, 1992).

Polysulfide sealants for aircraft use possess a Shore A hardness of 40 whilst the tensile strength is in the region of 1.5 MPa (Chemetall, (1995))

4.4. Current test procedures for evaluating sealants

4.4.1. Introduction

There are several reasons for testing sealants, these include:

- Obtaining information on cured performance, both short and long term
- Comparing or checking (quality control) the mechanical properties of a batch of sealants
- Comparing or checking substrate surface preparations
- Evaluating durability of a sealed system.

Sealant testing can be categorised as:

- Bulk specimen tests
- Sealant joint tests

Several factors can increase or reduce the performance of a bulk sample or test joint. For meaningful comparisons to be made of the test results there are important conditions that have to be met during the fabrication, cure and subsequent testing of the samples.

The parameters that can affect the performance of a bulk specimen or test joint include:

- Temperature
- Relative humidity
- The substrate used
- The thickness of the substrate
- The conditioning of the adherend surface, for example, as received, solvent wipe, gentle abrasion, heavy abrasion, bead blast, "Scotch Brite" etc.
- Test speed
- Specimen geometry

4.4.2. Bulk specimen tests

The bulk specimen tests are performed on the sealant material itself. The sealant is formed and cured in a mould in specific shapes and sizes. These are usually dumb-bell specimens, different sizes of prisms and various other sizes and shapes of moulded specimens.

The dumb-bell allows the determination of:

- tensile strength
- tensile modulus
- strain to failure.

The large prism allows the determination of:

- flexural strength
- flexural modulus
- creep (time dependent deformation).

From the smaller prisms Dynamic Mechanical Thermal Analysis (DMTA) tests can be performed from which the glass transition temperature (T_g) and Young's Modulus (E) can be established.

The various sizes of moulded sealant specimens allow the determination of:

- shrinkage
- water uptake
- colour retention
- weight loss
- hardness.

4.4.3. Sealant joint tests

There are several types of test available for establishing the mechanical properties of a sealant in a joint. The tests evaluate the mechanical and adhesion properties of the sealant to whatever the substrate and the surface treatment/preparation are. Consequently, it is important that the locus of failure is recorded and that the mechanism of the failure is understood.

At present the test procedures for evaluating seals and sealants are found in AITM (Airbus Industrie Test Method) and ISO (International Organization for Standardization) standards which evaluate shear strength, peel strength and physical properties such as shrinkage and slump. These procedures are summarised in **Appendix 3. Table 4.1** provides a summary of the methods, test parameters and data that can be obtained.

It should be recognised, however, that there are limitations as to how the results of these tests are interpreted. Variations in the specimens' fabrication and the tests themselves are operator-dependent, so there are bound to be variations in the test results even within a batch of test pieces made at the same time by the same operator. For example, if there are voids present in a dumbbell or prism specimen, or the specimen is damaged in some way, the tensile strength and strain to failure will not necessarily be consistent within a batch of specimens or with published data. Another important factor is the specimen geometry. To get consistent results, all of the test specimens, especially in the case of the dumbbells, need to have the same dimensions and also the optimum shape to reduce stress concentrations in the specimen (see BS 903 /ISO 37, Physical Testing of Rubber). Regardless of this, and other limitations, a lot of useful information can be obtained about *materials* from these tests. However, the performance of a *realistic joint system* can only be evaluated in the more elaborate test procedures described in **Sections 4.5** and **4.6**

Capability requirement	lap shear	linear de-bonding (Peel)	Dumb-bell test (ISO 37)	H-section adhesion test	Dynamic Mechanical Thermal Analysis (DMTA)	Full-size wingbox (Duke(2002))	QinetiQ Model Fuel Tank (Duke(2002))	OBU Model Sealed System (MSS)
Axial/flexural Loading	no	no	no	yes	yes	yes	yes	yes
Shear Loading	yes	yes	yes	no	yes	yes	yes	yes
Peel Loading	yes	yes	no	yes	no	no	no	no
Torsional Loading	no	no	no	maybe	yes	yes	yes	maybe
Fuel Exposure	yes	yes	yes	yes	yes	yes	yes	yes
Pressurisation	no	no	no	no	no	yes	yes	yes
Differential pressure across test specimen	no	no	no	no	no	no	no	yes
Temperature cycling	yes	yes	yes	yes	yes	yes	yes	yes
Differential temperature across skin boundary	no	no	no	no	no	yes	yes	yes
Fuel leak path across fuel/tank boundary	no	no	no	no	no	yes	yes	yes
Combined seal with rivets	no	no	no	no	no	yes	yes	yes
Safety Index, 1-5 (1=adaequate,5 =not adequate)	1	1	1	1	1	5	4	3
Relative cost	low	low	low	low	low	high	medium-high	medium-low

Table 4.1. Comparison of sealant joint tests against full size wing box and the MSS

4.5. Full size wing-box

The US Air Force Material Laboratories, Wright-Patterson, supported the construction of full-size integral fuel tanks in the qualification of a sealing system to be employed on a specific acquisition programme in the late 1970's. An illustration of the structural item with respect to the Hercules C-130 transport aircraft is shown in **Figure 4.8.**

The proposal covered the utilisation of the full-scale, structural, fatigue test item (an aircraft wing), which is mandatory for airworthiness requirements. Airworthiness certification is concerned with applying cyclic loads, representative of the aircraft's flight envelope, to the structural test item. The testing is conducted dry (without fuel) at temperatures that prevail in the test hall.

The principle proposed by Richardson(1989) was to conduct the structural fatigue test with the addition of fuel, subject to pressure and temperature cycles representative of actual flight conditions.

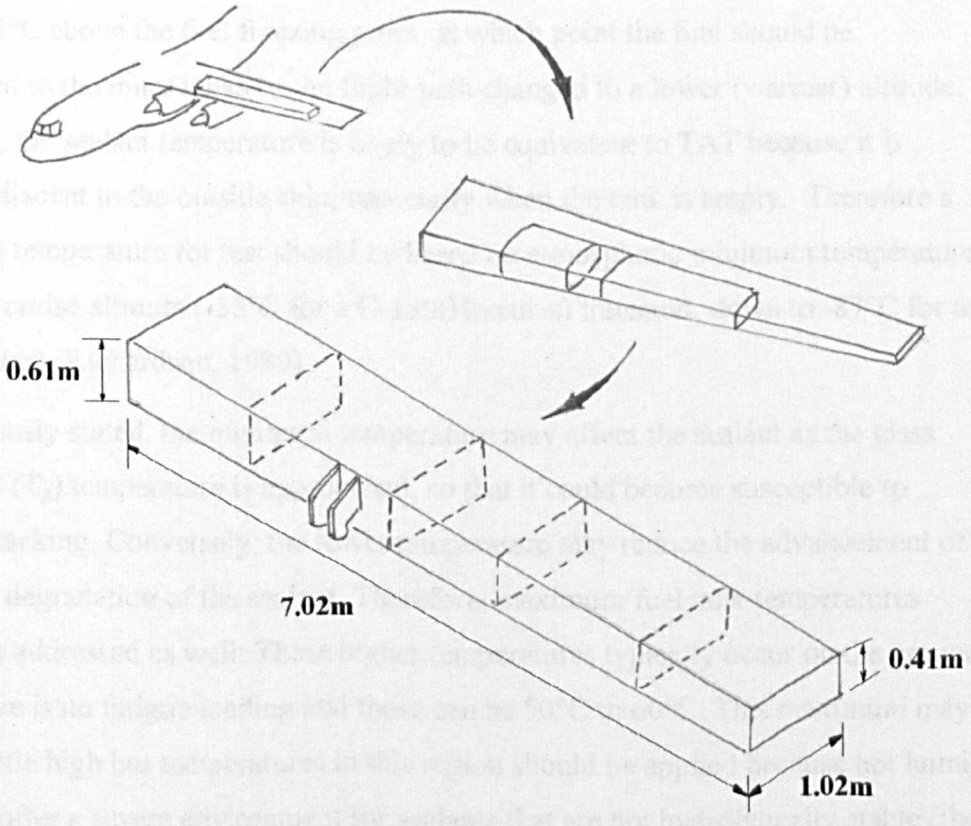

Figure 4.8 Full-size wing-box based on the C-130 incorporating five integral fuel tank bays (Richardson, 1989)

Richardson hypothesised that the best way to achieve spectrum shortening was by omission of low load range cycles. This meant that the test programme was to exclude load cycles producing stress changes below certain values and to also exclude load cycles thought not to have a detrimental effect on the fuel tank sealing integrity.

Peak load (gust peaks, heavy landings etc.) truncation was not recommended because peak loads can give rise to higher crack growth rates. Peak load truncation would also avoid those loads most likely to cause excessive deflection of bolted joints. These peak load cycles are the most likely to be detrimental to fuel tank integrity. A suitable method for low load omission is given in the paper (Richardson, 1989).

For an aircraft wing fuel tank, the temperature of the fuel begins to drop as soon as the aircraft takes-off and climbs to high altitudes. If the duration of the flight is sufficient for the outside temperature to completely 'soak' the fuel in the tank, then the temperature will eventually become equivalent to the Total Air Temperature (TAT).

Typical freezing points of aviation fuel are approximately -40°C for Jet A and -47°C for Jet A-1 (Chevron fuels, 2000). There are procedures in place whereby a warning is given at 5°C above the fuel freezing point, at which point the fuel should be transferred to the inner tanks or the flight path changed to a lower (warmer) altitude. However, the sealant temperature is likely to be equivalent to TAT because it is usually adjacent to the outside skin, especially when the tank is empty. Therefore a minimum temperature for test should be based on atmospheric minimum temperatures at design cruise altitude (-55°C for a C-130(Hercules) transport, down to -87°C for an F-16 fighter) (Richardson, 1989).

As previously stated, the minimum temperature may affect the sealant as the glass transition (T_g) temperature is approached, so that it could become susceptible to fatigue cracking. Conversely, the lower temperature may reduce the advancement of chemical degradation of the sealant. Therefore, maximum fuel tank temperatures should be addressed as well. These higher temperatures typically occur on the ground when there is no fatigue loading and these can be 50°C to 60°C. This maximum may seem a little high but temperatures in this region should be applied because hot humid climates offer a severe environment for sealants that are not hydrolytically stable (the decomposition of a chemical compound by reaction with water) (Meyer (1982)).

When compiling the test programme for the full scale fatigue test, Richardson (1989) found that:

- Sealant deterioration is predictable by the Arrhenius Law
- Significant sealant degradation does not occur below 120°F(48.9°C)
- Significant sealant degradation does not occur at sub-zero temperatures
- Humidity effects can be simulated by the addition of free water in the test tank
- Cyclic exposure is necessary to simulate aircraft usage conditions.

Consequently, the in-flight temperature data from a C-130 was reduced to a programme that could be applied in a short period of time, using the Arrhenius Law to convert time-temperature exposures to a shorter exposure at a different temperature to produce an equivalent sealant degradation.

A pressure spectrum was developed along with the temperature programme that simulated high manoeuvring loads above 1G.

Actual aircraft usage consists of ground time followed by flight time, with refuelling between each. To simulate actual aircraft usage the test spectrum is divided into six test cycles with fuel changes every five days.

This was the proposed environmental exposure programme for the full size fatigue test:

- 24 hours at -54°C with fuel
- 112 hours at 60°C fuel changed after exposure
- 24 hours at -54°C with fuel
- 21 hours at 48.9°C with fuel
- 6 hours at 60°C with fuel
- 15 hours at 60°C with ¼ full of fuel
- 8.3 hours at 71°C with ¼ full of fuel
- Humidity was regulated at 10gms of water/ ft^3 of tank volume.

This test cycle was repeated six times per 40,000 equivalent flight hours. One cycle takes 210.3 hours and therefore six will take 1261.8 hours (52.6days).

Full-scale dynamic and environmental testing of a fuel tank/aircraft wing filled with fuel requires a dedicated housing, a structural test framework, special enclosures for the heating and cooling system, a pressurisation system and a system of actuators to simulate the flight loads. The full-scale structure is cyclically loaded to a flight spectrum and the sealant material is fatigued with respect to actual service conditions. The approach carries an enormous cost penalty and there are considerable safety issues, which require special engineering solutions.

4.6. Modular wingbox or "Puffer Box"

A modular wingbox or "puffer box" is a small-scale integral wing tank (size varies but they are usually about 2.5 x 2.5 x 1 m). They are built exactly like the full-scale wing: with skin, interfay, sealed stringers, ribs and sealed fasteners. When assembled the structure is filled with fuel. It is then exposed to various thermal and pressure cycles, and, sometimes, physical loading. They are, needless to say, very expensive (costing around £150,000 to make and approximately £8,000 every time it is used due to the stripping down and resealing involved) and time consuming tests to conduct (Duke, 2002). By their very nature of construction they are generally only built by airframe OEM's (Original Equipment Manufacturers) and the air force (**Fig. 4.9**).

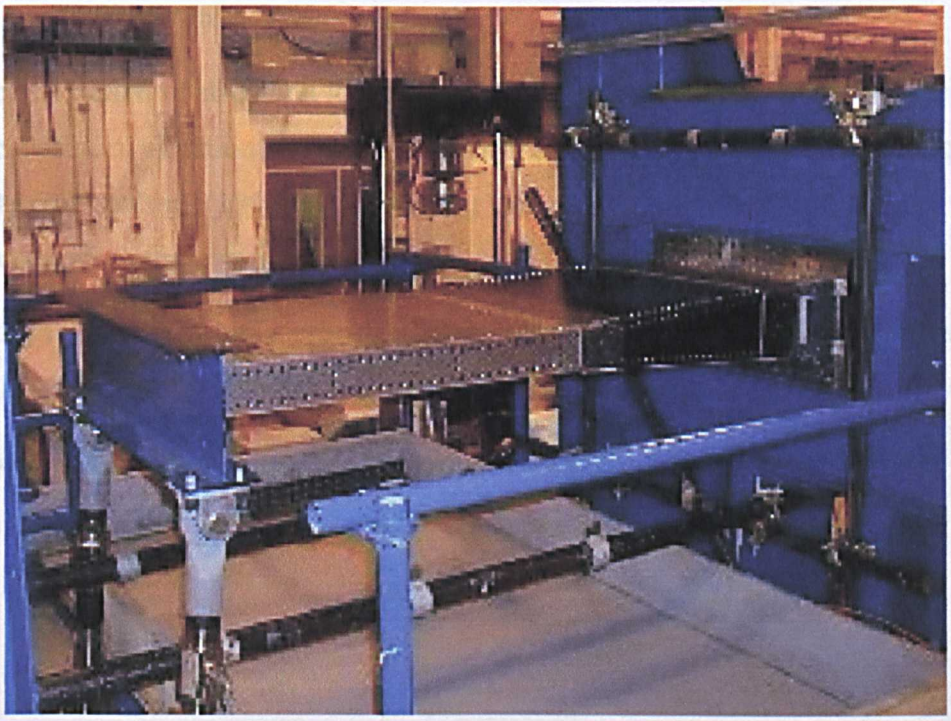

Figure 4.9 QinetiQ's Model Fuel Tank (based on modular wingbox)(Duke, (2002)).

4.7. Summary of overall requirements for testing seals for integral fuel tanks

Fuel leaks from aircraft integral tanks incur high costs due to the maintenance required to repair the leak and the reduction in aircraft availability. It is noteworthy that existing leak problems could be avoided if structural testing to certify fuel tank integrity had been performed in the development phase of the aircraft design. Particular aspects to be incorporated into a new approach to testing are that:

- Fuel tank testing must be done using realistic combinations of both flight loading and other environmental factors such as temperature, humidity and pressure.
- Test procedures should reflect realistic joint geometries, combinations of materials and assembly techniques. An ideal test set-up should allow different combinations of variables (materials, primers, sealants, fasteners) to be evaluated.
- The aging of the sealant systems as a result of chemical interaction with hydrocarbon fuels must be duplicated during testing to provide valid performance information during the expected service life of the fuel tank.
- This aging can only be accomplished by combining environmental exposures with the use of actual fuel in the test structure.
- A combination of structural loading, fuel inertia, fuel tank pressures, thermal and chemical effects, vibration and altitude all have detrimental influences on the fuel tank integrity (Richardson, (1989)). An ideal test procedure should therefore try to incorporate all of these variables.
- A dry cycle should be incorporated in the test because allowing any sealant to dry out causes shrinking and possible cracking (Healey, (1996))
- The procedure should be cost effective and safe.

5 Test coupon configuration

5.1. Analysis of stress in wings

The loading for the coupon test is based on a lower wing skin butt-strap joint for a typical Airbus single aisle aircraft. The primary purpose of the butt-strap is to join the skin panels. This part of the structure has had in-service fuel leak problems and has reasonably straightforward loading conditions. The two butt-strap joints on the lower wing skin form the joints between panels 1 and 2 at stringer 8 and between panels 2 and 3 at stringer 11 from rib 1 outboard to rib 20. Panel 2 contains the manholes for maintenance access to the wing-box (**Fig. 5.1**). A cross section of the typical structure of the butt-strap joint is shown in **Figure 5.2.**

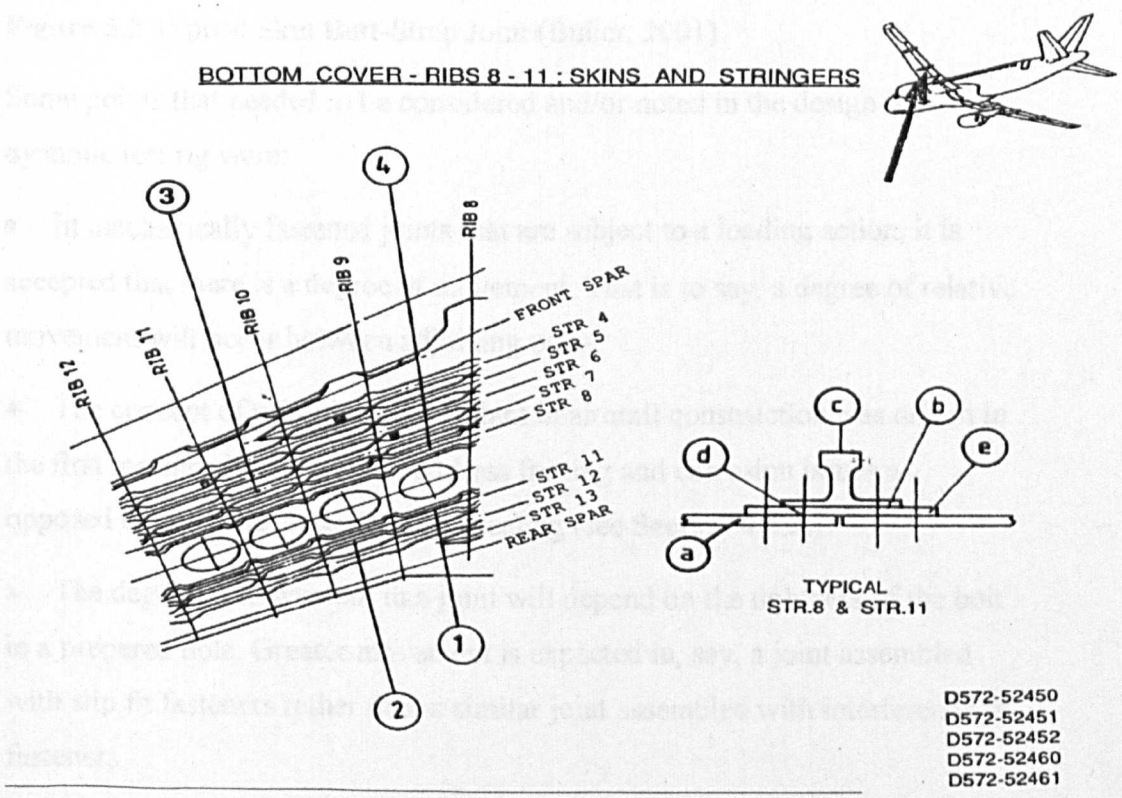

Figure 5.1 The location and detail of the lower wing skin butt-strap joint.

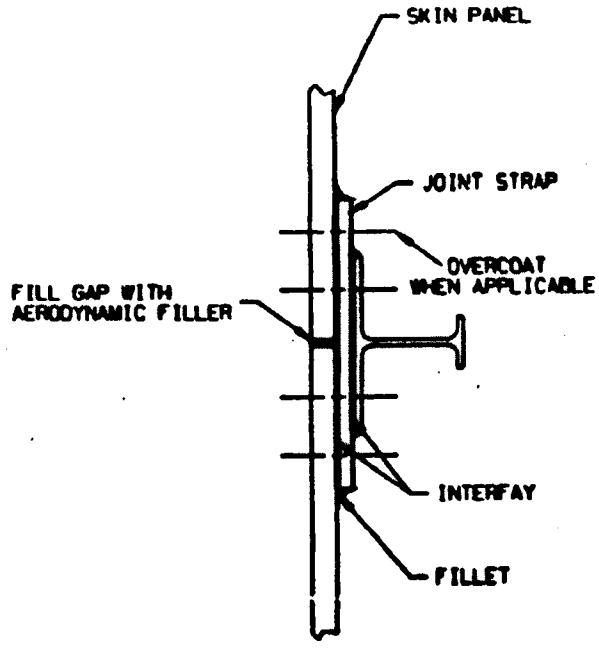

Figure 5.2 Typical Skin Butt-Strap Joint (Buller, 2001)

Some points that needed to be considered and/or noted in the design of a dynamic test rig were:

- In mechanically fastened joints that are subject to a loading action, it is accepted that there is a degree of movement. That is to say, a degree of relative movement will occur between adjoining parts.

- The concept of using interfay sealant in aircraft construction was driven in the first instance by the need to address fretting and corrosion issues as opposed to the achievement of fluid sealing (see **Section 4.2.3.**).

- The degree of movement in a joint will depend on the tightness of the bolt in a prepared hole. Greater movement is expected in, say, a joint assembled with slip fit fasteners rather than a similar joint assembled with interference fit fasteners.

- When a test joint is fitted into the test rig, a loading condition that provides similar movement (within the joint) to that experienced in joints on the aircraft should be applied.

5.2. Requirements of the model fuel tank

The main parameters were identified, discussed and agreed with the METEOR project team partners during the first year of this research project. They are listed below:

1. Aerostructure is designed to achieve a service life goal of 48 000 cycles but Airbus verify fatigue life to twice this figure i.e. 96 000 cycles.

2. A typical frequency range for load cycles is 1-5 Hz.

3. The peak stress occurs on the lower skin and is approximately 116 MPa. This is arrived at by:

- 1g Flight Stress: 46.4 MPa
- 30 foot per second (fps) Gust Stress: 69.6 MPa

Hence the stresses on the skin joints are: -

46.4 MPa ± 69.6 MPa = 116 MPa and –23.2 MPa.

4. Peak stresses occur:

- At take-off, due to downward bending.
- During a hard landing, i.e. on wet runway to avoid aquaplaning.
- And from upgusts or severe manoeuvres during flight.

5. A cyclic load should be applied to move the test piece both upwards and downwards with respect to the equilibrium position. A torsional load may be an option on the proposed test rig.

6. Factors/spectrum:

- Temperature -55° to +55°C.
- Pressure / synchronised with peak manoeuvre loads, based on hydrostatic pressure, possibly causes advancement of leak path tip.
- There should be no over-pressuring during refuelling.
- Fuel / refuelling typically occur once per flight, and the sealant probably remains immersed.
- Fuel tank drying during maintenance and repairs could be detrimental.

7. Cleaned and dried out fuel tanks tend to leak when fuel is re-introduced after prolonged lay-up or after repair. Wet/ dry cycling will therefore be investigated.

8. Fasteners should be included in order to prevent excessive strain in the joints, given that the actual strain level encountered by a real aerospace joint is very low. It was decided that ASNA 2027- 3 (3/16 inch diameter fasteners) should be used.

9. The aluminium alloy sheet should be 3-5 mm thick 2024 composition.

10. The pressures involved were around 3 psi (0.206 bar) to 5 psi (0.345bar). This may have to be increased to 35psi (2.41 bar) at a later stage to account for fuel inertia loads during flight manoeuvres.

11. The fluid involved should initially be water. Later testing should utilise non-flammable simulants or synthetic fuels but it must not be forgotten that the chemical effects upon the sealant systems being tested as a result of exposure to actual jet fuel is important.

12. Other fluids that come in contact with the sealants are de-icing fluid, water, various hydraulic fluids

13. Another factor is microbiological contamination.

14. Chemetall MC238B2 will be the reference sealant for all applications i.e. fillet, overcoat and interfay.

5.3. Early concept test rigs

5.3.1. Introduction

The aim of this project was to create a readily usable dynamic test procedure that can be easily run, accurately simulate real world dynamics and environmental conditioning, and provide reproducible results to qualify sealants in a more realistic manner than current testing methods allow.

To achieve this several concept ideas were drawn up, investigated and after discussion amongst the project partners a shortlist of viable concepts was investigated further. The following sections describe them briefly. The concept

that was eventually decided upon was "The Rivet Fastener (interference fit fastener) and Pressurised Tube" (**Section 5.3.4**.).

5.3.2. Box beam rig

The box beam sample is supported rigidly to the test frame at one end, whilst the other end is free to deflect (**Fig.5.3**). Cyclic displacements are applied to the free end of the test sample, and this will simulate the flexural movements that occur in a wing structure.

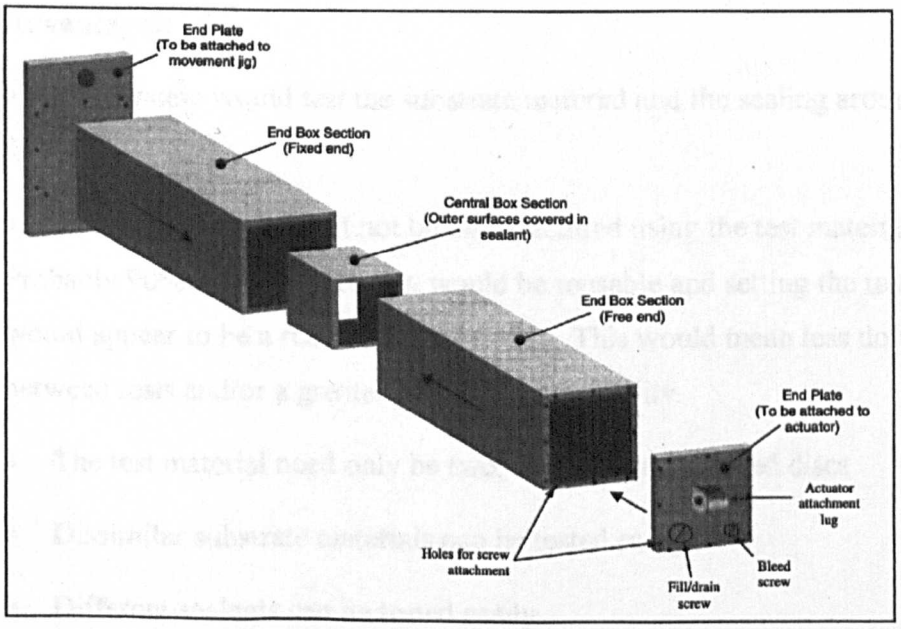

Figure 5.3. Box beam concept test rig (Jones, 2001).

This concept was not utilised for the following reasons:

- It would have been difficult to model realistically the joints involved
- It would have been difficult to utilise fasteners and maintain joint bondline thickness without distortion.
- This rig required the use of aircraft quality materials throughout, with the resultant expense and related manufacturing problems.

5.3.3. Screw fastener and pressurised tube

The design (**Figure 5.4**) comprises a sealed, pressurised tube with the test joint situated in the centre of tube. The test sealant is sandwiched between two bolted coupons. One end of the tube would be supported rigidly to a test frame

end plate, whilst the other end is free to deflect. Cyclic loads can be applied to the free end of the rig.

The loads can be applied using hydraulic or pneumatic actuators. These actuators could be computer controlled so that the applied loads and frequencies can be adjusted to suit different flight simulations. The test joint would be the weakest part of the tube, consequently, the applied sealant would experience the highest strains.

Advantages:

- This system would test the substrate material and the sealing around the fastener.
- The actual test rig need not be manufactured using the test material. Probably 90% or more of the rig would be reusable and setting the test up would appear to be a relatively easy matter. This would mean less down time between tests and/or a greater volume test capability.
- The test material need only be two, easily, manufactured discs
- Dissimilar substrate materials can be tested easily.
- Different sealants can be tested easily.
- Surface preparation and priming of the substrate can be altered and tested easily.

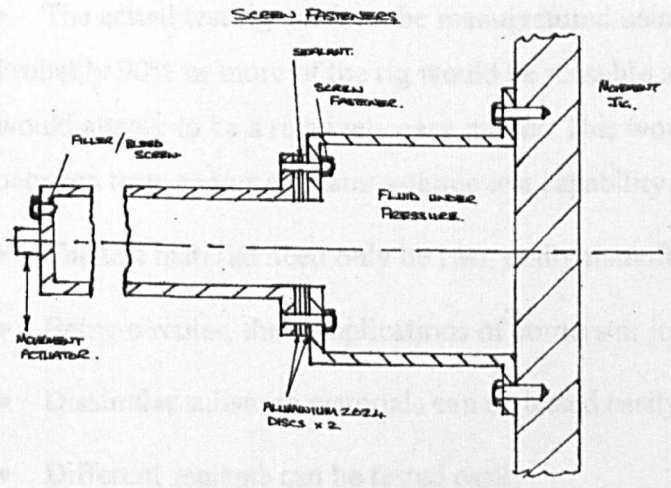

Figure 5.4. Screw fastener and pressurised tube concept.

5.3.4. Rivet fastener (interference fit fastener) and pressurised tube.

This configuration repeats a variation on the screw fastener and pressurised tube described in **Section 5.3.3**, with the added bonus that several joint configurations could, possibly, be tested. This design comprises a sealed, pressurised tube with the test joint situated in the centre of the tube (**Figure 5.5**). The test sealant is sandwiched between two bolted coupons of dissimilar size. One end of the tube would be supported rigidly to the test frame end plate, whilst the other end is free to deflect. Cyclic loads can be applied (axial and/or torsional) to the free end of the rig. This will simulate the flexural movements experienced by the wing during its working life.

The loads can be applied using hydraulic or pneumatic actuators. These actuators could be computer controlled so that the applied loads and frequencies can be adjusted to suit different flight simulations. The test joint would be the weakest part of the tube, consequently, the applied sealant would experience the highest strains (and hence the highest stress).

It was decided that the rivet fastener concept offered the best method of achieving the required test parameters.

Advantages:

- This system would test the substrate material and the sealing around the fastener.

- The actual test rig need not be manufactured using the test material. Probably 90% or more of the rig would be reusable and setting the test up would appear to be a relatively easy matter. This would mean less down time between tests and/or a greater volume test capability.

- The test material need only be two, easily manufactured discs

- Being circular, the complications of corners or joint-ends are eliminated

- Dissimilar substrate materials can be tested easily.

- Different sealants can be tested easily.

- Surface preparation and priming of the substrate can be altered and tested easily.

- It would allow the sealing of the riveted fasteners to be tested
- The potential for testing many joint configurations (with changes to the rig set-up).

This configuration appeared to model a simplified joint, as can be seen from **Figure 5.6**. The concept is shown in 3-D in **Figure 5.7.**

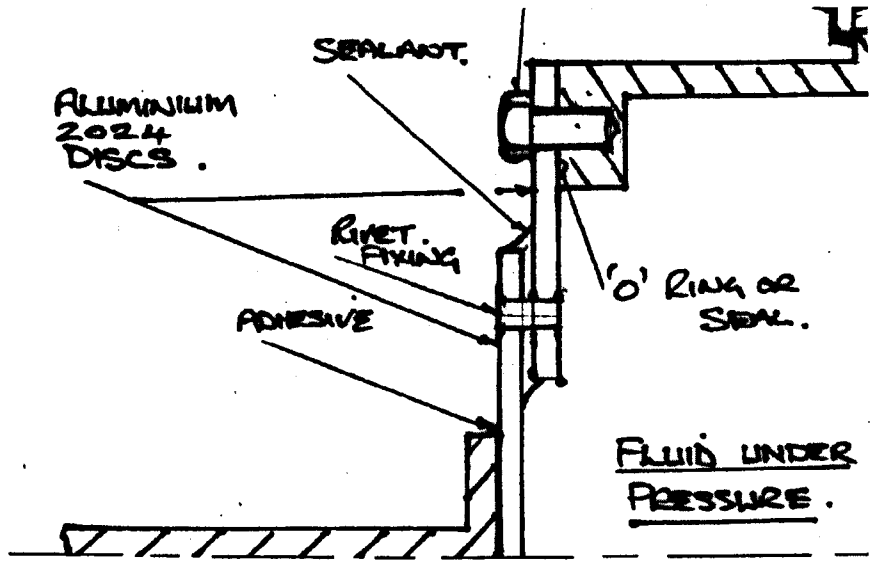

Figure 5.5 Rivet fastener and pressurised tube.

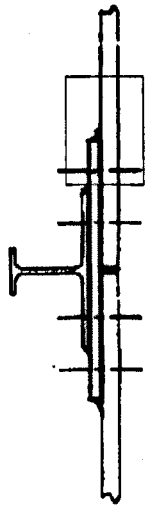

Figure 5.6. The Skin-Butt Strap joint. This shows the similarities between the two joint configurations.

5.4. Dimensions and scale

In the test parameters it can be seen that there is a requirement for 3-5mm thick aluminium sheet and aerospace fasteners to be utilised in the test rig. The thickness of the aluminium that the skin/butt-straps/stringers are manufactured from is at least 6.3 mm thick with the smallest diameter fasteners being 5/16 in. (7.94 mm)(there is a mixture of imperial and metric sizes used in the aircraft industry)(Buller,2002(a)). If a realistic model were to be designed to accurately model the stresses and strains experienced by the sealant joint then the thickness of the aluminium sheet used, the fasteners, along with the pitching and edge distances proportions would need to be scaled down to maintain dimensional constancy. It was initially felt that there would need to be at least five fasteners used in the test piece as well. In the final configuration, twelve fasteners were used.

5.5. Concept principles

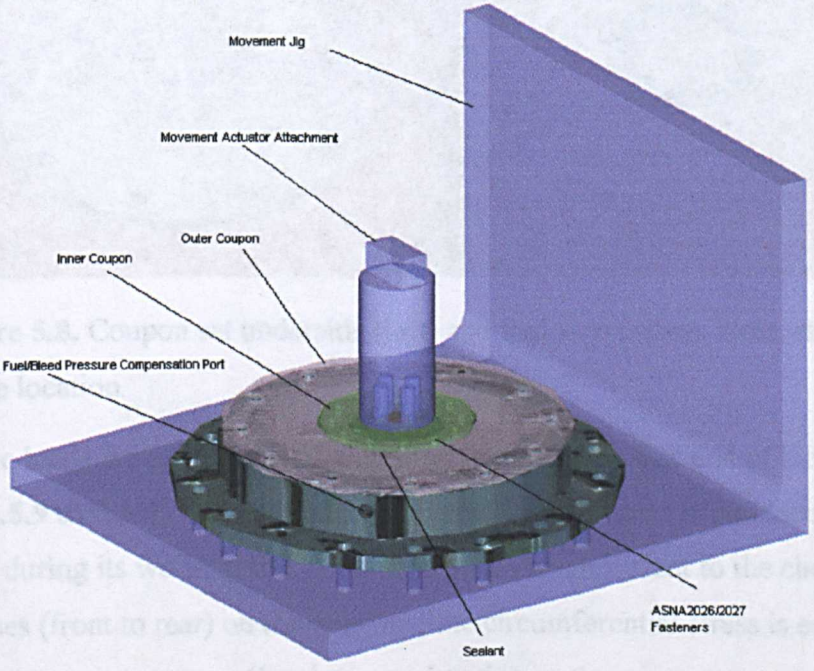

Figure 5.7 Early concept of the test rig (fasteners not shown).

The test sealant is sandwiched between the two bolted aluminium circular coupons of dissimilar size **(Fig.5.8)** mounted concentrically. The sealant used is Chemetall MC-238 B2 polysulfide sealant. The details of the fastening and sealing (interfay, fillet, and overcoat) represent variables that can be changed

to suit any particular test. The outer circular coupon is 216 mm diameter, with a central circular hole of 64 mm diameter; it is fabricated from aircraft quality 3.18 mm thick aluminium sheet (2024-T3 clad). The inner coupon of 104 mm diameter is formed from a billet of aluminium so that an integral threaded centre hub can be machined into it. A stainless steel threaded centre hub is then attached to this. The coupons are prepared in exactly the same way as an aircraft wing; they are degreased, pickled, anodised and finally painted to the relevant aircraft manufacturer's standards.

The test coupons are mounted as the base of a "Fuel Tank" or Pressure Pot (PP) that is structurally stiff and filled with jet fuel. The whole assembly is then mounted in a fatigue test machine. One end of the test rig is supported rigidly to the test frame end plate (load cell), whilst the other end is free to deflect (actuating ram).

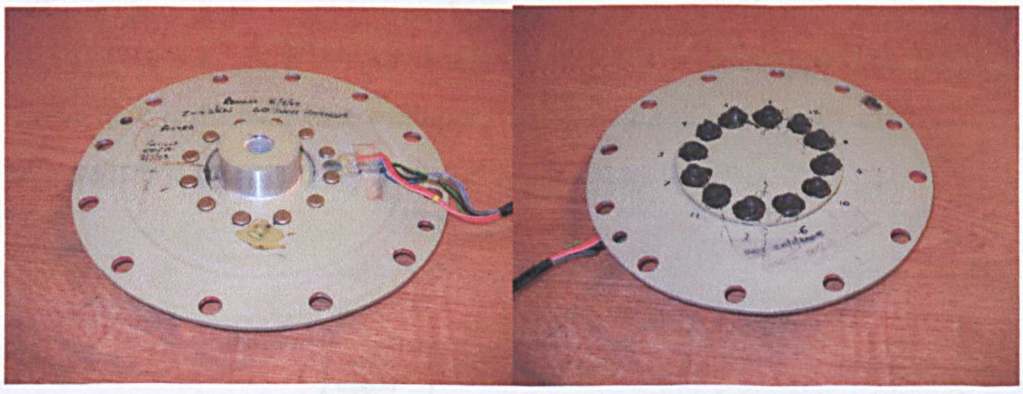

Figure 5.8. Coupon set underside (left) and fuel side (right). Note: the strain gauge location.

Cyclic loads are applied (axial and/or torsional) to the free end of the rig **(Figs.5.9 to 5.11)**. This simulates the flexural movements experienced by the wing during its working life. The radial stress is equivalent to the chordwise stresses (front to rear) on the wing and the circumferential stress is equivalent to the spanwise stresses (fuselage to wing tip) on the wing.

As mentioned previously, the loads can be applied using hydraulic or pneumatic actuators. The test joint is the weakest part of the rig, thus, the applied sealant experiences the highest strains (and hence the highest stress) and, in combination with the application of high and low temperatures and

varying pressures, this eventually leads to damage in the sealant system that promotes a leak of the jet fuel (that can be traced) **(Fig. 1.3).**

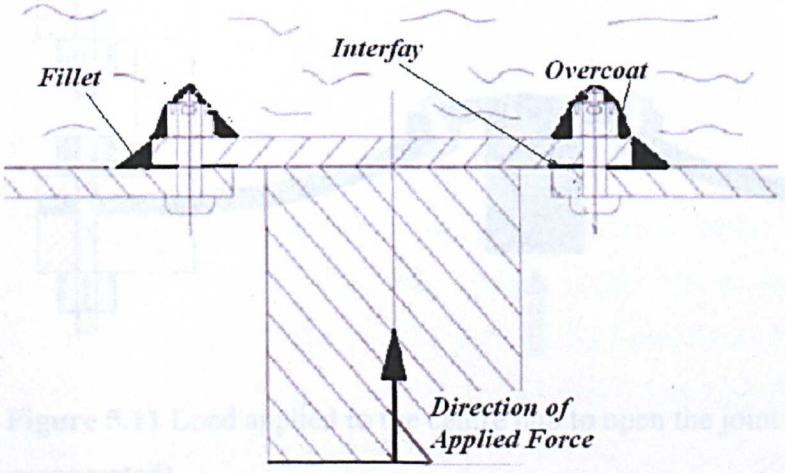

Figure 5.9. Section of the test coupons

Figs 5.10 to 5.12 show the movement applied to the test coupon. The design shown here is the later centre coupon/ hub configuration whereby the centre coupon/hub is machined from one piece of aluminium.

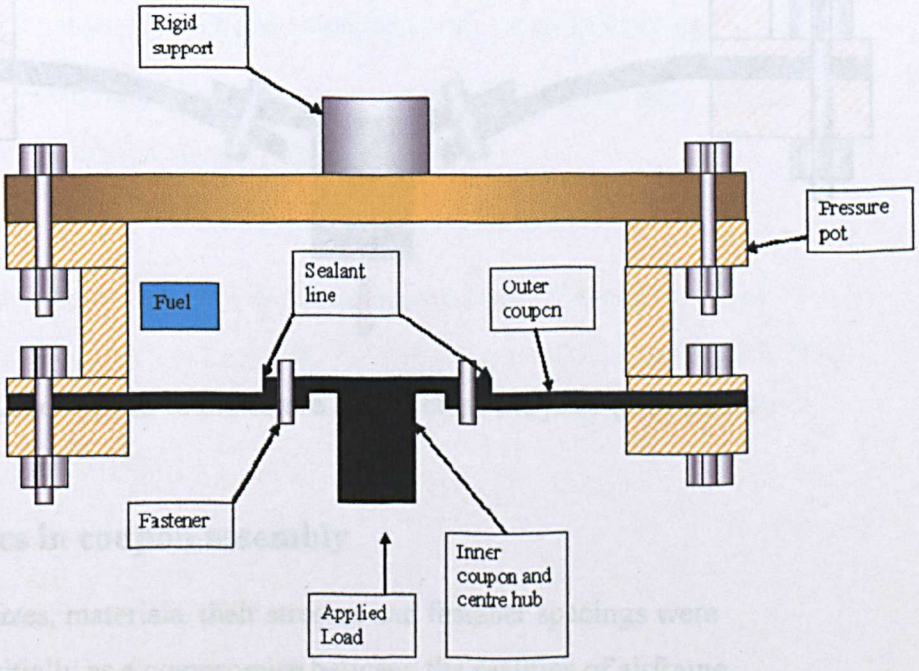

Figure 5.10 Sectioned general layout of the Pressure Pot (PP) and coupons

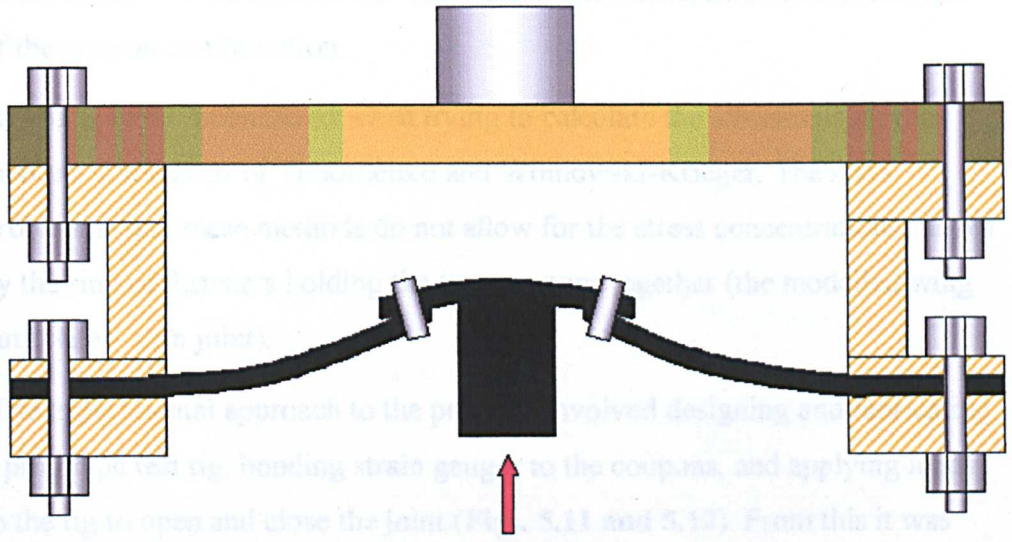

Figure 5.11 Load applied to the centre hub to open the joint (movement exaggerated)

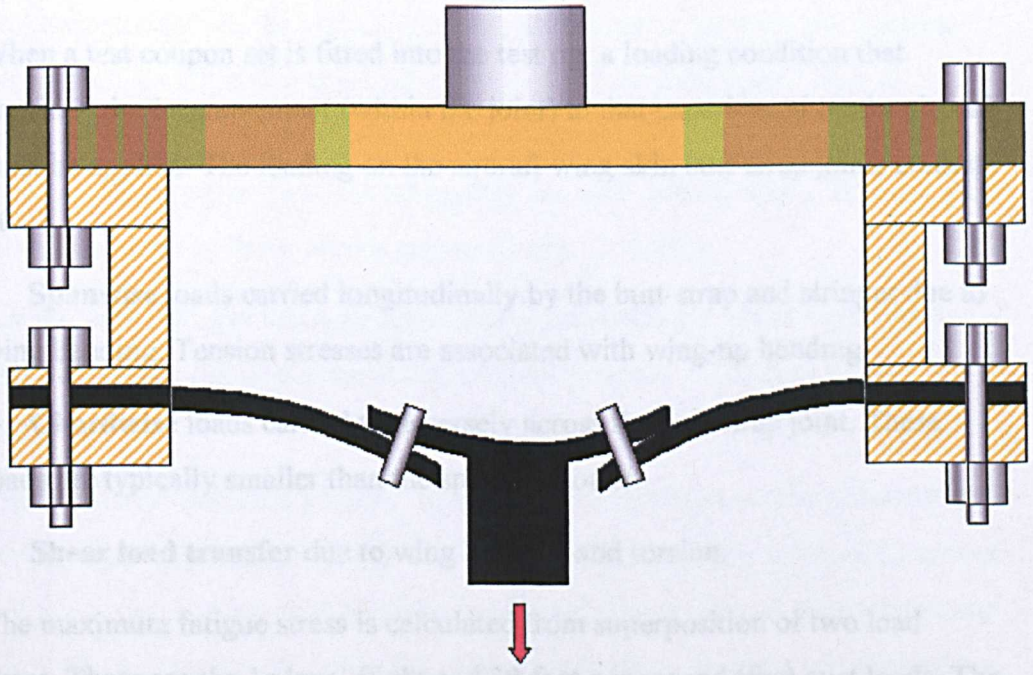

Figure 5.12 Load applied to the centre hub to close the joint (movement exaggerated)

5.6. Stresses in coupon assembly

The coupon sizes, materials, their stresses and fastener spacings were determined initially as a compromise between the realities of airframe

construction and the stresses derived from strain measurements on mock ups of the coupon configuration.

Problems were encountered when trying to calculate the stresses using the theoretical methods of Timoshenko and Woinowski-Krieger. The main problem is that these methods do not allow for the stress concentrations caused by the ring of fasteners holding the two coupons together (the modelled wing butt plate – skin joint).

The experimental approach to the problem involved designing and fabricating a prototype test rig, bonding strain gauges to the coupons, and applying loads to the rig to open and close the joint (**Figs. 5.11 and 5.12**). From this it was determined whether the measured stresses experienced by the Airbus A318 (**Table 5.1**) could be achieved in the laboratory.

5.7. Mechanical loading

When a test coupon set is fitted into the test rig, a loading condition that provides similar movement (within the joint) to that experienced on the aircraft must be applied. The loading on the aircraft wing skin butt-strap joints consists of:

- **Spanwise** loads carried longitudinally by the butt-strap and stringer due to wing bending. Tension stresses are associated with wing-up bending.
- **Chordwise** loads carried transversely across the butt-strap joint. These loads are typically smaller than the spanwise loads.
- **Shear load transfer** due to wing bending and torsion.

The maximum fatigue stress is calculated from superposition of two load cases. These are the 1g level flight and 30 foot per second (fps) gust loads. The following stresses for the spanwise skin stresses in a particular rib bay are given by Buller (2002(a)):

- 1g Flight Stress: **46.4 MPa**
- 10fps Gust Stress: **23.2 MPa**

A maximum gust of 30fps leads to a Gust Stress of **69.6 MPa**. The maximum (spanwise) fatigue stress for this element is then:

46.4 MPa + 69.6 MPa = 116.0 MPa.

The Chordwise and Shear stresses derived in a similar way are shown in **Table 5.1**.

Spanwise stresses (MPa)	**Chordwise stresses(MPa)**	**Shear stresses(MPa)**
116.0	**41.7**	**53.5**

Table 5.1. Direct and shear fatigue stress for skin joint configurations (Buller(2002(a)).

It was felt that these stresses may be too high to achieve, realistically, on the test rig in the laboratory. However, it is possible to replicate the relative proportions between the various stresses, i.e. the ratios between the stresses, because it was felt that this would certainly load the joint higher than in normal flight and, consequently, could shorten the time required to test the joint configuration and sealant adequately (or until failure) whilst keeping the stresses within the linear elastic region (Buller, 2002(b)).

For the initial fatigue test a **1g flight stress (46.4MPa) ± 10fps flight gusts (23.2MPa)** was decided upon at the required frequency of **5 Hz** (Taylor, 2003).

The similarity between Bullers' skin stresses **(1g flight stress (46.4MPa) ± 10fps flight gusts (23.2MPa))** and the equivalent coupon stresses (achieved using a epoxy bonded centre hub rather than the later integral centre hub/inner coupon) can be seen in **Table 5.2**. The experimental stresses were calculated from strain gauge data obtained in a similar way as for the integral centre hub, as discussed later.

Several adhesives were tried but found to be unreliable and unable to withstand fatigue testing in tension, especially at the low temperatures, required in the MSS. On later testing, the applied loads remained the same but the coupon gauge stresses were reduced because of the use of the integral centre hub /inner coupon (**See Table 5.4**).

Buller's skin stress (MPa)	Coupon gauge stress (MPa)	Load applied to centre hub (kN)
23.2	24.9	1.5
46.4	45.7	3.0
69.6	67.8	4.5

Table 5.2. Buller's skin stress, coupon equivalent circumferential stresses and applied loads.

To test the integral centre hub design static load testing was carried out using strain gauges **(Fig. 5.13)** to check that the stresses obtained were within the test parameters. The method by which the stresses are calculated from the strain gauge readings can be found in **Appendix 7**.

The loads can be applied to either open (tension) or close (compression) the sealant joint. The maximum load that could be applied to the coupons before permanent deformation (damage) was detected was between 6.5kN and 7kN. As the joint is to be fatigued the loads need to be lower than this to achieve a reasonable fatigue life. Static loads of 4 and 4.5kN were applied in opposite directions to load the joint in tension and compression respectively to gauge whether the stress levels would be appropriate for fatigue loading.

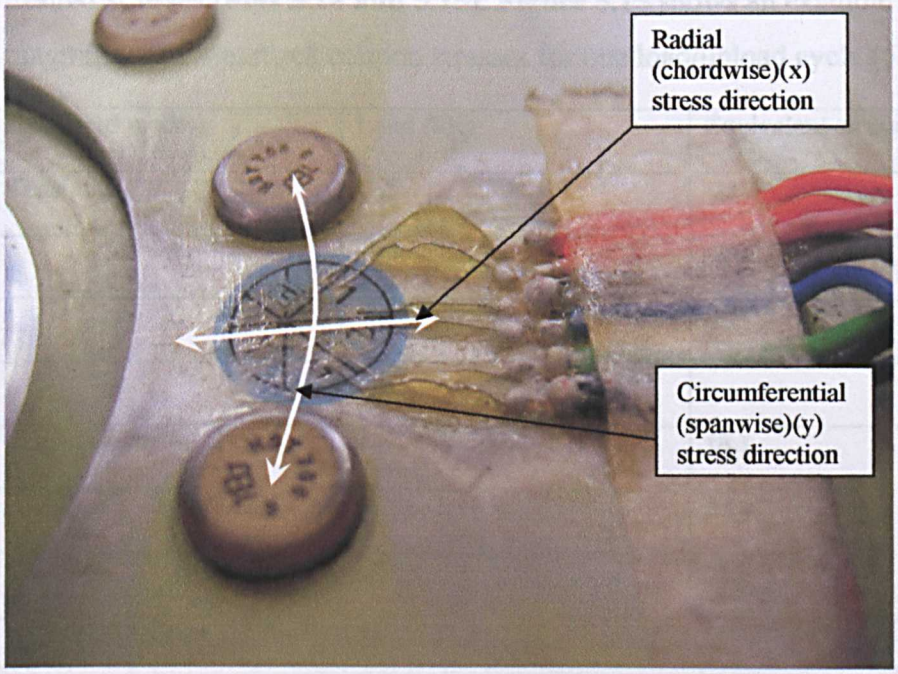

Figure 5.13 Test coupon strain gauge showing circumferential and radial stress

The results showed that with the sealant in tension, the proportions of the stresses achieved were close to the proportions of the stresses referred to by Buller (2002(a))(**Table 5.3).**

	Radial(σ_r) (MPa)	Hoop(σ_θ) (MPa)	Shear(τ) (MPa)	Ratio ($\sigma\theta/\sigma r$)	Ratio ($\tau/\sigma r$)
Theoretical stresses (Buller, 2002(a))					
Fatigue stress skin	**41.7**	**116**	**53.5**	**2.78**	**1.28**
Fatigue stress butt-strap	**52.1**	**112.3**	**66.9**	**2.15**	**1.28**
Experimental static load check					
Single coupon, joint in tension. Max load 4kN	**-19.2**	**-49.85**	**-15.32**	**2.59**	**0.80**
Single coupon, joint in compression. Max load 4.5kN	**11.4**	**56.9**	**22.75**	**4.99**	**1.99**

Table 5.3. Stress comparison with Buller (2002(a)).

From static and dynamic testing, the loads imposed on the coupons by the fatigue machine were modified to keep the proportions correct **(Table 5.4)**. However, the joint tension fatigue load had to be increased to achieve the desired stresses **(Figs 5.14 and 5.15). Figure 5.15** shows an example of the magnitudes of measured coupon stresses for one load/unload cycle (5Hz).

Joint load mode	Load (kN)	Equivalent stress (MPa)
Tension	**-1.5**	**-21.3**
	-3.0	**-39.2**
	-4.5	**-55***
Compression	**1.5**	**18.1**
	3	**37.1**
	4.5	**56.9**

*** Projected stress, see figure 5.14**

Table 5.4. Loads and equivalent stresses

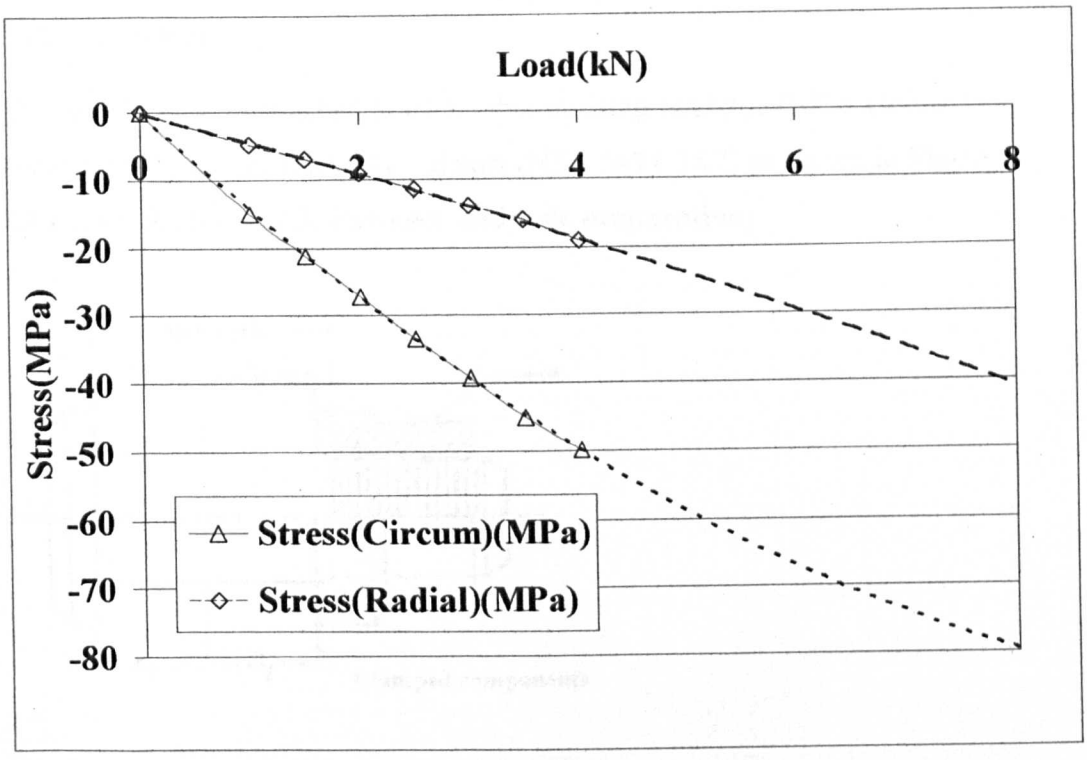

Figure 5.14 Static stress against load with a trendline showing the predicted stresses at higher loads.

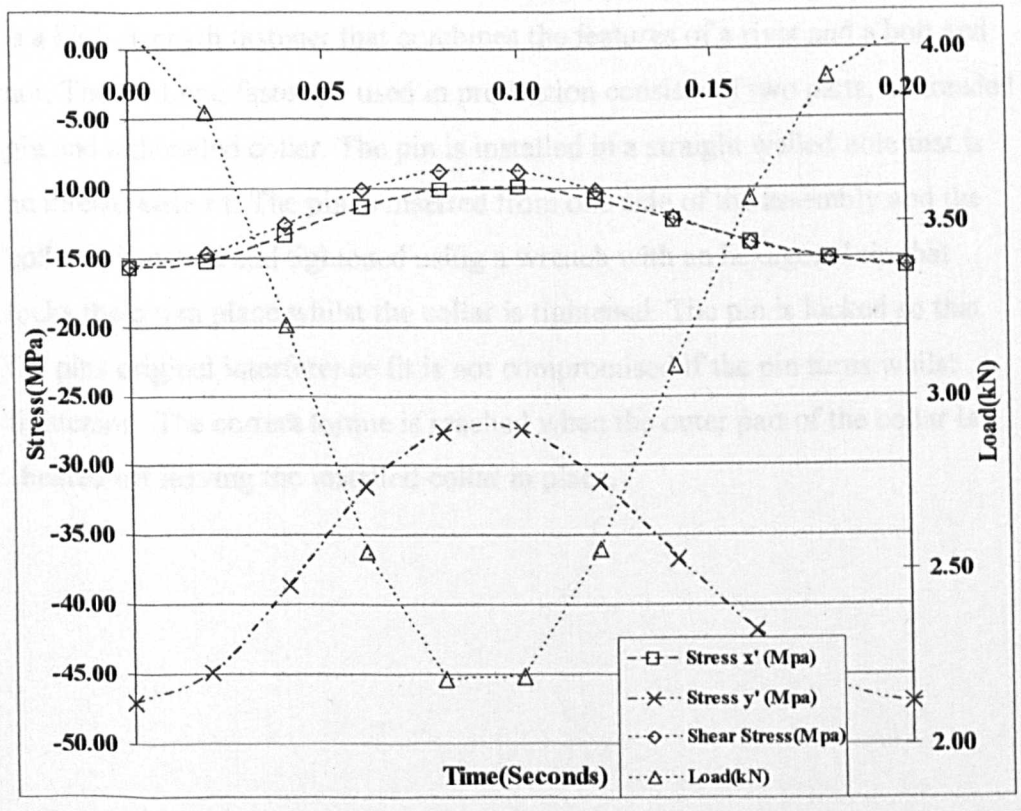

Figure 5.15 Example dynamic stress / load against time, joint in tension at 5Hz.

5.8. Fasteners

The two discs were attached to each other utilising twelve, 3/16" Titanium fasteners (ASNA 2027HK3-4) and nuts (NSA 5474-3K7) as shown in **Figure 5.16.** (see **Section 3.2.2. Fastener and hole preparation**).

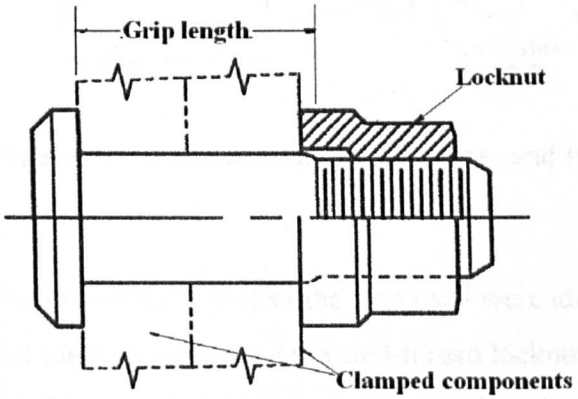

Figure 5.16. Titanium fastener and locknut.

The fasteners used were of the Hi-Lock type (**Fig. 5.17**). The Hi-Lock fastener is a high strength fastener that combines the features of a rivet and a bolt and nut. The Hi-Lock fasteners used in production consists of two parts, a threaded pin and a threaded collar. The pin is installed in a straight walled hole that is an interference fit. The pin is inserted from one side of the assembly and the collar is installed and tightened using a wrench with an hexagonal tip that locks the pin in place whilst the collar is tightened. The pin is locked so that the pins original interference fit is not compromised if the pin turns whilst tightening. The correct torque is reached when the outer part of the collar is sheared off leaving the installed collar in place.

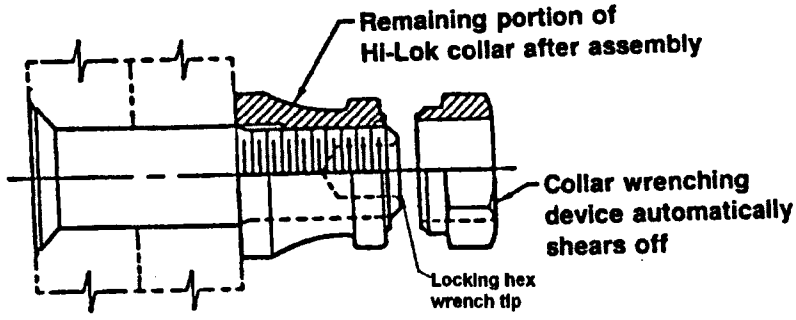

Figure 5.17. Hi-Lock titanium fastener and locknut (Bennett, 1990)

For the research project the pins used were identical to those described above but the nuts were the deformed-thread locknut type (see **Section 3.2.2.3 Locking methods**). These were used because the Hi-Lock wrench and lock tip are expensive pieces of equipment and were deemed unnecessarily expensive for the project. Instead, a calibrated torque wrench and an adapted ¼ inch drive to enable an Allen key to be used to lock the pin whilst applying the torque was thought to be adequate.

5.9. Finite Element Analysis (FEA)

5.9.1. Introduction

This section details the finite element analysis (FEA) of the test coupons. The FEA analysis was carried out as a precursor to the fabrication of the first test coupons (with inconclusive results) and in parallel to the development of the MSS. This was done to enable a comparison to be made with the stresses obtained from the strain gauges and, ideally, to optimise the design of the coupons further.

The aim of this part of the research was to:

- Compare the experimental results, obtained using strain gauges, with those obtained from FEA
- To carry out a limited parametric study to optimise the design or show that other joint configurations can be produced that exhibit the same proportion of circumferential to radial stress
- To determine the maximum and minimum theoretical principal strains experienced by the sealant in the joint.

Finite Element Modelling

Finite Element Analysis (FEA) is a computational technique that is often used to model the physical response of a structure. The first step of any finite element analysis is to divide the actual geometry of the structure using a collection of discrete portions called finite elements. The elements are joined together by shared nodes. The collection of nodes and finite elements is known as the mesh (**Fig. 5.18**).

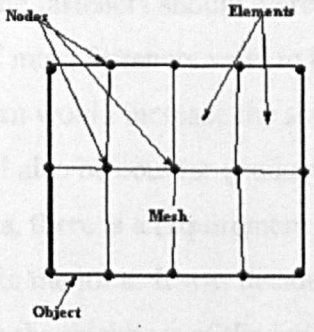

Figure 5.18 A simple structure in FEA illustrating the various parts of a model.

In the analysis, it is assumed that the variable to be determined (in this case load) acts on each element in a predefined manner. This means that loads can be transferred between the elements of adjacent elements that share nodes. The number and type of elements is chosen to ensure that the distribution of the variable over the whole body is adequately approximated. In a stress analysis problem, the finite element software calculates the displacements of the nodes and from this information, the stresses and strains in the elements are determined. Boundary conditions are applied to prevent unlimited rigid body motion and to apply the actual real life constraints.

The analysis of the MSS coupon set typify a few of the problems that are encountered when carrying out FEA. The main one is that FEA programs can only provide accurate results if the program is given the correct inputs (material specifications etc.) and that the model itself is constructed properly within the FEA program. Incorrect FEA results usually include idealization errors, i.e. those that come from simplifying the real world. Errors arise when compromises, or simplifications, are made within the model. The FE analysis of the coupon set was no different and required several simplifications and assumptions included in the model to enable the model to run in a realistic timeframe and gain some meaningful results.

A limited parametric study was carried out to try to optimise the design. One detail that it was felt would be inadvisable to alter was the pitch and size of the fasteners. Altering the pitch of the fasteners would be counterproductive for several reasons. Firstly, one of the parameters set out by Airbus (UK) was that the pitch and size of the fasteners should be representative of a real aircraft wing. Secondly, if more fasteners were to be used the pitch would have to be altered and this in turn would increase the size of the MSS. Reducing the number of fasteners would also be counter-productive in that, to be able to obtain some statistical data, there is a requirement for the coupon set to have a number of fasteners used in the joint. It was decided that the only component that could be changed was the thickness of the inner or outer coupon either both or in combination. The magnitude of the stresses are important but, as previously mentioned, real maxima could not be achieved realistically in the

laboratory (certainly not with the equipment and budget available) although the proportions of the circumferential and radial stresses (spanwise and chordwise stresses respectively) were (Buller (b)(2002)).

The analysis of the coupon set was initially carried out using ABAQUS version 6.2 with the final model being created in ABAQUS version 6.6.

5.9.2. Model Definition

The test coupons were loaded only within the linear elastic region as would be the case in a real joint, avoiding any damage and distortion to the coupons over the long periods and high cycle rates that the test required. For this reason the following model material parameters were used to determine the stress distribution within the coupons:

- Linear elastic behaviour
- Isotropic material properties

This was thought to be a good approximation of how the structure was expected to behave and formed the basis for the FEA of the MSS coupon set.

A 30° section (wedge) was enough to model the important features using symmetry as a boundary condition. The final model was constructed as a single object, revolved through 30° **(Fig.5.19)**. This produced a $1/12^{th}$ slice of the complete coupon set that had all of the components within it, together with the representative material properties assigned to the various regions within the model. This ensured a relatively short computation time whilst trying to maintaining reasonably accurate results.

The boundary condition around the outside perimeter was "clamped," allowing no translation or rotational movement **(Fig. 5.20)**.

The other two sides of the wedge required the use of two co-ordinate systems as shown in **Fig. 5.20** to define the alignment of the Z symmetry (**BC1** and **BC2**). Full details can be found in **Appendix 8**.

The main focus of the analysis was the prediction of stress at the position of the stacked rosette strain gauge in the experimental coupons **(Fig. 5.13).** This position coincides with N**ode 93 (Fig. 5.19)**. The mesh included 4-node tetrahedral elements. This was selected because of problems with non-convergence using 8-node hexagonal elements. (See **Appendix 8**).

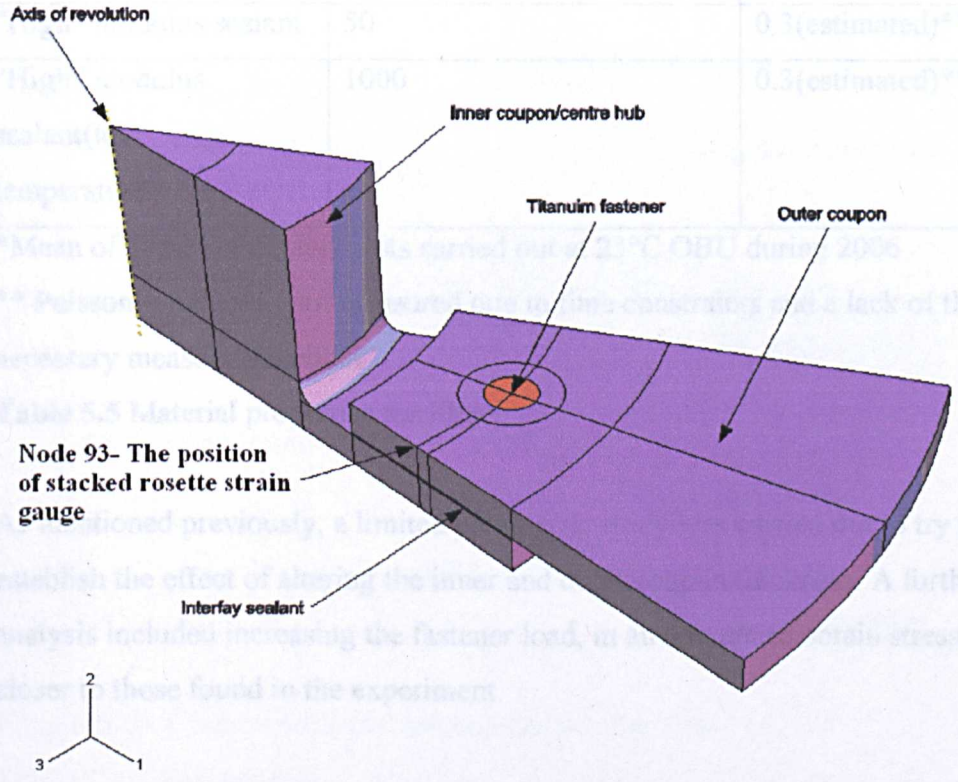

Figure 5.19 Coupon set components

Similar problems were encountered with this model if the measured sealant properties were used directly, resulting in a gross distortion of the model elements. Due to the low stiffness of the sealant material's properties it was found that if the Modulus of the sealant was increased from 2.52 MPa (±0.92) (the average and SD of various dumbbell tests carried out at OBU during 2006) to 50 MPa, the modelled sealant interfay behaved in a more realistic and expected manner. This is not necessarily unrealistic as the modulus of the sealant at low temperatures (worse case scenario) can reach 1GPa (Healey, 1996) (see **Section 8.4.2. DMTA results).** Another aspect that needs to be addressed is that the estimated Poissons's ratio of 0.3 may be to low. **Appendix 8** contains images of the MSS FEA results that illustrate the effect of sealant modulus on the sealant interfay joint area.

The material properties used in the analysis are shown in **Table 5.5**

Material	Young's Modulus(E) MPa	Poisson's ratio(υ)
Aluminium2024 T3	72400	0.33
Titanium 6AL-4V	114000	0.34
Chemetall MC 238-B2	2.52 (±0.92) *	0.3(estimated)**
"High" modulus sealant	50	0.3(estimated)**
"High" modulus sealant(low temperature)	1000	0.3(estimated)**

*Mean of dumbbell sealant tests carried out at 23°C OBU during 2006

** Poisson's ratio was not measured due to time constraints and a lack of the necessary measuring devices

Table 5.5 Material properties for FEA

As mentioned previously, a limited parametric study was carried out to try to establish the effect of altering the inner and outer coupon thickness. A further analysis included increasing the fastener load, in an attempt to obtain stresses closer to those found in the experiment.

The parametric variations used are shown in **Table 5.6**

Altered parameter	Altered Specification
Thinner outer coupon Standard inner (3.18mm)	2.4 mm
Standard outer coupon (3.18mm) Thicker inner	4.77 mm
Thicker outer coupon Standard inner (3.18mm)	4.77 mm
Standard fastener load =103.7N/mm^2	
Fastener load increased 10%	114.07N/mm^2
Fastener load increased 100%	204.4N/mm^2

Table 5.6 Parametric variations used

Figure 5.20 shows the placement of loads that were applied to the coupon set, the clamping forces from the fastener and the position of Node 93 (strain gauge position).

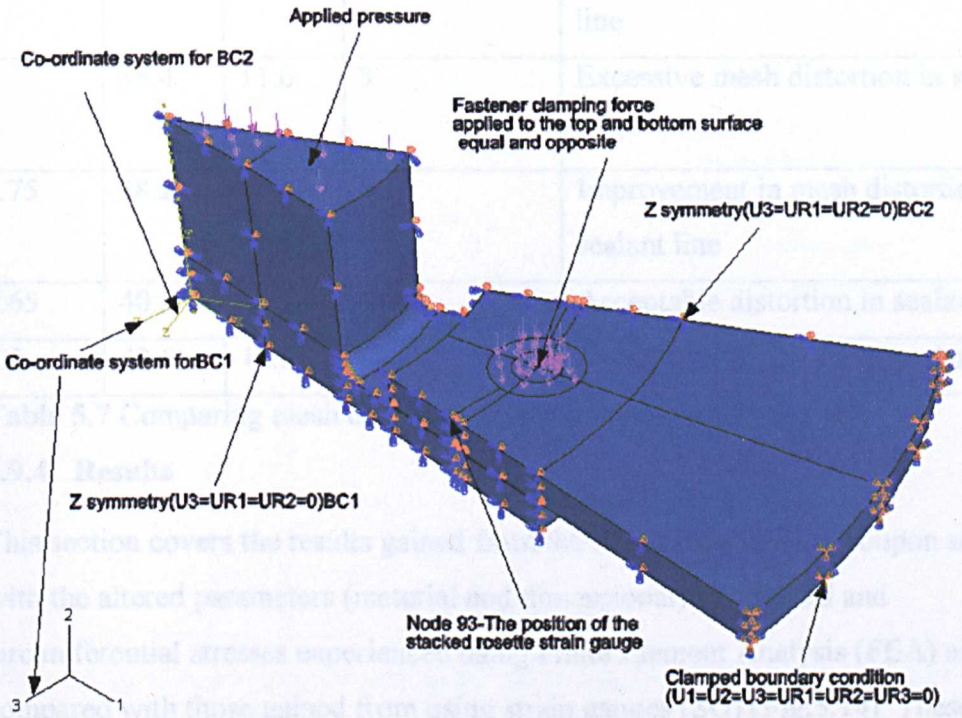

Figure 5.20. Coupon set loads and boundary conditions

5.9.3. Convergence test

To ensure that the mesh density used was suitable, a convergence test was carried out. This required several analyses to be performed on the same model but with varying mesh densities. As the mesh density increases, the results should converge to the numerically correct value. However, as the values converge with the increased mesh density a "law of diminished returns" will apply whereby for more accurate results the analysis will take much longer to complete to no great advantage. Therefore a balance must be made between the accuracy of the results and the time taken to complete the analysis. **Table 5.7** shows the maximum stresses achieved using the various mesh densities and the computational time required to achieve them using a 4kN load with the sealant in compression. The higher the mesh density number, the coarser the mesh (larger elements but with less elements in the section to be analysed). A mesh size of 0.65 was deemed appropriate.

Mesh density	Stress ($\sigma_{Circum.}$)	Stress (σ_{Radial})	Approximate time to solve (minutes)	Comments
1.25	38.3	11.8	2 .5	Excessive mesh distortion in sealant line
1	38.4	11.6	3	Excessive mesh distortion in sealant line
0.75	38.2	10.8	4	Improvement in mesh distortion in sealant line
0.65	40.5	11.2	6.5	Acceptable distortion in sealant line
0.5	42.6	12.5	30	Acceptable distortion in sealant line.

Table 5.7 Comparing mesh density, stress and time to solve the FEA

5.9.4. Results

This section covers the results gained from the FEA of the various coupon sets with the altered parameters (material and dimensional). The radial and circumferential stresses experienced using Finite Element Analysis (FEA) are compared with those gained from using strain gauges (SG) **(Fig.5.14)**. These stresses are then proportioned ($\sigma_{circum}/\sigma_{radial}$) enabling comparisons to be made between those results supplied by Buller (Buller, R.D. (a) (2002), the FEA and the strain gauges. The complete set of results for the various coupon sets, along with the dimensions used in the various FE models, can be found in **Appendix 8.**

5.9.4.1. Results for the standard coupon set (3.18mm thick)

The material properties used in all of the following FE analyses, where the coupon dimensions are altered, are the same for each test. These are shown in **Table 5.8.**

Material	Young's Modulus(E) MPa	Poisson's ratio(υ)
Aluminium2024 T3	72400	0.33
Titanium 6AL-4V	114000	0.34
High modulus sealant	50	0.3(estimated)

Table 5.8 Material properties for the FEA models where the coupon dimensions are altered.

Fig. 5.21 shows the circumferential and radial stress against load for the standard coupon set. **Fig. 5.22** shows proportioned stress against load for the standard coupon set.

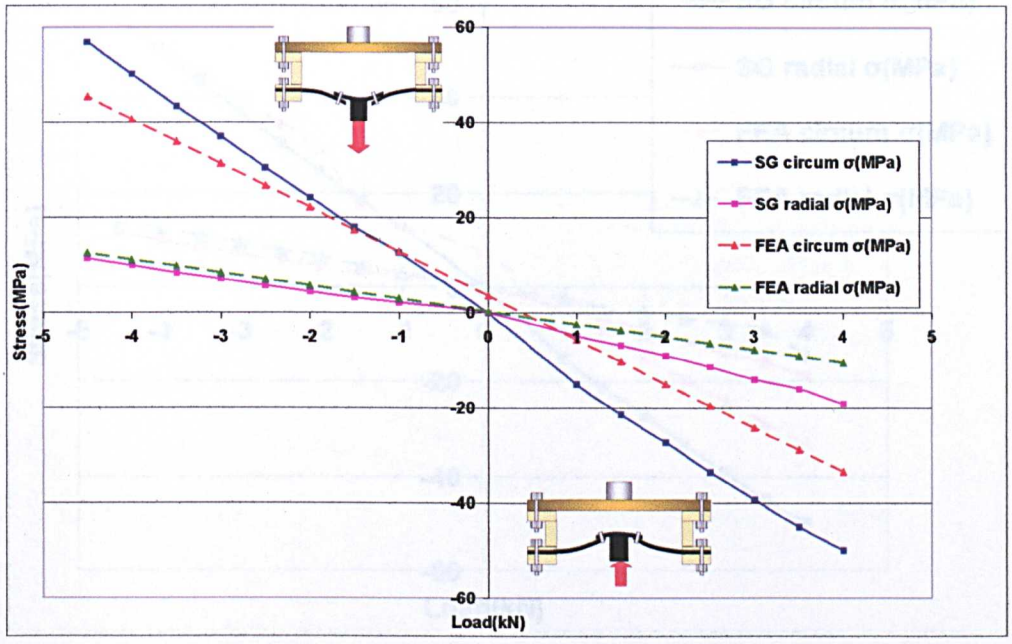

Figure 5.21 Circumferential and radial stress against load for the standard coupon set.

Note: The two diagrams showing the direction of the force apply to all of the following graphs.

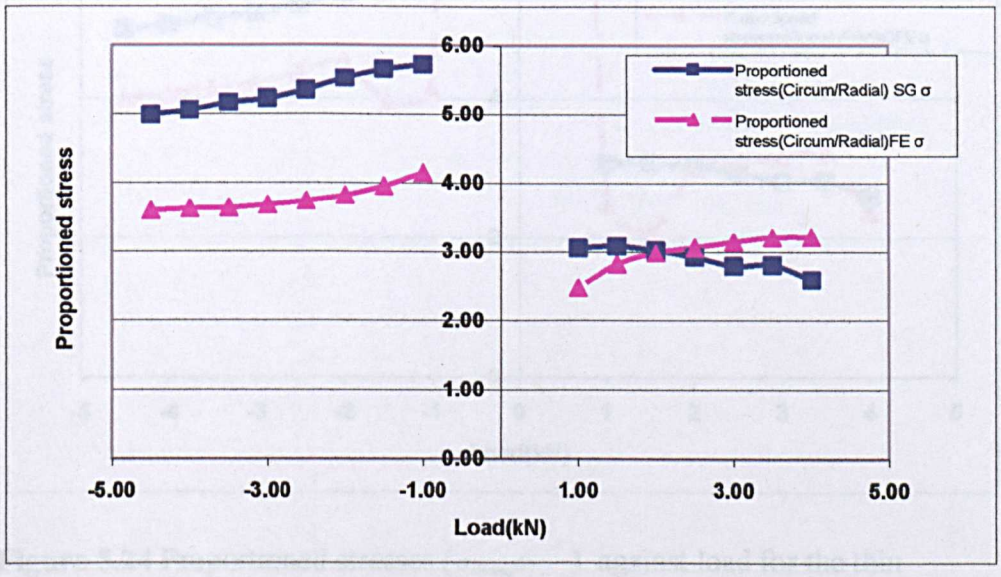

Figure 5.22 Proportioned stresses ($\sigma_{circum}/\sigma_{radial}$) against load for the standard coupon set

5.9.4.2. Results for the thin (2.4mm) outer coupon

Fig. 5.23 shows the stress against load for the thin (2.4mm) outer coupon. **Fig. 5.24** shows proportioned stress against load for the thin (2.4mm) outer coupon.

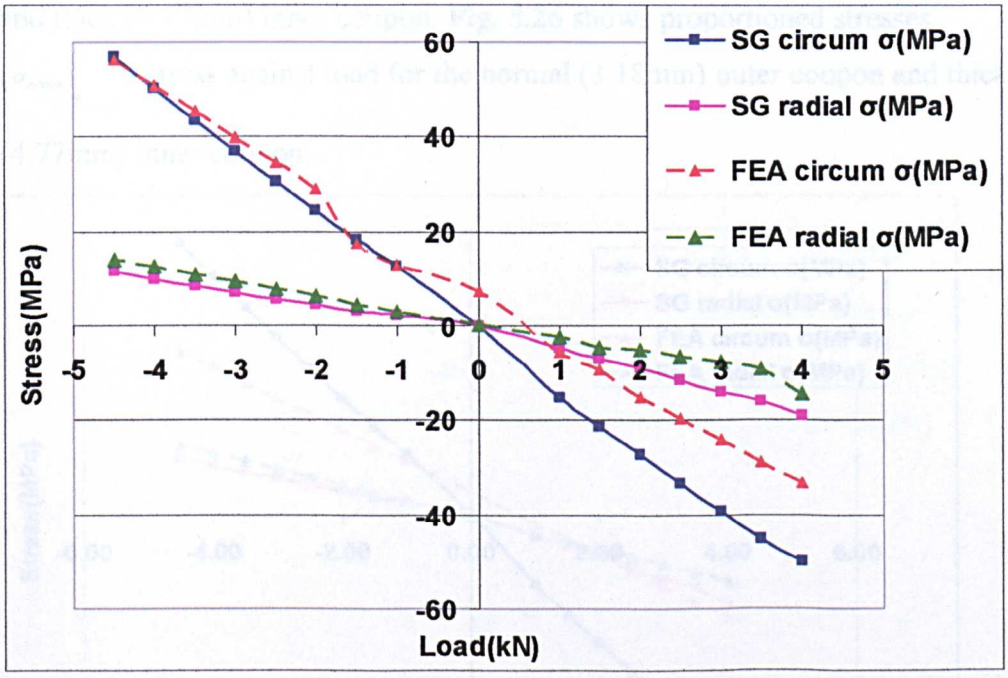

Figure 5.23 Circumferential and radial stress against load for the thin (2.4mm) outer coupon

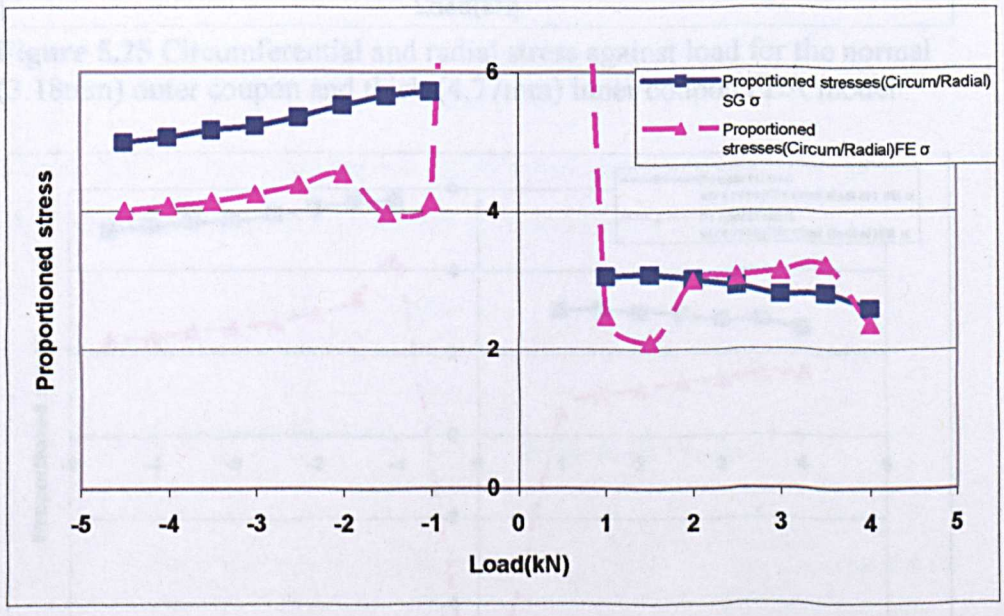

Figure 5.24 Proportioned stresses ($\sigma_{circum}/\sigma_{radial}$) against load for the thin (2.4mm) outer coupon

5.9.4.3. Results for the normal (3.18mm) outer coupon and thick (4.77mm) inner coupon

Fig. 5.25 shows the stress against load for the normal (3.18mm) outer coupon and thick (4.77mm) inner coupon. **Fig. 5.26** shows proportioned stresses ($\sigma_{circum}/\sigma_{radial}$) stress against load for the normal (3.18mm) outer coupon and thick (4.77mm) inner coupon.

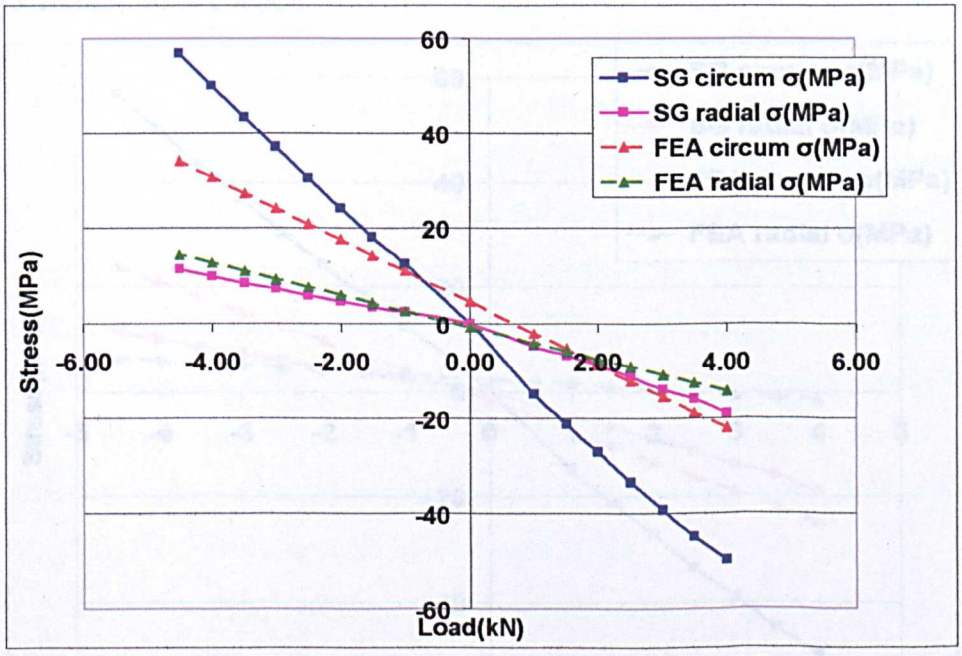

Figure 5.25 Circumferential and radial stress against load for the normal (3.18mm) outer coupon and thick (4.77mm) inner coupon FEA model

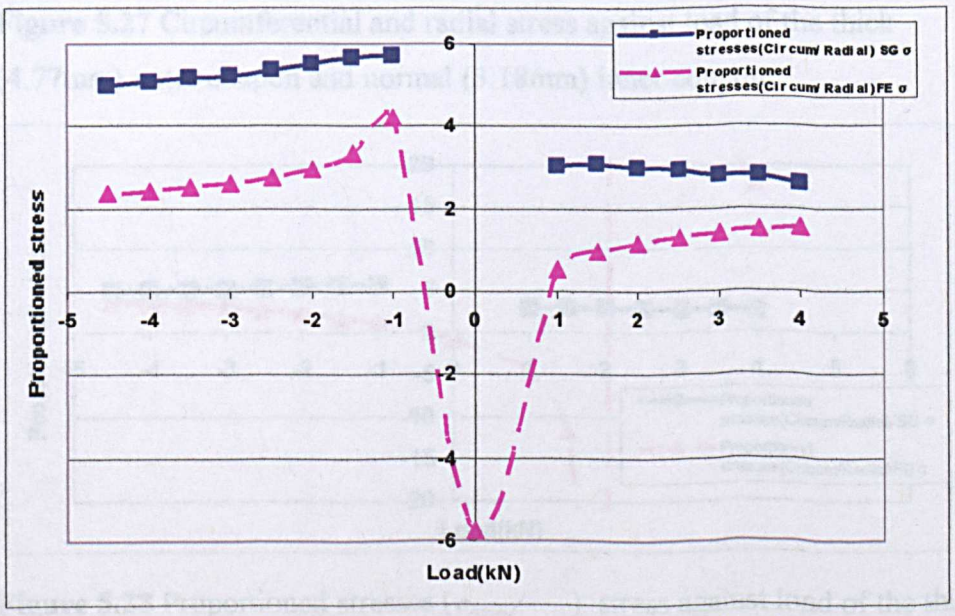

Figure 5.26 Proportioned stresses ($\sigma_{circum}/\sigma_{radial}$) stress against load for the normal (3.18mm) outer coupon and thick (4.77mm) inner coupon FEA model

5.9.4.4. Results for the thick (4.77mm) outer coupon and normal (3.18mm) inner coupon

Fig. 5.27 shows the stress against load for the thick (4.77mm) outer coupon and normal (3.18mm) inner coupon. **Fig. 5.28** shows proportioned stresses ($\sigma_{circum}/\sigma_{radial}$) against load for the thick (4.77mm) outer coupon and normal (3.18mm) inner coupon.

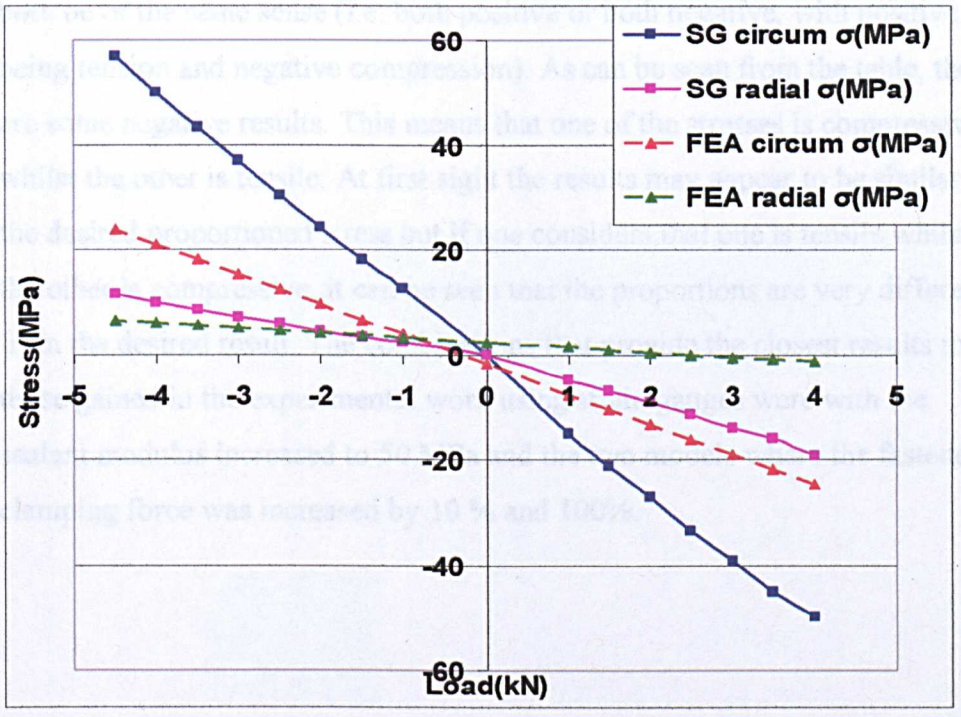

Figure 5.27 Circumferential and radial stress against load of the thick (4.77mm) outer coupon and normal (3.18mm) inner coupon

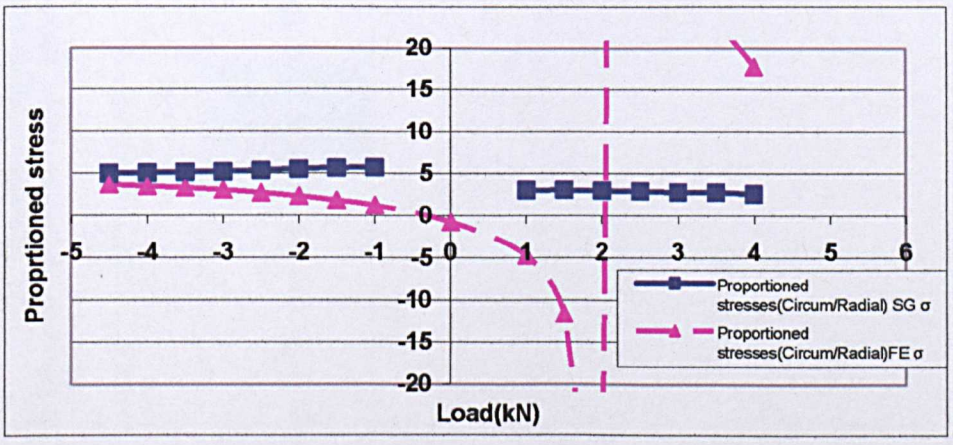

Figure 5.28 Proportioned stresses ($\sigma_{circum}/\sigma_{radial}$) stress against load of the thick (4.77mm) outer coupon and normal (3.18mm) inner coupon

5.9.4.5. Results gained from altering various FEA test parameters

Several other model parameters were altered with the tests run at the minimum and maximum loads to see if the FEA model results could show better correspondence with the real world strain gauge results. The results are compared **Table 5.9**. It must be remembered that the proportioned stress results should always be positive because they are derived from the circumferential stress divided by the radial stress, which in this model should both be of the same sense (i.e. both positive or both negative, with positive being tension and negative compression). As can be seen from the table, there are some negative results. This means that one of the stresses is compressive whilst the other is tensile. At first sight the results may appear to be similar to the desired proportioned stress but if one considers that one is tensile whilst the other is compressive, it can be seen that the proportions are very different from the desired result. The combinations that provide the closest results to those gained in the experimental work using strain gauges were with the sealant modulus increased to 50 MPa and the two models where the fastener clamping force was increased by 10 % and 100%.

	Experimental using strain gauges						FEA					
Modified model parameters	Strain gauge 4.5kN load sealant compressed			Strain gauge 4kN load sealant in tension			FEA 4.5kN load sealant compressed			FEA 4kN load sealant in tension		
	Circuml δ (MPa)	Radial δ (Mpa)	Proportioned stresses (Circum /Radial) δ	Circum δ (MPa)	Radial δ (Mpa)	Proportioned stresses (Circum /Radial) δ	Circum δ (MPa)	Radial δ (Mpa)	Proportioned stresses (Circum /Radial) δ	Circum δ (MPa)	Radial δ (Mpa)	Proportioned stresses (Circum /Radial) δ
Sealant modulus (Strain gauge results) 2.52 MPa	56.90	11.40	4.99	-49.85	-19.20	2.60	24.6	34.7	0.71	-58.5	-12.9	4.53
Sealant modulus 50 MPa							45.3	12.6	3.60	-33.4	-10.4	3.21
Sealant modulus 72.4GPa (aluminium)							22.6	3.95	5.72	-35.5	5.72	-6.21
Sealant modulus 1GPa (equivalent to -50°C)							36.8	5.7	6.46	-27.5	6.42	-4.28
Fastener force increased 10%							45.8	12.4	3.69	-32.9	-10.2	3.23
Fastener force increased 100%							49.1	12.8	3.84	-29.53	-9.8	3.01

Table 5.9 Comparison stresses for modified model parameters

5.9.5. FEA Result of maximum sealant strain experienced

Some limited FEA was carried out to determine what principal strains (maximum and minimum) the polysulfide sealant experienced under the most extreme test conditions (maximum load and the highest modulus 1GPa (equivalent to a temperature of -50°C)) (Healey, 1996).

The principal strain readings were taken along the centre of the sealant line (**Fig.5.29**). The outside of the fuel tank, the dry side, is at 0 mm and the inside of the fuel tank, where the fuel is in contact with the sealant, is 20mm. **Figure 5.30** shows the principal strains for the sealant joint in tension and **Figure 5.31** shows the principal strains for the sealant joint in compression.

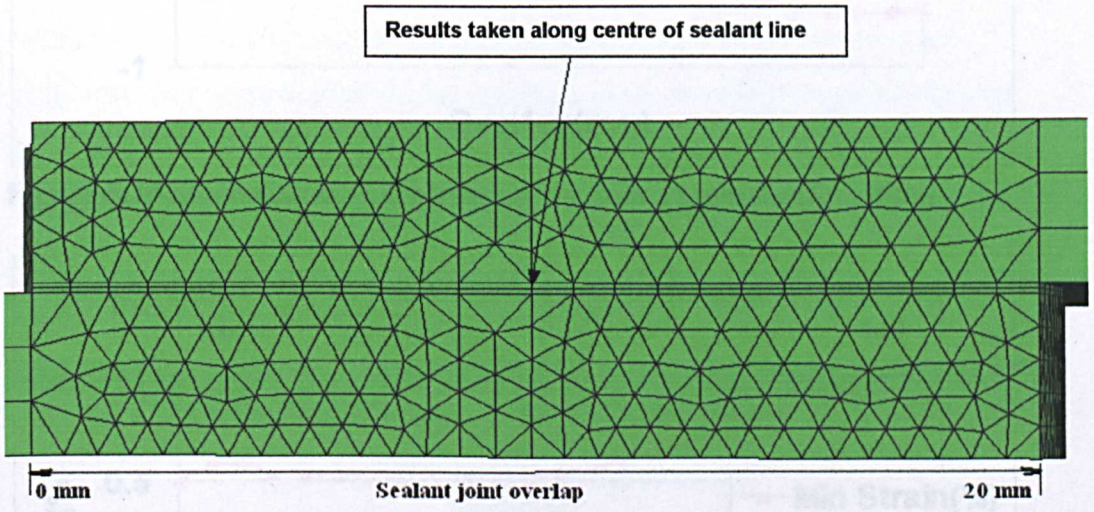

Figure 5.29 Centre of the sealant line from where the FE results were taken

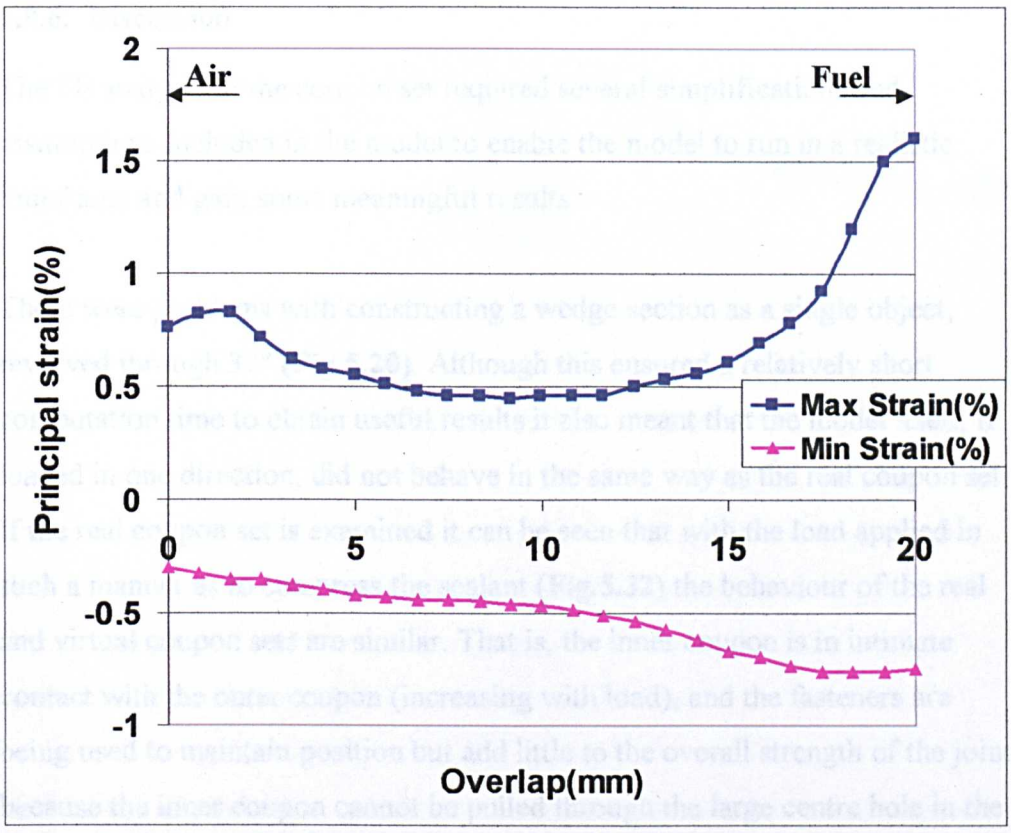

Figure 5.30 Strain distribution across sealant joint in tension **(P=4.0kN)**

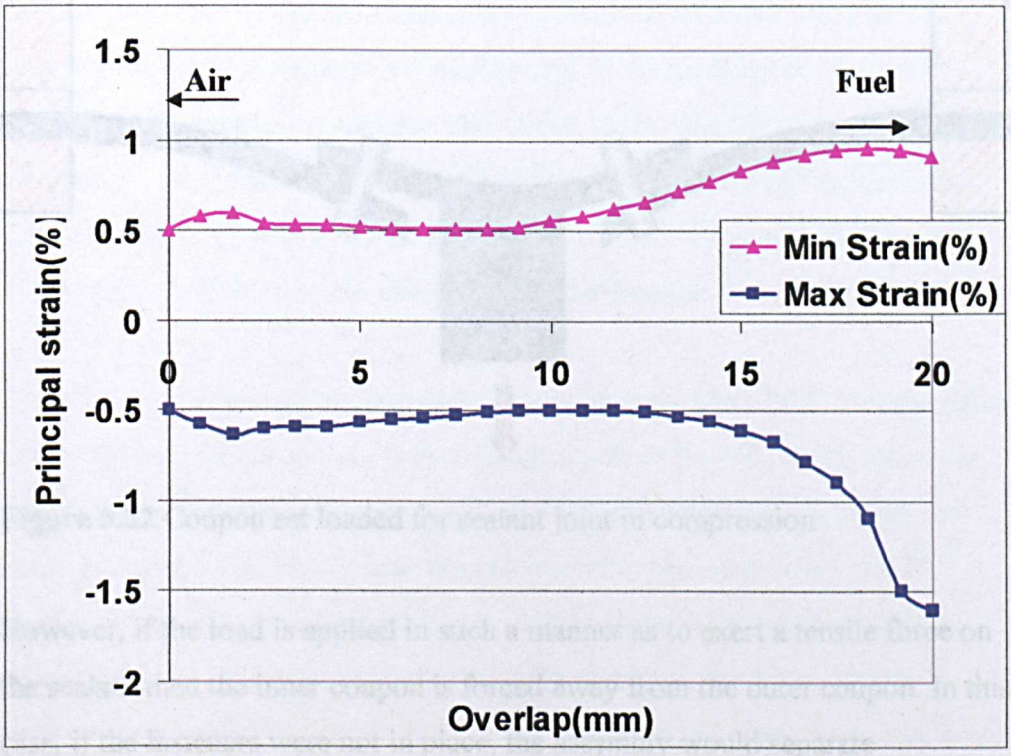

Figure 5.31 Strain distribution across sealant joint in compression **(P=-4.5kN)**

5.9.6. Discussion

The FE analysis of the coupon set required several simplifications and assumptions included in the model to enable the model to run in a realistic timeframe and gain some meaningful results.

There were problems with constructing a wedge section as a single object, revolved through 30° **(Fig.5.20)**. Although this ensured a relatively short computation time to obtain useful results it also meant that the model itself, if loaded in one direction, did not behave in the same way as the real coupon set. If the real coupon set is examined it can be seen that with the load applied in such a manner as to compress the sealant **(Fig.5.32)** the behaviour of the real and virtual coupon sets are similar. That is, the inner coupon is in intimate contact with the outer coupon (increasing with load), and the fasteners are being used to maintain position but add little to the overall strength of the joint because the inner coupon cannot be pulled through the large centre hole in the larger coupon.

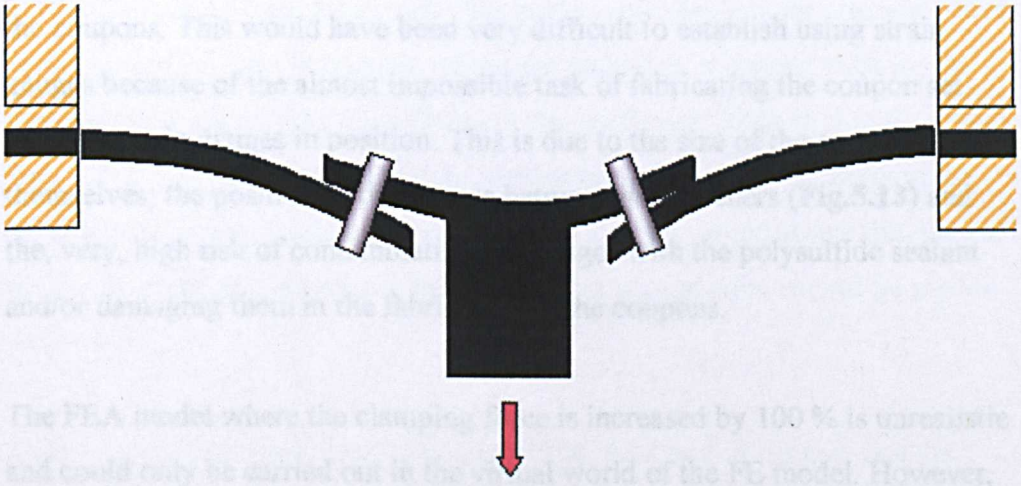

Figure 5.32 Coupon set loaded for sealant joint in compression

However, if the load is applied in such a manner as to exert a tensile force on the sealant then the inner coupon is forced away from the outer coupon. In this case, if the fasteners were not in place, the assembly would separate completely **(Fig.5.33)**. In these circumstances the FE results and the strain gauge results differ significantly.

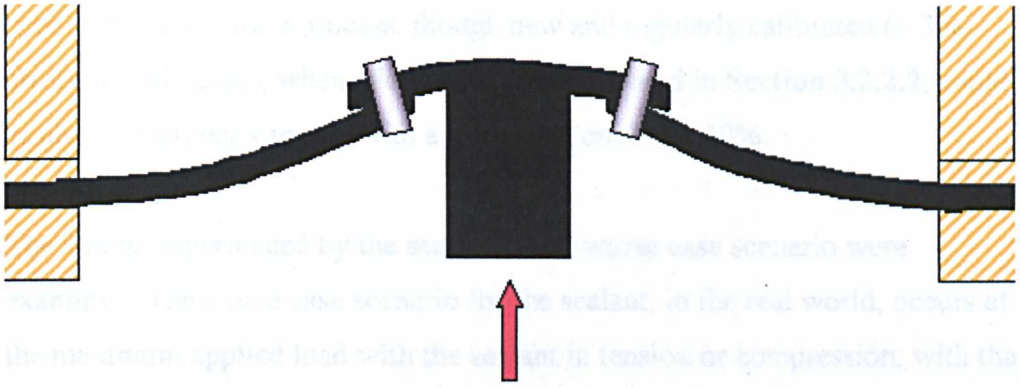

Figure 5.33 Coupon set loaded for sealant joint in tension

From this it can be seen that if the results for the FE results for the joint in compression and the strain gauge reading results are compared they give similar stress and strain characteristics. However, the results for the joint loaded in tension are quite different to the experiment.

One thing that the FEA model could predict was the residual stresses caused by the fasteners themselves as they are tightened, with no loads imposed on the coupons. This would have been very difficult to establish using strain gauges because of the almost impossible task of fabricating the coupon set with the strain gauges in position. This is due to the size of the gauges themselves; the position of the gauges between the fasteners (**Fig.5.13**) and the, very, high risk of contaminating the gauges with the polysulfide sealant and/or damaging them in the fabrication of the coupons.

The FEA model where the clamping force is increased by 100 % is unrealistic and could only be carried out in the virtual world of the FE model. However, the 10% increase in fastener force did give better results. This could be the result of several differences between the experimental coupon set and FE model. The experimental coupon set is held together with fasteners with a different head area for the nut and screw. However, in the FE model the fasteners' nut and screw head are both the same size. Another factor that could introduce residual stress is that the fasteners in the experimental coupon set are an interference fit; this means that they will cause a certain amount of distortion to the coupons in the fabrication stage. Finally, the torque wrench

used in the fabrication process, though new and regularly calibrated (± 3% error on load range), when added to the factors listed in **Section 3.2.2.2**, could easily be applying a torque with a margin of error of ±10%.

The strains experienced by the sealant in the worse case scenario were examined. The worse case scenario for the sealant, in the real world, occurs at the maximum applied load with the sealant in tension or compression, with the temperature at -55°C. At this temperature the Modulus of the sealant can increase from approximately 2.52 MPa at 23°C (an average taken from sealant testing, see **Chapter 8**) to 1GPa, or more, at -55°C (Healey, 1996). This means that the sealant turns from an elastomer capable of quite high movement capability (>400% at 23°C (Naftoseal, 1998)) to a material that is below its glass transition temperature (T_g) where its movement capability is reduced dramatically (at best less than 300% but could be as low as 25% (Healey, 1996).

If **Figs 5.30 & 5.31** are examined, they are very similar in their characteristics. With the sealant joint in tension, where the sealant is in contact with the jet fuel, on the outside of the joint (20mm), the maximum strain is slightly greater than 1.5%. With the sealant joint in compression the maximum strain in the same area is, again, slightly greater than 1.5%. It was noted above that the FE results from the models where the sealant joint is in tension should be treated with caution.

The proportioned stress results shown in **Fig. 5.22** would suggest that the stresses recorded in the experiment are about 50% greater than those predicted in the FEA. This would suggest that the proportions of the strains would be the same, meaning that the strain of ≈1.5% should be increased by the same factor to achieve parity with the experiment. This would increase the maximum principal strain to ≈2.25%. Even this strain of ≈2.25% is well below the movement capabilities of even the sealant at -55°C.

Another important factor that should be mentioned is that the principal strains were taken from the centre line of the sealant joint and this is not the area

where the greatest strain is experienced, which is actually at the ends of the sealant joint at the sealant-substrate interface. However, in examining the FE results it was found that the increase in strain at the sealant-substrate interface was negligible and so it was felt that the use of the centre line for the strain readings was acceptable and a lot easier to collate.

If all of the above observations are examined, they would suggest that the sealant does not necessarily fail due to excessive strain and the reasons for the fuel leaks may be attributed to other factors.

5.9.7. Conclusions

The results from the FE analysis of the MSS coupon set would seem to suggest that:

- Care must be taken in the construction of the model within the FE program to ensure that compromises, simplifications and assumptions are reduced. Their effects must be recognised as such, with the subsequent results used only as an indicator.
- The coupon configuration chosen (both coupons 3.18mm thick) would appear to provide the optimum results.
- The sealant does not appear to fail due to excessive strain under the maximum load conditions.
- More work should be carried out separating the coupon set into the various components (model the fasteners, the coupons and the sealant interfay joint as separate components and establish more accurate sealant specifications from experiments) within the FE model to produce more comprehensive information (this was beyond the scope of this project in both time and financial expenditure).

6 Mechanics of the system

Introduction

This section describes the main mechanical parts of the MSS and their function within the MSS structure. The engineering drawings for the main components of the MSS can be found in **Appendix 9**.

6.1. Test coupon set

The test coupon set comprises two circular plates that are fastened and sealed. A mechanism was developed that subjects a circular lap joint to cyclic axial stresses whilst simultaneously imposing a range of experimental parameters. The whole assembly is located within a closed circular chamber or "pressure pot". The circular lap joint is assembled using aerospace fasteners and sealed, and it simulates a wing skin butt-strap joint in a real aircraft. However, by making it circular the complications of corners and joint-ends are eliminated **(Fig.6.1).** The test sealant is sandwiched between the two bolted aluminium circular coupons of dissimilar size **(Fig. 6.2)** mounted concentrically. The two discs are attached to each other utilising twelve, 3/16" titanium fasteners (ASNA 2027HK3-4) and nuts (NSA 5474-3K7). The sealant used was Chemetall MC238B2. Sealant may be used in the test joint as required, for example, interfay plus overcoat with no fillet or only fillet and no interfay, etc.

The details of the fastening and sealing (interfay, fillet, and overcoat) represent variables that can be changed to suit any particular test.

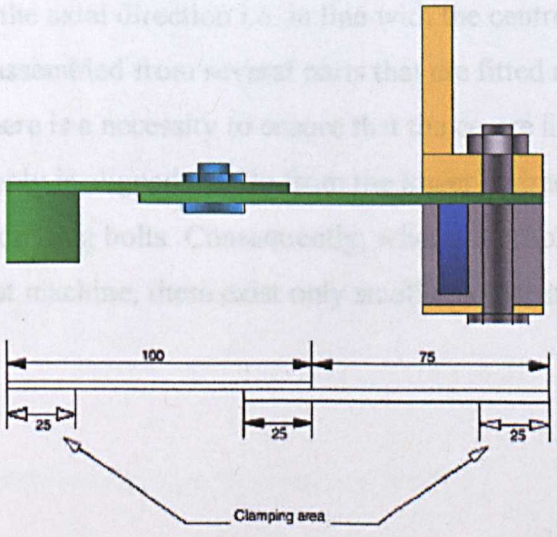

Figure 6.1 The similarity of the test coupon joints (top) to a lap joint.

A hub in the centre coupon is attached to a device that provides cyclic axial loading. In early prototypes it was found that the centre coupon needed to be reinforced in the centre to avoid deformation due to the localised loads imposed by the fatigue machine. Early prototype inner coupons consisted of an aluminium 2024 T3 circular plate with a diameter of 104 mm and 3.18mm thick. An aluminium centre hub was attached to the centre coupon using 3M 9323 structural epoxy adhesive. A problem with this arrangement is that it wouldn't allow the centre hub to be loaded in tension because adhesives, especially at low temperatures, can be weak when loaded in tension. This was later changed to an integral inner coupon/centre hub assembly **(Fig.6.2)**, again manufactured from a single block of aluminium 2024 T3 measuring 105mm x 105mm x 26mm. This enables loads to be applied in tension and in compression, as well as in torsion if required. Another important factor is the inclusion of a radius between the centre hub and the coupon to reduce the stress concentration that exists at this point if loaded in tension **(Fig.6.2 arrow)**. The first fatigue test coupon set failed because the radius was not included and the result was that the centre hub was pulled from the inner coupon in tension, leaving a large circular hole in the small coupon. The inner coupon is prepared to the same standards as those of the full size aircraft (i.e. cleaned degreased, deoxidised, anodised and painted). The outer circular coupon is unchanged from the early prototypes.

To get reliable test results, in fatigue, the only load that should be imposed on the coupons is in the axial direction i.e. in line with the centre of the coupons. As the test rig is assembled from several parts that are fitted together with slide fit clamp bolts, there is a necessity to ensure that the centre line of the pressure pot/coupon assembly is aligned axially from the lower hydraulic ram through to the load cell mounting bolts. Consequently, when the whole assembly is attached to the test machine, there exist only small residual stresses in the sealant joint.

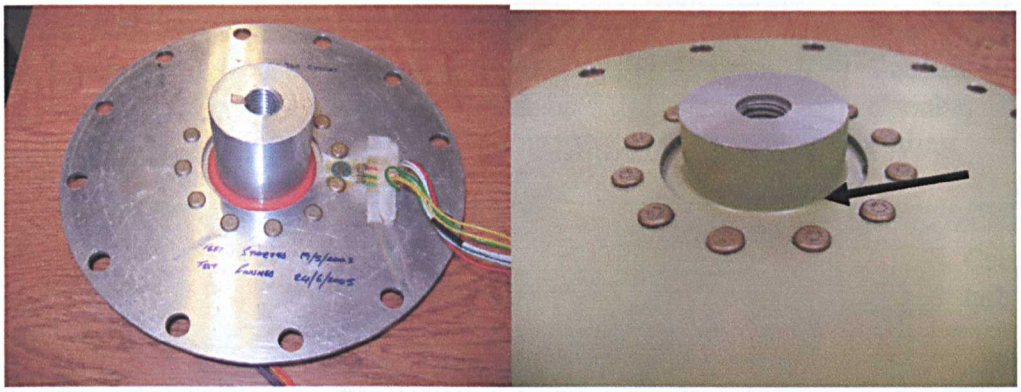

Figure 6.2 Prototype coupon set with a bonded centre hub (left) and the later integral inner coupon/centre hub assembly (right). The arrow illustrates the position of the 2mm radius.

A schematic cross section through the pressure pot assembly is shown in **Fig.6.3.** The test coupon set can be seen towards the bottom of the figure. The actual components are shown in **Fig. 6.4.**

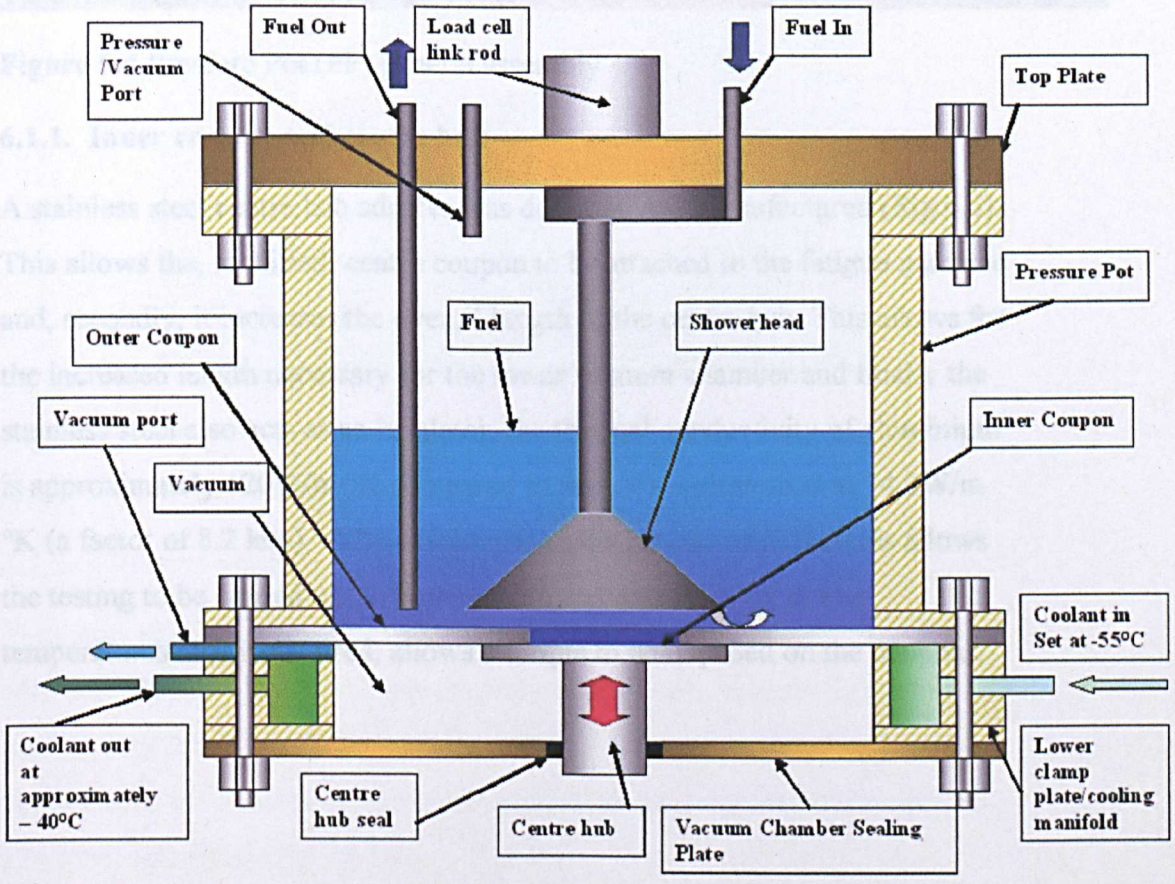

Figure 6.3 Cross-section through the Pressure Pot (PP).

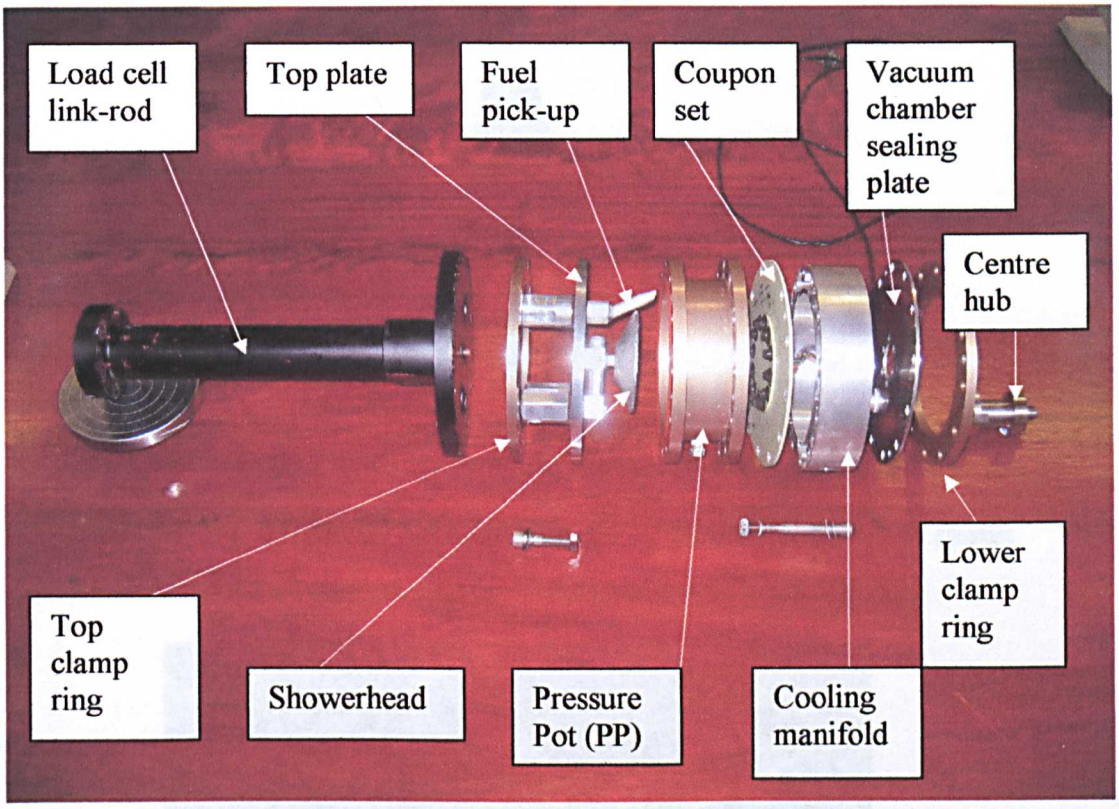

Figure 6.4 Pressure Pot (PP) general assembly

6.1.1. Inner coupon and centre hub

A stainless steel centre hub adapter was designed and manufactured **(Fig.6.5).** This allows the, modified, centre coupon to be attached to the fatigue machine and, secondly, it increases the overall length of the centre hub. This allows for the increased length necessary for the lower vacuum chamber and finally the stainless steel also acts as an insulator; the thermal conductivity of aluminium is approximately 120W/m °K compared to that of stainless steel at 14.6W/m °K (a factor of 8.2 less). The advantages to the project were that this allows the testing to be carried out in both tension and compression at low temperatures and, if required, allows a torque to be imposed on the coupons.

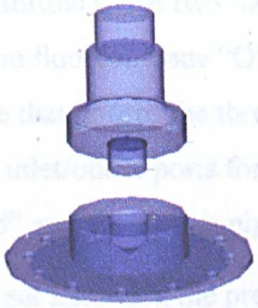

Figures 6.5 Modified inner coupon and stainless steel centre hub.

Fig. 6.6 shows the coupon set being aligned during assembly. This also shows the showerhead, the alignment pins (arrowed) and the silicone "O" ring.

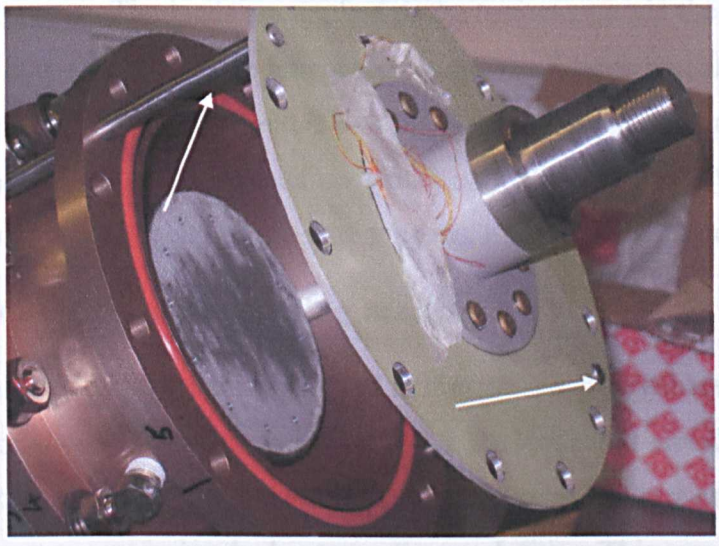

Figure 6.6 The coupon set (including the modified inner coupon and centre hub) being aligned during assembly.

6.1.2. Outer coupon

The outer circular coupon is unchanged from the early prototype. It is 216 mm diameter, with a 64 mm diameter central circular hole, fabricated from aircraft quality 3.18 mm thick aluminium sheet (2024-T3 clad) prepared to the same standards as those of the full size aircraft (i.e. cleaned degreased, deoxidised, anodised and painted).

6.2. Pressure pot

The test coupon set is mounted as the base of a "Fuel Tank" or Pressure Pot (PP) that is structurally stiff and filled with jet fuel **(Fig.6.4).** The pressure pot

has a bolted flange at either end for the top plate and the coupon set (and the lower clamp plate /cooling manifold). The two flanges have a machined groove to accommodate a large fluorosilicone "O" ring at each end. The top of the tank is an aluminium plate that houses the three ports (one for pressure/vacuum and the two inlet/outlet ports for the test fluid). From beneath the top plate the "Showerhead" and the pickup pipe are fastened **(Fig.6.4).**

The top plate and the coupon set sandwich the pressure pot. They are secured by two sets of 12 x 10mm nuts and bolts and sealed by the two fluorosilicone "O" rings. The whole assembly is then mounted in a fatigue test machine. One end of the test rig is supported rigidly to the test frame end plate (load cell) via the link-rod and the thick steel top plate, whilst the other end is free to deflect (the actuating ram). The loads are applied to the test coupon via the stainless steel centre hub. One end of the hub is attached to the fatigue machine actuating ram, whilst the other end is screwed into the hub of the smaller inner coupon. The typical maximum load applied is only 5kN, or about 5% of the maximum load cell capacity of the stiff frame of a Mayes fatigue machine.

6.3. Lower clamp plate/cooling manifold

A Julabo refrigerated circulator was used to impose the different temperature regimes upon the test coupons **(see Section 7.2 Refrigerated circulator)**. It is necessary to enable the coolant from the circulator to be in direct contact with the test coupon to maximise the heat transfer capabilities. This was achieved by manufacturing a lower clamp plate/cooling manifold **(Fig. 6.7)**. The whole assembly is shown in **Fig.6.8**.

The manifold was machined from one piece of aluminium. Aluminium was chosen for two reasons. Firstly, to ensure that the materials used in the pressure pot assembly (including the coupons) must be made only from materials used in the full size wing, reducing the effects of galvanic corrosion and any other related problems. Secondly, aluminium exhibits a high degree of thermal conductivity (approximately 120W/m °K); this means that heat from the MSS, and in particular the coupon set, can be conducted away quickly. The manifold consists of a square section, doughnut shaped ring with a deep groove machined into the top side. The top of the groove is sealed by the outer

coupon itself using Loctite 518 sealant. Loctite 518 is a single component, anaerobic sealant that was used instead of a gasket to ensure maximum heat transfer. The coolant is introduced to the groove via an insulated hose through a drilling in the outer wall. The coolant has to travel around the groove, because of a machined plug in the groove, and flows back out of another drilling and back to the circulator via the coolant flow control solenoids and another insulated hose. The coolant flow control solenoids divert the coolant, either back to the circulator directly or through the coolant/fuel heat exchanger. The lower end of the lower clamp plate/cooling manifold is sealed by an aluminium plate with a vacuum hose attachment and a boss attached to the centre with two "O" ring seals through which the stainless steel centre hub is located. The two "O" rings seal the chamber, allowing it to serve as the vacuum chamber beneath the test coupon set.

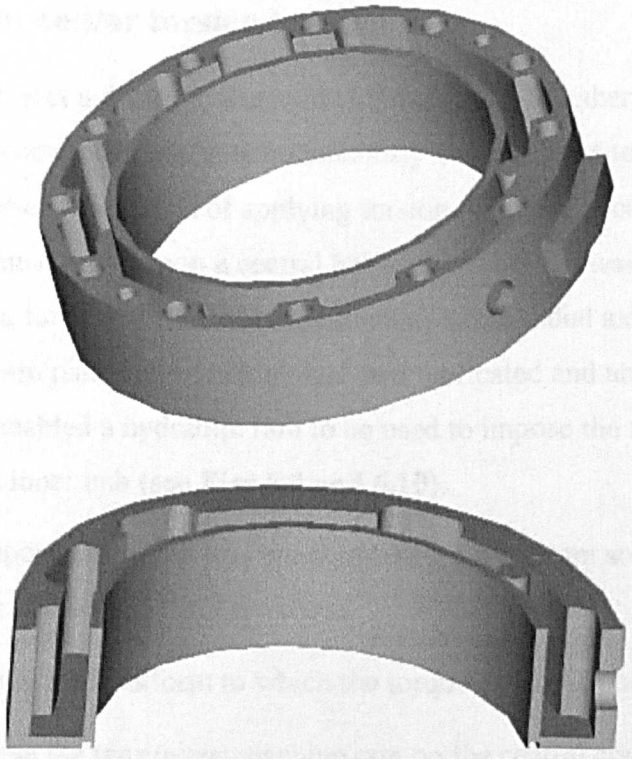

Figure 6.7. Modified lower clamp plate/cooling manifold. The bottom section sketch shows the depth of the coolant groove and the groove for the "O" ring that seals the vacuum chamber.

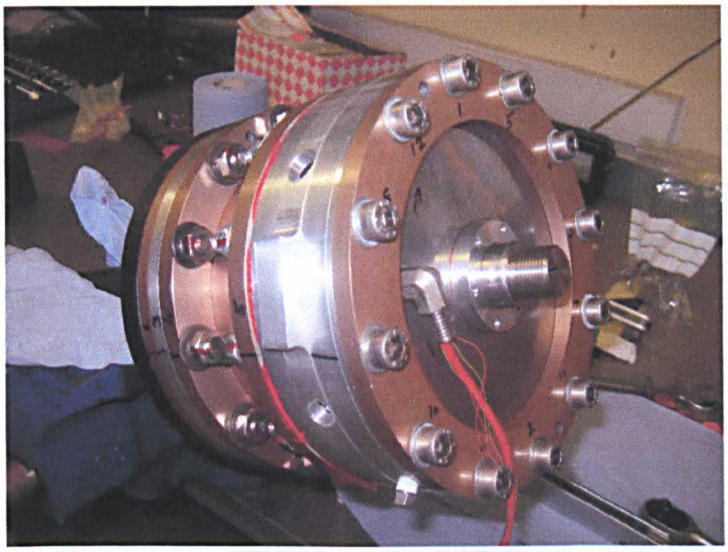

Figure 6.8. Modified lower clamp plate/cooling manifold in position on the pressure pot assembly. The lower vacuum plate and centre hub seal housing can also be observed along with the vacuum outlet and the thermocouple leads.

6.4. Tension and/or torsion loading

Early in the project a decision was made to investigate whether applying torsion to the coupon set whilst simultaneously being subject to axial fatigue could be achieved. A method of applying torsion to the inner coupon was required. To the inner coupon a central hub and torque arm was fabricated and attached, and a force was applied perpendicular to the radial axis of the coupons. A base plate and reaction plate was fabricated and attached to the test rig. This enabled a hydraulic ram to be used to impose the force, in torsion, to the inner hub (see **Figs 6.9 and 6.10**).

The inner coupon centre hub was attached using 5 No. 8mm socket head screw fasteners. The hub served three purposes:

- To provide a stiff platform to which the torque arm could be attached.
- To centralise the tensile test machine ram on the central coupon.
- To stiffen the central coupon to enable more force to be applied to the joint

The coupon assembly was then attached to the mild steel base and secured using 8 No. 16mm steel nuts and bolts, tightened to 40Nm.

The whole assembly was then fitted to a Nene universal test machine and the load applied. Stress concentrations will exist between the drilled holes for the fasteners. This is where the rectangular rosette strain gauges were bonded. The consequent strain was obtained from the strain gauges and from these strains the principal strains and their directions, and hence the stresses, were calculated. This investigation was carried out very early in the project and the pressure pot hadn't been fabricated at this point.

Figure 6.9. The second prototype in the "Nene" test machine. The hydraulic system can also been seen along with the switch unit and strain gauge meter.

Figure 6.10. The test rig in the "Nene" test machine. (Showing the test rig configured for applying torque).

There were several reasons why this avenue of testing was not followed, the main one being financial. The fatigue machine required would need to be of a bi-axial type that cost £70k to £90k at 2006 prices. However, there is no reason why a bi-axial load could not be applied to the test coupon in the future.

7 Environmental and control system

7.1. Introduction

The Model Sealed System (MSS) can be thought of as a modular test system that can simulate a combination of structural loading, fuel inertia, tank pressures, thermal and chemical effects. The general layout of the MSS, complete with control system and the various components involved with the environmental system, is shown in **Figure 7.1.**

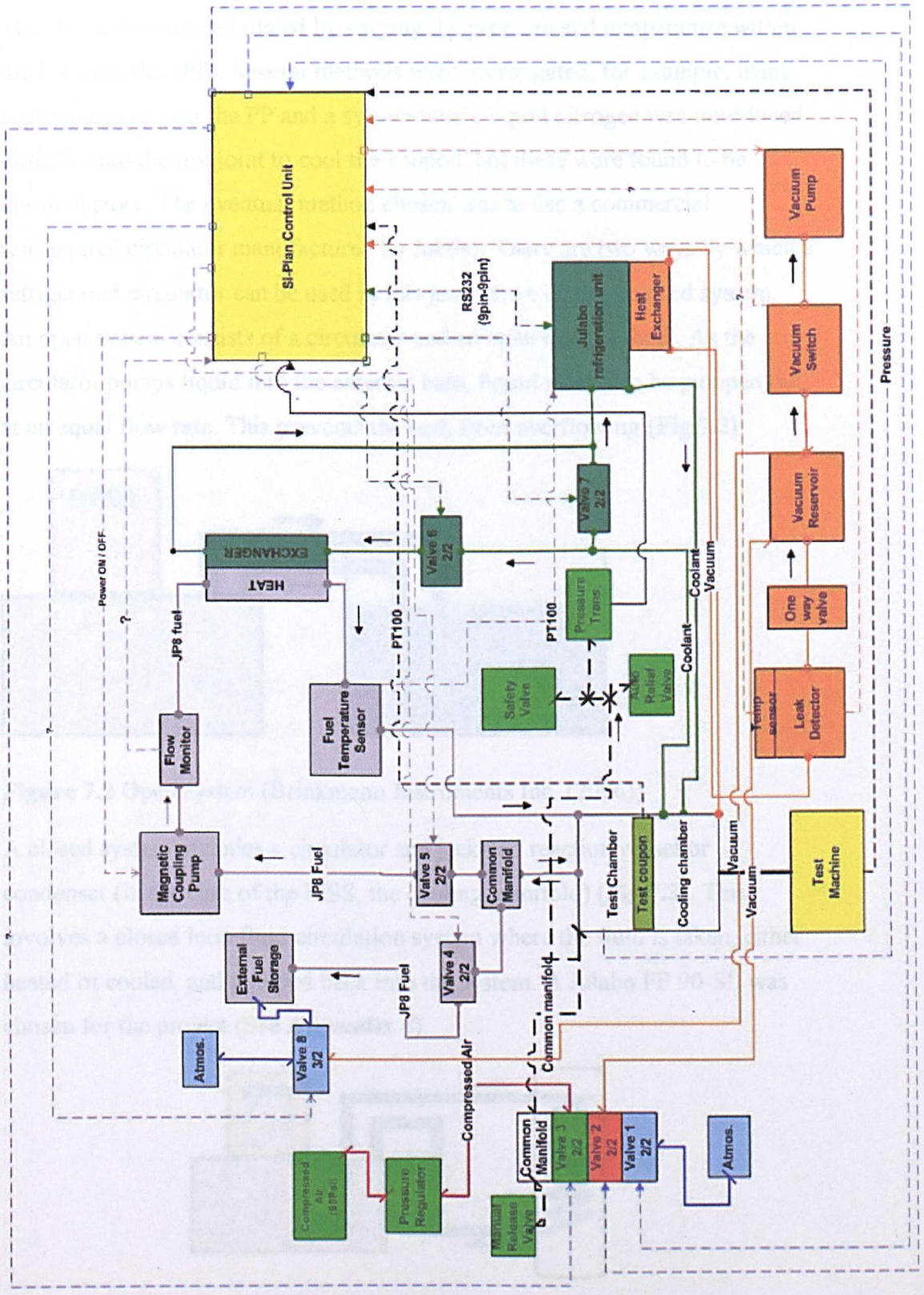

Figure 7.1 The components of the Model Sealed System (MSS)

7.2. Refrigerated circulator

Thermal effects are simulated by varying the pressure and temperature within the Pressure Pot (PP). Several methods were investigated, for example, using heating tape to heat the PP and a system where liquid nitrogen was introduced directly onto the test joint to cool the coupon, but these were found to be unsatisfactory. The eventual method chosen was to use a commercial refrigerated circulator manufactured by Julabo. There are two ways by which a refrigerated circulator can be used in this project; an open or closed system. An open system consists of a circulator and an open external bath. As the circulator pumps liquid into the external bath, liquid must also be pumped out at an equal flow rate. This prevents the bath from overflowing **(Fig.7.2)**.

Figure 7.2 Open system (Brinkmann Instruments Inc. (2006))

A closed system includes a circulator and jacketed reaction vessel or condenser (in the case of the MSS, the cooling manifold) **(Fig.7.3)**. This involves a closed loop fluid circulation system where the fluid is taken, either heated or cooled, and pumped back into the system. A Julabo FP 90-SL was chosen for the project **(See Appendix 4)**.

Figure 7.3 Closed system (Brinkmann Instruments Inc. (2006))

Heating and cooling bath/circulators are the most versatile because of their wide temperature range and their ability to change temperature quickly. Besides choosing a unit that meets the required temperature range, a critical specification is cooling capacity. In general, the higher the cooling capacity the better. A large cooling capacity bath/circulator will be able to reach low temperatures much faster than a small cooling capacity bath/circulator (Eble, 2001). Additionally, a large cooling capacity bath/circulator may not cost much more than a small cooling capacity bath/circulator. This means that for a small amount of extra money, it may be possible to cool two or three applications with one larger cooling capacity unit against one application with a smaller cooling capacity unit. This can save time but, more importantly, may also be a factor when the heating and cooling cycle for aviation fuel is addressed using, possibly, a synchronized array of Model Sealed Systems.

A powerful refrigeration system was chosen, not only to achieve -50°C, but also to compensate for the additional energy generated by the pump. The Julabo FP90-SL is capable of raising the temperature to 100°C (**Fig. 7.4**) **(Note: the Thermal HY bath fluid (a thin HC based fluid), used in the Julabo, has a flash point of 62°C**). This means that the same system that is used to cool the MSS can also be utilised to heat up the MSS. However, there is a downside to using the Julabo in this manner. The Julabo's bath fluid capacity is 22 litres. If the temperature of this fluid is brought up to 50°C, by the Julabo, to heat up the MSS and then the Julabo is used to bring the temperature down to -50°C, the time taken (and the energy wasted) is increased considerably.

Figure 7.4 The Julabo FP90-SL

Another important factor in choosing a bath/circulator is the pumping capability. There are two specifications of importance: pump flow and pump pressure. Most manufacturers specify flow rates with zero back pressure i.e. fluid flows directly out of the pump with no tubing or anything else connected to it. This is not a real-world situation. As back pressure to a pump increases, the flow will decrease. Therefore, it is important that a bath/circulator with a high pump pressure capability is chosen.

The first method considered of applying temperature involved the use a plate heat exchanger that incorporated two circuits. The primary circuit would be connected to an appropriate refrigerated circulator which would cool and circulate an appropriate thermal fluid (Julabo's Thermal HY fluid) at temperatures down to -50°C. The secondary circuit would then have to be connected to a pump which would circulate the aviation fluid through the test rig and out and around to the plate heat exchanger.

The second method considered involved directing the heat/cold fluid directly at the area of interest on the coupon & immediate surroundings **(Fig.7.6)**. The

eventual method chosen involved both of these systems, the use of a heat exchanger and directing the heat/cold fluid directly at the coupon & immediate surroundings by redesigning the lower parts of the pot to act as a heat exchanger and also use the fuel as a re-circulating coolant directed at the coupon **(see Section 7.3)**.

A cross section through the prototype Pressure Pot assembly (without the cooling manifold or vacuum chamber) is shown in **Fig.7.5.** The modified Pressure Pot incorporating the cooling manifold and vacuum chamber is shown in **Fig.7.6**.

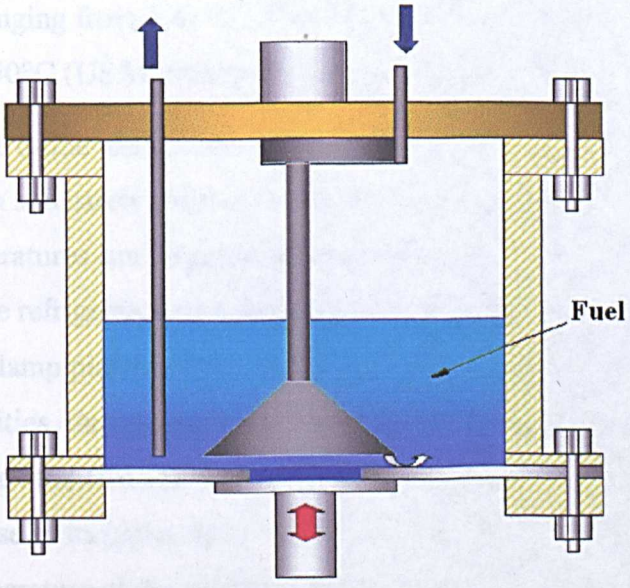

Figure 7.5 The MSS before environmental modifications

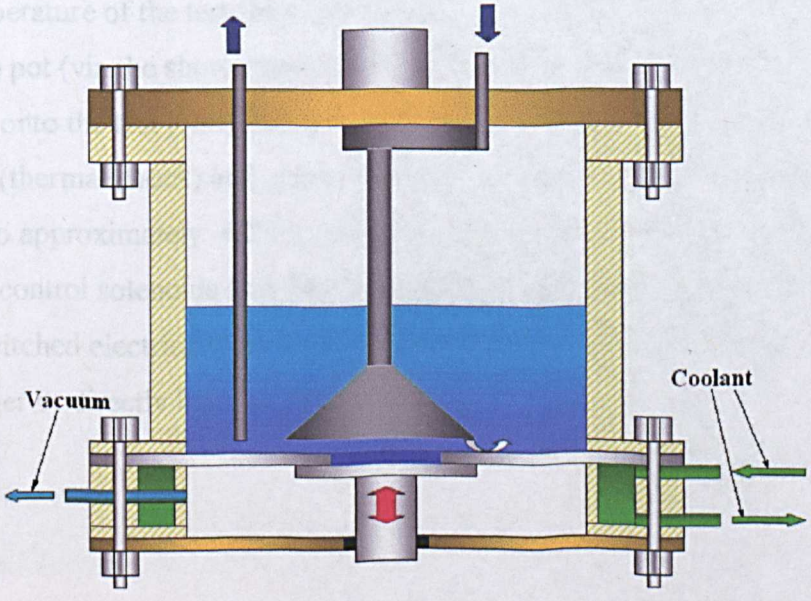

Figure 7.6 The MSS incorporating the new environmental modifications.

7.3. Temperature control

To carry out an evaluation of sealant materials for aircraft it is necessary to expose the sealed joint system to typical dynamic and environmental parameters representative of actual flight conditions. If the test coupon is tested at or near its T_g (glass transition temperature (see **Section 4.3.4**)) the sealant will no longer behave as an elastomer, where it will be able to flex and still maintain its ability to seal, but will behave like a very stiff gasket where the sealant will not be able to perform as it was designed to do and leaks may occur. This means that the coupon set needs to be able to experience temperatures ranging from – 41°C (A340-600, 40000-42000ft, Mach 0.83) to approximately 50°C (USAF transport) (Buller, 2002).

The temperature of the test coupon set is controllable from approx. -60°C to 50°C (for health and safety reasons the maximum temperature is set at 30°C). Different temperatures can be generated at different times in the test cycle. The coolant from the refrigerated circulator flows through a heavily insulated hose into the lower clamp plate/cooling manifold **(Fig. 7.6).** To maximise the heat transfer capabilities, the coolant from the circulator is in direct contact with the test coupon. The modified lower clamp plate/cooling manifold acts as a large heat sink because of its high rate of thermal conductivity, and this helps to reduce the temperature of the pressure pot and test fluid quickly. To speed this up, returning coolant is diverted through a heat exchanger. This in turn lowers the temperature of the test fluid (JP8) which, when pumped back into the pressure pot (via the showerhead attachment that directs the cold test fluid directly onto the test joint), helps to reduce the temperature of the test joint quickly (thermal shock) and generally lower the temperature of the MSS (down to approximately -40°C). This is controlled by a diverter manifold with coolant control solenoids (see **Fig.7.7, valves 6 and 7)** that enables the coolant to be switched electrically by the controller to flow, either through the heat exchanger or directly back into the Julabo.

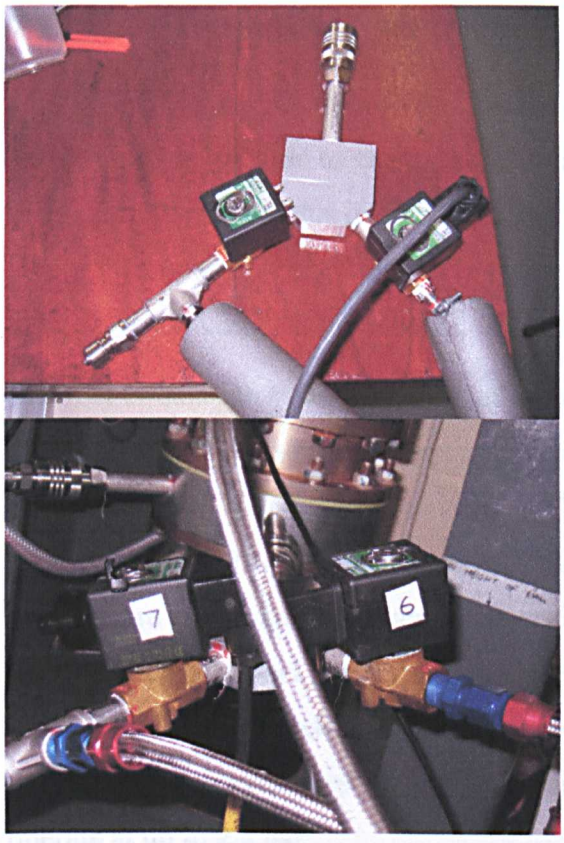

Figure 7.7 Coolant control solenoids (**valves 6 and 7**) and manifold.

The temperature of the sealed joint is taken from a PT100 temperature sensor attached to the coupon at the test joint (**Fig 7.8**). The temperatures are recorded on the data logging facility of the Si-Plan controller.

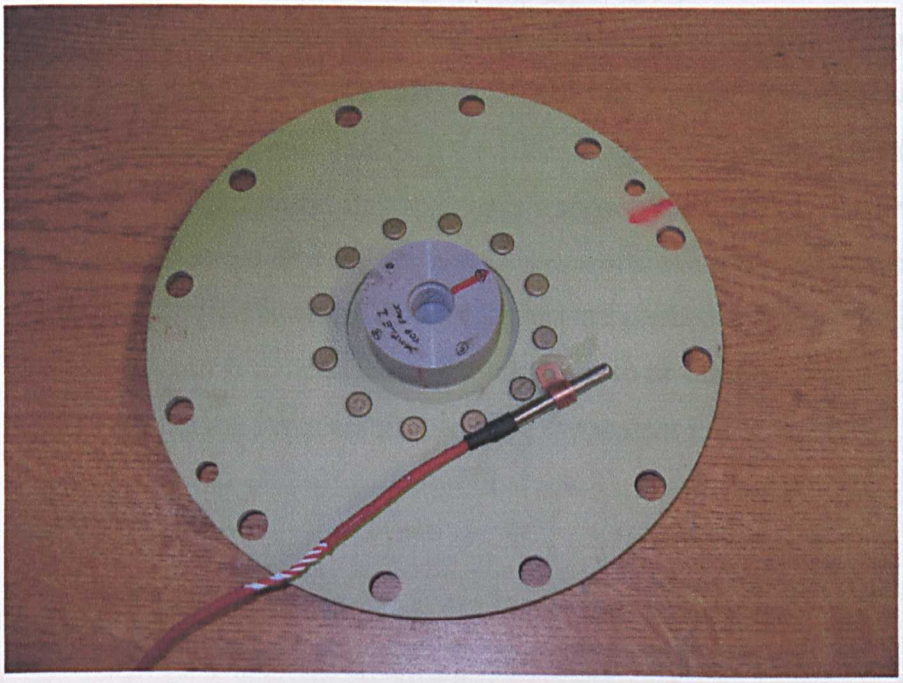

Figure 7.8 PT100 temperature sensor location.

7.4. Fuel circulation system

A pumping system was used to introduce cold fuel directly on to the test joint and to circulate the fuel to generate wet and dry cycles into the MSS test spectrum. To achieve this it is necessary to have the ability to completely empty the pressure pot of fuel and to pump the fuel through a heat exchanger to use a proportion of the Julabo's cooling medium to cool the fuel.

The fuel circulation system consists of the fuel flow control solenoid valves that divert the fuel to either the external fuel tank or via the magnetic coupling fuel pump and "Rotorflow" visual/digital flow meter, through the coolant/fuel heat exchanger where the temperature of the fuel is logged with a PT100 temperature sensor and back into the pressure pot via the showerhead. For safety reasons, the fuel hoses used are Speed-Flex Teflon-lined stainless steel braided hose with Speed-Seal threaded aluminium hose ends. All components have to be able to withstand the system pressure, typically 1 bar but able to operate at up to 2.2 bar.

7.4.1. Showerhead

The system allows approximately 1.5 litres of JP8 jet fuel to be circulated. The top plate of the pressure pot has ports for fuel inlet and outlet plus a port for air pressure or vacuum. The outlet port has a pick-up pipe attached that is situated just above the coupon set whilst the inlet port has a "Showerhead" that is situated over the coupon test seal **(Fig. 7.9).** The concept of the "Showerhead" is to "crash" cool the joint and fill the MSS rapidly. The "Showerhead" is a small, flat, circular vessel that looks like a showerhead, with the outlet (the base) for the test fluid being the same dimensions as a small coupon and rotated by 15° (the fasteners in the coupons are pitched at 30° intervals) . This enables the cold JP8, from the heat exchanger, to be directed onto the area (land) between the fasteners thus cooling the sealant joint quickly.

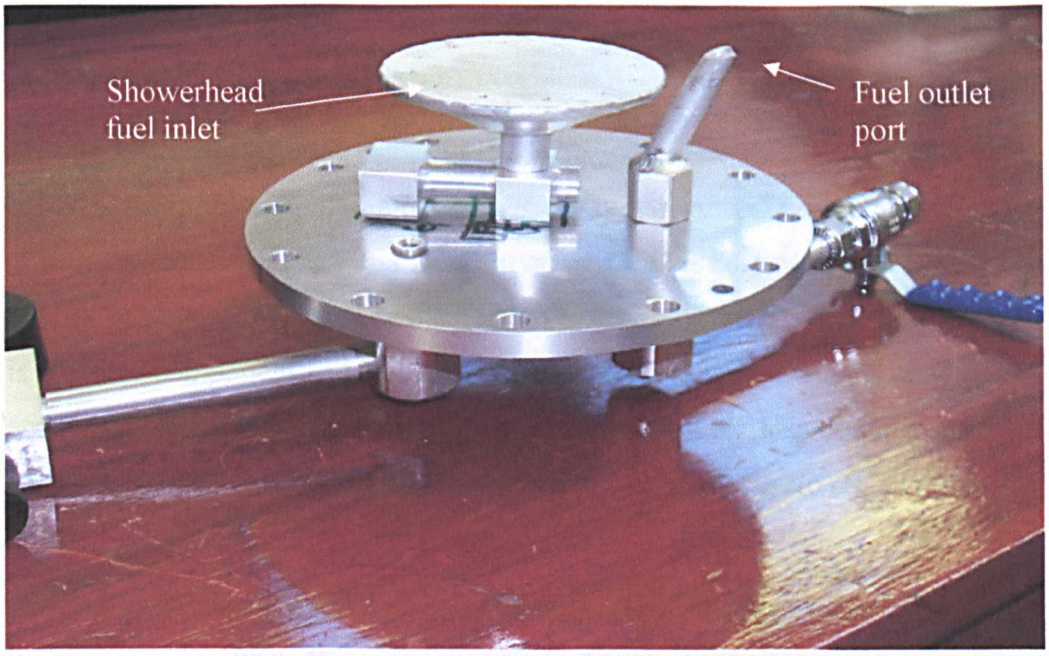

Figure 7.9 Showerhead assembly attached to the top plate

7.4.2. Magnetic coupling pump

Several types of pump were considered. Peristaltic pumps and diaphragm pumps were investigated for their suitability. Watson-Marlow Bredel are the world's largest manufacturer of peristaltic pumps, tube pumps and hose pumps. Watson-Marlow Bredel were approached and the temperatures that would be utilised in the test routine were disclosed to them, but they stated that their pumps, or rather the hoses used, would not be able to operate at sustained temperatures of –50°C reliably.

KNF Neuberger manufacture a range of diaphragm pumps and vacuum systems. Unfortunately, as before, when KNF Neuberger were approached and the temperatures that would be utilised in the test routine were disclosed to them they stated that the diaphragms in their pumps, again, would not be able to operate at sustained temperatures of –50°C reliably.

Many pumps utilize a dynamic seal on the pump shaft. These types of seals, either mechanical seal or packed glands, rely on the control of fine clearances to minimize pump leakage. However, these seals require cooling and lubrication across the seal face. This cooling is often provided by a controlled leak of the process fluid, resulting in environmental contamination or

contamination of the process fluid. Dynamic seals also convert friction to heat. In the MSS this is not be desirable.

Micropump manufacture a reliable "leak-free" magnetic coupling pump **(Fig. 7.10)**. A magnetic coupling pump consists of two magnets, a drive magnet that attaches to the motor shaft and a driven magnet that is completely sealed within the pumphead and is connected to the driving gear. The driven magnet is a wetted component and is totally encapsulated. The two magnets couple automatically such that the drive magnet turns the driven magnet and gears without physical contact. This means that there are no dynamic seals in the pump.

Decoupling occurs when the pump load exceeds the coupling torque between the two magnets. This feature can act as a safety device to prevent damage to the pump and motor as well as associated piping. The magnets can be recoupled by bringing the motor to a complete stop, then eliminating the cause of the decoupling and restarting. This was the pump that was decided upon.

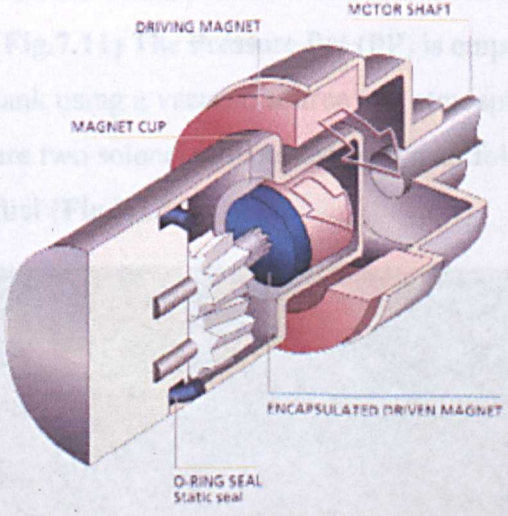

Figure7.10 The working principles of a magnetic coupling pump (Micropump).

The specifications for the series 101 Micropump are:

- Flow Rate Range 0 to 28 l/min
- Temperature Range, Pump Seal -50°C to 176°C.

There are a couple of relatively small drawbacks with these types of pump. The first is that they cannot draw fluid from dry, in other words they need priming with fuel. The second is that although the quoted head capability is 10 metres for this pump, it has been found that the pump works more efficiently with as little head as possible. To overcome the first problem a priming sub-programme can be inserted in the test programme that involves applying system pressure to the fuel inside the PP for 18 seconds; applying system vacuum to the external fuel tank and opening valve No.4. for 2 seconds; then immediately opening valve No.5 and circulating the fuel using the pump. The second problem is overcome by ensuring that all of the components within the fuel circulation system are at the same level, thereby reducing the head as much as possible.

7.4.3. External fuel tank

It is necessary for the Pressure Pot (PP) to be emptied of fuel to allow for a drying cycle. An auxiliary fuel tank was designed and manufactured along with the various connections and fitted to the Model Sealed System (MSS). **(Fig.7.11)** The Pressure Pot (PP) is emptied and refilled from the external fuel tank using a vacuum source and atmospheric pressure with no problems. There are two solenoids mounted on a manifold that control the empty /fill flow of fuel **(Fig.7.12).**

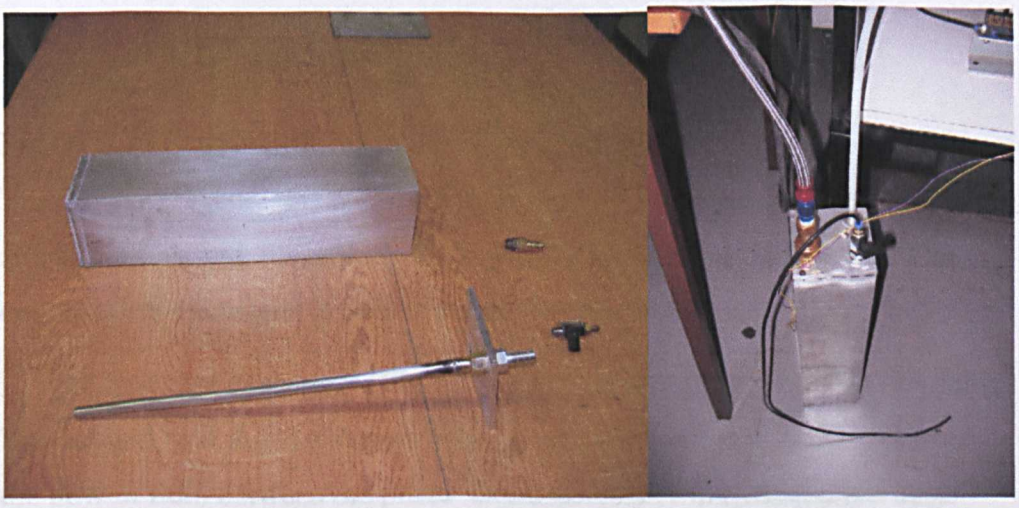

Figure 7.11 External fuel tank components (left) and in situ (right).

Figure 7.12 Fuel control solenoids (**No. 4 and 5**) and manifold.

7.4.4. Heat exchanger

A heat exchanger utilizes the fact that heat transfer occurs when there is a difference in temperature. In a heat exchanger, there is a cold stream and a hot stream. The two streams are separated by a thin, solid wall **(Fig 7.13).** The wall must be thin and conductive in order for heat exchange to occur, but the wall must be strong enough to withstand any pressure by the fluid.

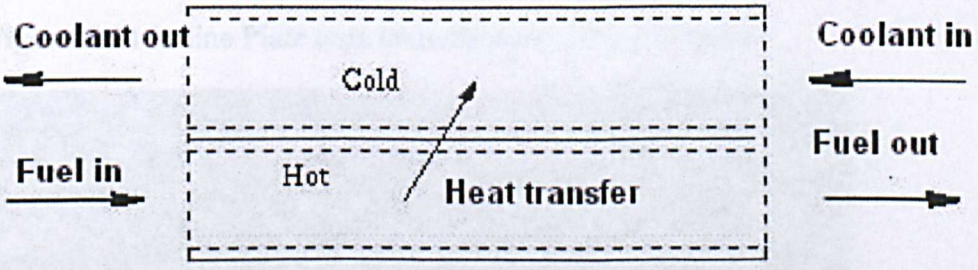

Figure 7.13 Simple flow diagram showing heat transfer in a heat exchanger. This flow arrangement is called **counter-current**. If the direction of one of the streams is reversed, the arrangement is called **co-current** flow. A **counter-current** heat exchanger provides more effective heat transfer.

A plate type heat exchanger **(Fig.7.14)** consists of plates to separate the fluids. The hot and cold fluids alternate between each of the plates. Baffles control the flow of fluid between the plates. Because each of the plates has a large surface area, there is an extremely large heat transfer area. This means that a plate type heat exchanger, as compared to a tube and shell type, is capable of transferring much more heat. This high heat transfer efficiency means that

plate type heat exchangers are usually (i) very small and (ii) a lot cheaper than their tube and shell counterparts. **Figure 7.15** shows the plate type heat exchanger as used on the MSS.

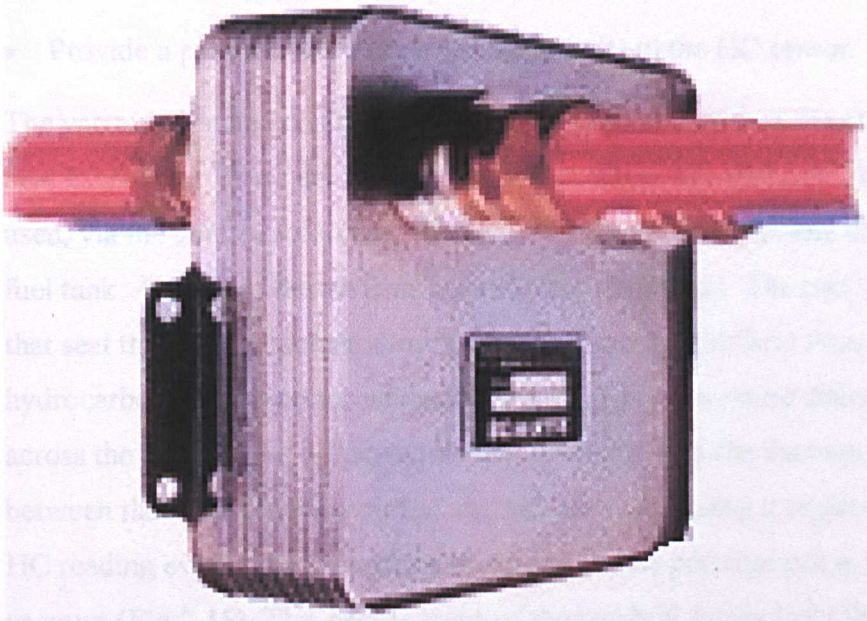

Figure 7.14 In-line Plate type manufactured by E.J. Bowman.

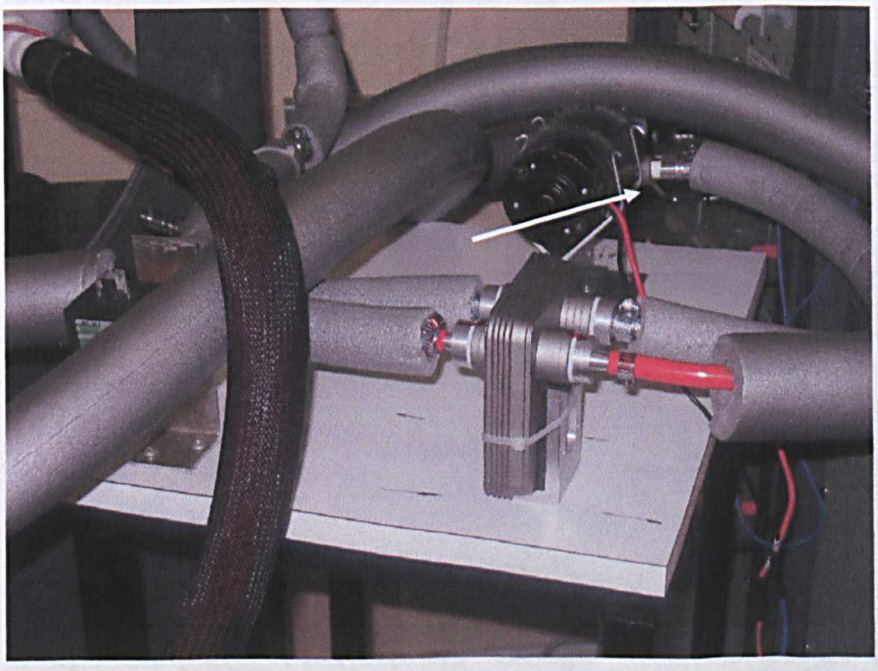

Figures 7.15 The In-line plate heat exchanger, with the magnetic coupling "Micropump" in view behind (arrowed), on the fuel circulation system stand.

7.5. Vacuum system

The vacuum system performs several functions:

- Empty/fill the pressure pot and external fuel tank
- Provide a pressure differential across the test joint
- Provide a path for fuel vapour (hydrocarbon) to the HC sensor.

The vacuum system consists of the pump, a control switch, a reservoir and a heat exchanger. There are various ports from where the vacuum is drawn and used, via the control solenoids, to empty/fill the pressure pot and the external fuel tank. Air is also drawn from beneath the coupon set. The two "O" rings that seal the lower chamber allow a certain amount of airflow through the hydrocarbon (HC) detector whilst still maintaining a pressure differential across the joint. There is also a one-way valve fitted in the vacuum hose between the vacuum reservoir and the HC detector to stop it registering a high HC reading every time the external fuel tank or the pressure pot is subjected to vacuum **(Fig 7.16).** This causes some of the residual fumes from the fuel in the pressure pot or external tank to be drawn through the HC detector and these fumes register a leak, thereby stopping the test.

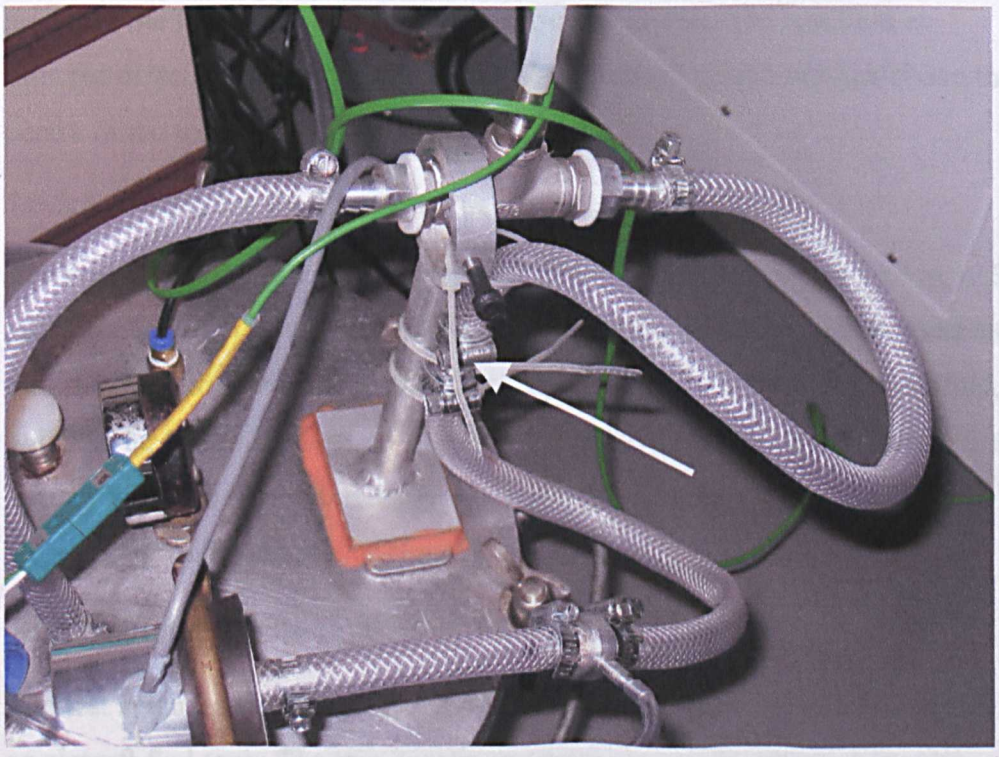

Figure 7.16 The one-way valve (arrowed)

7.5.1. Pressure Pot and external fuel tank empty/fill system

The valves within the MSS are operated via the Si-Plan controller (**see 7.8 Control system**). The basic sequences for filling and emptying the Pressure Pot and external fuel tank are described in the following sections. It should be noted that the valves in the common manifold, the fuel diverter manifold and the coolant manifold are programmed so that only one valve in each component can be ON at one time. The following operations are achieved using only atmospheric pressure and system vacuum. **Figure 7.1** shows the various components in the system.

7.5.1.1. Filling the Pressure Pot

The pressure in the PP is reduced to 20 to 25 in Hg (0.67 to 0.85 bar) by valve No. 3 being ON in the common manifold; this introduces a slight vacuum into the inside of the PP. Valve No.8 is a 3/2 valve **(Fig. 7.17)** that can switch two inlets to a common outlet, in this case switching the common outlet, to the external fuel tank to either atmospheric pressure or system vacuum. Valve No.8 allows atmospheric pressure to act on the surface of the fuel (that has been already filled to the correct level) in the external fuel tank. At the same time valve No.4 will be ON to allow the fuel to flow from the external fuel tank into the PP to the required level, ready for the test. The test fluid is directed directly onto the joint via the "Showerhead" positioned just above the centre of the test coupon.

7.5.1.2. Emptying the Pressure Pot

The pressure in the external fuel tank is reduced to 20 to 25 in Hg (9.8 to 12.3 psi or 0.67 to 0.85 bar) by operating valve No. 8 to introduce a slight vacuum into the inside of the external fuel tank. Valve No.2 in the common manifold, will also be ON to allow atmospheric pressure to act on the surface of the fuel in the PP. At the same time, valve No.4 will be ON to allow the fuel to flow from the PP to the external fuel tank.

7.6. Pressure system

The test apparatus has two chambers which simulate the inside and outside of an aircraft fuel tank. The test coupon forms a boundary between these two

chambers. Fuel inertia and tank pressures can be simulated by introducing a pressurised gas (inert, for safety reasons) into the pressure pot. This acts on the test fluid which stresses the sealant slightly. The more important factor that can be combined with the above is to introduce a slight vacuum into the lower cooling manifold centre chamber, below the test coupons, to simulate the pressure differential experienced by the wing during flight. This would, in effect, pull the fuel through the interfay joint and possibly causing an advancement of a leak path tip.

This is achieved with the use of control solenoids **(Fig.7.17)** that switch either compressed air, atmospheric pressure or vacuum to various parts of the MSS. These valves are also used to empty and refill the pressure pot from the external fuel tank.

Mounting brackets for the new control solenoids were attached to the control solenoids and they, in turn, were attached to the valve stand.

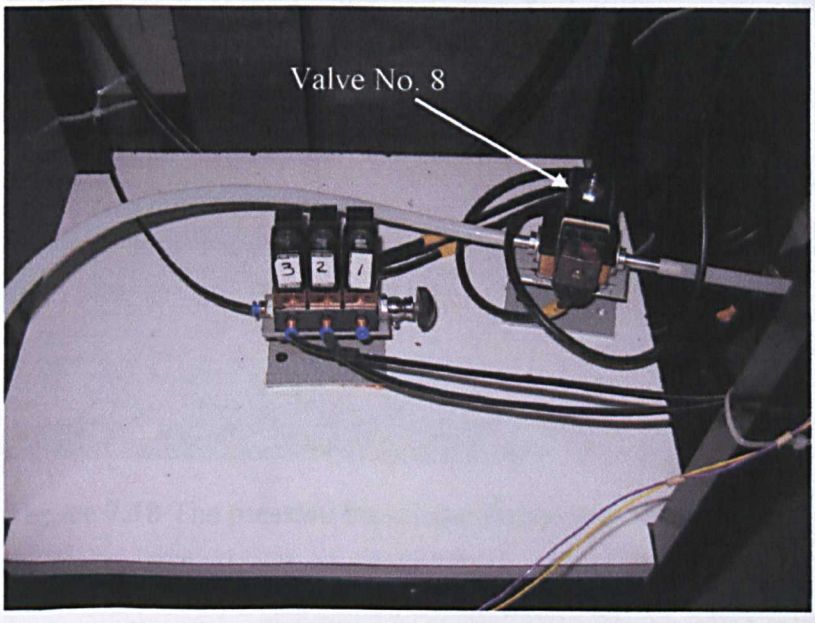

Figure 7.17 Common manifold with atmospheric pressure valve (**No.1**), vacuum valve (**No.2**) and pressure valve (**No.3**) (see **Fig. 7.1**). 3/2 valve **No.8** (arrowed) can also be seen.

Health and Safety issues have been addressed. As well as an automatic safety relief valve, there is a manual release valve and a pressure transducer attached to the Pressure Pot (PP) **(Fig.7.18).** The pressure transducer enables the control system to:

- Monitor and record the pressure within the PP
- Enable a shut down procedure should there be a sudden rise in pressure. This should not happen because of the spring relief valve, but it could ice-up and seize closed
- Enable a comparison to be made between the readings from the pressure transducer and the hydrocarbon (HC) detector. For example, if a leak is detected with the HC detector and, simultaneously, there is a drop in pressure in the PP, it may be possible to dispense with the HC detector system altogether and only use a pressure drop system for leak detection.

Figure 7.18 The pressure transducer (white arrow), pressure indicator (centre), pressure relief valve (bottom) and the supply hose (black arrow).

The pressures can range from 0.85 bar (12.3 psi) to 2.4 bar (35 psi) (gauge pressures). Pressures above atmospheric are set using a Norgren pressure regulator, whilst the pressures below atmospheric are controlled by turning the vacuum pump on/off using a vacuum switch connected to the Si-Plan controller.

7.6.1. Pressure differential across test joint

This is achieved by switching ON valve No.3 in the common manifold, allowing a preset air pressure to act on the surface of the fuel in the PP. Air is also drawn from beneath the coupon set by the vacuum pump via a hose that also draws any leaked hydrocarbon (HC) fumes to the HC detector.

7.7. Hydrocarbon leak detection

The hydrocarbon (HC) sniffer **(Fig.7.19)** has two functions:

- Detect a fuel leak
- Inform the control system of a leak to enable shut down of the test.

The HC detector is a solid state detector manufactured by Figaro (a Figaro LPM-2610 was used). The HC detector module is enclosed in an aluminium housing **(Fig.7.19)** which is in turn situated in the vacuum hose that leads from the vacuum chamber below the test coupon.

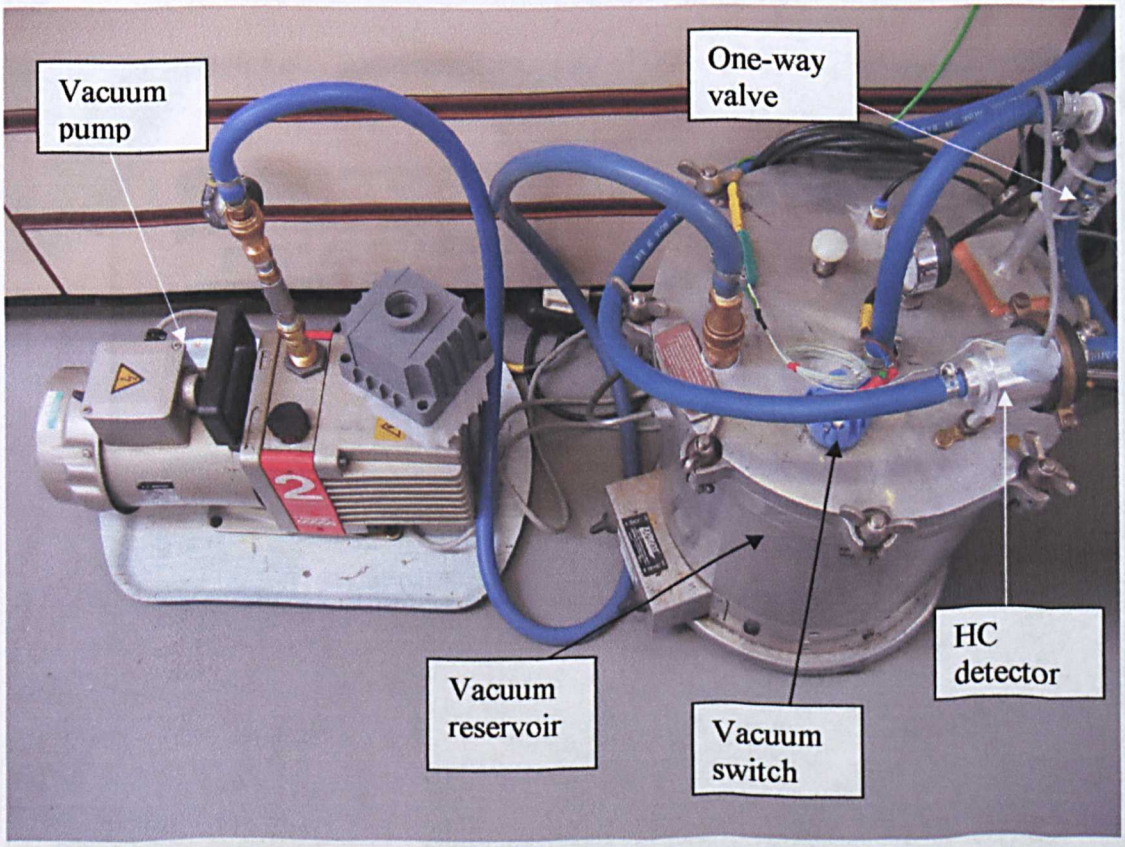

Figure 7.19 Vacuum system pump and reservoir housing components.

Attached to this housing is a K-type thermo-couple to log the temperature of the HC detector. The HC detector does not work below -10°C, so it has to be situated in such a manner that the through flow of air has a chance to warm up. To achieve this, the air drawn from below the test coupon has to be warmed. A heat exchanger was fabricated and attached to the hot air outlet vent of the refrigerated circulator. This utilises the hot air discharged from the circulator and warms the air flow from below the test coupon to room temperature (approx. 23°C) **(Fig.7.20).** The controller uses the reference voltage and an output voltage from the detector to establish if there is a rise in the HC content of the sampled air. A 5V DC voltage is applied to the detector. Within the detector there is a heated gas sensor. The reference voltage (V_{ref}) is about 2.5 V whilst the output voltage (V_{out}) is around 0.75V. When the gas sensor module is exposed to a higher than normal concentration of hydrocarbons in the airflow the value of V_{out} will reach or exceed the value of V_{ref}. When the value of V_{out} exceeds the value of V_{ref}, a safety trip on the controller stops the test.

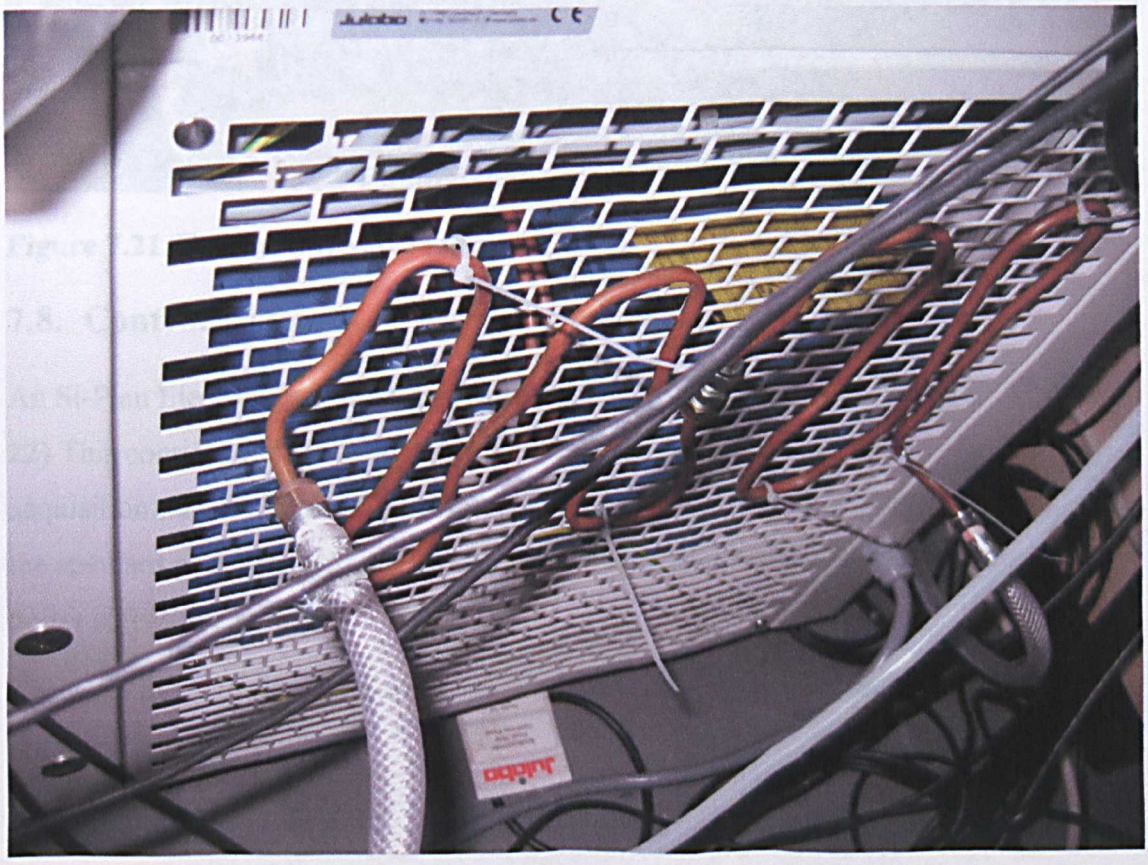

Figure 7.20 Heat exchanger mounted on rear of Julabo

The HC sniffer hose also required a one way valve to be manufactured and installed in the vacuum hose to stop the HC sniffer reading hydrocarbons whenever the pressure pot or the external fuel tank were emptied/filled **(Fig.7.21).**

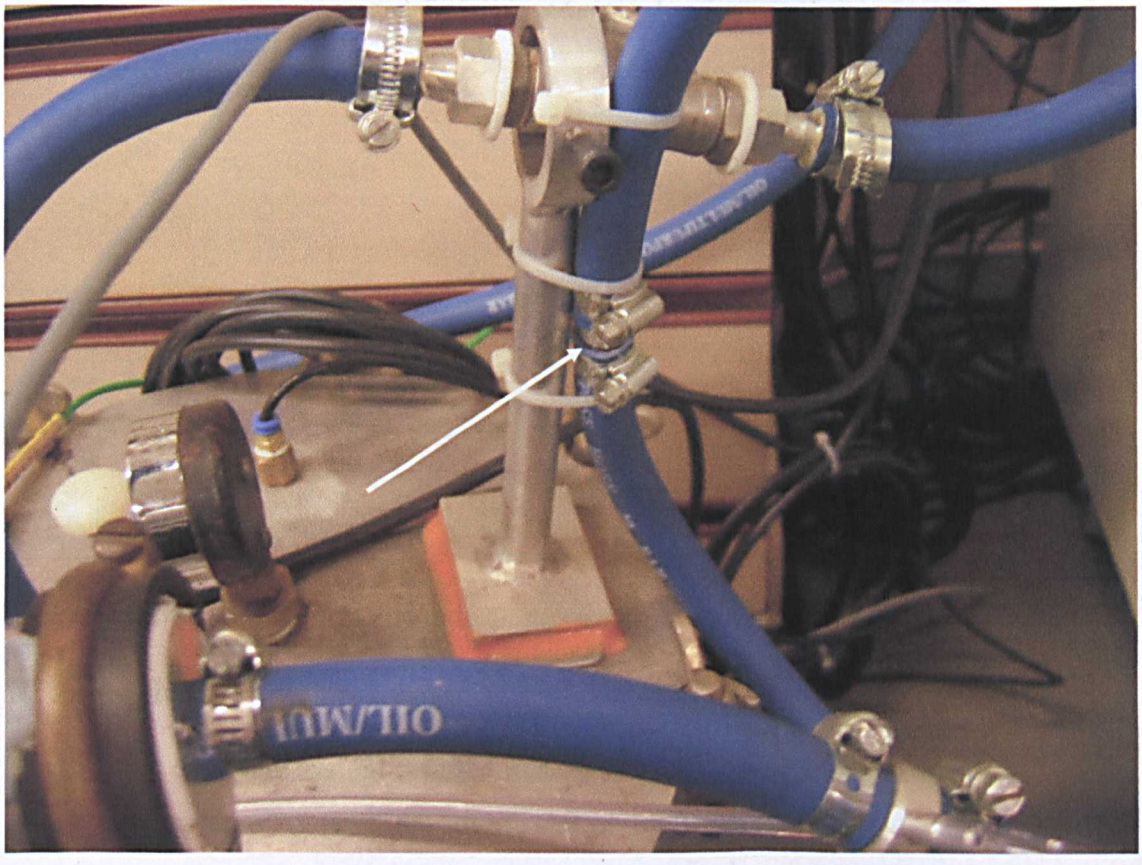

Figure 7.21 The one-way valve (arrowed)

7.8. Control system

An Si-Plan Electronics control and data acquisition system was used **(Fig.7. 22)** This consists of a 1 x 879 32-bit digital servo-controller and data acquisition unit, configured for single axis operation. The operating software is the standard package, with bespoke software designed by Si-Plan, by their in-house software engineers.

The MSS has several temperature and pressure sensors in the system. These are there to:

- Log data
- Act as sensors for alarms that enable the controller's adjustable trips to stop the test if certain parameters are exceeded.

The function of these sensors is described in the appropriate section of text.

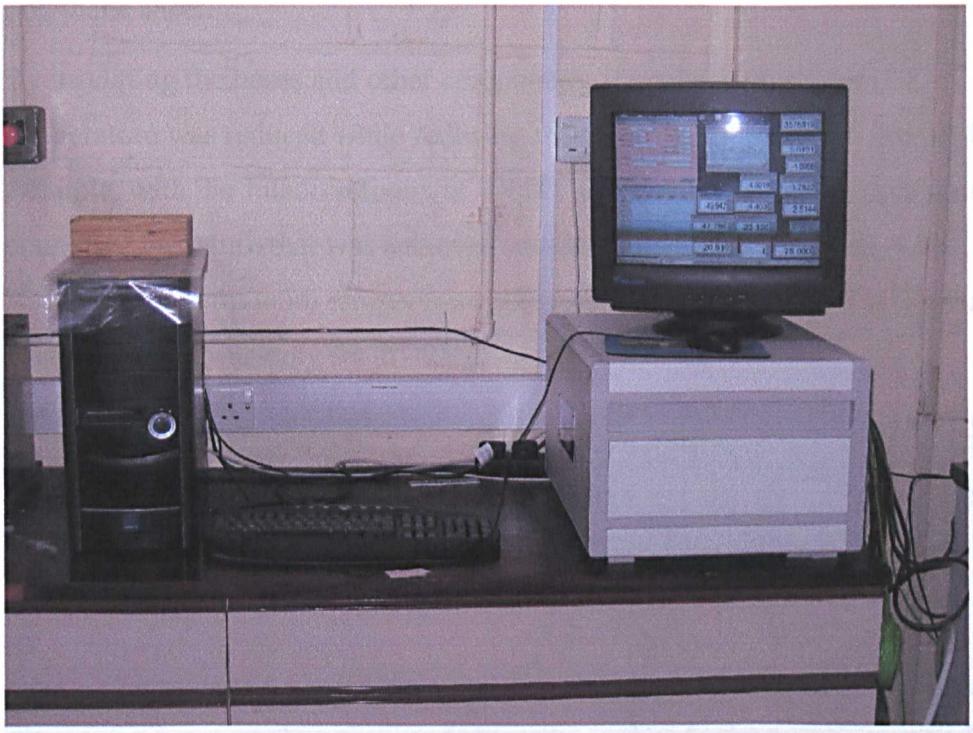

Figure 7.22 Si-Plan control and data acquisition system

7.9. Insulation

Trials of the complete system resulted in a build up of excessive ice around the base of the Pressure Pot (PP), the supply and return hoses for the Julabo and several other components. If the ice build up around the base of the PP was left unchecked the ice would have completely filled the gap between the outside of the PP and the "Mayes" fatigue actuating ram. This would have meant that the load applied by the fatigue machine wouldn't have been applied to the coupon but to the PP itself with the coupon seeing no load. This problem was overcome by removing the PP cover, allowing the test rig to dry out completely, applying insulation material around the base of the PP and wrapping the insulation material with a thin film of polythene. This stopped water condensing on the insulation and the consequent build up of ice **(Fig.7.23).**The ice build up on the hoses etc. was overcome by removing the hoses from the Julabo and, as before, applying insulation material around the hoses where they were in contact and wrapping the hoses with a thin film of polythene and refitting the hoses. The other components, for example the heat

exchanger, were wrapped in insulating material and, again, wrapped with polythene sheet.

By insulating the hoses and other components the minimum coupon temperature was reduced while reducing the set temperature of the Julabo. For example, with the Julabo setpoint at –90°C, without insulation the minimum coupon temperature that was achieved was around –48°C. However, with insulation, the minimum temperature achieved was around – 59°C while the Julabo setpoint was only set at –75°C.

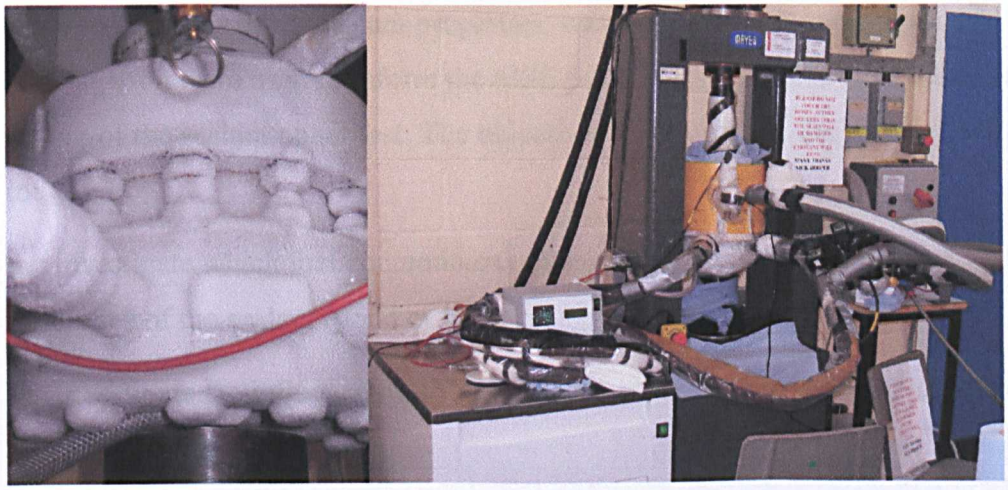

Figure 7.23 PP without (left) and with insulation (right).

8 Testing of sealants used in the project

8.1. Small scale tests

This chapter contains summary data from the results of both small-scale coupon tests and the MSS evaluation. The complete results of the test programmes can be found in **Appendix 6**.

8.1.1. Introduction

A limited investigation, into which typical fluids (jet fuel, water and saline solution) that can affect sealant properties, was undertaken. Results from this investigation were used to inform the MSS parameters to accelerate the time to failure of the sealant under test. The objectives of this part of the research were to:

- Investigate which fuel contaminants (water (fresh and salt)) affect the properties of the sealant (good or bad).
- Investigate the influence of different temperatures on the sealant properties.

Three types of test were used:

- Dumb-bell
- H-type joints
- Dynamic Mechanical Thermal Analysis (DMTA).

Table 8.1 shows the information that can be achieved with each test.

Type of Test	Young's Modulus (E) GPa	Peak Stress (σ_{peak})	Peak Strain (ε_{peak})	Failure Stress (σ_{fail})	Failure Strain (ε_{fail})	Glass transition temperature (T_g)	Adhesion
Dumb-bell	✓	✓	✓	✓	✓	✗	✗
H-Type	✓*	✓**	✓**	✓	✓	✗	✓
DMTA	✓	✗	✗	✗	✗	✓	✗

Table 8.1 Type of test used and results gained

Note:

* Secant modulus usually at 60% or 100% extension or any other elongation decided by the parties concerned.** These are usually used in a comparative or qualitative test

The sealant used was Chemetall MC-238 B2 in all cases. The sealant was supplied in a Semkit package. The Semkit package is a complete plastic cartridge assembly which stores, mixes, and applies multiple component adhesives and sealants etc. The Semkit package assures accurate proportioning of the materials since the pre-measured components are stored in separate compartments within the cartridge. To use the material, the mixing instructions are followed and the sealant is applied directly from the Semkit package.
The conditioning used for the specimens cured in air was 23°C ± 2°C and a relative humidity of 50% ± 5%. The temperature used for the fluids (jet fuel, de-ionised water and saline solution) was 23°C ± 2°C.
The following is a brief explanation off the tests. More in details are provided in **Appendix 3.**

8.2. Dumb-bell test (ISO 37)

In a dumb-bell test, sealant (or adhesive) is poured in to a mould and covered. Once cured, the specimen produced is carefully removed from the mould and inspected for air bubbles etc (**Fig 8.1**). If the sample is deemed satisfactory an average cross sectional area is calculated from the central part of the specimen.

The dumb-bell specimen is placed in a tensile testing machine and an extensometer is used to record tensile strain in the central narrow portion. A force is exerted until the test piece fails. From the failure load and other measurements taken, the bulk properties of the sealant (Young's modulus, ultimate tensile strength (stress) etc.) can be determined.

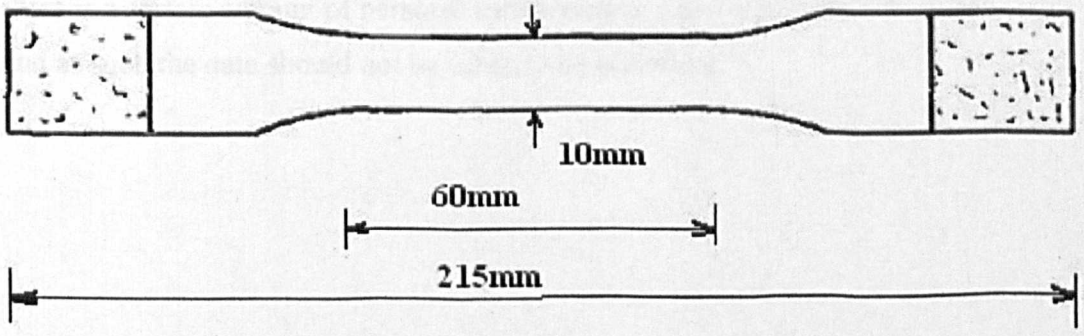

Figure 8.1 Dumb-bell specimen (Not scaled) (From Adams and Wake, 1984)

There are a number of points that should be noted:

- Sealants exhibit high strains to failure
- A standard extensometer could not be used because of the displacements involved and the softness of the specimens
- A high strain rate was used (500mm/min) to try to instigate an early failure
- During testing, a number of the tests ended when the sample just slipped from the jaws rather than breaking the specimen.
- Ultimate strength or failure strength could not be ascertained from these tests.

The dumb-bell test was used primarily to determine the Young's Modulus of the sealant upon 14 days air cure, and after immersion in jet fuel, water and saline solution over the different time periods (a further 14, 28 and 56 days). The test matrix is shown in **Table 8.2** and 3 replicates were used for each condition **See Appendix 6**.

Young's Modulus was calculated from the linear portion of the stress/strain curve before yielding occurs, as illustrated by the red line in **Fig. 8.2.** The test machine used for this portion of the testing possessed a function in the test program whereby a line can be manoeuvred to overlay the stress/strain curve from which the modulus is calculated by the test program. This means that there is a certain amount of personal interpretation involved in the calculation and as such the data should not be taken to be definitive.

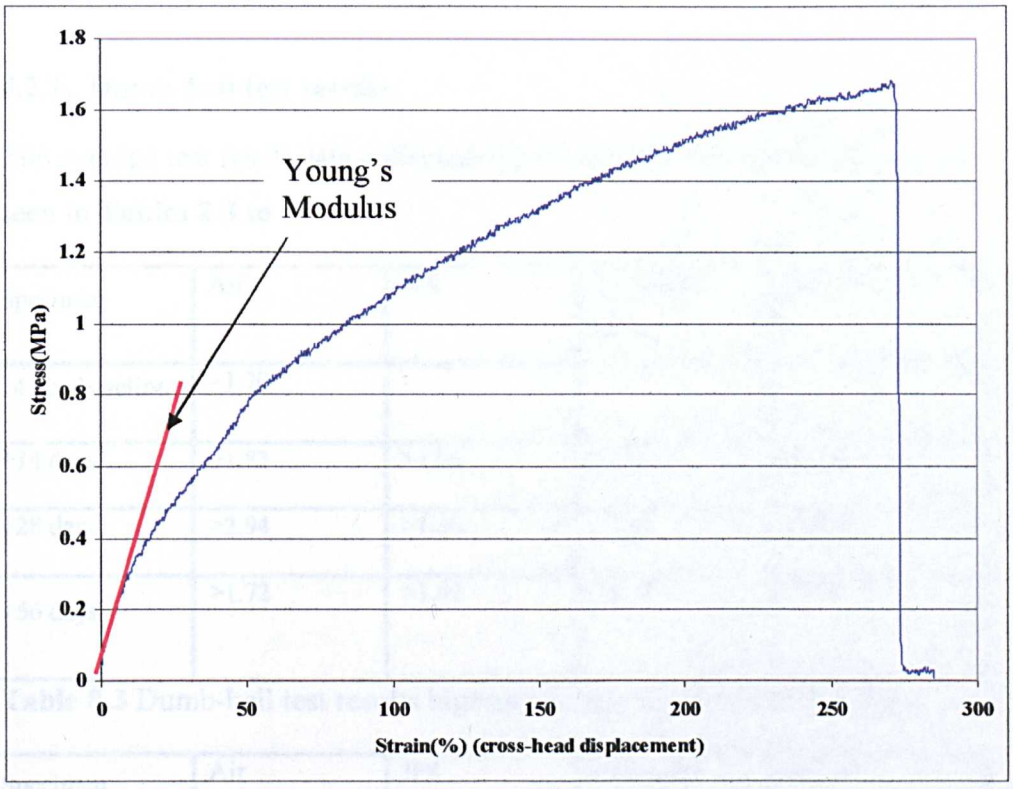

Figure 8.2 Example dumb-bell test result

Test configuration	**Test medium**				
Dumb-bell	**Air**	**JP8 jet fuel**	**Deionised Water**	**Saline solution (10%ww)**	**Total**
14 day baseline	3				3
+14 days	3	3	3	3	12
+28 days	3	3	3	3	12
+56 days	3	3	3	3	12

Table 8.2 Number of dumb-bell specimens.

8.2.1. Dumb-bell test results

The average test result data collected from the dumb-bell specimens can be seen in **Tables 8.3 to 8.5**

Specimen	Air	JP8	Deionised water	Saline
14 day baseline	>1.70			
+14 days	>1.83	>1.96	>1.80	>2.04
+28 days	>2.94	>1.56	>1.41	>1.16
+56 days	>1.72	>1.42	>1.48	>1.57

Table 8.3 Dumb-bell test results highest average stress measured (MPa)

Specimen	Air	JP8	Deionised water	Saline
14 day baseline	>317			
+14 days	>297	>342	>347	>332
+28 days	>279	>273	>281	>278
+56 days	>301	>281	>323	>306

Table 8.4 Dumb-bell test results average peak strain (%)

Specimen	Air	JP8	Deionised water	Saline
14 day baseline	2.61			
+14 days	4.51	2.42	4.05	2.76
+28 days	1.63	1.57	1.32	1.77
+56 days	2.65	2.50	2.34	2.63

Table 8.5 Dumb-bell test results average Youngs Modulus (MPa)

8.2.2. Discussion

No specific aerospace test procedure is currently in place for the testing of sealant dumb-bells. The method adopted is that defined in the British Standard BS 903-A2: 1995 Physical testing of rubber – Method for determination of tensile stress-strain properties (BS 903, 1995). This standard is written for the testing of rubber but this polysulfide sealant exhibits very similar properties and characteristics. However, there is a problem with using this standard for testing sealant. With rubber, the sample to be tested is usually supplied in the form of a sheet of uniform thickness and the dumb-bell samples are cut from this sheet to size with special dies and cutters. The sealant that was to be tested in this project (MC-238 B2) comes in a "Semkit" whereby the two components are pre-mixed within the "Semkit" container, the container is then fitted to some sort of application device(manual or pneumatic sealant gun) and used to either apply the sealant on initial assembly or to repair a fuel leak in service. This meant that the sealant, either, had to be moulded into a sheet of polysulfide to a certain thickness, and then cut to shape using the correct dies and cutters quoted in the standard (neither of which, moulds or cutters, the author had access to within the timeframe of the project) or to simply use adhesive dumb-bell moulds (which the author did have access to and in the numbers required) to mould the sealant dumb-bells. The latter was the system used. Unfortunately, this raised another problem, the size of the dumb-bells themselves. The standard overall length dumb-bell quoted within BS 903-A2 is 75-115 mm with the test length in the centre measuring 24-35 mm long by 4-6 mm wide, whereas the adhesive dumb-bell moulds gave the sealant dumb-bells an overall length of 215 mm with the test length in the centre of 60 mm by 10 mm wide **(Fig. 8.1)**. This explains why nearly all of the specimens pulled from the test machine jaws rather than breaking in tension. In hindsight, it would have been a better decision to use the correct dies and cutters to manufacture the dumb-bell specimens but it must be remembered that this testing was not going to produce new test data but confirmation of existing test results already carried out by several other establishments.

The results show that for the 14 day baseline test the Chemetall MC-238 B-2 sealants tensile strength of 1.7 MPa had exceeded the minimum requirement

tensile strength for Airbus UK (AIMS 04-05-001, Airbus, 2000) of 1.4 MPa. The results for the 14 day baseline test were also comparable to Chemetalls' own figures (Chemetall, 1995) of 2.1MPa.

The results of the dumb-bell testing were mainly inconclusive. As previously mentioned, if the results of the tests are studied it can be seen that most of the samples slipped from the jaws of the tensile test machine before they failed. Consequently, failure stress and strain could not be collated for most of the tests. The data for Young's Modulus shows that because there is a certain amount of personal interpretation involved in the calculation, the data should not be taken to be definitive and as such the results are inconclusive.

A simple overview is given in **Table 8.6** to show the relative effect of fluids on the properties of the sealant.

Fluid	Average Peak Stress*	Average Peak Strain	Average Modulus
JP8	↓	=	↑
Deionised Water	↓	=	↑
Saline	↓	=	=

* little or no change up to 14 days with a decrease thereafter.

Key: ↓ indicates a decrease in sealant property

↑ indicates an increase in sealant property

= indicates little or no change in sealant property

Table 8.6 Effect of fluid on sealant properties in comparison to identical dumb-bell tests in air

8.3. H-Type joint specimen

Tensile adhesion properties were investigated using H-type section joints, made with aluminium substrates; the dimensions are shown in **Figure 8.3**. These were manufactured to the protocols set out in BS EN ISO 8339:2005. See **Appendix 3.**

The test matrix is shown in **Table 8.7** and 3 replicates were used for each condition. The adhesion qualities were not determined because Airbus standard aluminium surface treatment was not used. However, in order to ensure adequate adhesion, fine grit blasting (180-220 mesh alumina) was used to prepare the bonding surfaces of the aluminium specimens. H-section samples allow for more surface area to be in contact with test fluid than lap shear samples and the H-section samples were immersed in jet fuel, water and saline solution over the different time periods (a further 14, 28 and 56 days) and compared with the baseline test in air at 14 days **(Table 8.8).**

Test configuration	**Test medium**				
H-section type	**Air**	**JP8 jet fuel**	**Deionised Water**	**Saline solution 10% ww**	**Total**
14 day baseline	3				3
14 days	3	3	3	3	12
28 days	3	3	3	3	12
56 days	3	3	3	3	12

Table 8.7 Number of H-type specimens.

In an H-type test the two test substrates are placed parallel to each other and a block of PTFE is affixed between them with tape; the resulting void in the centre can be filled with the test sealant (avoiding voids and bubbles etc) to provide a bead 50 x 12 x 12 mm **(Fig. 8.3)**. The test piece is allowed to cure for the recommended time period, the PTFE blocks are then removed and the finished specimen can either be tested or placed in an environmental (and/ or immersed in a test medium) chamber for a certain period prior to testing. The

specimen is tested in a tensile test machine and subjected to a pull at a defined strain rate (**NOTE:** 14 and 28 day = 6mm/min, 56 day = 12mm/min) until failure occurs. Values for failure load and extension at failure were recorded. These were converted to failure stress and failure strain. The level of adhesion can be determined by measuring the area of cohesive/adhesive failure and quoting as a percentage of the total area of the test.

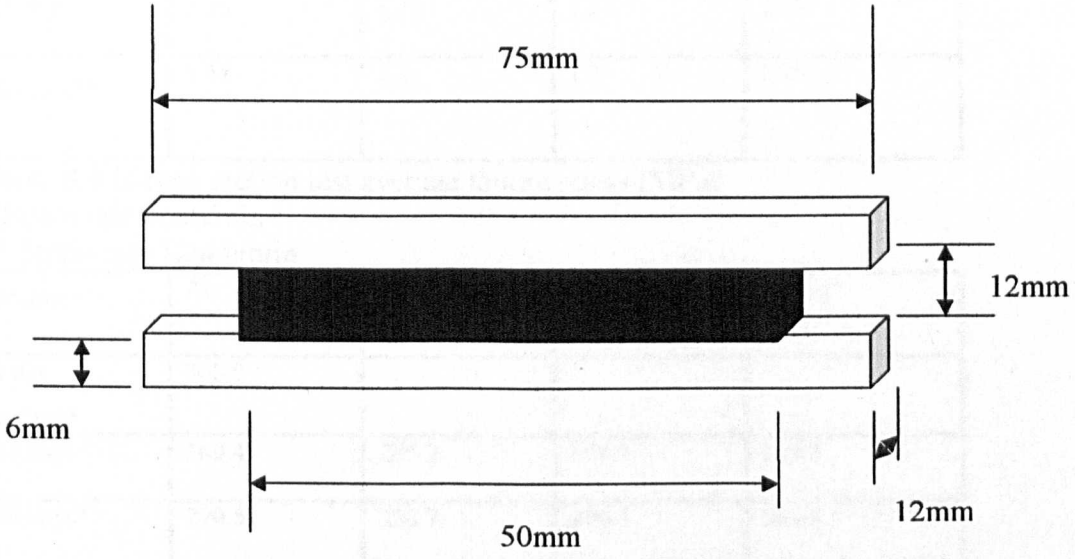

Figure 8.3 Typical H-Type test specimen

8.3.1. H-type section results

The data collected from baseline H-type section specimens can be seen in **Table 8.8.**

Specimen Number	Maximum Load(N)	Peak Stress(MPa)	Peak Extension (%)	60 % Secant Modulus (MPa)	Failure Mode
HBL 14-1	631	1.05	302	0.464	10% adhesive
HBL 14-2	1016	1.69	299.3	0.772	Light cohesive
HBL 14-3	1068	1.78	301.3	0.796	10% adhesive
Average and standard deviation	905±238	1.51±0.04	300.9±1.4	0.68±0.19	

Table 8.8 H-type test results 14 day baseline cure at 23°C 50%RH

The data collected from H-type section specimens can be seen in **Tables 8.9 to 8.11**

Specimen	Air	JP8	Deionised water	Saline
14 day baseline*	1.51			
+14 days*	1.46	1.31	1.38	1.07
+28 days*	1.36	1.33	1.23	1.17
+56 days**	1.44	1.21	1.2	1.19

Table 8.9 H-type section test average failure stress (MPa)
* Strain rate 6mm/min
** Strain rate 12mm/min

Specimen	Air	JP8	Deionised water	Saline
14 day baseline*	300.9			
+14 days*	360.4	286.2	359.0	204.3
+28 days*	270.5	326.7	296.3	303.3
+56 days**	299.4	313.1	302.4	281.6

Table 8.10 H-type section test average failure strain (%)
* Strain rate 6mm/min
** Strain rate 12mm/min

Specimen	Air	JP8	Deionised water	Saline
14 day baseline*	0.68			
+14 days*	0.52	0.58	0.60	0.62
+28 days*	0.59	0.59	0.58	0.51
+56 days**	0.6	0.56	0.57	0.59

Table 8.11 H-type section test average secant modulus (MPa) at 60 % extension
* Strain rate 6mm/min
** Strain rate 12mm/min

8.3.2. Discussion

This test regime is used extensively in the construction and glazing industry. It has several advantages as illustrated by Clark (2001). These are that:

- They are easy to manufacture
- Test fluids can easily access the bulk of the sealant and the bondline, thus enabling the tensile and adhesion properties to be determined after a relatively short immersion period
- Dissimilar substrates can be used
- Fatigue cycling can be carried out
- The effects of varying the strain rate can be investigated.

Figure 8.4 shows an example load extension graph for the H-type section test (14 day baseline test for MC-238 B2).

Clark carried out tests on several aerospace sealants (PR-1422 A and B along with PR-1440 A and B) using the H-type test configuration using various surface treatments. The specimens were cured for 14 days (at 25°C) and tested along with two sets that were immersed in either synthetic jet fuel or distilled water for a further 7 days (at 60°C). **Table 8.12** and **Figures 8.5** and **8.6** enables a comparison to be made of the results of H-type testing of PRC De-Soto's 1442(A+B) and 1440(A+B) tested by Clark (2001) and Chemetall MC238-B2 (Hooper).

Figure 8.4 Results of 14 day baseline test.

Test	Sealant	Average stress (MPa)	Average strain (%)	Failure mode
Clark (2001)				
14 days air cure @25°C	PR1422-A	1.24	144.5	CF
	PR1422-B	1.43	199.0	CF
	PR1440-A	1.17	260.0	CF
	PR1440-B	2.02	284.5	CF
7 days in synthetic jet fuel @ 60°C	PR1422-A	1.01	144.5	CF
	PR1422-B	1.30	150.0	CF
	PR1440-A	1.06	233.5	CF
	PR1440-B	1.38	166.5	CF
7 days in distilled water @ 60°C	PR1422-A	1.27	148.5	CF
	PR1422-B	1.30	133.0	CF
	PR1440-A	1.13	250.0	CF
	PR1440-B	1.68	276.0	CF
Hooper				
14 days air cure @25°C (Baseline)	MC 238-B2	1.51	300.9	CF
14 days in jet fuel @ 23°C	MC 238-B2	1.31	286.2	CF
14 days in deionised water @ 60°C	MC 238-B2	1.38	359.0	CF

Table 8.12 Comparison of the results of H-type testing of PRC De-Soto's 1442(A+B) and 1440(A+B) tested by Clark (2001) and Chemetall MC238-B2 (Hooper). (NOTE: CF = Cohesive Failure)

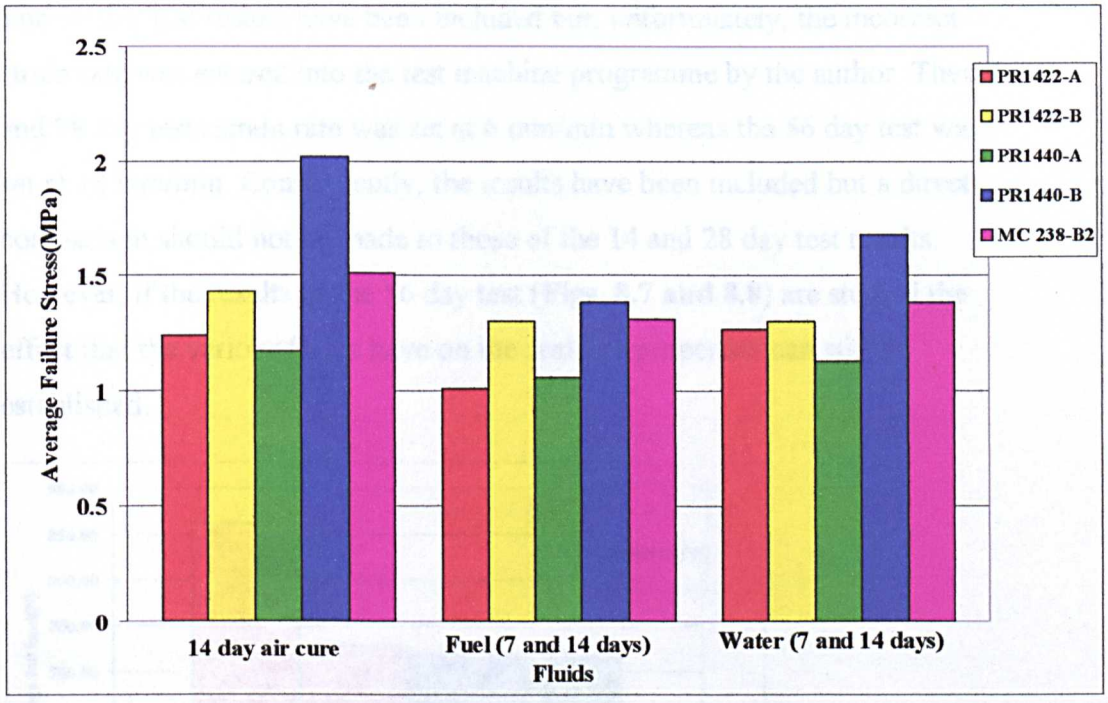

Figure 8.5 The effect of various fluids on average failure stress at 7 days (PR sealants) (Clark, (2001)) and 14 days (MC 238-B2 sealant) (Hooper).

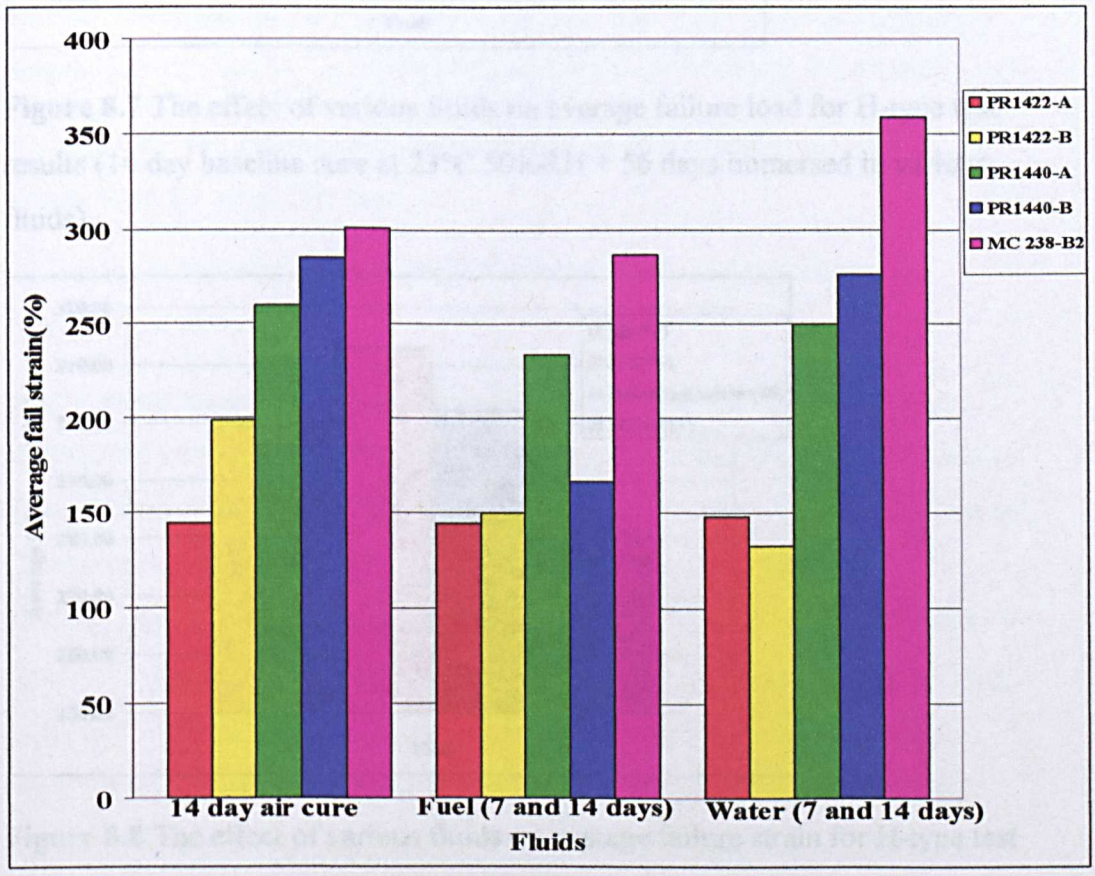

Figure 8.6 The effect of various fluids on average failure strain at 7 days (PR sealants) (Clark, (2001)) and 14 days (MC 238-B2 sealant) (Hooper).

The 56 day test results have been included but, unfortunately, the incorrect strain rate was entered into the test machine programme by the author. The 14 and 28 day tests strain rate was set at 6 mm/min whereas the 56 day test was set at 12 mm/min. Consequently, the results have been included but a direct comparison should not be made to those of the 14 and 28 day test results. However, if the results of the 56 day test (**Figs. 8.7 and 8.8**) are studied the effect that the various fluids have on the sealants properties can still be established.

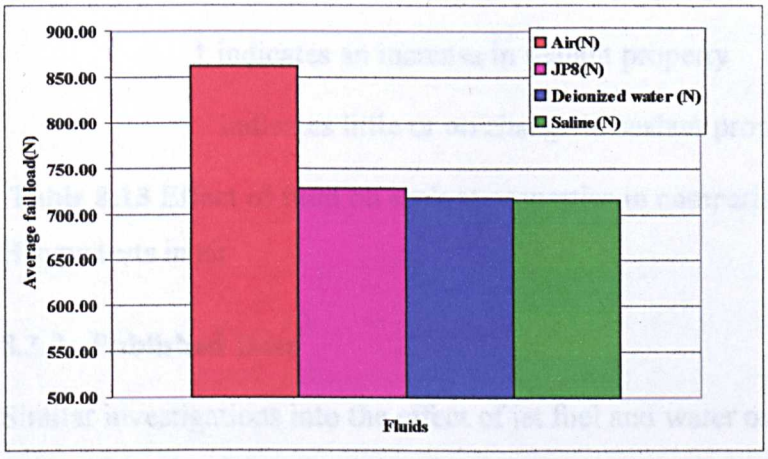

Figure 8.7 The effect of various fluids on average failure load for H-type test results (14 day baseline cure at 23°C 50%RH + 56 days immersed in various fluids).

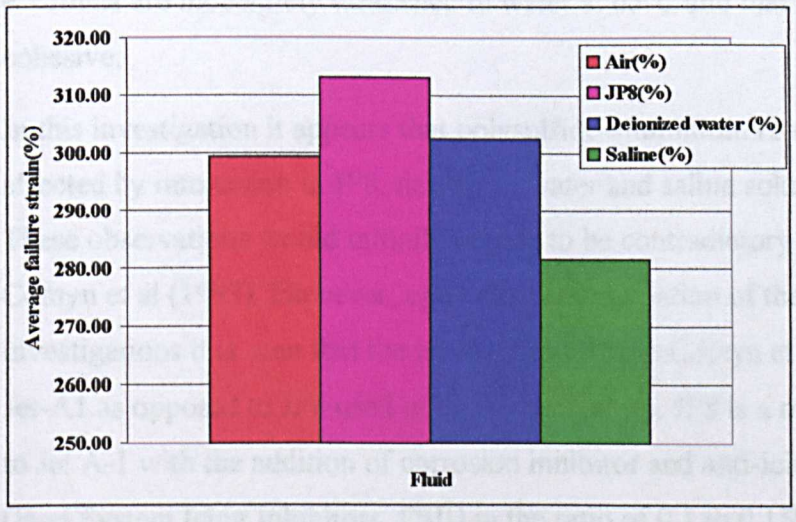

Figure 8.8 The effect of various fluids on average failure strain for H-type test results (14 day baseline cure at 23°C 50%RH + 56 days immersed in various fluids).

A simple overview is given in **Table 8.13** to show the relative effects of fluids on the properties of the sealant.

Fluid	Failure Stress	Failure Strain	Secant modulus
JP8	↓	↑	=
Deionised Water	↓	↑	=
Saline	↓	↓	=

Key: ↓ indicates a decrease in sealant property

↑ indicates an increase in sealant property

= indicates little or no change in sealant property

Table 8.13 Effect of fluid on sealant properties in comparison to identical H-type tests in air

8.3.3. Published Data

Similar investigations into the effect of jet fuel and water on the properties of polysulfide-aluminium lap joints by Comyn et al (1997) have shown that:

- Joints are not weakened on immersion in jet-fuel or water at room temperature for up to 160 days.
- Joints are moderately weakened in water at 65°C and that failure is cohesive.

In this investigation it appears that polysulfide-aluminium H-type joints are affected by immersion in JP8, deionised water and saline solution for 56 days. These observations would initially appear to be contradictory to the findings of Comyn et al (1997). However, upon closer examination of the two investigations it is seen that the jet fuel used by the Comyn et al (1997) was Jet-A1 as opposed to JP8 used in this investigation. JP8 is a military equivalent to Jet A-1 with the addition of corrosion inhibitor and anti-icing additives (Fuel System Icing Inhibitors, FSII) in the ratio of 0.1 to 0.15% by volume (ConocoPhilips, 2006). As shown in the findings of Comyn et al (1997), antifreeze greatly weakened the strength of polysulfide-aluminium lap joints and so that may account for the loss in strength observed by the author.

8.4. Dynamic Mechanical Thermal Analysis (DMTA)

Dynamic Mechanical Thermal Analysis (DMTA) is a method by which the viscoelastic properties of a material can be determined while the specimen is loaded dynamically and its temperature changed. Dynamic mechanical testers apply a periodic stress or strain to a sample and measure the resulting strain or stress response. Measured stiffness is frequently converted to a modulus to enable sample comparisons and damping is commonly referred to as $\tan\delta$, representing the phase lag between an applied sinusoidal force and resulting displacement or the measured phase lag between the applied stimulus and the response. $\tan\delta$ is proportional to the ratio of energy dissipated/ energy stored **(Tritec 2000)**.

DMTA was used to find the glass transition temperature (T_g) and the Young's modulus (E) of the sealant. This involved several tests after the samples were immersed in jet fuel, water and saline solution over the different time periods (a further 14, 28 and 56 days) and compared with the baseline test in air at 14 days. **See Appendix 6.**

DMTA testing was carried out on rectangular samples measuring 43 x 8 x 3 mm **(Fig.8.9)**. These were prepared at the same time and in the same moulds as the dumb-bell specimens. **Table 8.14** lists the number DMTA tests undertaken and 3 replicates were used in each condition.

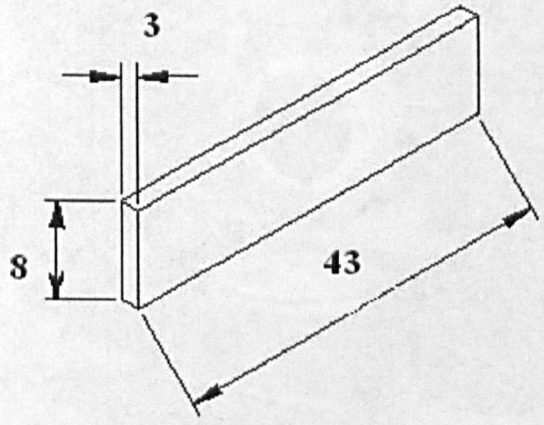

Figure 8.9 DMTA specimen dimensions (mm) (drawing not scaled)

8.4.1. Procedure

The specimens were cut to size and fitted in the DMTA test machine **(Figure 8.10)**. However, there is a problem because MC 238 B-2 is rubber-like at ambient temperature and consequently the sample will deform and even split when the drive shaft and base mounting clamps are tightened beyond finger tight. This problem was overcome by preconditioning the sample before the test was carried out. This was achieved by:

- Attaching the fixing clamps finger tight and fitting the cover
- Cooling the sample from room temperature to well below the sealants T_g (at least -70°C) in the environmental chamber of the DMTA using liquid nitrogen
- Cooling the sample to -70°C at the set ramp rate (5°C/min) and holding hold at this temperature for a set period of time (5 minutes) to ensure the entire specimen was at the required temperature (and the sealant specimen is a lot stiffer, glass like)
- Removing the cover and, very quickly, retightening the clamp plate screws to a uniform torque and then restarting the test at the required ramp rate (3°C/min) to the end temperature.

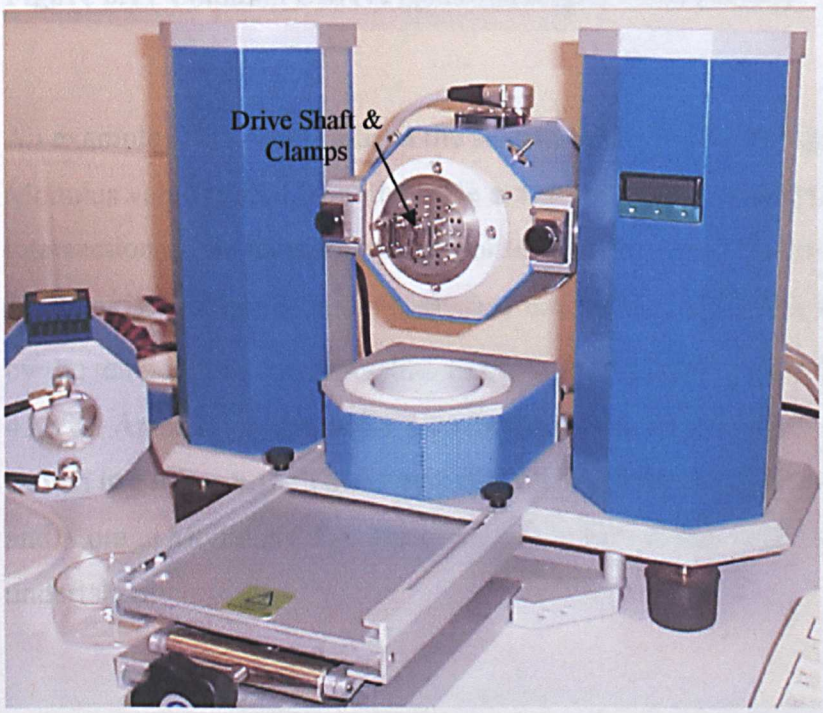

Figure 8.10 Tritec 2000 Dynamic Mechanical Thermal Analyzer (DMTA)

The most common analysis points when using DMTA are shown in **Figure 8.11**, they are:

- Extrapolated onset of decrease in storage modulus
- Point of inflection of the decrease in storage modulus
- Peak of loss modulus
- Peak of tan delta ($\tan \delta$)

Figure 8.11 Common DMTA result **(Mulligan et al. (2000))**

An example DMTA graph from the sealant test is shown in **Figure 8.12**. The Modulus value is read from the scale at the point corresponding to an intersection of the modulus curve. For example at -41.3 °C, the Young's Modulus (E) of the specimen is approximately 68.1 MPa. The T_g is determined by the temperature corresponding to the peak in tan delta ($\tan \delta$) in this case 41.3°C. An example graph for a **14 day Baseline cure sample No. 14-3** is shown in **Figure 8.13**. This shows the points on the curve for peak tan δ (T_g) and Storage Modulus (T_g). **Table 8.14** lists the number DMTA tests undertaken.

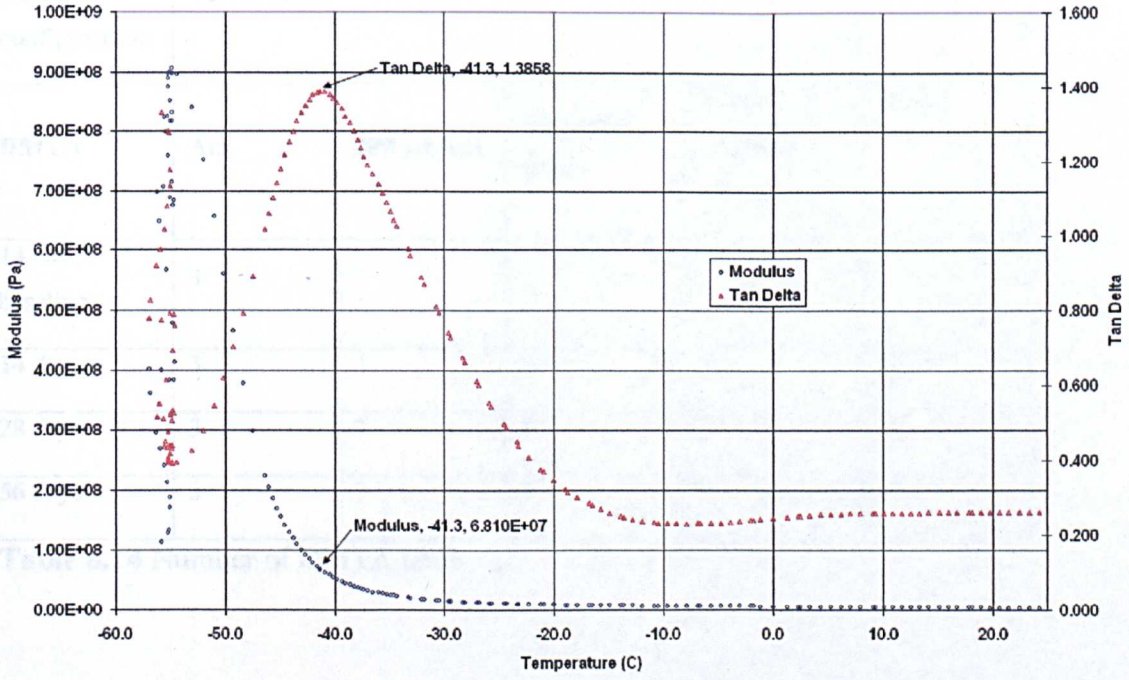

Figure 8.12 Example DMTA result (baseline test air cure 14 days).

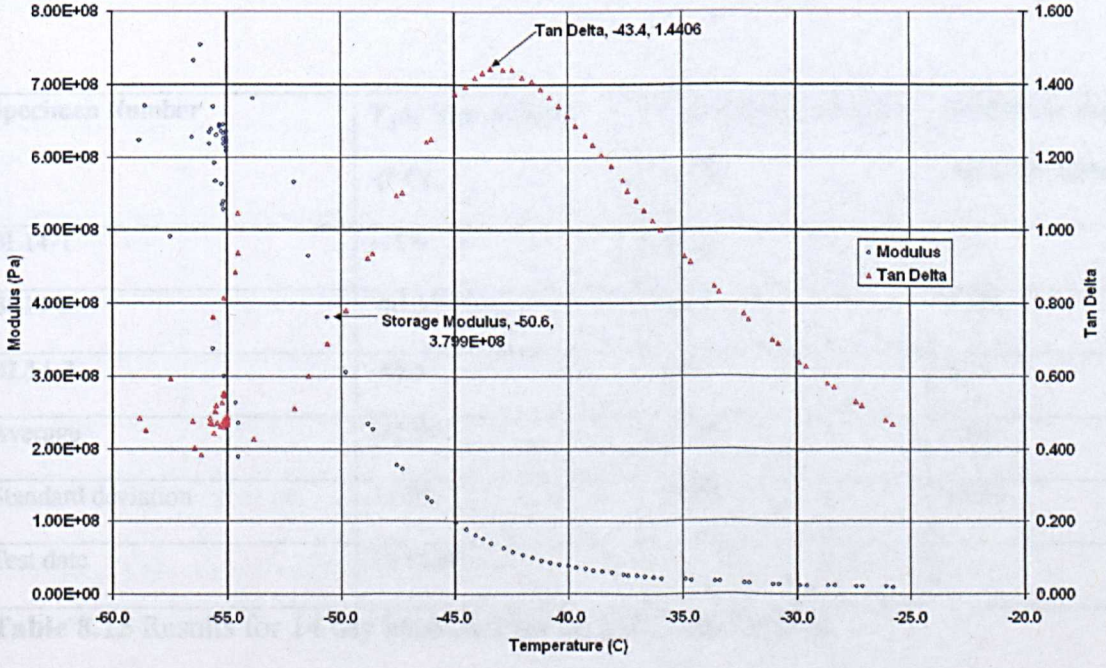

Figure 8.13 Example DMTA 14 day Baseline cure sample No. 14-3 (see **Table 8.16**).

Test configuration	Test medium				
DMTA	**Air**	**JP8 jet fuel**	**Deionised Water**	**Saline solution 10% ww**	**Total**
14 day baseline	3				3
14 days	3	3	3	3	12
28 days	3	3	3	3	12
56 days	3	3	3	3	12

Table 8.14 Number of DMTA tests

8.4.2. DMTA results

The data collected from DMTA specimens can be seen in **Tables 8.16 to 8.18.** The baseline results are shown in **Table 8.15.**

Specimen Number	T_g@ Tan δ Peak (° C)	T_g@ Storage modulus (° C)	Modulus@ approx -55°C (E) GPa
BL14-1	-41.6	-49.9	1
BL14-2	-40.9	-49.3	1.374
BL14-3	**-43.4**	**-50.6**	**0.75**
Average	-41.97	-49.93	1.04
Standard deviation	±1.29	±0.65	±0.31
Test date	16.06.06		

Table 8.15 Results for 14 day baseline cure @ 23°C and 50%RH.

Specimen	Air	JP8	Deionised water	Saline
14 day baseline	-42			
+14 days*	-39	-43	-42	-41
+28 days*	-40	-42	-38	-38
+56 days*	-39	-43	-39	-38

Table 8.16 T_g @ Tan δ Peak (° C) (*Stated date + up to 4 days)

Specimen	Air	JP8	Deionised water	Saline
14 day baseline	-50			
+14 days*	-47	-51	-49	-49
+28 days*	-48	-50	-47	-49
+56 days*	-48	-51	-48	-47

Table 8.17 T_g @ Storage modulus (° C) (*Stated date + up to 4 days)

Specimen	Air	JP8	Deionised water	Saline
14 day baseline	1.0			
+14 days*	1.3	0.8	0.6	1.2
+28 days*	1.3	0.9	1.6	1.5
+56 days*	1.2	0.7	1.7	2.1

Table 8.18 Modulus @ approximately -55°C (E) GPa (*Stated date + up to 4 days)

The results are also presented in block diagrams in **Figures 8.14 and 8.15** for ease of comparison.

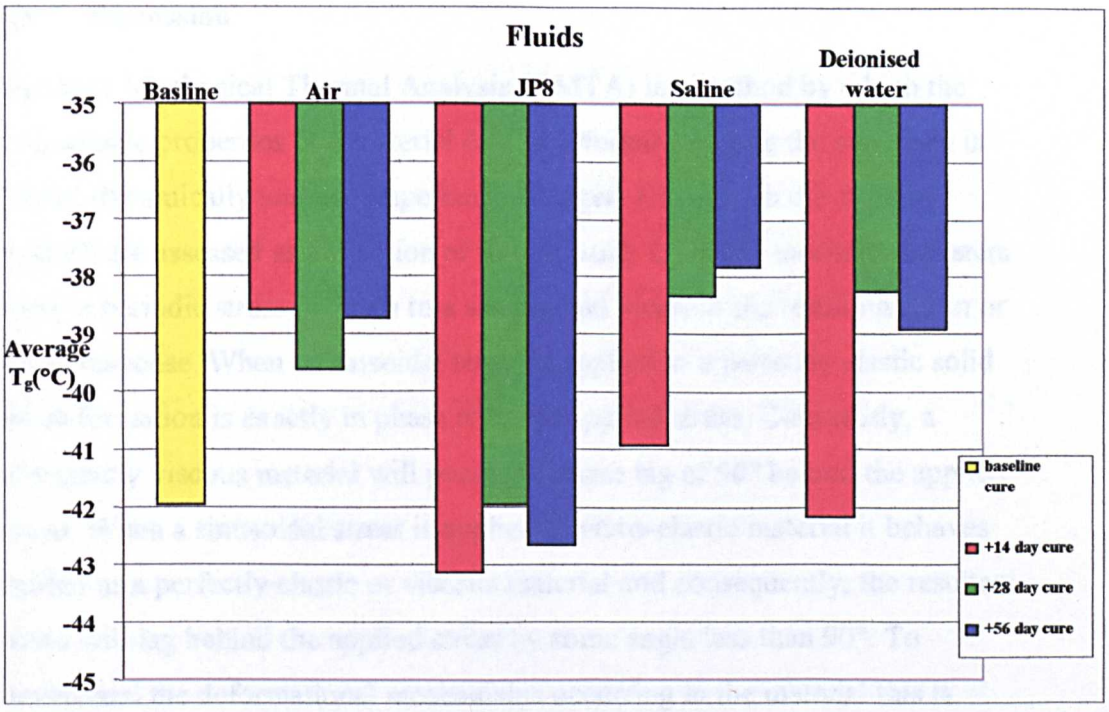

Figure 8.14 The effect of long term fluid exposure on the glass transition temperature (T_g)

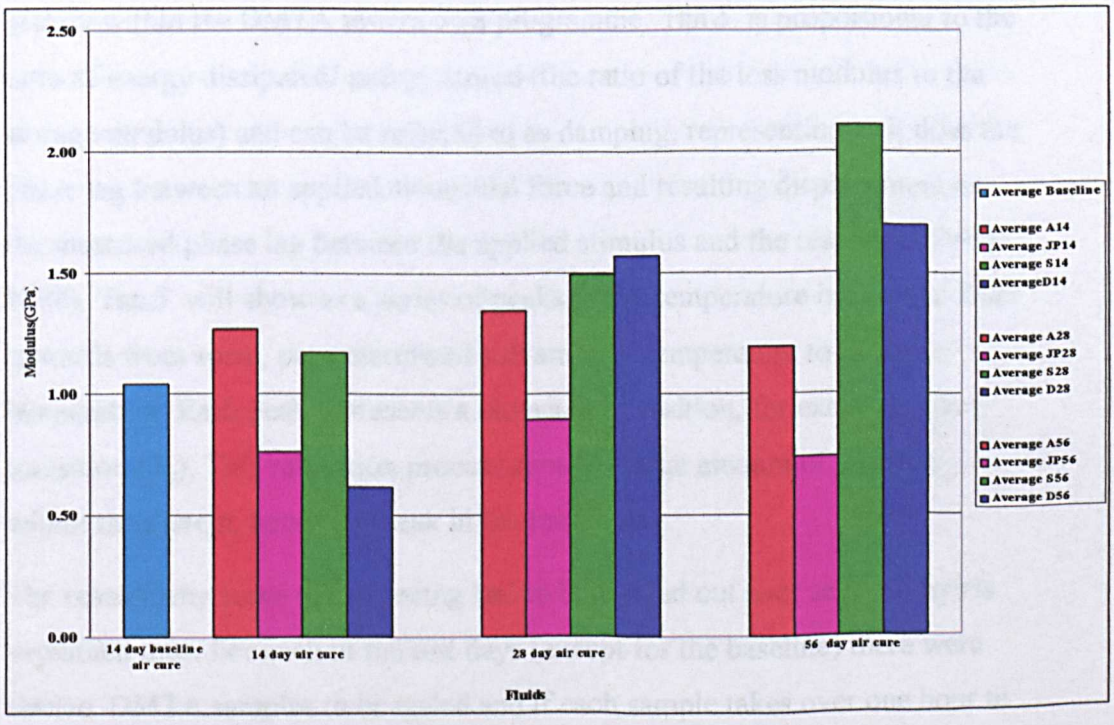

Figure 8.15 Average modulus (GPa) at approximately -55°C

8.4.3. Discussion

Dynamic Mechanical Thermal Analysis (DMTA) is a method by which the viscoelastic properties of a material can be determined while the specimen is loaded dynamically and its temperature changed. Changes in the dynamic modulii are assessed as a function of temperature. Dynamic mechanical testers apply a periodic stress or strain to a sample and measure the resulting strain or stress response. When a sinusoidal stress is applied to a perfectly elastic solid the deformation is exactly in phase with the applied stress. Conversely, a completely viscous material will possess a phase lag of 90° behind the applied stress. When a sinusoidal stress is applied to visco-elastic material it behaves neither as a perfectly elastic or viscous material and consequently, the resultant strain will lag behind the applied stress by some angle less than 90°. To understand the deformational mechanisms occurring in the material this is resolved into an in-phase and out-of-phase response. By comparing the input signal and the output signal values of the loss modulus (the elastic response) of the material are determined. Values of storage modulus (the viscous response) and $\tan\delta$ are calculated from the equations of motion of the mechanical system within the DMTA testers own programme. $\tan\delta$ is proportional to the ratio of energy dissipated/ energy stored (the ratio of the loss modulus to the storage modulus) and can be referred to as damping, representing as it does the phase lag between an applied sinusoidal force and resulting displacement or the measured phase lag between the applied stimulus and the response **(Tritec 2000)**. $\tan\delta$ will show as a series of peaks as the temperature is scanned from upwards from some, pre-determined sub ambient temperature to the melt temperature. Each peak represents a molecular transition, for example, glass transition (T_g). This relaxation process causes a large amount of damping within the system, hence the peak in the $\tan\delta$ curve.

The reason why some of the testing had to be carried out over several days is explained thus. For each of the test days (except for the baseline) there were twelve DMTA samples to be tested and if each sample takes over one hour to test, then the minimum time taken to test the 12 samples is 12 hours. Unfortunately, when consideration is made for having to refill the nitrogen dewar etc. the time can be increased by at least 6 hours.

A possible reason why the modulii of the specimens vary at ambient temperature whilst the T_g remains, roughly, the same may be due to the presence of voids within the specimens. Young's modulus is the measure of the stiffness of a material. If the sealant contains voids, then it is less stiff and a lower modulus will be measured. Conversely, the T_g is a measure of the relaxation point of polymer chains within the sealant. Whether voids are present or not the material will always change from a brittle, glass like condition, to a much more flexible and rubbery condition, at approximately the same temperature (T_g).

However, **Figure 8.15** indicates that there is a trend for the Modulus to increase at a temperature of -55°C for the deionised water (deionised water from 28 days) and the saline samples over the samples for air and jet fuel at the same temperature. Healey's report for Airbus (Healey,1996) states that at temperatures below the T_g the sealants that had been tested became very stiff with an estimated moduli of around 1000 MPa (1GPa). **Figure 8.15** shows that whilst the 14 day baseline cure modulus is indeed 1040MPa (1.04GPa), and the air cure and JP8 cure remain fairly constant (after an initial increase for the air cure and decrease for the JP8 cure) at around 1270 MPa (1.27GPa) for air cure and 800 MPa (0.8GPa) for the JP8 immersed, the moduli of the deionised water and saline samples increase dramatically at 56 days (after 28 days for the deionised water) to an average of 1690MPa (1.69GPa) for deionised water immersed and 2110 MPa (2.11GPa) for the saline immersed. The presence of saline solution in the test programme and Airbus test requirements seems to derive from the use of seawater to displace fuel from tankers in some areas of the world (Meyer, 1982 and Healey, 1996).

Saline solution was not selected for use in the MSS, initially, because of the inherent corrosion problems. However, when the combined results of the DMTA test and the H-type tests are examined, it is clear that consideration should be given to the inclusion of saline solution and, to a lesser extent, deionised water in future test programmes.

A simple overview of the results is given in **Table 8.19.**

Fluid	DMTA	
	Modulus	Tg
JP8	↑	↑
Deionised Water	↓	↓
Saline	↓	↓

Key: ↓ indicates a decrease in sealant property

↑ indicates an increase in sealant property

Table 8.19 Effect of fluid on sealant properties in comparison to identical DMTA tests in air

8.5. Evaluation of the Model Sealed System (MSS)

Four coupon sets were evaluated at Oxford Brookes University. The coupon configurations are shown in **Table 8.20.** In all cases the sealant was Chemetall MC-238 B2. The coupon sets were tested using combinations of fatigue and static loads along with the other test parameters (temperature, pressure etc.). These parameters and associated results are discussed in **Section 9.2**.

Test coupon number	Test coupon sealant configuration	Test duration(days)
01-05	overcoat and fillet	72 days in total (with 44 days environmental conditioning(i.e. below -50°C).
01-06	overcoat and fillet	11 days
02-06	overcoat and fillet	127 days, NO leak (OBU were requested by Airbus to stop test and make new coupon set). For the final 14 days of the test, the test programme was altered slightly to promote a leak and a leak was detected after 135 days in total (see **Appendix 10**).
03-06	Interfay and wet assembly, NO fillet or overcoat	No leak detected after 25 days

Table 8.20 Coupon identity, configuration and length of test

8.5.1. Safety cut-outs

The safety cut–outs on the MSS worked well on several occasions over the period October 2005 to December 2006. The hydrocarbon detection system was the main safety method by which the tests were terminated.

As an example, on 2nd November 2006 (coupon set 03-06) the MSS switched itself off. **Figure 8.16** shows the hydrocarbon detector reference voltage (HC V_{ref}) and the hydrocarbon detector output voltage (HC V_{out})**(Section 7.7 Hydrocarbon leak detection).** The arrow in **Figure 8.16** illustrates the point at which the HC V_{out} exceeded the 2.45volt (HC V_{ref}) at which point the MSS safety cut-out stopped the test. The time (about 7 minutes) between the peaks on the HC V_{out} coincides with the time between the vacuum switch turning off the vacuum pump and atmospheric pressure leaking into the system. The resultant pressure increase in the system, and the vacuum switch turning the vacuum pump on again to maintain the depression in the system, drew the hydrocarbon fumes through the hydrocarbon detector housing **(Fig.7.19)** thereby increasing the HC V_{out}.

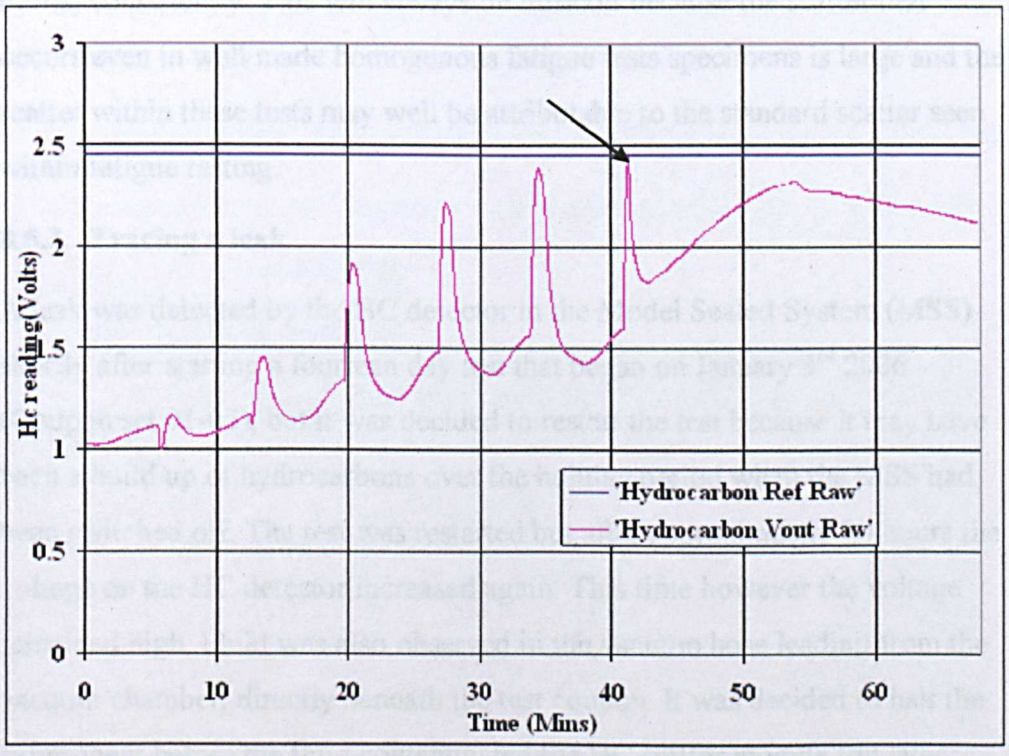

Figure 8.16 Hydrocarbon detector voltages detecting a leak.

8.5.2. Coupon sets

Three coupon sets exhibited leaks. The first was after approximately 72 days (with 44 days environmental conditioning (i.e. below -50°C)). This coupon set was in the MSS whilst the controller and Julabo were being fitted to the MSS, and commissioning and familiarisation of the equipment was being carried out. Consequently, temperatures, loads etc. were not logged adequately, but it showed that a leak could be initiated within a reasonable time span. The second set leaked within 11 days at temperatures down to -55°C. This may have been a particularly badly made joint and may be unrepresentative. The third set leaked after 135 days (there was no leak evident at 127 days at which point the author was requested by Airbus to stop the test and make a new coupon set). For the final 14 days of the test, the test programme was altered slightly to promote a leak and a leak was detected after 135 days in total **(see Appendix 10).**

This shows that the concept does work but more research needs to be carried out to define a test regime that produces a joint failure within a certain time frame, consistently. This will always be difficult because the scatter that occurs even in well made homogenous fatigue tests specimens is large and the scatter within these tests may well be attributable to the standard scatter seen within fatigue testing.

8.5.3. Tracing a leak

A leak was detected by the HC detector in the Model Sealed System (MSS) shortly after starting a fourteen day test that began on January 3rd 2006 (Coupon set 01-05), but it was decided to restart the test because it may have been a build up of hydrocarbons over the holiday period when the MSS had been switched off. The test was restarted but after approximately 20 hours the voltage on the HC detector increased again. This time however the voltage remained high. Fluid was also observed in the vacuum hose leading from the vacuum chamber, directly beneath the test coupon. It was decided to halt the experiment before the fluid contaminated the HC sniffer module (on later inspection it was found that the fluid had indeed contaminated the HC sniffer module).

The Model Sealed System (MSS) was removed from the fatigue machine and dismantled. A visual inspection of the coupon set was carried out with no obvious leaks detected. It was decided to trace the leak in a similar manner to that used when tracing a leak in a bicycle tyre, using compressed air and a bowl of water and watching the air bubbles escape from the puncture. To carry this out it was decided to reinstall the coupon set in the Pressure Pot (PP) assembly and use the pressure pot as a pressure vessel and use water to trace the leak from the sealant joint. To achieve this, the pressure pot assembly had to be assembled in a slightly different manner to facilitate the detection of air bubbles as follows:

- The lower cooling manifold and cover were not fitted.
- The assembly was inverted
- The whole assembly fitted in the "Nene" tensile test machine **(Fig.8.17)**
- The resulting hollow formed by the coupon and the clamp plate was filled with a fluid(water)
- A compressive load was applied to the inner coupon centre hub (4.5kN) to open the joint
- Compressed air (2.5 bar) was introduced to the inside of the PP **(Fig.8.18)**
- The above was carried out and a leak was detected **(Figs.8.19 and 8.20)**

Figure 8.17 and 8.18 The MSS fitted into the Nene test machine (left) with the air pressure gauge reading (right)

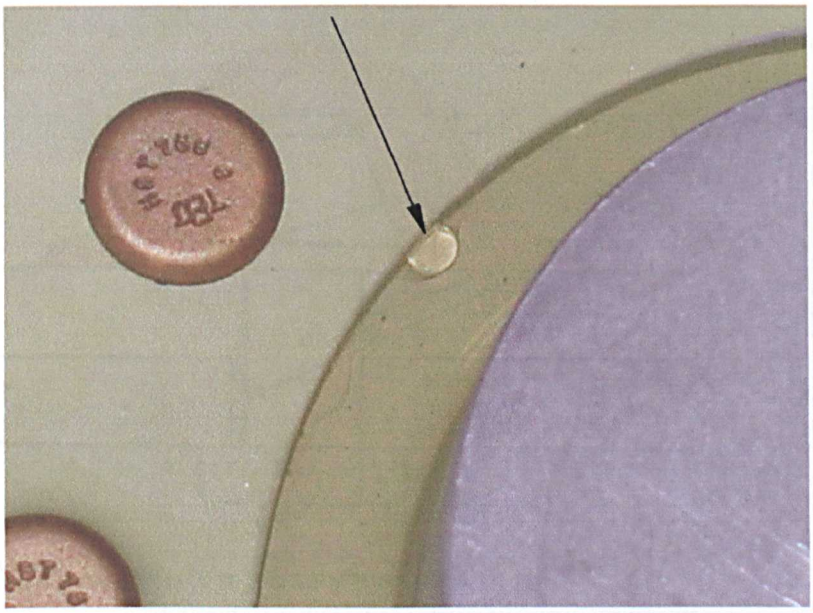

Figure 8.19 Air bubble (arrowed) from sealant joint leak

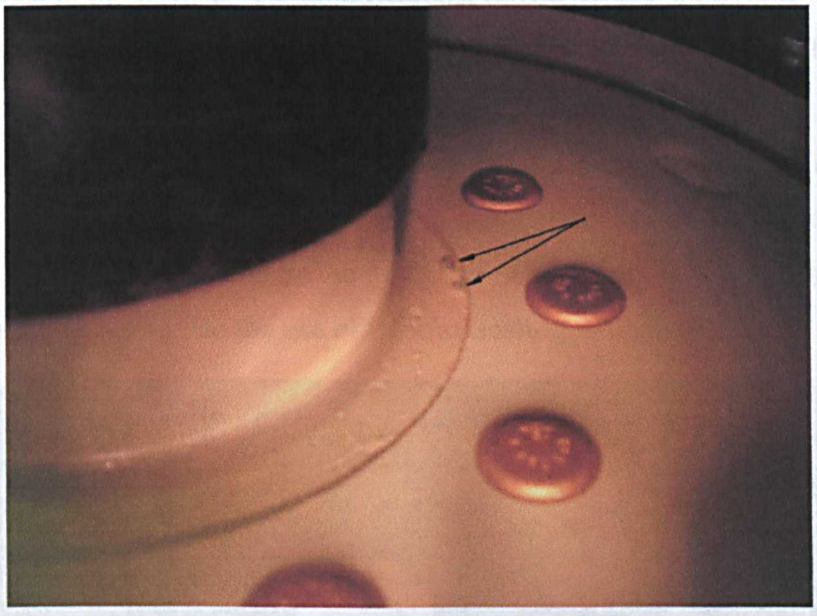

Figure 8.20 Air bubbles (arrowed) from sealant joint leak

Figure 8.21 shows an example of a primary leak path, that is a leak that exists because of gaps in the components. The majority of leaks are from primary leak paths (i.e. gaps in the metal plates) and not secondary leak paths which are leak paths via the fasteners hole only (Taylor (2002) (a)).

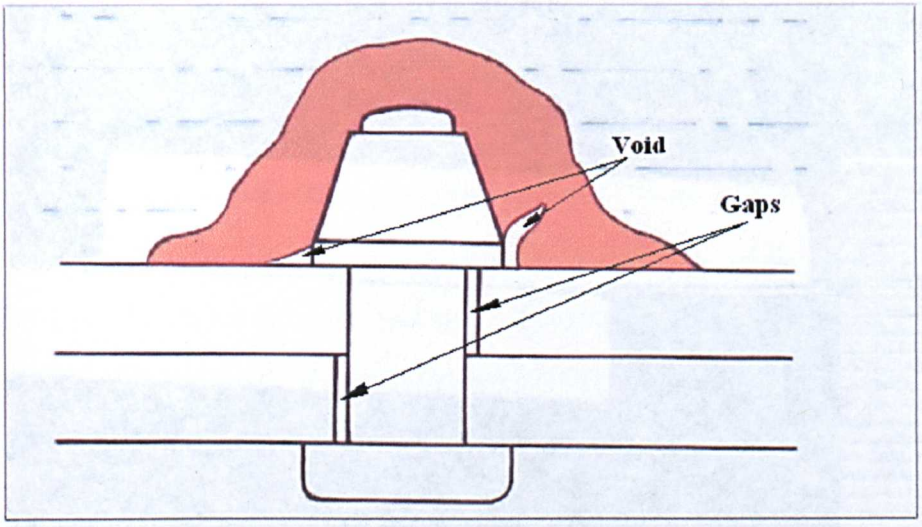

Figure 8.21 Example of a primary leak path

Figure 8.22 shows a close up of the titanium fastener in section. Several voids can be seen in the fastener's sealant overcoat (arrowed) and a possible instigator of a secondary leak path. **Figure 8.23** shows that the width of the interfay joint increases in the zone between the fasteners; this is known as quilting. From **Figure 8.23** it would appear that the interfay may be as much as 0.5 mm thick, but this is misleading and is generally nearer to 0.2mm (Buller, 2002(a)). This could be the instigator of a primary leak path and explains the necessity for the use of interfay sealing in the joints.

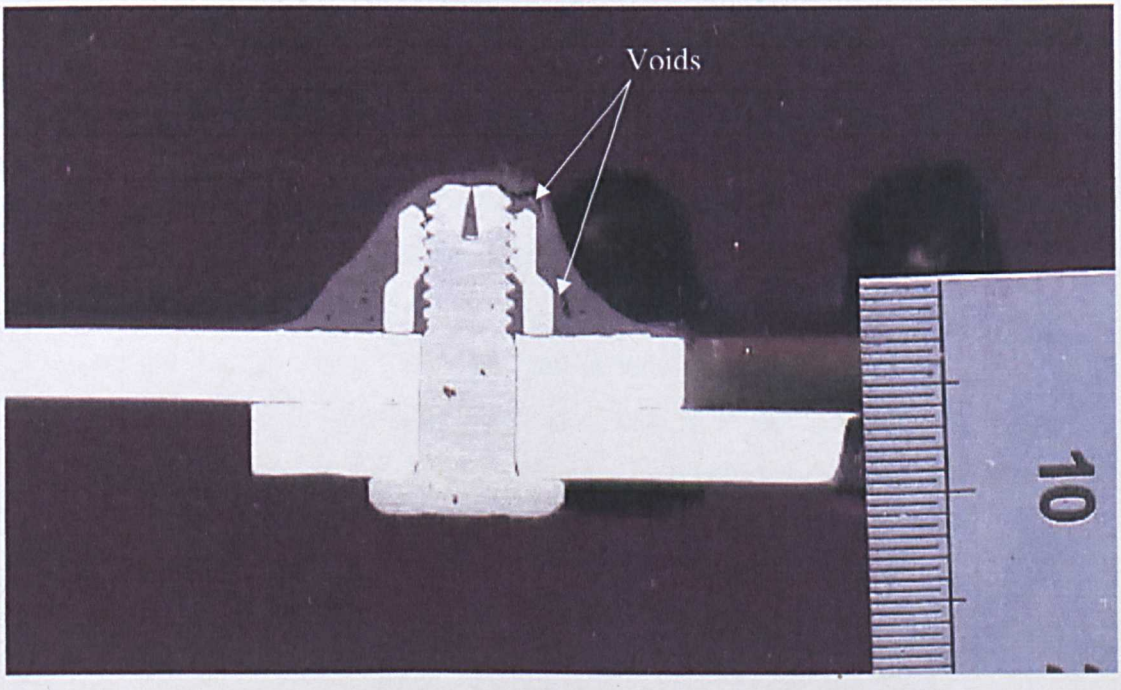

Figure 8.22 Titanium fastener and joint in section, showing several voids in the sealant

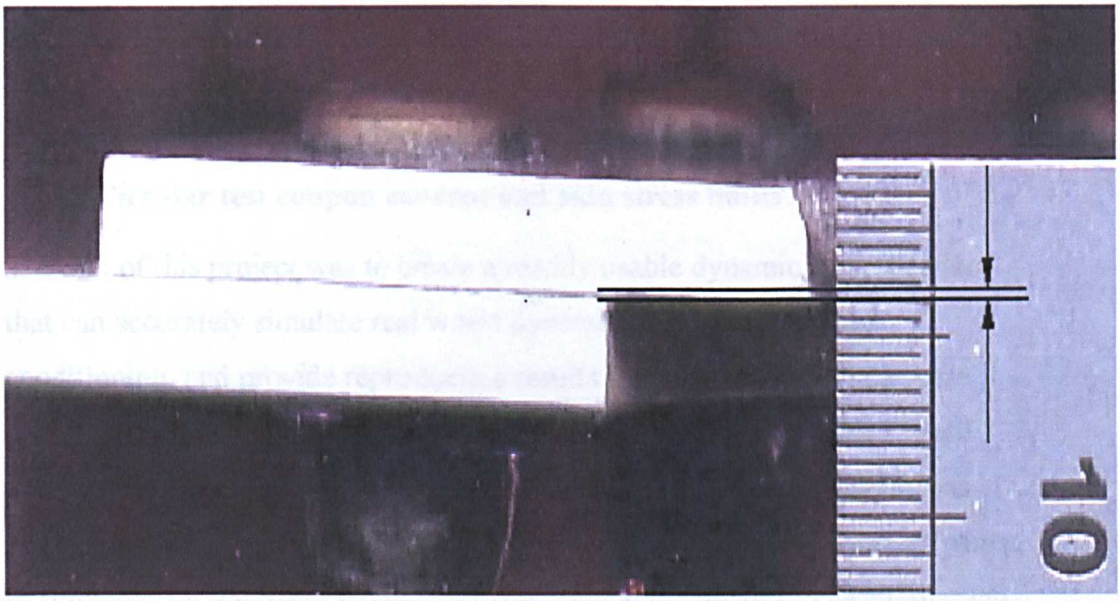

Figure 8.23 Coupon section midway between the fasteners.

8.5.4. Summary

The MSS performed within the set parameters laid down by Airbus UK at the beginning of the research (See **Section 2.2.3**) and a leak was instigated in the sealant joint on several coupon sets. The safety cut-outs performed as per their design specifications and stopped the test programme when a boundary condition was exceeded. The fuel leaks themselves, though not major, were noticeable in that they produced sufficient hydrocarbon vapour to be detected; in one case, a leak was visible in the vacuum hose leading from the vacuum chamber beneath the test coupon. Other factors such as the time-scale of testing are discussed in Chapter 9.

9 Discussion

9.1. Model Sealed System (MSS)

9.1.1. Circular test coupon concept and skin stress limits

The aim of this project was to create a readily usable dynamic test procedure that can accurately simulate real world dynamics and environmental conditioning, and provide reproducible results to qualify sealants in a more realistic manner than current testing methods allow. To achieve this several concept ideas were drawn up, investigated and the circular test coupon was adopted. This method subjects a circular lap joint to cyclic axial stresses whilst simultaneously imposing a range of experimental parameters. The circular lap joint is assembled using aerospace fasteners and sealed, and it simulates a wing skin butt-strap joint in a real aircraft. However, by making it circular the complications of corners and joint ends are eliminated. The loading used in the coupon test is based on a lower wing skin butt-strap joint for a typical Airbus single aisle aircraft. This part of the structure has had in-service fuel leak problems, has reasonably straightforward loading conditions and was deemed by Airbus to be a suitable sealed joint to provide the focus for a test configuration.

Problems were encountered when trying to calculate the stresses in the coupon using theoretical methods because these equations do not allow for the stress concentrations caused by the ring of fasteners holding the two coupons together. The coupon sizes, materials, their stresses and fastener spacings were determined initially as a compromise between the realities of airframe construction and the stresses derived from strain measurements on mock-ups of the coupon configuration. The experimental approach to the problem involved designing and fabricating a prototype test rig, bonding strain gauges to the coupons, and applying loads to the rig to open and close the joint. From this it was determined whether the measured stresses experienced by the Airbus A318 could be achieved in the laboratory. Initially, it was felt that these stresses may be too high to achieve, realistically, on the test rig in the laboratory. However, it was decided that the relative proportions between the various stresses was important, enabling the test coupons to replicate the

relative proportions between the various stresses. The final loads used did produce stresses higher than experienced in normal flight conditions by allowing for some flight gusts (10 fps). The aircraft can experience gusts of up to 30 fps but this would be unusual and consequently the time required to test the joint configuration and sealant adequately should be significantly reduced in comparison to real aircraft time to failures (Buller, (2002)(b)).

Some points that needed to be considered and/or noted in the design of a dynamic test rig were referred to in **Section 5.1**. Briefly, these were that some movement will exist between adjoining parts in mechanically fastened joints that are subject to a loading action, the use of interference fit fasteners will reduce this movement, that the loads applied should provide similar movement to that experienced in joints on the aircraft, and that using interfay sealant was first introduced to reduce the effects of fretting (caused by movement) and corrosion rather than as a fuel tank sealant.

9.1.2. Mechanics of the system and limitations

The test coupon set comprises two circular plates that are fastened and sealed. The test sealant is sandwiched between the two bolted aluminium circular coupons of dissimilar size **(Fig. 6.2)** mounted concentrically. The two discs are attached to each other utilising twelve, 3/16" titanium fasteners and nuts. Initial problems with load application were overcome by using a hub rather than reinforcing the inner coupon. This raised three problems. Firstly, by using fasteners to attach the hub a secondary leak path through the fasteners could be initiated and secondly, if adhesive were used to attach the hub, at the low temperatures that the test regime require the adhesive would only really be suitable for use in compression and not tension. Thirdly, if a torque load was to be applied to the test coupons at a later stage in the test programme, fasteners would have to be used. These three problems were overcome by making an inner coupon with an integral centre hub. A very important factor is the inclusion of a radius between the centre hub and the coupon to reduce the stress concentrator that exists at this point if loaded in tension **(Fig.6.2 arrow)**.

The test coupon set is mounted as the base of a "Fuel Tank" or Pressure Pot (PP) that is structurally stiff and filled with jet fuel. The top of the tank is an aluminium plate that houses the three ports (one for pressure/vacuum and the

two inlet/outlet ports for the test fluid). From beneath the top plate the "Showerhead" and the pickup pipe are fastened.

The whole assembly is then mounted in a fatigue test machine. One end of the test rig is supported rigidly to the test frame end plate (load cell) via the thick steel top plate and pushrod, whilst the other end is free to deflect (the actuating ram). The loads are applied to the test coupon via the stainless steel centre hub. One end of the hub is attached to the fatigue machine actuating ram, whilst the other end is screwed into the hub of the smaller inner coupon. The typical maximum load applied is only 5kN.

The desire to thermally "shock" the coupon meant that there was a need to keep thermal masses low and the heat transfer rates high. This was achieved by directing the hot/cold coolant directly at the area of interest (the coupon & immediate surroundings). It entailed maximising heat transfer by redesigning the lower parts of the pot to act as a heat exchanger and using the fuel as a recirculating coolant directed at the coupon. This maximised the temperature difference between the coolant fluid and the MSS. This was achieved by designing a lower clamp plate/cooling manifold through which the heating/cooling medium would flow and, in so doing, it is in intimate contact with the test coupon increasing the heating/cooling rate. Along with the lower vacuum plate and centre hub seal housing, this also acts as a vacuum chamber beneath the test coupon to provide a pressure differential across the sealant joint.

9.1.3. Environmental and dynamic control system

The Model Sealed System (MSS) can be considered to be a modular test system that can simulate structural loading, but can also simulate fuel inertia, tank pressures, thermal and chemical effects.

9.1.3.1. Data acquisition and control

An Si-Plan Electronics control and data acquisition system was used. This consists of a 1 x 879 32-bit digital servo-controller and data acquisition unit, configured for single axis operation. The operating software is the standard package, with bespoke software writing designed by Si-Plan, by their in-house software engineers.

9.1.3.2. Temperature

Initial testing involved the use of liquid nitrogen (N_2) to cool the PP. A cryogenic chamber was fabricated that fitted in the (limited) space of the "Mayes" fatigue machine. Cooling was achieved by a combination of:

- Putting a sealed, glass jar with the test fluid inside, in a freezer cabinet at approximately -30°C and flooding the coupon, rapidly, using a vacuum system.
- Manufacturing a manifold that fits over the joint area on the outside of the test coupons and pumping liquid nitrogen directly on to the joint.

This "Crash Cooled" the joint adequately and introduced a thermal shock to the sealant system. The nitrogen cooling system was then used to maintain a low temperature for a cooling cycle of the fatigue test. To raise the temperature to the required +50°C, an electric heating coil (tape) was wound around the pressure pot with the temperature regulated by a temperature control unit using a thermocouple.

Environmental and fatigue testing using this method began in April 2004 (environmental testing only from January/February 2004). The heating system worked very well and performed to expectations. Unfortunately, the liquid nitrogen cooling system only worked for a total of 6 days (with low temperatures between -30°C to -40°C maintained for about 4 hours per session, for a total of 24 hours at low temperature) before several components failed, either partially or completely, in quick succession. The failures were:

- The already, noisy, nitrogen lift pump eventually lost its efficiency and required renewal or reconditioning.
- The control valve for the liquid nitrogen and/or the control unit itself failed completely.

A more complete description of the above problems is provided by Hooper et al (2004). In May 2004, it was clear that the cryogenic system employed was not reliable enough or controllable enough for the project. A refrigerated circulator was then adopted to impose the various test temperature parameters. Julabo suggested the use of a heat exchanger to cool the fuel which in turn

would cool the PP. The reason for the use of a heat exchanger was that the Julabo could not cool the jet fuel directly because the fuel would damage the unit. This method was decided against and the use of the cooling manifold was eventually used. The refrigerated circulator was used to heat/cool the fluid medium, that was in turn circulated through the lower clamp plate/cooling manifold and in the return hose a heat exchanger to heat/cool the circulating test fluid(JP8) was used. The size and output of the refrigerated circulator were important factors that had to be taken into account. In order to maximise heat transfer rates, using a cooler that can deliver very low temperatures would be optimal, remembering that rate of flow of energy depends on the temperature difference in the system. This led the author towards systems with a working temperature range at about -85 or -90°C. The volume of the refrigerated circulators tank was also a consideration. A large volume tank would allow us to have a large cold sink and a hot sink ready to switch in, especially useful if operating a bank of multiple MSSs. The Julabo FP90-SL was the final choice of refrigerated circulator.

The temperature of the test coupon set is controllable from approx. -60°C to 50°C (for health and safety reasons the maximum temperature used was 30°C). Different temperatures can be generated at different times in the test cycle. The coolant from the refrigerated circulator flows through a heavily insulated hose into the lower clamp plate/cooling manifold. To maximise the heat transfer capabilities, the coolant from the circulator is in direct contact with the test coupon. The modified lower clamp plate/cooling manifold acts as a large heat sink because of its high rate of thermal conductivity, and this helps to reduce the temperature of the pressure pot and test fluid quickly. To speed this up, returning coolant is diverted through a heat exchanger. This in turn lowers the temperature of the test fluid (JP8) which, when pumped back into the pressure pot (via the showerhead attachment that directs the cold test fluid directly onto the test joint), helps to reduce the temperature of the test joint quickly (thermal shock) and generally lower the temperature of the MSS (down to approximately -40°C).

The temperature of the sealed joint is taken from a PT100 temperature sensor attached to the coupon at the test joint. The temperatures are recorded on the data logging facility of the Si-Plan controller.

9.1.3.3. Pressure

The test apparatus has two chambers which simulate the inside and outside of an aircraft fuel tank. The test coupon forms a boundary between these two chambers. Fuel inertia and tank pressures can be simulated by introducing a pressurised gas (inert, for safety reasons) into the pressure pot. This acts on the test fluid, stressing the sealant slightly. More importantly a slight vacuum into the lower cooling manifold centre chamber can be combined with the above, below the test coupons, to simulate the pressure differential experienced by the wing during flight. This, in effect, pulls the fuel through the interfay joint, possibly causing an advancement of a leak path tip.

Health and Safety issues were addressed. As well as an automatic safety relief valve, there is a manual release valve and a pressure transducer attached to the Pressure Pot (PP). The pressure transducer enables the control system to:

- Monitor and record the pressure within the PP
- Enable a shut down procedure should there be a sudden rise in pressure. This should not happen because of the spring relief valve, but it could ice-up and seize closed
- Enable a comparison to be made between the readings from the pressure transducer and the hydrocarbon (HC) detector. For example, if a leak is detected with the HC detector and, simultaneously, there is a drop in pressure in the PP, it may be possible to dispense with the HC detector system altogether and only use a pressure drop system for leak detection.

The pressures can range from 12.3 psi (0.85 bar) to 35 psi (2.4 bar) (gauge pressure). Pressures above 1 bar are set using a Norgren pressure regulator, whilst the pressures below 1 bar are controlled by turning the vacuum pump on/off using a vacuum switch connected to the Si-Plan controller.

9.1.4. Leak detection

The requirement for leak detection is to not only to detect the presence of a leak, but also to trace the leak from its point of exit to its point of origin.

Leak testing encompasses procedures for one or more of the following:

- Locating (detecting and locating leaks)
- Determining the rate of leakage
- Continuously monitoring for leaks.

Many methods of leak testing are available. For the detection of fuel leaks from an aircraft integral fuel tank, the following methods are most applicable:

- Sniffing Test with Helium Tracer Gas and a Mass Spectrometer
- Sniffing Test with Halogen Tracer Gas
- Chemical Detection with Ammonia Tracer Gas
- Hydrocarbon Leak Detection (Hydrocarbon "Sniffer")
- Pressure Decay Test
- Bubble Emission Techniques
- Acoustic Emission
- Visual Techniques.

The most sensitive methods are listed first. All the methods, with the exception of the pressure decay test, measure the leak location but not the leak rate. The pressure decay test measures the leak rate but not the leak location.

In the early stages of the project, getting the coupons to leak, being able to trace the leak, and being able to establish when the leak occurred, was the focus of testing.

Initially, visual methods were used. It required the component under test to be filled with the test fluid (with, maybe, a leak detector colourant added). An investigation into the possibility of using time-lapse techniques with a video camera and taking one second of video a minute had been considered. The test rig could then be left running unattended and if a leak was detected, it would

have been relatively easy to establish when the leak occurred. This method was discounted earlier in the project for several reasons, one being the space available beneath the test coupon, especially using the liquid nitrogen **(See Section 9.1.3.2)** for the lens of the camera and secondly, the definition of the available camera was not particularly good.

Another visible method of leak detection is based on the application of coloured or fluorescent liquid penetrants. The liquid penetrant should be applied to ensure complete coverage of one surface without allowing penetrant to touch the opposite surface. Immediately after application of the penetrant, the developer should be applied to the opposite surface. Fluorescent liquid penetrants have a greater sensitivity than the coloured dye penetrants. Leaks are then detected by visual observation, with the use of optical aids (such as mirrors, magnifiers etc) if required. This method (with some modifications) was adopted for an initial test to see if the joint would leak with no sealant applied at all **(Fig. 9.1)** (A more complete description of the above is provided by Hooper et al (2003)**).**

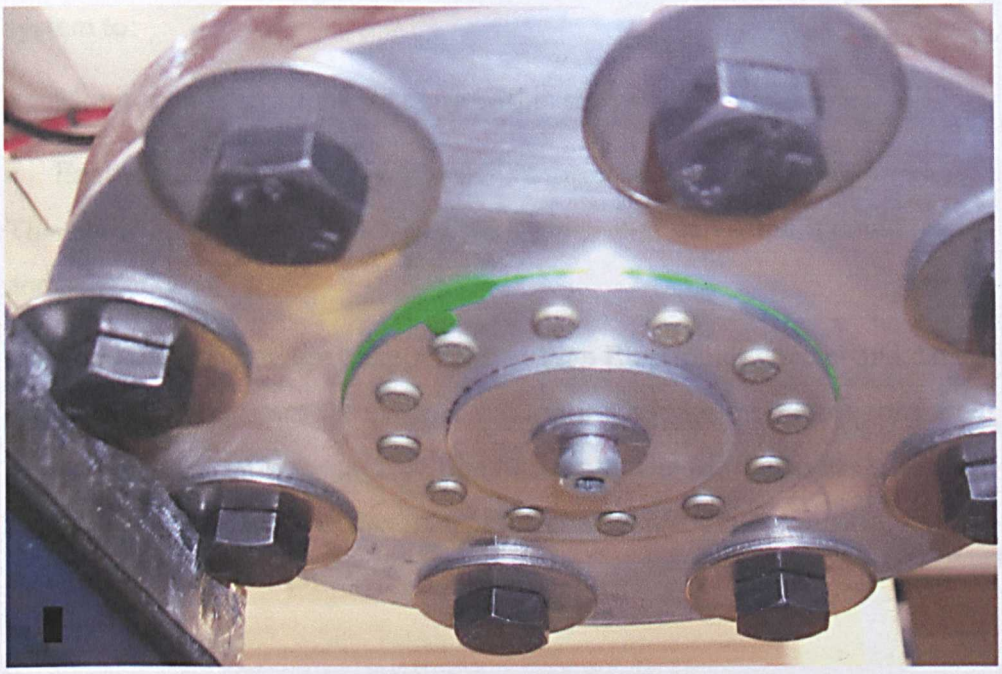

Figure 9.1 An early leak test using green dye to trace the leak from a joint with no sealant applied. This is the fluid leak at approximately twenty-four hours.

The hydrocarbon (HC) detector used in the MSS is a solid state device manufactured by Figaro (model LPM-2610) (described in **Section 7.7.).** Basically, it works by comparing a reference voltage (V_{ref}) against an output voltage (V_{out}) from the detector that increases if there are hydrocarbons detected. When the value of V_{out} exceeds the value of V_{ref}, a safety trip on the controller stops the test. The HC detector as used in the MSS at present is not capable of measuring a leak rate because this would require that the module's output voltage (V_{out}) was calibrated to a known HC concentration (ppm in air) in the flow of air from beneath the test coupon. This would require a more sophisticated (and expensive) HC sensor.

9.1.5. Safety features

Health and Safety issues have been addressed in the design of the MSS. On the Pressure Pot (PP), several systems are used to ensure that the pressure is maintained within the prescribed safety limits. As well as an automatic safety relief valve, there is a manual release valve and a pressure transducer attached to the Pressure Pot (PP) **(Fig.7.18).** The pressure transducer enables the control system to:

- Monitor and record the pressure within the PP.
- Enable a shut down procedure should there be a sudden rise in pressure. This should not happen because of the spring relief valve, but it could ice-up and seize closed.

To avoid overloading the coupons the Si-Plan Electronics control and data acquisition system uses safety trips that trip if the loads on the coupons are exceeded by the fatigue machine (load control). The MSS also has several temperature and pressure sensors that the control and data acquisition system uses. These are there to:

- Log data
- Act as sensors for alarms that enable the controller's adjustable trips to stop the test if certain parameters are exceeded.

The function of these sensors is described in the appropriate section of text.

9.1.6. Robustness

By the end of the project the Phase 2 Model Sealed System (MSS) could be left to run for very long periods without any external interference at all, except to monitor the results. There were a variety of problems in the early stages (described in various monthly progress reports to Airbus UK) ranging from:

- Leaks from the flow meter
- Fuel leaking from fuel hoses(rectified by fitting" Speed-Flex" hoses with screw couplings instead of braided hose and "Jubilee" type hose clips)
- Problems with atmospheric condensation freezing on the various components resulting in unacceptable ice build up on the MSS and related components, and the resultant reduction in the insulating capabilities of the insulating material. This was rectified by wrapping a lot of the components with Clingfilm and/or thin polythene sheet
- A couple of problems with communication between the Si-Plan Electronics controller and the Julabo refrigerated circulator
- Some minor problems with the Julabo refrigerated circulator were rectified under warranty and did not re-occur
- Ice crystals forming in the supply hoses from the Julabo, blocking the supply of coolant to the MSS.

9.1.7. Changing the specimen

The specimen can be changed relatively easily. This does, however, involve an almost complete strip down of the Pressure Pot (PP) after draining the various fluids (coolant into the Julabo and fuel into the external fuel tank), disconnecting all of the various fuel and coolant hoses along with the vacuum/pressure hose and disconnecting the various pressure and temperature sensor cables. The lower part of the pressure pot itself can then be stripped to gain access to the coupon set. The top part need not be stripped allowing the top plate and the related parts to be undisturbed.

A new clamp is bonded to the coupon as near to the sealant joint as possible. A new PT100 temperature sensor is fitted into the clamp and the new coupon is fitted into the PP, renewing any "O" rings disturbed. Special attention should

be paid to tightening the ring of clamp bolts evenly and ensuring that the alignment pins are used to ensure alignment and centralisation (**Fig. 9.2**). The PP is then refitted into the fatigue machine, the various electrical, fluid pressure and vacuum hoses are reconnected. A short test programme is then run to check the integrity of the various seals and hoses at different temperatures and pressures; this also allows a check to be carried out that ensures that the controller and the Julabo are connected and operating correctly. If everything is functioning correctly, the required test programme can be installed in the controller and the new test can begin. The total time taken for a typical procedure is approximately 8 hours.

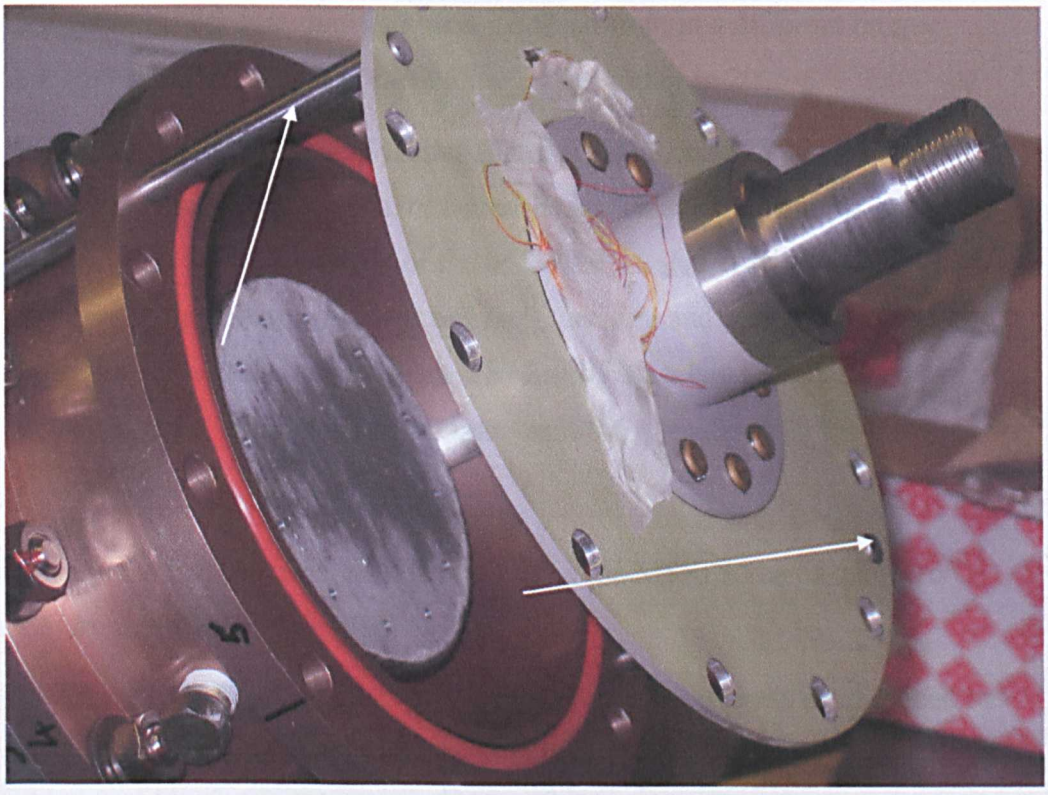

Figure 9.2 The coupon set (including the modified inner coupon and centre hub) being aligned during assembly. This shows the showerhead, the alignment pins (arrowed) and the silicone "O" ring.

9.1.8. Replication and manufacture of additional systems

The replication and manufacture of additional systems has, to a certain degree, already been carried out at Oxford Brookes University (OBU). The blank (No holes drilled) coupon sets are manufactured on site at OBU, sent to Airbus UK at Filton where the coupons are cleaned, degreased, deoxidised, anodised and finally painted they are then returned to OBU for the holes to be drilled and reamed. The coupons have the sealant applied as per required and the fasteners fitted and allowed to cure for the pre-requisite time before being fitted to the Pressure Pot (PP) for inclusion within the Model Sealed System (MSS). As well as the above, two complete PP assemblies were drawn and manufactured at OBU for assembly at Airbus UK, Filton. These were slightly different to those at OBU because they had been modified to fit in a different fatigue machine at Filton. This was carried out by the author in 2005-6.

For multiple Model Sealed Systems to run simultaneously there is a need for two or more fatigue machines, or a modification made to the upper and lower mountings to facilitate the use of the added PP's together with modifications to the various pipe unions (coolant and fuel), vacuum and pressure hoses, and the sensor and solenoid control cables. The Julabo has a large enough cooling/heating capacity for more than one MSS.

9.1.9. Limitations of the system

There are several limitations inherent within the MSS. Some of them are compromises relating to cost.

As discussed in **Section 5.7** it was felt that the actual stresses experienced by the wing may be too high to achieve, realistically, on the test rig in the laboratory. However, it has been shown that it is possible to replicate the relative proportions between the various stresses experienced by the wing.

The thickness of the aluminium that the skin/butt-straps/stringers are manufactured from is at least 6.3 mm, with the smallest diameter fasteners being 5/16 in. (7.94 mm). If the test coupons had been manufactured from materials of these dimensions there would have been several problems:

- For the coupons to have had a representative number of fasteners (12) the coupon's outside diameter would have to be approximately 363mm instead of

216mm. This would not normally have been a problem but for the size of the fatigue machine in the laboratory, with the insulation and the inlet and outlet ports fitted, the pressure pot only just fitted in the available space in the "Mayes" fatigue machine (**Figure 9.3**).

- The thermal mass of the MSS had to be kept as low as possible to enable the prescribed temperatures to be reached. It must be remembered that the initial method used to heat and cool the MSS was by electric tape to heat, and liquid nitrogen and cooled synthetic fuel to cool, so again size was an important issue.

If a realistic model were to be designed to more precisely duplicate the maximum stresses and strains experienced by a real sealant joint, then the thickness of the aluminium sheet used, the fasteners, along with the pitching and edge distances proportions would need to be scaled down to maintain dimensional constancy. The final coupons were manufactured from 3.18 mm thick aluminium sheet fastened with 3/16" (4.762mm) titanium fasteners. The coupon sizes, materials, their stresses and fastener spacings were determined initially as a compromise between the realities of airframe construction and the stresses derived from strain measurements on mock ups of the coupon configuration. It was initially felt that there would need to be at least five fasteners used in the test piece. In the final configuration, twelve fasteners were used. This gave a greater number of possible leak paths available per test.

Some of the other limitations of the MSS are that:

- To enable shear forces to be exerted on the coupons a new fatigue machine would have to be purchased or the old one modified. Unfortunately, neither of these options were viable due to financial limitations.

- The number of sealant joint types that can be tested using the MSS is limited at the moment

- At the moment the MSS can only inform that a leak is present; it cannot trace the leak or quantify the extent of the leak

- The size of the PP restricts the amount of test fluid (jet fuel) that can be in contact with the sealant joint. Geometry affects the rate of fluid penetration into the sealant and the extraction of material back out. For example, thinner

specimens equilibrate faster than thick ones (Healey, 1996). This means that if there is a limited amount of fuel in the MSS, extractives from the sealant may dissolve into the fuel and alter its properties in relation to long term testing of the sealant. In the real world the fuel in the tank is used, and the tank refilled many times with fresh fuel which may or may not affect the performance of the sealant in the tank. This means that the fuel in the MSS should be changed frequently.

- The size of the sealant joint itself means that there is only a very small sealant joint in the test coupon (104mm diameter or 326 mm long), in relation to the full size aircraft (an Airbus A 380 has a wingspan of 262ft or 80 m) and, as Keller (2004) (**Appendix 5**) wrote in a private communication "I recently saw 40-year-old OEM applied sealant in B-52's and it looked great. Further, sealed wing parts from a retired B-52 of this vintage were tested at Wright-Patterson AFB and they still met the lap shear requirements of the specification." This suggests that of all the many metres of joints in an aircraft wing, only a relatively low percentage actually leak (this was also confirmed by Taylor, 2006(a)), so to get this small length of sealed test joint to leak in a representative timescale is challenging.

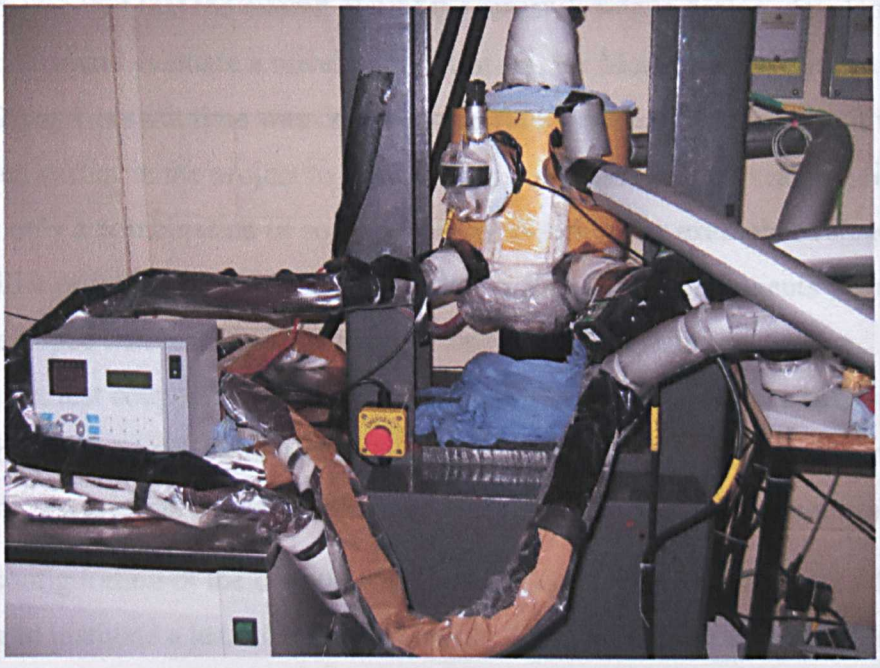

Figure 9.3 The Pressure Pot (PP) situated within the fatigue machine

9.1.10. Problems in the development of the MSS

The main problem encountered was having to use liquid nitrogen to cool the MSS. A Julabo refrigerated circulator was first suggested (by the author) as the method of controlling the temperature of the MSS in April of 2003. Unfortunately, the financial constraints imposed by Airbus at the time meant that two separate systems had to be used, one to heat and another to cool the MSS. These systems were wholly inadequate for the reason previously described. This meant that from April 2003 when Julabo were first contacted until delivery of the Julabo in July 2004, progress on the MSS was slow due to designing, manufacturing and testing a system that only worked for a few consecutive days at best.

9.2. Evaluation of sealed joint systems

9.2.1. Selection of coupon configuration, loading, environment and timescale

A complete sealant joint can be tested using the MSS with all of the components present, for example, interfay, fillet, wet assembled fasteners and overcoat, but this tends to lengthen the test time before a leak occurs. It must be remembered that the overall aim of the research was to design, develop, fabrication and evaluate a novel sealant test rig, (or Model Sealed System (MSS)) and as such time was of paramount importance. Consequently, it was decided earlier in the project to manufacture aerospace quality, sealant joints using only a combination of some of the components, for example overcoat and fillet or interfay and wet assembly, but not all of the components at once. It was hoped that this would instigate a leak in a shorter time scale (For example, test coupon set 02-06 only had overcoat and fillet sealant application and this test was still running at 123 days with no leak) and would allow a realistic assessment of the MSS's performance within a suitable timeframe.

The configuration of the coupon within the MSS is an important factor when trying to instigate a leak in the sealant joint. The coupons are assembled in the manner shown in **Figure 9.4,** rather than that shown in **Figure 9.5,** for two reasons (note that the loads in both instances will result in the joint being opened). Firstly, the length of the sealant joint is longer in this configuration,

allowing a greater length of sealant to be in contact with the jet fuel increasing the chance of a leak occurring. Secondly, to instigate a leak, the load should be applied in such a manner as to enable the joint to open rather than close. If the configuration shown in **Figure 9.7** is used the joint can open but the inner coupon /hub will be subjected to a stress raiser at the junction of the hub and inner coupon (arrow **Fig. 9.7**) that could result in premature failure of the inner coupon /hub assembly(**see Section 6.1, Test coupon set**). **Figure 9.6** shows the smaller resultant angle that is present if the coupon configuration shown in **Figure 9.7** is used.

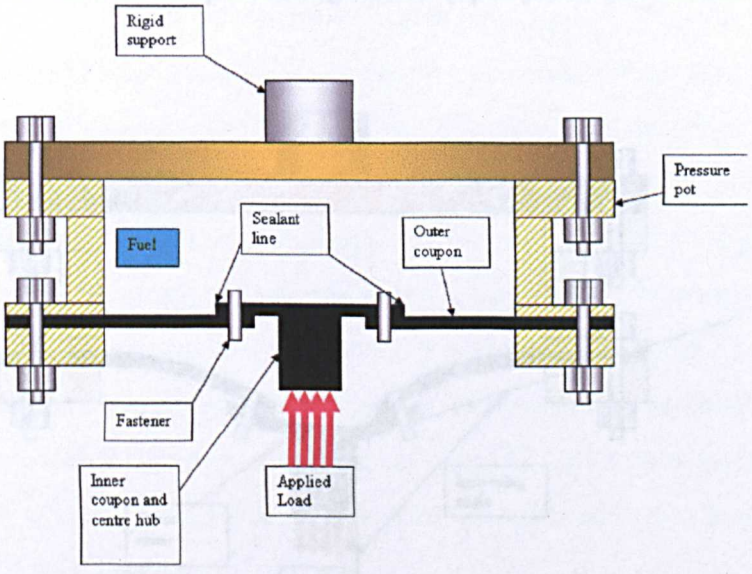

Figure 9.4 Conventional coupon configuration (open joint)

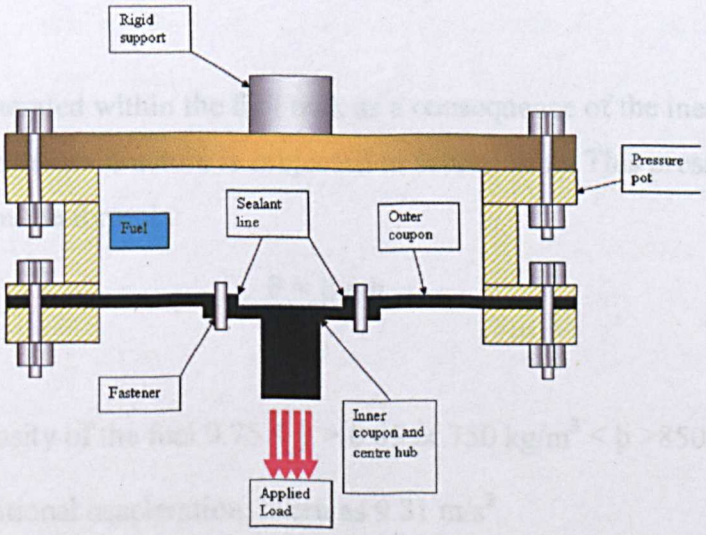

Figure 9.5 Alternative coupon configuration (open joint)

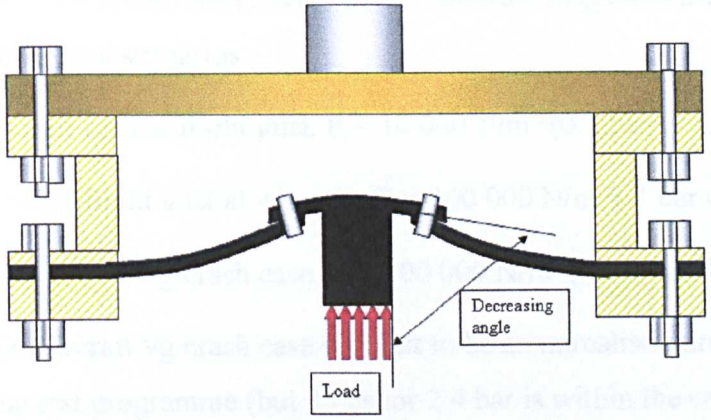

Figure 9.6 Conventional coupon configuration (open joint) (movement exaggerated)

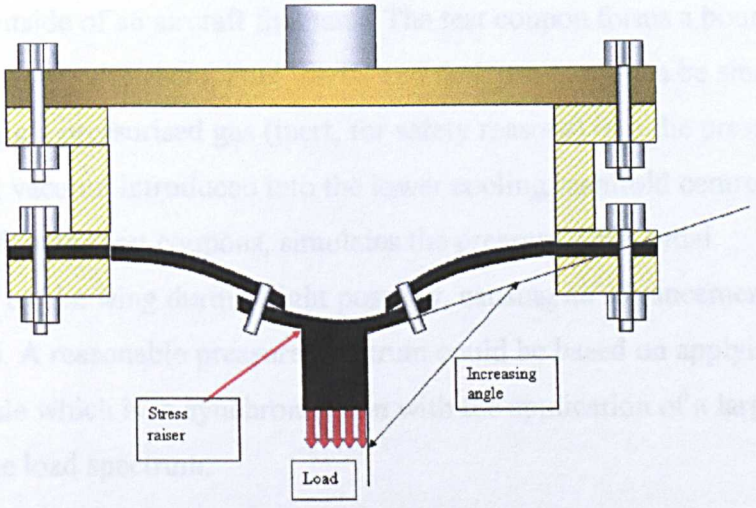

Figure 9.7 Alternative coupon configuration (open joint) (movement exaggerated)

Pressure is generated within the fuel tank as a consequence of the inertia of the fuel when the aircraft structure is subjected to acceleration. This pressure (P) is calculated from the formula:

$$P = \rho g h$$

Where:

- ρ is the density of the fuel $0.75 < \rho > 0.85$ or $750\ kg/m^3 < \rho > 850 kg/m^3$
- g is gravitational acceleration, taken as $9.81\ m/s^2$
- h is the depth of the fluid above point P in metres(m)

Figures supplied from Airbus (UK) (Taylor, 2003(b)) suggested these pressures for several scenarios:

- Large aircraft typical flight gust. P = 10 000 N/m ^{2}(0.1 bar or 1.45 psi)
- Large aircraft flight gust at wing tip. P = 100 000 N/m ^{2}(1 bar or 14.5 psi)
- Large size aircraft 9g crash case. P = 500 000 N/m ^{2}(5 bar or 72.5 psi)

The large size aircraft 9g crash case was felt to be an unrealistic pressure to include in the test programme (but 35 psi or 2.4 bar is within the capabilities of the MSS). Airbus stipulated that the total pressure must be representative of the aircraft cycles identified above, i.e. cycles in the range 10 000 N/m ^{2}(0.1 bar) < P < 100 000 N/m ^{2}(1 bar). The PP has two chambers which simulate the inside and outside of an aircraft fuel tank. The test coupon forms a boundary between these two chambers. Fuel inertia and tank pressures can be simulated by introducing a pressurised gas (inert, for safety reasons) into the pressure pot. A slight vacuum introduced into the lower cooling manifold centre chamber, below the test coupons, simulates the pressure differential experienced by the wing during flight possibly, causing an advancement of a leak path tip. A reasonable pressure spectrum could be based on applying a pressure cycle which is in synchronisation with the application of a large load in the fatigue load spectrum.

9.2.2. Axial and torque loading

Early in the project a decision was made to investigate the application of torsion to the coupon set whilst simultaneously being subject to axial fatigue **(Section 6.4)**. With the integrated centre hub and inner coupon, excluding the use of adhesive or bolted connections between the centre hub and inner coupon, this would have been a relatively easy modification to perform. Unfortunately though, as previously mentioned, there were several reasons why this avenue of testing was not followed, the main one being financial. The fatigue machine required would need to be of a bi-axial type that cost £70k to £90k at 2006 prices. However, there is no reason why a bi-axial load could not be applied to the test coupon in the future.

9.2.3. Influence of coupon quality on results

The quality of the coupons themselves, the finish before and after the application of the various Airbus surface conditioning procedures, the machining of the fastener holes and the application of the sealant are all governed by the various Airbus ABP (Airbus Process Specifications) and the materials (aluminium plate, titanium fasteners and the MC-238 B2 polysulfide sealant) governed by AIMS (Airbus Industrie Material Specification). These were adhered to unless Airbus requested modification, as in the case of sealant application (see **Section 9.2.1**).

An important factor that needed to be addressed was the alignment of the coupons. Because the loads are applied in an axial direction, it is important that the coupons are aligned concentrically. This ensures that the stresses experienced by any part of the coupon are the same, such as the stresses between any of the fasteners in the sealant joint. This was a particular problem earlier in the project with the bonded centre hub requiring an alignment tool to be designed and manufactured to allow the adhesive to cure in the correct alignment. With the integrated centre hub and inner coupon, this was unnecessary.

The application of the sealant and the assembly of the coupons can lead to anomalies if a statistical analysis is to be carried out. It is important to exclude as many variables as possible from the manufacture of the coupons. Using the same materials for the coupons themselves, the same fasteners and sealant from the same batch should reduce these variables. However, these coupons are assembled manually and although carried out by a skilled technician this will introduce some variability. Additional variables can range from the temperature and humidity in the assembly area, variations in the cleanliness and probably most important of all, the skill of the various technicians when carrying out the preparatory machine work, the consequent sealant application and assembly of the coupons. To reduce this, one option may be to have a single location, with the same individuals carrying out the various machining and assembly operations, thereby reducing some of the many variables that can be introduced in the manufacture of the test coupons. Some of the causes of fuel tank leaks are discussed and illustrated in **Section 8.5.3.**

9.2.4. Typical test regimes used in the research

No single environmental condition is the single ingredient in degradation of fuel tank containment integrity. A combination of structural loading, fuel inertia, tank pressures, thermal and chemical effects, influence the structural integrity of the fuel tanks. A test spectrum can be written for the control system that addresses some of these parameters. An example flight cycle is shown below.

- **Start position –** Room temperature
  Fuel exposure
  Atmospheric pressure
  Zero load
- **Stage 1 -** Cooling to -55°C
  Fill tank and circulate fuel
  2 hours duration
  Apply a pressure pulse to the fuel (6 x 5 second pulses)
  Static loading, 4.5kN, closing the sealant joint
- **Stage 2 -** Cooling to -55°C
  2 hours duration
  Circulate fuel
  Cyclic loading, 5 Hz (-1.5kN to -4.5kN, opening the sealant joint)
- **Stage 3 -** Cooling to -55°C
  2 hours duration
  Circulate fuel
  Cyclic loading, 5 Hz (1kN to 4kN, closing the sealant joint)
- **Stage 4 -** Cooling to -55°C
  2 hours duration
  Circulate fuel
  Cyclic loading, 5 Hz (-1.5kN to -4.5kN, opening the sealant joint)

Repeat stages 1 to 4, three times for a total of 24 hours. This is then repeated, in this case 14 times, which is equivalent to a 14 day test.

This was the basis for the first test programmes. This was modified to provide some additional test parameters throughout the test programme. The Si-Plan control system allowed a programme to be written that provided a comprehensive test subjecting the test joint to several stresses, pressures and temperatures.

- **Start position –** Room temperature
  No fuel in PP
  Atmospheric pressure
  Zero load
- **Stage 1 -** Cooling to -55°C
  Fill PP and circulate fuel
  2 hours duration
  Apply a pressure pulse to the fuel (6 x 5 second pulses)
  Static loading, 4.5kN, closing the sealant joint

- **Stage 2 -** Cooling to -55°C
  2 hours duration
  No fuel circulation
  Cyclic loading, 5 Hz (-1.5kN to -4.5kN, opening the sealant joint)

- **Stage 3 -** Cooling to -55°C
  2 hours duration
  Circulate fuel
  Cyclic loading, 1 Hz (1kN to 4kN, closing the sealant joint)

- **Stage 4 -** Cooling to -55°C
  2 hours duration
  No fuel circulation
  Cyclic loading, 5 Hz (-1.5kN to -4.5kN, opening the sealant joint)

Repeat stages 1 to 4, three times for a total of 24 hours. This is then repeated, in this case 4 times.

It was found that after a minimum of approximately 4 days (but sometimes it was as much as 10 days) the MSS began to heat up whilst the Julabo refrigerated circulator was still registering -55°. The fault was eventually traced to a blockage that took a few days to form in the coolant pressure hose. To rectify the problem an extra stage was inserted at the end of the fourth day. This stops ice crystals forming and eventually blocking the coolant feed pipes from the Julabo.

Stage 5 - Heat to 20°C
Circulate fuel
2 hours duration
Static loading, -4.5kN, opening the sealant joint

Stage 5 only occurs once every four days. This cycle of 5 stages is then repeated as many times as required or until a leak occurs.

9.2.5. Leak detection and definition of failure

Several systems can be used to stop the test, but only one if a leak is detected, the hydrocarbon detector (sniffer). As previously described, if a leak is detected, the gas sensor module is exposed to a higher than normal concentration of hydrocarbons in the airflow. This, in turn, sends a signal to the controller and a safety trip on the controller stops the test.

This method will not quantify the leak but rather it recognises that there is an increase in hydrocarbons and stops the test. Care must be taken that the hydrocarbons in question are not the coolant from the refrigerated circulator leaking. If it is coolant rather than fuel, it is relatively easy to discern which fluid is leaking by smell and observing from where the leak appears to have originated.

Once it has been established from where the hydrocarbons have originated, and if it is not the cooling system, then the test is deemed to be finished because the test joint has failed.

The next step is to remove the test coupon from the PP and try to trace the leak either using the method described in **Section 9.1.4** or the other methods described in **Section 8.5.3**

9.2.6. Timescale of testing

9.2.6.1. Full scale fatigue test

This section has been included to illustrate some of the problems that have been encountered by previous projects and the timescale of the tests involved.

The MSS at OBU was initially developed to carry out coupon tests to help in the development of a full scale test item that was to be used by Airbus UK to investigate the integrity of sealant systems for in service aircraft fuel tanks. The duration of the full scale fatigue test proposed by Airbus was based on the Design Service Goal (DSG) for the Single Aisle aircraft (Airbus 318). To meet the certification requirements of the regulatory authorities, it is necessary to demonstrate that a fatigue life twice that of the DSG for the aircraft in the full scale fatigue test can be achieved. It was felt that it was not practical to test for the full duration of DSG x 2 using a combined load and environmental

spectrum due to the time constraints of the programme due to the length of time that a DSG x 2 would take (Buller, 2002(a)). It was therefore necessary to design the test using a truncated or shortened load spectrum together with superimposed pressure, temperature and fuel cycles. The DSG of the Single Aisle aircraft (Airbus 318) is 48000 flight cycles (FC) (A flight cycle is a take-off and landing cycle). To put this into perspective, Richardson (1989) states that the design life of a Lockheed C-130 Hercules was assumed to be 40,000 flight hours giving a projected life of 30 years.

The construction of the full-size, integral fuel tanks at Air Force Material Laboratories, Wright-Patterson, U.S.A.F, is covered in **Section 4.5**. It was proposed that a full-scale, structural, fatigue test item (an aircraft wing), which is mandatory for airworthiness requirements be constructed. Airworthiness certification is concerned with applying cyclic loads, representative of the aircraft's flight envelope, to the structural test item. The testing is conducted dry (without fuel) at temperatures that prevail in the test hall. The proposal was used to conduct the structural fatigue test with the addition of using fuel, subject to pressure and temperature cycles representative of actual flight conditions.

The in-flight temperature data from a C-130 was reduced to a programme that could easily be applied in a short period of time, using the Arrhenius Law to convert time-temperature exposures to a shorter exposure at a different temperature to produce an equivalent sealant degradation.

Actual aircraft usage consists of ground time followed by flight time, with refuelling between each. To simulate actual aircraft usage the test spectrum was divided into six test cycles with fuel changes every five days.

The test cycle was repeated six times per 40,000 equivalent flight hours. The length of one cycle was 210.3 hours, therefore six cycles took 1261.8 hours (52.6days) to complete.

There were problems with this system, the main ones being fatigue damage and safety. If the timescale of the test is examined it would suggest that a minimum of nearly 60 days is required. In fact this was not the case. The time required to reach the equivalent of 60,000 flight hours testing the C-130 test

tank was nearer to nine months (allowing for repairs and inspections) (Richardson, 1989).

Full-scale structural testing is appropriate for airworthiness certification purposes and is the ultimate Model Fuel Tank (MFT). However, it is not a suitable tool for experimental materials testing for research purposes and Airbus have not, as yet, built a full scale Model Fuel Tank (MFT).

9.2.6.2. The Model Sealed System (MSS)

The Model Sealed System (MSS) at OBU was developed initially to carry out coupon tests. However, the MSS itself quickly developed into a stand alone mechanism for the future evaluation of sealant materials for commercial or military aircraft, that could expose realistic sealed joint systems to typical dynamic and environmental parameters representative of actual flight conditions. Unlike the Full Scale Model Fuel Tank (FSMFT), the MSS can provide an adequate tool for experimental testing for research purposes. The MSS achieves this through the combination of applied fatigue and/or static loads, and the application of the environmental parameters of fuel, pressure and temperature in a relatively compact, cheap and safe mechanism. Unlike the FSMFT, the lower fatigue loads applied result in relatively low stresses (representing 1g flight stress and 30fps gust (**Section 5.7**))that replicate the relative proportions between the various stresses experienced by the aluminium coupons and the titanium fasteners (representing the wing skin and fasteners in real life) and this certainly loads the joint more highly than in normal flight. Consequently, this should shorten the time required to test the joint configuration and sealant adequately, but the stresses are not high enough to cause any damage to the coupons or fasteners themselves. More research needs to be carried out to define a test regime that produces a joint failure within a certain time-frame, consistently. So far it has caused joint failure at 11, 44 and 135 days. Recalling the test durations in **Table 8.21,** the average length of a test before a fuel leak occurs can be seen to be 75 days. From this it can be seen that more coupons have to tested in the MSS, using the same test regimes, to identify patterns of data that relate to variations in test parameters to enable some meaningful statistical analysis to be carried out and a test programme defined.

9.2.7. Comparisons of data with conventional testing

There are several ways in which the results can be evaluated and presented. The MSS can employ dynamic and environmental cycling as two independent testing regimes, or combined as one synergistic test to instigate an earlier failure. As such the MSS can be used to develop an enhanced capability for the evaluation of aircraft wing fuel tank sealing materials and sealing performance for in-service aircraft. This mechanism can, along with the FSMFT, the modular wing-box and even Mallory and Elmers (1978) Wright-Patterson Bench "Dynamic" Apparatus to some extent, be used to:

- Indicate inadequacies in the design of the joint
- Aid in the selection and type of sealant used
- Carry out evaluation and comparative tests on new experimental sealants early in their development when only a small sample of the test sealant may be available for testing
- Carry out Preliminary screening of sealants for new aircraft.

The results obtained from the above tests cannot reveal the sealants' physical qualities as determined from conventional testing using the methods described in **Appendix 3.** The data must not therefore replace conventional testing, but should be used alongside as valuable complementary information about potential system performance.

9.3. Recommended test regime for the evaluation of sealed joint system and sealant selection

9.3.1. Recommended MSS test programme

The test programmes referred to in **Section 9.2.4** were used to (i) investigate the MSS control system,(ii) to provide familiarisation with the control system and (iii)to undertake preliminary testing to try to instigate a leak within a reasonable time frame.

Any *new* programme should include an improved spectrum of physical and environmental parameters that include some of the parameters covered in the previous text **(Section 9.2.4),** as well as some new parameters tailored to suit.

These new parameters would include imposing a permanent 1bar pressure (14.7 psi) (gauge pressure) inside the PP. This, together with the depression that exists below the test coupon of 20 to 25 in Hg (9.8 to 12.3 psi or 0.67 to 0.85 bar), would ensure that there is always a pressure differential across the joint (except at those times when it is required for the test fluid to be moved to and from the PP to the external fuel tank). The pressure differential amounts to a difference of 0.15 to 0.33 bar (2.4 to 4.9psi) across the joint. This would increase if the pressure pulsations (35 psi or 2.4 bar, that simulate high manoeuvre G loads, are applied increasing the pressure differential to 1.55 to 1.73 bar (22.7 to 25.2 psi). This would, in effect, pull the fuel through the interfay joint. The programme would also include longer times between cycles to bring the test more in line with real flight times.

Start position – Room temperature
No fuel in PP
Atmospheric pressure
Zero load

- **Stage 1 -** Cooling to -55°C
  Fill PP and circulate fuel
  6 hours duration
  Apply an internal air pressure to PP
  Apply a pressure pulse to the fuel (6 x 5 second pulses)
  Static loading, 4.5kN, closing the sealant joint

- **Stage 2 -** Cooling to -55°C
  6 hours duration
  Apply an internal air pressure to PP
  No fuel circulation
  Cyclic loading, 5 Hz (-1.5kN to -4.5kN, opening the sealant joint)

- **Stage 3 -** Cooling to -55°C
  6 hours duration
  Apply an internal air pressure to PP Circulate fuel
  Cyclic loading, 1 Hz (1kN to 4kN, closing the sealant joint)

- **Stage 4 -** Cooling to -55°C
  6 hours duration
  Apply an internal air pressure to PP
  No fuel circulation
  Cyclic loading, 5 Hz (-1.5kN to -4.5kN, opening the sealant joint)

Stages 1 to 4 total 24 hours. This is then repeated four times for a total of 4 days.

To rectify the problem of ice crystals forming **(Section 9.2.4)** the extra stage is inserted at the end of the fourth day.

Stage 5 - Heat to 20°C
Circulate fuel
Apply an internal air pressure to PP
2 hours duration
Static loading, -4.5kN, opening the sealant joint

Finally, if all Health and Safety issues have been addressed, the higher temperatures used in the test should be increased to address the temperature related sealant degradation issues referred to by Meyer(1982) and the assumptions referred to in Richardson's paper that suggests that:

- Significant sealant degradation does not occur below 120°F(48.9°C)
- Significant sealant degradation does not occur at sub-zero temperatures

The modified stage could be:

Stage 5 - Heat to 50°C
Circulate fuel
8 hours duration
Apply (using an inert gas) an internal pressure to PP
Static loading, -4.5kN, opening the sealant joint

Stage 6 - Heat to 50°C
Circulate fuel
8 hours duration
Apply (using an inert gas) an internal pressure to PP
Cyclic loading, 5 Hz (-1.5kN to -4.5kN, opening the sealant joint)

Stage 7 - Heat to 50°C
Circulate fuel
8 hours duration
Apply (using an inert gas) an internal pressure to PP
Cyclic loading, 1 Hz (1kN to 4kN, closing the sealant joint)

Stages 1 to 4 total 24 hours. This is then repeated four times for a total of 4 days.

Stages 5, 6 and 7 would take 24 hours to complete at which point the programme would return to stage 1 to repeat the cycle.

To simulate a dry tank cycle, another stage could be inserted. This could simulate the storage cycle when the sealant could dry out and crack (Healey, 1996). Stages 5, 6 and 7 could be replaced by a drying cycle. The modified stage could be:

Stage 5 - Heat to 50°C
Drain fuel from PP
15 days duration
Apply (using an inert gas) an internal pressure to PP
Static loading, 4.5kN, closing the sealant joint

Stage 6 - Heat to 50°C
Drain fuel from PP
15 days duration
Apply (using an inert gas) an internal pressure to PP
Static loading, -4.5kN, opening the sealant joint

Of course, increasing the temperatures to over 50°C would take the temperature of the fuel to temperatures in excess of its flash point (38°C) and as such would render the test extremely dangerous.

9.3.2. Sealant selection protocols

The tests could be separated into two types of test:

- A test to failure on several coupons tested at the same time using several MSSs. This will enable some meaningful results to be collated and a statistical analysis to be carried out on the test coupon sealant configuration, the sealant itself, and to validate the MSS itself.

- A Quality Control (QC) test for sealants. After validation, the MSS could be used as a QC check to:

    - Ensure that sealed systems exceed a certain standard set by the end user

    - Grade sealants into classes.

Altering the severity or focusing on different parameters in the test, the sealant could be graded to enable the sealant to be used in the manner that suits its physical attributes the best. **Table 9.1** shows an example of the possible

sealant test criteria that a sealant of a certain hypothetical class might have to pass. The tests would be carried out over a prescribed time-frame for the different sealants.

Hypothetical sealant class basic acceptance	Static load	Fatigue load	Test Fluid	High G loads	Temperature conditioning		Pressure Differential	Wet/Dry cycle	
					Hot	Cold		Wet	Dry
Class 1	✓	✖	✓	✖	✓	✖	✓	✓	✖
Class 2	✖	✓	✓	✖	✖	✓	✓	✓	✖
Class 3	✓	✓	✓	✓	✓	✓	✓	✓	✓

Table 9.1 Test spectrum to differentiate a hypothetical sealant class criteria.

10 Conclusions

The aims and objectives set out at the beginning of the project were achieved.

The hypothesis that states that fuel tank testing must be accomplished using actual jet fuel and using realistic combinations such as structural loading, fuel inertia, tank pressures, thermal and chemical effects is accepted within the aerospace industry (Richardson (1989). To achieve this, the design, development, fabrication and evaluation of a novel sealant test rig (Model Sealed System (MSS)) was successfully carried out.

10.1. Development of the MSS

A mechanism was developed that subjects a circular lap joint to cyclic axial stresses whilst simultaneously imposing a range of experimental parameters. At the heart of the MSS lies the novel coupon set. The test sealant is sandwiched between the two bolted aluminium circular coupons of dissimilar size mounted concentrically. The resultant circular lap joint is assembled using aerospace fasteners and sealed, and it simulates a wing skin butt-strap joint in a real aircraft. However, by making it circular the complications of corners and joint ends are eliminated.

As the MSS is now a modular test system that can simulate a combination of structural loading, fuel inertia, fuel tank pressures, thermal and chemical effects, it would appear that most of the requirements set out in Richardson's hypothesis and Keller's statement (see **Introduction** and **Appendix 5**) have been addressed and overcome.

Early indications are that the MSS with the Si-Plan data logging and control system enables:

- Test programs to be written relatively easily
- Real flight data to be imported to the control module (although this has not been tried yet).
- The MSS to be a fully automatic test machine with programmable fatigue, environmental, pressure and empty/fill cycles.

- The MSS to have safety cut-outs to stop a test if any of the test parameters are exceeded.

- The MSS to be programmed for tests of any duration.

Most importantly the MSS causes a leak to occur and detects it in a representative aerospace standard joint within a realistic time frame using realistic test parameters.

The MSS can also enable the:

- Evaluation and comparative testing on new experimental sealants to be carried out early in their development

- Preliminary screening of sealants for new aircraft to be accomplished

- Maintenance and operational cost to be reduced, since field use conditions can be simulated, thereby reducing the need for costly and time consuming flight tests.

10.2. Data obtained from the MSS

More data needs to be obtained from the MSS to define a test regime that produces a joint failure within a certain time-frame, consistently. So far it has caused joint failure at 11, 44 and 135 days. This shows that the concept does work but more research needs to be carried out to define a test regime that produces a joint failure within a certain time frame, consistently.

10.3. Data from the small scale testing

The results of the dumb-bell testing were mainly inconclusive because of several factors (i.e. the size and geometry of the specimens). The results show that, generally, exposure to the various fluids resulted in a decrease in the sealants peak stress capability when compared to exposure in air.

The H-type joint tests gave comparable results to those achieved by Clark (2001) and it appears that polysulfide-aluminium H-type joints are weakened by immersion in JP8, deionised water and saline solution for 56 days. It also suggests that saline solution affects the failure stress and strain of the sealant and could be the basis of future work.

Dynamic Mechanical Thermal Analysis generally confirmed the results of testing carried out by Airbus (Healey, 1996) and others and confirmed that the storage modulus T_g for MC-238 B2 polysulfide sealant is around -47 to -51°C. It also confirmed Healy's findings in that the Modulus at -55°C (the temperature at which the MSS can operate) increases considerably from around 2.25 MPa to around 1000MPa (1GPa), with an extreme case of 2110 MPa (2.11GPa) for immersion in saline solution for 56 days. This also suggests that saline solution affects polysulfide sealant.

10.4. FEA of the coupon set

The results from the FE analysis of the MSS coupon set indicate that:

- Reasonable correlation was obtained between the actual and predicted stresses for a joint in compression
- The coupon configuration chosen (both coupons 3.18mm thick) results in the best compromise of stresses in the materials to satisfy the MSS design parameters
- The sealant should not fail due to excessive strain under the maximum load conditions.

10.5. Recommendations for future work

The PP should be in an insulated self contained environmental cabinet attached to a designated fatigue machine. The control valves and related hoses should also be contained within an insulated cabinet. All of the coolant hoses and fuel hoses should be kept as short as possible to reduce heat loss (and gain). The inclusion of a dehumidifier for the air supply to the inside, of both, the PP environmental chamber and the control valve/hose cabinet would reduce ice build up and the related problems. The inclusion of a dehumidifier within the air inlet system (especially to the pressure pot) would also reduce the condensation, and hence un-metered water, within the fuel system.

Future work should also include the use of torsion within the fatigue cycle, this is because even though early, preliminary, stress analysis using strain gauges and the prototype coupons (with slip fit fasteners) (**Section 6.4**) were inconclusive (and financially beyond the scope of the project at that time). It is

felt that the inclusion of torsion within the fatigue cycle would increase the stresses on the sealant, the coupon set and especially the fasteners, instigating a comparable leak to those experienced in the real integral fuel tank.

In the future, the MSS may enable realistic physical and environmental cycles to be simulated, enabling qualitative and comparative testing of combinations of sealants, joint geometries, substrates, surface preparations and cure times. During Phase 1 of the MSS development there was interest in the MSS from other, unrelated, departments within Airbus UK (and an undisclosed outside supplier) as to whether the MSS could be used in the development and testing of new products (West (2003)). In the same conversation it was disclosed that the project was not just for fuel tank sealants but that other materials will be utilised in the test matrix for example, composites, plastics etc.

REFERENCES

ABAQUS /CAE users manual (2001),Version 6.2, Hibbitt, Karlsson and Sorenson

ABAQUS /CAE users manual (2003),Version 6.4, ABAQUS,Inc

Adams, R. D. and Wake, W. C. (1984), Structural Adhesive Joints in Engineering, Elsevier Applied Science Publishers Ltd, Essex.

Advisory Group for Aerospace Research and Development (AGARD) (1989) Fuel Tank Technology, Report No.771, NATO.

Airbus Industries Material Specification (AIMS) 04-05-(000-012) BAE Systems CD ROM issued September 2001.

Airbus UK Ltd. AIMS 04-05-001 Airbus Industrie Material Specification, Sealants, General Purpose, Material Specification. Airbus UK Ltd, Filton, Bristol, September 2000

Airbus UK Ltd. AIPS 98-02-001 Airbus Industrie Process Specification, Material and Process Concession, Application of Phosphoric Acid Anodising for Repairs, February 1996.

Airbus UK Ltd. AITM 2-0013 Airbus Industrie Test Method, Determination of sealant adhesion by linear debonding test, Airbus UK Ltd, Filton, Bristol, November 2000.

Airbus UK Ltd. AITM 7-0006 Airbus Industrie Test Method, Assessment of sealant compatibility, Airbus UK Ltd, Filton, Bristol, November 1995.

Airbus UK Ltd. AITM 1-0030 Airbus Industrie Test Method, Determination of lap shear strength, Airbus UK Ltd, Filton, Bristol, November 1995.

Airbus UK Ltd. AITM 2-0033 Airbus Industrie Test Method, Sealants: Determination of slump, Airbus UK Ltd, Filton, Bristol, November 1996.

Airbus UK Ltd. AITM 2-0035 Airbus Industrie Test Method, Sealants: Determination of shrinkage, Airbus UK Ltd, Filton, Bristol, June 1996.

Airbus UK Ltd. AITM 1-0036 Airbus Industrie Test Method, Sealants – Determination of assembly time, Airbus UK Ltd, Filton, Bristol, November 1995.

Airbus UK.CD-ROM. Updated 2003.

Anderson, D. and Eberhardt, S. (2001). Understanding Flight, McGraw-Hill, New York, , ISBN 0-07-136377-7

Barnard, R. H. and Philpot D.R. (1989). Aircraft Flight, Harlow, Longman Scientific & Technical.

Barrett, R. (1990). NASA reference publication 1228.

Bennett R.T. (1990). Fastener Design Manual, NASA,

Birch, S.(2001). Aerospace Engineering, July, pp21-24.

Brinkmann Instruments (2006), Inc. www.brinkmann.com.

British Standards Institution. Physical testing of rubber, BS 903 A2 (ISO37), 1995.

British Standards Institution. Building and construction, determination of tensile properties (extension to break), BS EN ISO 8339, 2005.

Buller. R.D. (2002) (a). "Study to Support Meteor WP6- Large Wing Fuel Tank Technology." W.S. Atkins Report No.CJ1079_005/R01, January, 2002.

Buller, R.D. (2002) (b). Private communication. June 18th 2002.

Campbell. J. "Effects of Shot Peening Processing on the Fatigue Behavior of Three Aluminum Alloys and TI-AL-4V", Army Research Laboratory, Aberdeen. Weapons and Materials Research Directorate. 5th April 2001.

Chemetall, Qualification Report Naftoseal Aircraft Sealants, AIMS, Airbus UK. 1995.

Chevron Aviation Fuels Technical Review (FTR-3), 2000, Bacha J. et al, Chevron Products Company.

Clark, L. (2001) "The Measurement of the Tensile Adhesion Properties of Aerospace Sealants" SAE VI, Bristol, 4-6th July, 2001.

Coanda, H. (1938) US Patent No 2,108,652 date 15.02.

Comyn, J. (1997) Adhesion Science, The Royal Society of Chemistry, Cambridge, 1997.

Comyn J. Day J. and Shaw, S. (1997). "Durability of Aluminium- sealed Joints in Jet-fuel, Water and Antifreeze" International Journal of Adhesion and Adhesives. Vol.17 No.3 (pp. 213-221).

ConocoPhilips (2006), JP-8 Marketing Specification, FMP No. 1014,as per MIL-DTL-83133E, 1/04/2006

Dawson, G. (1989)."The Repair of Aircraft Integral Fuel Tanks in the RAF" NATO AGARD-R-771.

Duke P. (2002). QinetiQ report for DTI "Model Fuel Tank Feasibility Study Review" Appendix 6: Consideration by QinetiQ of test apparatus for assessing the integrity of sealed joints with regards to fuel leaks (pp.12-18).

Eble.D (2001). How to choose a refrigerated and heating circulator. R&D Magazine.

Floyd, J. (1958) The Canadian Approach to All-Weather Interceptor Development, The Journal of the Royal Aeronautical Society.

Giles G. L. (2003) Design-oriented analysis of aircraft fuselage structures. NASA. Langley Research Center, Hampton, Virginia.

Global Climatic Data for Developing Military Products. US Dept of Defence Handbook, MIL-HDBK-310,1997.

Healey M.J. (1996). " Degradation of Sealants in Service: Physio-Chemical and Mechanical" British Aerospace Report No. B23/96/0083, January 1996.

Hooper M., Hutchinson A. and Broughton J.(2003). Model Fuel Tank Test Rig Development, Phase 1 Final Report, June 2003.

Hooper M., Hutchinson A. and Broughton J. (2004). Aero-Seal Project, Model Fuel Tank Test Rig Development (MSS Construction), Phase 2. Progress Report, January to December.

Hunsicker H.Y. (1987). " Metals Handbook, vol. 13". ASM.

Hutchinson. A.R. (2000). " Durability of Aircraft Integral Fuel Tank Sealing". Project Proposal, October.

Jones, T. (2001). Internal report, Oxford Brookes University.

The International Aluminium Institute (2000).

Keller, W.(2004). Private communication, (March)

Kemmerer, R. (1992). "Improvements in Sealant Technology for Aircraft Production- A Move Towards Environmental and user Friendliness". Proceedings from 13th International European Conference, SAMPE, Germany, May 11-13, (pp. 445-456).

Kutta, M.W.(1902). Thesis on aerodynamics to the Technische Hochschule at Munich.

Lee, T.C.P. (1999). "Properties and Applications of Elastomeric Polysulfides" RAPRA Review report, Vol.9 No. 10.

Mallory. R and Elmer V. (1978). "Dynamic Laboratory Evaluation of Integral Fuel Tank Sealants" National SAMPE 10th Technical Conference, (pp.598-609), Oct. 17-19.

Meyer, R.E. (1982). "Polysulfide Sealants for Aerospace" Part 1. SAMPE Journal (pp. 6-10), December.

Meyer R.E. (1983). "Polysulfide Sealants for Aerospace" Part 2. SAMPE Journal (pp. 27-36), March.

MIL-S-8802F. (1997) "Sealing Compound, Temperature-resistant, Integral Fuel Tanks and Fuel Cell Cavities High Adhesion".

Mulligan, D, Gnaniah, S. and Sims, G.(2000). "Thermal Analysis Techniques for Composites and Adhesives", Measurement Good Practice Guide, No. 32, pp. 9-16, National Physics Laboratory (NPL).

Naftoseal qualification report, MC-238 B2,Naftoseal, Frankfurt, 1998.

Niu, M.(1988). Airframe Structural Design (2nd edition), Hong Kong Conmilit Press Ltd. 1988.

Paris. P.C. (1998). "Fracture Mechanics and Fatigue: A Historical Perspective". Fatigue and Fracture of Engineering Materials and Structures. Vol. 21(5) p535,

Panek J.R. and Cook J.P. (1991). Construction Sealants and Adhesives (pp. 107-127) Wiley and Sons, Inc.

Quilter, A. Head of Strength Analysis Group, ESDU International. "Composites in Aerospace Applications"

Richardson, M.D. (1989). "Integral Fuel Tank Certification and Test Methods", Fuel Tank Technology, NATO AGARD-R-771.

Sheridan. G.N. (1989). "Integral Fuel Tank Practise at British Aerospace" NATO AGARD-R-771.

Taylor. M. Airbus UK, Various diagrams and private communication. (between 2001-2005)

Thompson, J.E. (1990). "Design Consideration Unique to Sealants", Adhesive and Sealants, Vol. 3, Engineered Materials Handbook, ASM International.

Tritec 2000 DMA manual, DMA Theory – Principles of DMA, v1.43

Vishay Group (2003). "Strain Gauge Technology". www.vishay.com

West. C. (Airbus UK, MSS project manager 2002-3) Private communication. September 11th 2003.

Appendix 5

A copy of an email sent in 2004, reproduced with the kind permission of Bill Keller

From: Keller, Bill [bill.keller@prc-desoto.com]
Sent: 13 January 2004 15:14
To: Oxford Brookes University
Subject: RE: E-contact Message

Importance: High

A "puffer box" is a small-scale integral wing tank (size varies but the one I last saw under test at the Boeing C-17 plant was about 10ft X 12 ft. with a root of about 2.5 ft.). They are built exactly like the full-scale wing: fay sealed stringers, ribs, sealed fasteners. When assembled, they fuel it ,then expose it to various heat and pressure cycles, and sometimes physical loading. They are, needless to say, very expensive and time consuming tests to conduct. By their very nature of construction they are generally only built by airframe OEM's and the air force's.

I do not know your background and experience level in this field. If you review the cornerstone material specs for fuel tank sealants, namely AMS-S-8802 (on which the majority of all global aircraft fuel sealant specs are still based), you will note that the baseline tests to assess physical performance are 180^0 peel, and lap shears. Thus far these tests have proved well because our sealants have provided field performance when properly applied of 40+ years.

I recently saw 40-year-old OEM applied sealant in B-52's and it looked great. Further, sealed wing parts from a retired B-52 of this vintage were tested at Wright-Patterson AFB and they still met the lap shear requirements of the spec.

Now the "Holy Grail" question that our Industry is looking for: Can a simple test method be developed that is less cumbersome than a "puffer box", but more real world than peels and lap shears? Such a method must be easily run in a materials lab, reproducible, and accurately simulate the real world dynamics of an aircraft integral tank.

Does your department have a travel budget? I am very serious. If you are working towards the Holy Grail test that I noted, then I would definitely invite your group to present a paper at our SAE subcommittee.

Best regards,

Bill

Appendix 6
The results of sealant tests carried out in the Joining Technology Research Centre (JTRC) at Oxford Brookes University in 2006

Introduction

A limited investigation, into which typical fluids (jet fuel, water and saline solution) that can affect sealant properties, was undertaken. Results from this investigation were used to inform the MSS parameters to accelerate the time to failure of the sealant under test. The objectives of this part of the research were to:

- Investigate which fuel contaminants (water (fresh and salt)) affect the properties of the sealant (good or bad).
- Investigate the influence of different temperatures on the sealant properties.

Three types of test were used:

- Dumb-bell
- H-type joints
- Dynamic Mechanical Thermal Analysis (DMTA).

Table 6.1 shows the information that can be achieved with each test.

Type of Test	Young's Modulus (E) GPa	Peak Stress (σ_{peak})	Peak Strain (ε_{peak})	Failure Stress (σ_{fail})	Failure Strain (ε_{fail})	Glass transition temperature (T_g)	Adhesion
Dumb-bell	✓	✓	✓	✓	✓	×	×
H-Type	✓*	✓**	✓**	✓	✓	×	✓
DMTA	✓	×	×	×	×	✓	×

Table 6.1 Type of test used and results gained

Note:

*** Secant modulus usually at 60% or 100% extension or any other elongation decided by the parties concerned.** These are usually used in a comparative or qualitative test**

The sealant used was Chemetall MC-238 B2 in all cases. The conditioning used for the specimens cured in air was 23°C ± 2°C and a relative humidity of 50% ± 5%. The temperature used for the fluids (jet fuel, de-ionised water and saline solution) was 23°C ± 2°C.

6.1. Dumb-bell test (ISO 37)

The bulk properties of the sealant was determined after immersion in jet fuel, water and saline solution over the different time periods (14, 28 and 56 days) and compared with the baseline test in air at 14 days.

6.1.1. 14 day cure

6.1.1.1. 14 day baseline cure

The data collected from all three dumb-bell specimens can be seen in Table 6.2.

Specimen Number	Maximum stress (MPa)	Peak strain(%)	Young's Modulus (MPa)	Locus of Failure
BL 14-1	1.735	337.7	2.214	No break. Slipped from jaws.
BL 14-2	1.740	318.3	3.071	No break. Slipped from jaws.
BL 14-3	1.625	295.9	2.543	No break. Slipped from jaws.
Average and Standard deviation	1.70±0.06	317±21	2.61±0.43	
Date samples made-15/06/2006	Age at test -14days	Test date-19/06/2006	Test temperature-30°C RH-30%	Test speed -500mm/min

Table 6.2 Dumb-bell test results baseline cure at 23°C 50%RH

The results of the dumb-bell test show that the initial value of Young's Modulus may be taken as **2.61 MPa** with a standard deviation of **0.43 MPa.**

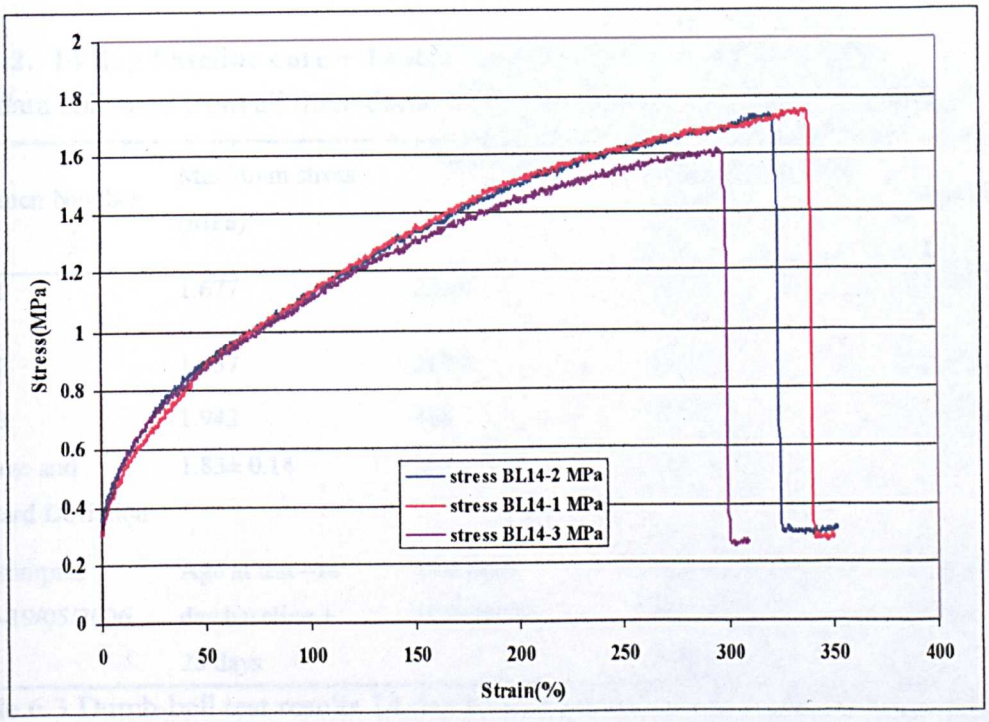

Figure 6.1 Results of 14 day baseline test.

6.1.1.2. 14 day baseline cure + 14 day cure in air@23°C and 50%RH

The data collected from all three dumb-bell specimens can be seen in **Table 6.3.**

Specimen Number	Maximum stress (MPa)	Peak strain(%)	Young's Modulus (MPa)	Locus of Failure
A14-1	1.677	253.8	5.037	No break.
A14-2	1.857	319.4	4.912	No break.
A14-3	1.942	318	3.578	No break.
Average and Standard Deviation	1.83± 0.14	297 ± 37.5	4.51 ± 0.8	
Date samples made-19/05/2006	Age at test –14 day baseline + 28 days	Test date-16/06/2006	Test temperature-31.1°C RH-25%	Test speed - 500mm/min

Table 6.3 Dumb-bell test results 14 day baseline cure + 14 days @ 23°C 50%RH

The results of the dumb-bell test show that Young's Modulus may be taken as **4.51MPa** with a standard deviation of **0.8 MPa.**

NOTE: Sample A14-1 data didn't log correctly consequently it has been left from the graph.

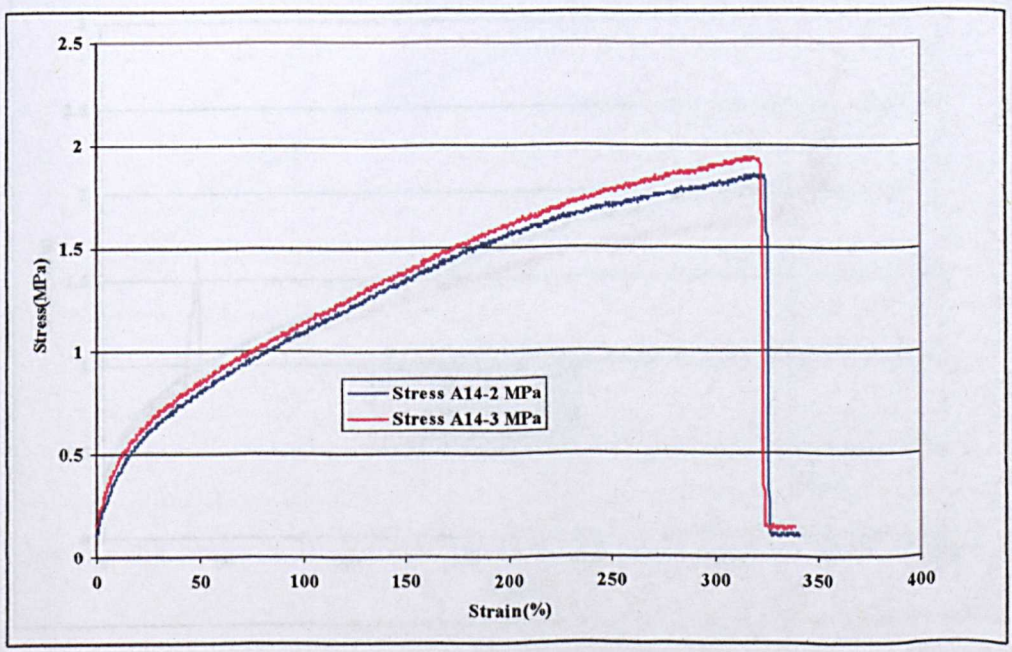

Figure 6.2 Results of 14 day baseline test + 14 days air @ 23°C 50%RH

6.1.1.3. 14 day baseline cure @23°C and 50%RH+14 days in saline solution (10%ww)

The data collected from all three dumb-bell specimens can be seen in **Table 6.4.**

Specimen Number	Maximum stress (MPa)	Peak strain(%)	Young's Modulus (MPa)	Locus of Failure
S14-1	2.06	280.8	2.92	10% void.
S14-2	1.90	284.6	2.73	10% void
S14-3	2.15	430	2.64	No break. Curve deleted from graph.
Average and Standard Deviation	2.04± 0.13	331.8 ± 85.06	2.76± 0.14	
Date samples made-19/05/2006	Age at test –14 day baseline + 28 days	Test date-16/06/2006	Test temperature-31.1°C RH-25%	Test speed - 500mm/min

Table 6.4 Dumb-bell test results 14 day baseline cure at 23°C 50%RH + 14 days in saline solution

The results show that Young's Modulus may be taken as **2.76 MPa** with a standard deviation of **0.14 MPa.**

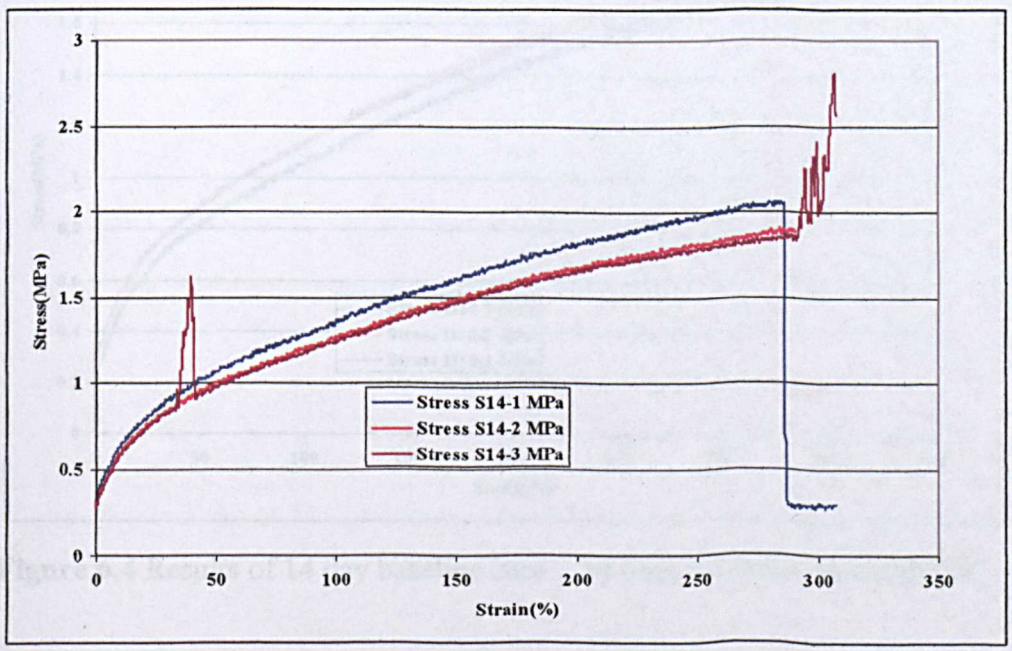

Figure 6.3 Results of 14 day baseline test + 14 days saline

6.1.1.4. 14 day baseline cure @23°C and 50%RH+14 days in deionised water@23°C

The data collected from all three dumb-bell specimens can be seen in **Table 6.5**

Specimen Number	Maximum stress (MPa)	Peak strain(%)	Young's Modulus (MPa)	Locus of Failure
D14-1	1.778	354.1	4.292	10% void.
D14-2	1.83	319.3	4.398	20% void.
D14-3	1.87.	367.9	3.472	Slipped from jaws. No break.
Average and Standard Deviation	1.80± 0.04	347.1± 25.04	4.05± 0.5	
Date samples made-19/05/2006	Age at test –14 day baseline + 28 days	Test date-16/06/2006	Test temperature-31.1°C RH-25%	Test speed - 500mm/min

Table 6.5 Dumb-bell test results14 day baseline cure at 23°C 50%RH + 14 days in de-ionised water.

The results show that Young's Modulus may be taken as **4.05 MPa** with a standard deviation of **0.5 MPa.**

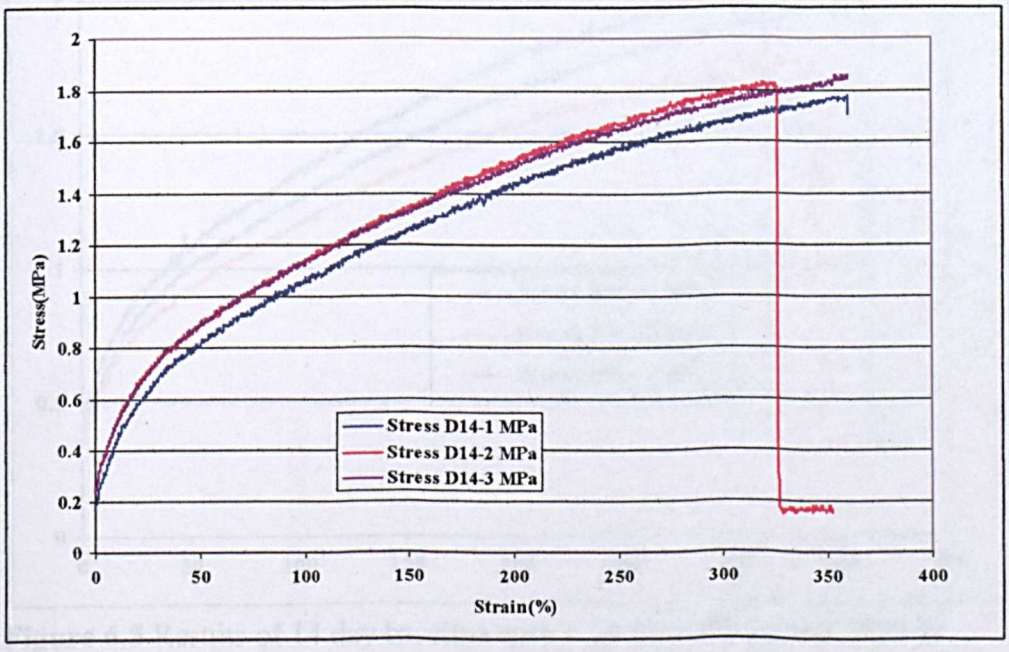

Figure 6.4 Results of 14 day baseline cure + 14 days deionised water@23°C

6.1.1.5. 14 day baseline cure @23°C and 50%RH +14 days in jet fuel (JP-8).

The data collected from all three dumb-bell specimens can be seen in **Table 6.6**

Specimen Number	Maximum stress (MPa)	Peak strain(%)	Young's Modulus (MPa)	Locus of Failure
JP14-1	1.998	352.8	2.531	No break.
JP14-2	1.784	356.9	2.297	No break.
JP14-3	2.094	315.2	2.423	30% void
Average and Standard Deviation	1.96 ± 0.16	341.63± 22.98	2.42± 0.12	
Date samples made-19/05/2006	Age at test –14 day baseline +	Test date-16/06/2006	Test temperature-31.1°C RH-	Test speed - 500mm/min

Table 6.6 Test results 14 day baseline cure at 23°C 50%RH + 14 days in JP-8.

The results show that Young's Modulus may be taken as **2.41 MPa** with a standard deviation of **0.11 MPa**.

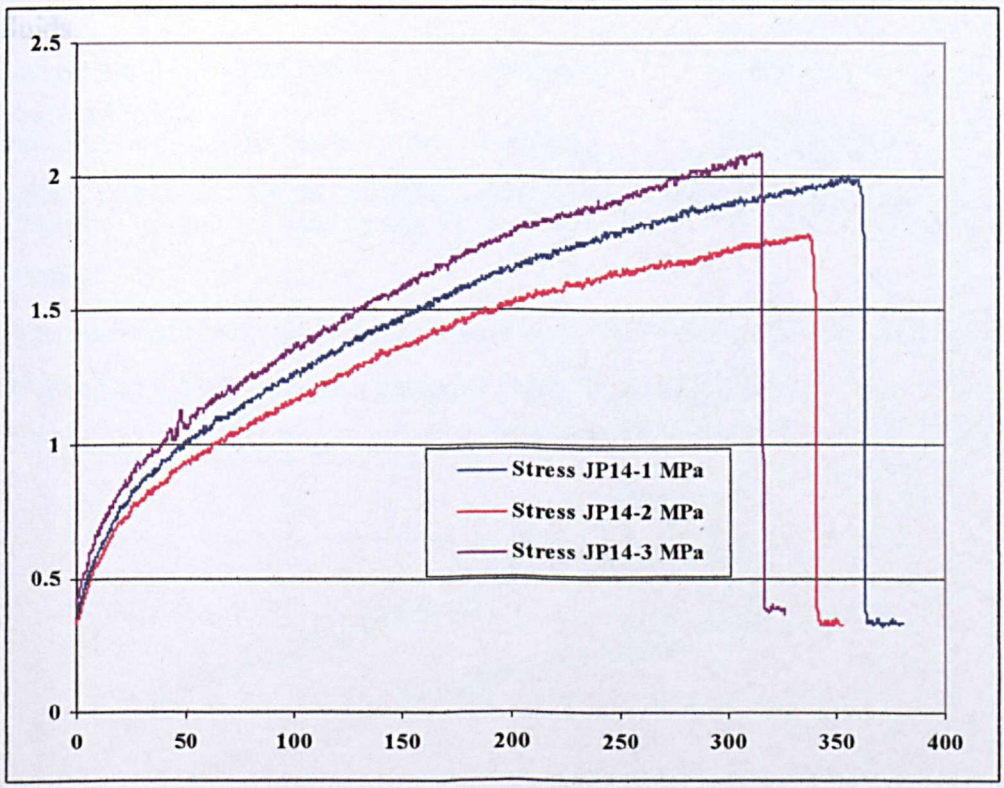

Figure 6.5 Results of 14 day baseline cure + 14 days JP8 jet fuel @23°C

6.1.1.6. 14 days immersion in fluids combined results

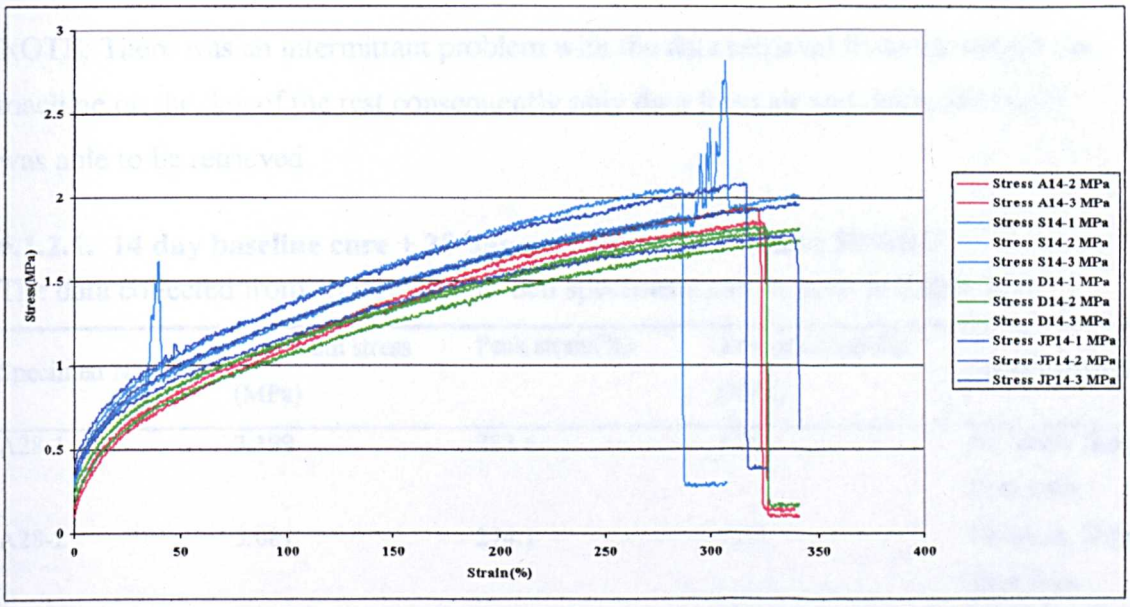

Figure 6.6 Combined results of 14 day baseline cure + 14 days immersed in various fluids.

6.1.2. 28 day cure

NOTE: There was an intermittant problem with the data retrieval from the tensile test machine on the day of the test consequently only data from air and deionised water was able to be retrieved.

6.1.2.1. 14 day baseline cure + 28 day cure in air@23°C and 50%RH

The data collected from all three dumb-bell specimens can be seen in **Table 6.7.**

Specimen Number	Maximum stress (MPa)	Peak strain(%)	Young's Modulus (MPa)	Locus of Failure
A28-1	3.199	283.6	1.70	No break. Slipped from jaws.
A28-2	3.081	274.1	1.53	No break. Slipped from jaws.
A28-3	2.543	279.5	1.66	No break. Slipped from jaws.
Average and Standard deviation	2.94±0.35	279.1±4.76	1.63± 0.09	
Date samples made-5/06/2006	Age at test - 14 day baseline + 28 days	Test date-18/07/2006	Test temperature-32°C RH-35%	Test speed - 500mm/min

Table 6.7 Dumb-bell test results 14 day baseline cure + 28 day cure in air@23°C and 50%RH

The results of the dumb-bell test show that the initial value of Young's Modulus may be taken as **1.63 MPa** with a standard deviation of **0.08 MPa.**

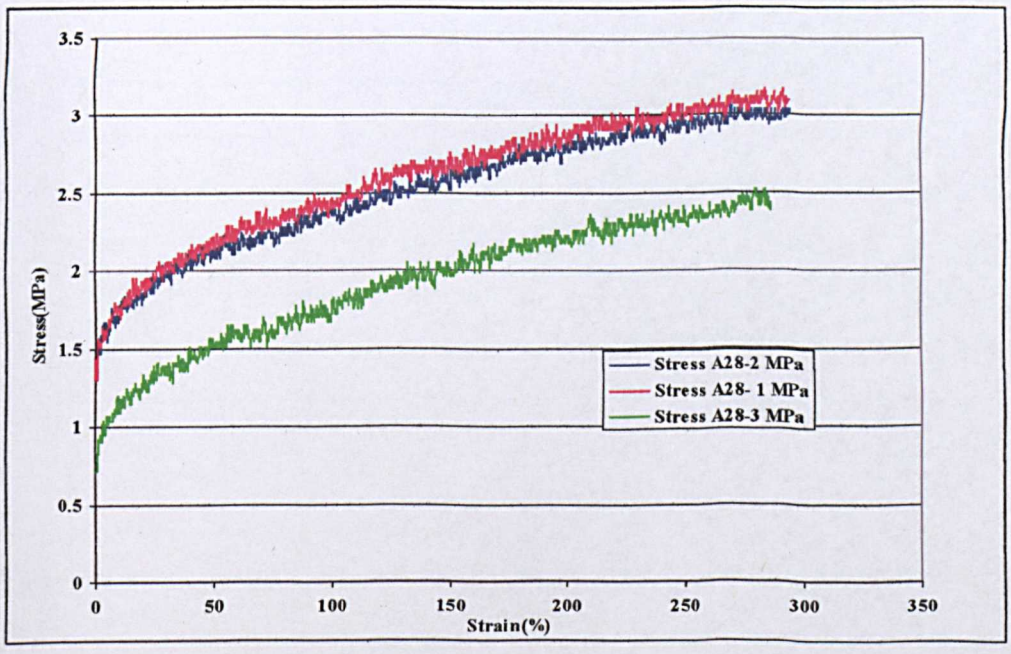

Figure 6.7 Combined results of 14 day baseline cure + 28 days air @ 23°C 50%RH

6.1.2.2. 14 day baseline cure @23°C and 50%RH+28 days in saline solution (10%ww)

The data collected from all three dumb-bell specimens can be seen in **Table 6.8**

Specimen Number	Maximum stress (MPa)	Peak strain(%)	Young's Modulus (MPa)	Locus of Failure
S28-1	1.113	280.1	1.656	No break. Slipped from
S28-2	1.214	277	1.88	No break. Slipped from jaws.
Average and Standard deviation	1.16±0.07	278.5±2.19	1.77± 0.16	
Date samples made-5/06/2006	Age at test – 14 day baseline + 28 days	Test date-18/07/2006	Test temperature-32°C RH-35%	Test speed - 500mm/min

Table 6.8 Dumb-bell test results 14 day baseline cure + 28 day cure in saline solution.

The results of the dumb-bell test show that the initial value of Young's Modulus may be taken as **1.76 MPa** with a standard deviation of **0.16 MPa**.

6.1.2.3. 14 day baseline cure @23°C and 50%RH+28 days in deionised water@23°C

The data collected from all three dumb-bell specimens can be seen in **Table 6.9**

Specimen Number	Maximum stress (MPa)	Peak strain(%)	Young's Modulus (MPa)	Locus of Failure
D28-1	1.598	271.2	1.131	No break. Slipped from jaws.
D28-2	1.516	282.5	1.506	No break. Slipped from jaws.
D28-3	1.119	289.5	1.335	No break. Slipped from jaws.
Average and Standard deviation	1.41±0.26	281±9.23	1.32 ± 0.19	
Date samples made-5/06/2006	Age at test - 14 day baseline + 28days	Test date-18/07/2006	Test temperature-32°C RH-35%	Test speed - 500mm/min

Table 6.9 Dumb-bell test results 14 day baseline cure + 28 day cure in de-ionised water

The results of the dumb-bell test show that the initial value of Young's Modulus may be taken as **1.32 MPa** with a standard deviation of **0.18 MPa.**

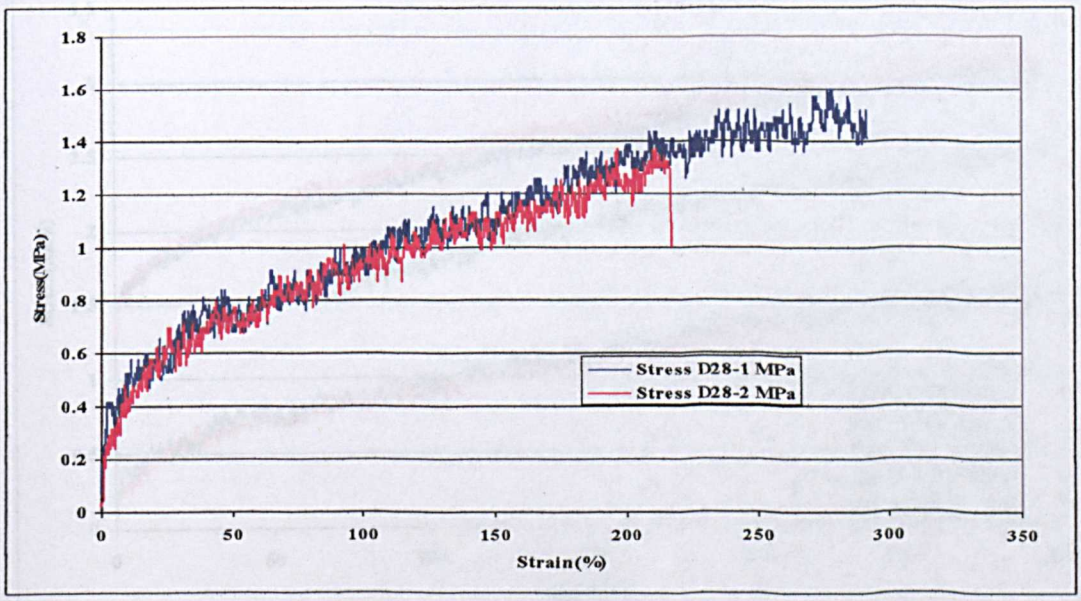

Figure 6.8 Combined results of 14 day baseline cure + 28 days deionised water @ 23°C .

6.1.2.4. 14 day baseline cure @23°C and 50%RH +28 days in jet fuel (JP-8)@ 23°C.

The data collected from all three dumb-bell specimens can be seen in **Table 6.10**

Specimen Number	Maximum stress (MPa)	Peak strain(%)	Young's Modulus (MPa)	Locus of Failure
JP28-1	1.543	284.3	1.738	No break. Slipped from jaws.
JP28-2	1.13	267	1.543	No break. Slipped from jaws.
JP28-3	2.01	267	1.441	No break. Slipped from jaws.
Average and Standard deviation	1.56±0.44	272.76±9.99	1.57 ± 0.15	
Date samples made-5/06/2006	Age at test - 14 day baseline + 28 days	Test date-18/07/2006	Test temperature-32°C RH-35%	Test speed - 500mm/min

Table 6.10 Dumb-bell test results 14 day baseline cure + 28 day cure in JP8 jet fuel at 23°C

The results of the dumb-bell test show that the initial value of Young's Modulus may be taken as **1.57 MPa** with a standard deviation of **0.15 MPa**.

6.1.2.5. 28 days immersion in fluids combined results

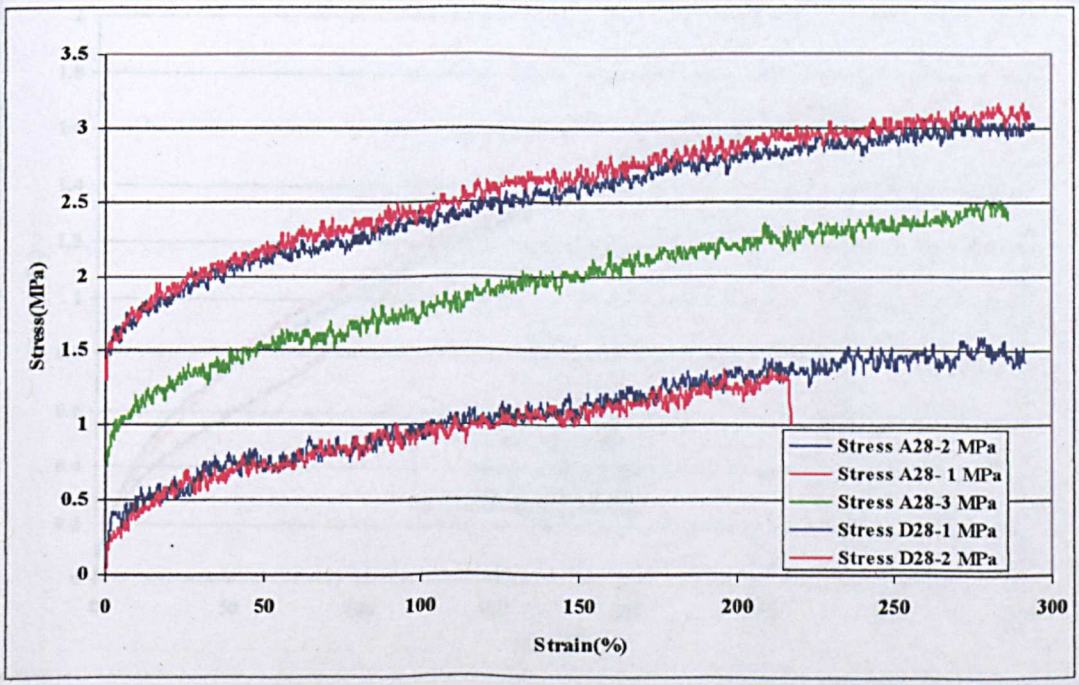

Figure 6.9 Combined results of 14 day baseline cure + 28 days immersed in various fluids.

6.1.3. 56 day cure

6.1.3.1. 14 day baseline cure + 56 day cure in air@23°C and 50%RH

The data collected from all three dumb-bell specimens can be seen in **Table 6.11**

Specimen Number	Maximum stress (MPa)	Peak strain(%)	Young's Modulus (MPa)	Locus of Failure
A56-1	1.657	279.9	3.241	Small voids
A56-2	1.683	270.6	2.774	No break. Slipped from jaws.
A56-3	1.828	351.8	1.928	No break. Slipped from jaws.
Average and Standard deviation	1.72±0.09	300.8±44.44	2.65± 0.67	
Date samples made-19/05/2006	Age at test -14 day baseline + 56 days	Test date-28/07/2006	Test temperature-32°C RH-35%	Test speed - 500mm/min

Table 6.11 Combined results of 14 day baseline cure + 56 days in air@23°C.

The results of the dumb-bell test show that the initial value of Young's Modulus may be taken as **2.64 MPa** with a standard deviation of **0.66MPa.**

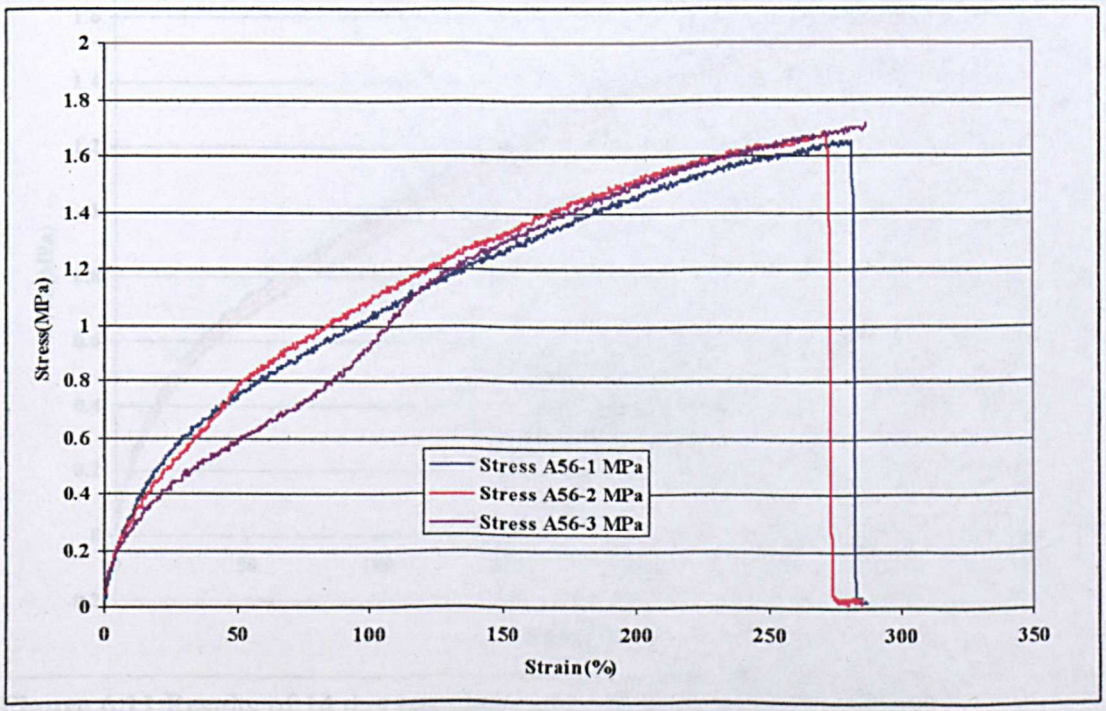

Figure 6.10 Results of 14 day baseline cure + 56 days air @ 23°C 50%RH

6.1.3.2. 14 day baseline cure @23°C and 50%RH+ 56 days in saline solution (10%ww)

The data collected from all three dumb-bell specimens can be seen in **Table 6.12**

Specimen Number	Maximum stress (MPa)	Peak strain(%)	Young's Modulus (MPa)	Locus of Failure
S56-1	1.66	317.2	2.918	Small voids
S56-2	1.59	302.4	2.576	No break. Slipped from jaws.
S56-3	1.47	298.3	2.408	No break. Slipped from jaws.
Average and Standard deviation	1.57 ±0.10	305.97±9.94	2.63± 0.26	
Date samples made-19/05/2006	Age at test - 14 day baseline +56 days	Test date-28/07/2006	Test temperature-32°C RH-35%	Test speed - 500mm/min

Table 6.12 Combined results of 14 day baseline cure + 56 days in saline solution.

The results of the dumb-bell test show that the initial value of Young's Modulus may be taken as **2.63 MPa** with a standard deviation of **0.26MPa**.

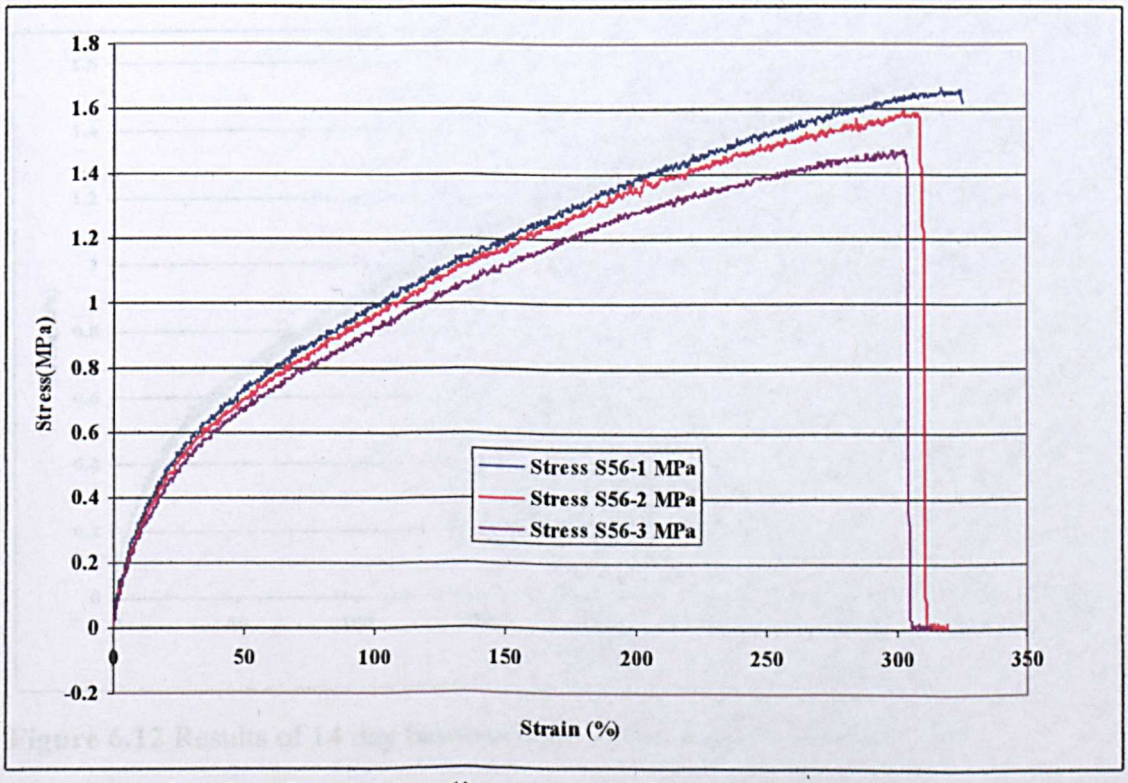

Figure 6.11 Results of 14 day baseline cure + 56 days in saline solution.

6.1.3.3. 14 day baseline cure @23°C and 50%RH+ 56 days in deionised water@23°C

The data collected from all three dumb-bell specimens can be seen in **Table 6.13**

Specimen Number	Maximum stress (MPa)	Peak strain(%)	Young's Modulus (MPa)	Locus of Failure
D56-1	1.508	324.6	2.371	No break. Slipped from jaws
D56-2	1.47	328.3	2.304	No break. Slipped from jaws
D56-3	1.47	316.7	2.336	Small voids
Average and Standard deviation	1.48 ±0.02	323.2±5.93	2.34 ± 0.03	
Date samples made-19/05/2006	Age at test – 14 day baseline +56 days	Test date-28/07/2006	Test temperature-32°C RH-35%	Test speed - 500mm/min

Table 6.13 Combined results of 14 day baseline cure + 56 days in de-ionised water.

The results of the dumb-bell test show that the initial value of Young's Modulus may be taken as **2.34 MPa** with a standard deviation of **0.03 MPa**.

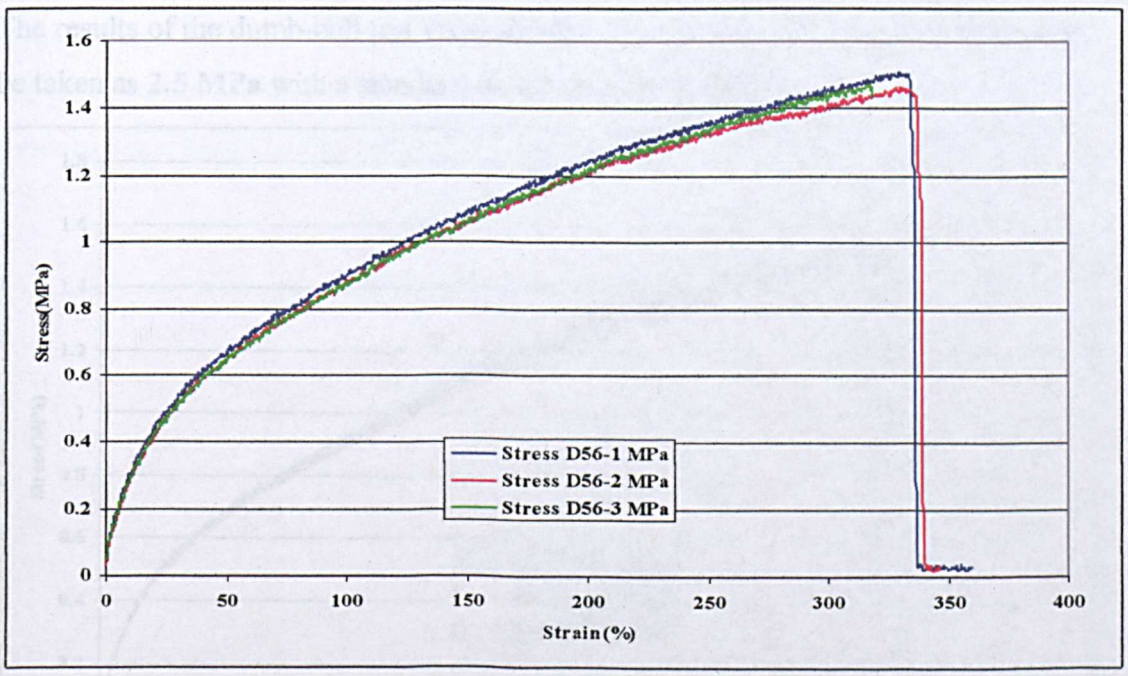

Figure 6.12 Results of 14 day baseline cure + 56 days in de-ionized water.

6.1.3.4. 14 day baseline cure @23°C and 50%RH + 56 days in jet fuel (JP-8)@ 23°C.

NOTE: Samples JP56-1 to 3 had dried out before the test due to fuel evaporation leaving them above the fuel level. Sample JP56-4 had remained immersed in the fuel for the full 56 days.

The data collected from all three dumb-bell specimens can be seen in **Table 6.14**

Specimen Number	Maximum stress (MPa)	Peak strain(%)	Young's Modulus (MPa)	Locus of Failure
JP56-1	1.437	278.9	2.432	Small voids
JP56-2	1.158	175.1	2.483	Small voids
JP56-3	1.519	324.9	2.597	
JP56-4	1.57	347.1	2.49	
Average and Standard deviation	1.42 ±0.18	281.5± 76.4	2.5 ± 0.07	
Date samples made-19/05/2006	Age at test – 14 day baseline +56 days	Test date-28/07/2006	Test temperature-32°C RH-35%	Test speed - 500mm/min

Table 6.14 Combined results of 14 day baseline cure + 56 days in JP8 jet fuel.

The results of the dumb-bell test show that the initial value of Young's Modulus may be taken as **2.5 MPa** with a standard deviation of **0.07 MPa.**

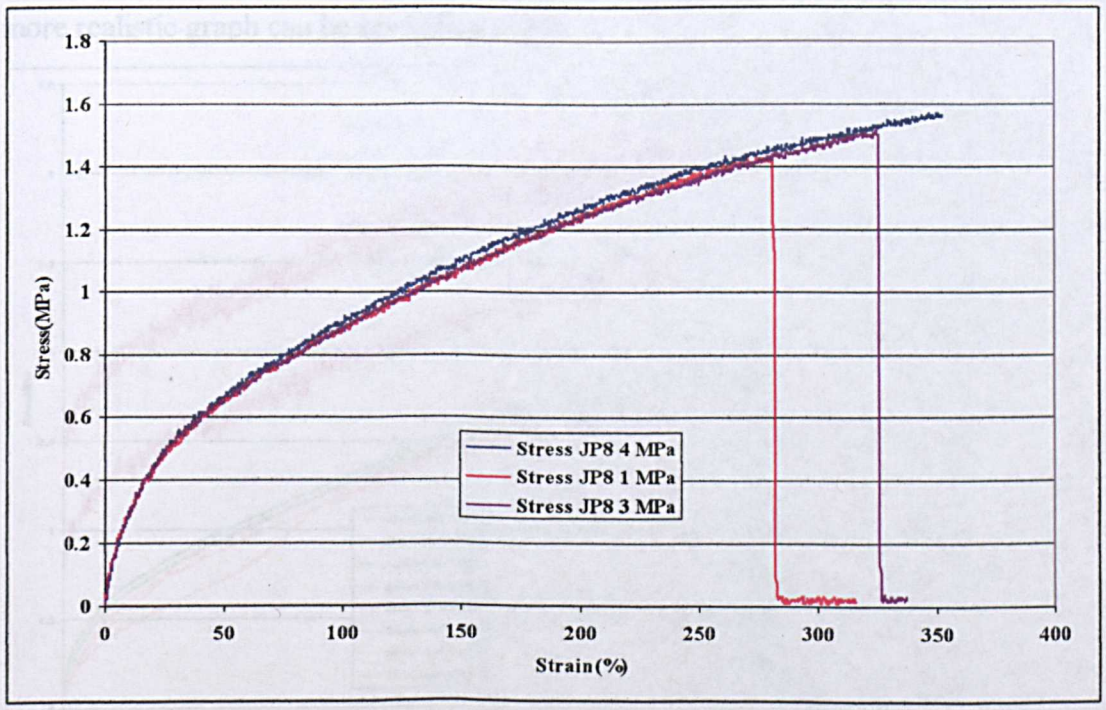

Figure 6.13 Results of 14 day baseline cure + 56 days in JP8 jet fuel.

6.1.3.5. 56 days immersion in fluids combined results

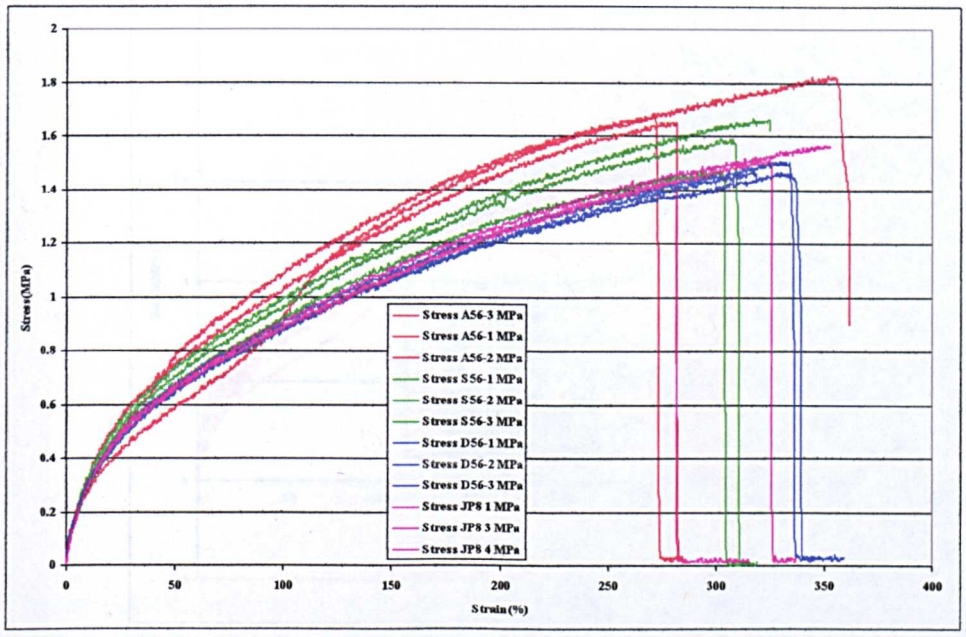

Figure 6.14 Combined results of 14 day baseline cure+ 56 days immersed in various fluids.

6.1.4. Combined results-Air

It can be seen that on initial inspection the 28 day cure appears to alter the properties of the sealant **(Fig. 6.15).** On closer inspection it can be seen that the load hadn't zeroed correctly giving an artificially high reading initially. If this is modified then the more realistic graph can be seen **(Fig. 6.16).**

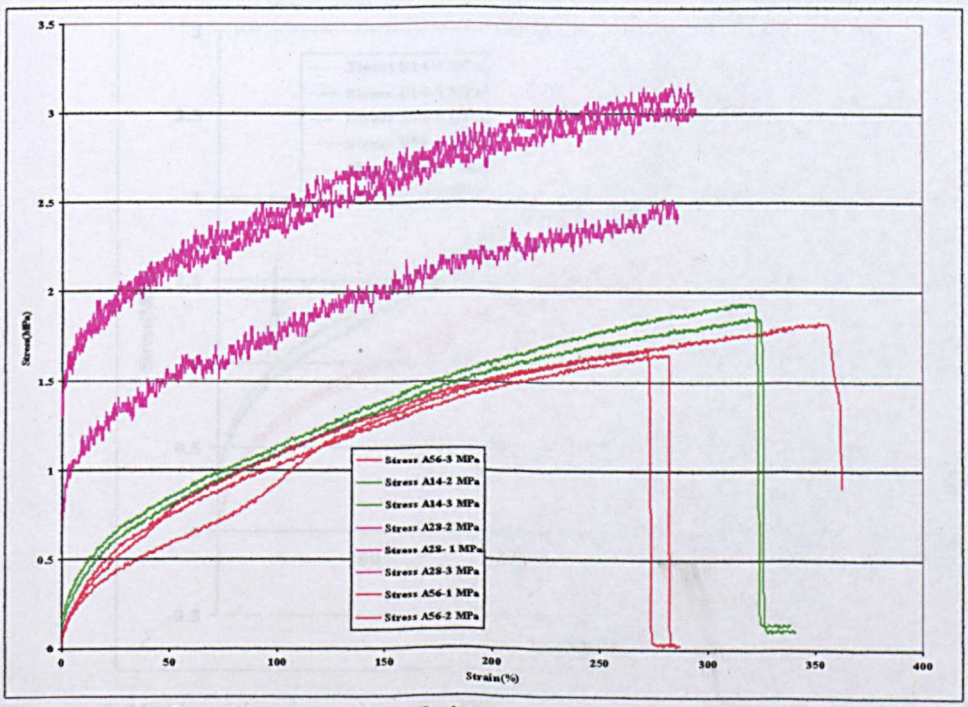

Figure 6.15 Combined results of air.

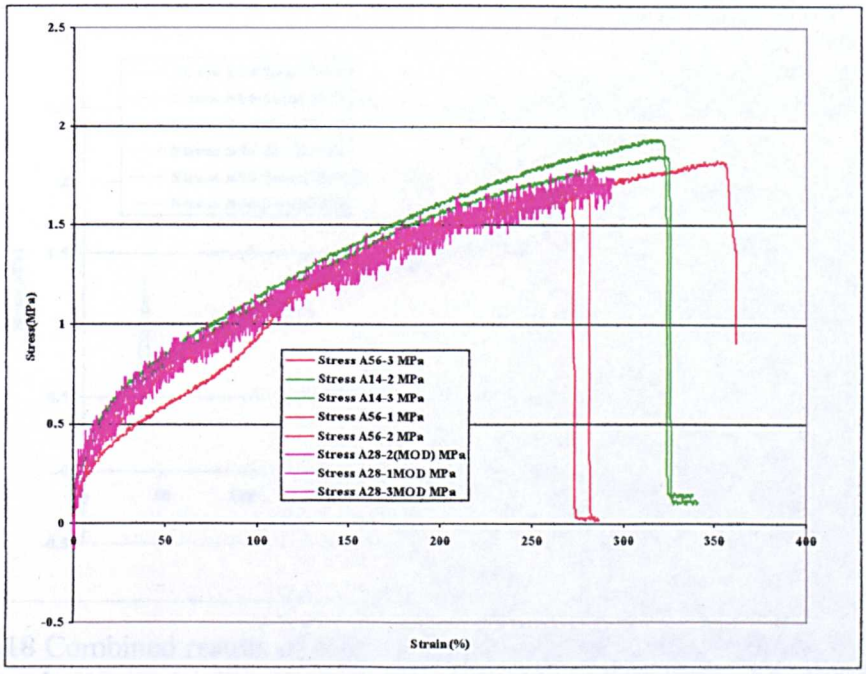

Figure 6.16 Combined results of air with the constant removed (stresses recalibrated to zero) from 28 day test results.

6.1.5. Combined results-Saline

It can be seen that on initial inspection the 14 day cure appears to alter the properties of the sealant **(Fig.6.17).** On closer inspection it can be seen that the load hadn't zeroed correctly giving an artificially high reading initially. If this is modified then the more realistic graph can be seen **(Fig. 6.18).**

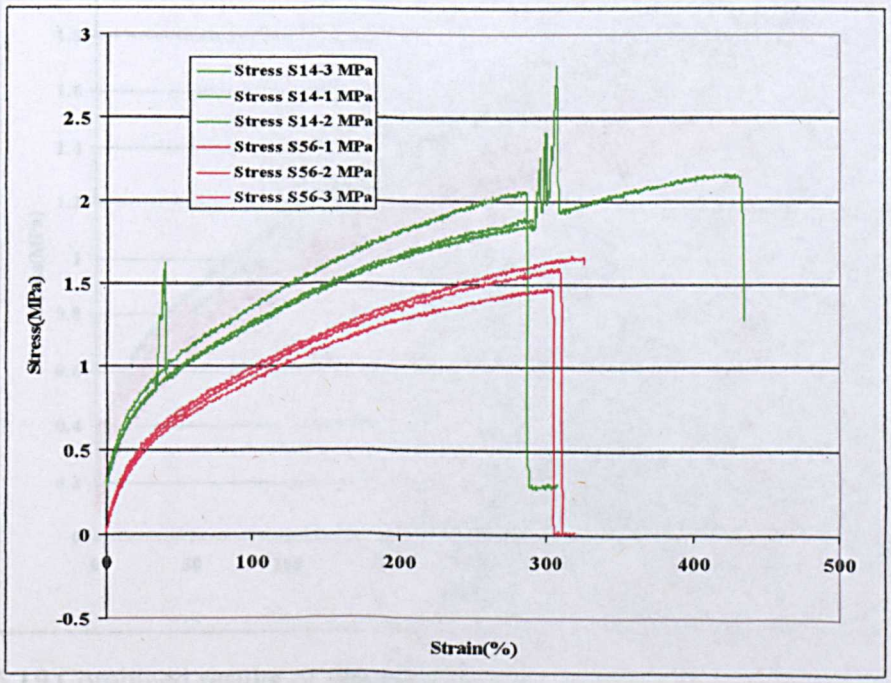

Figure 6.17 Combined results of saline.

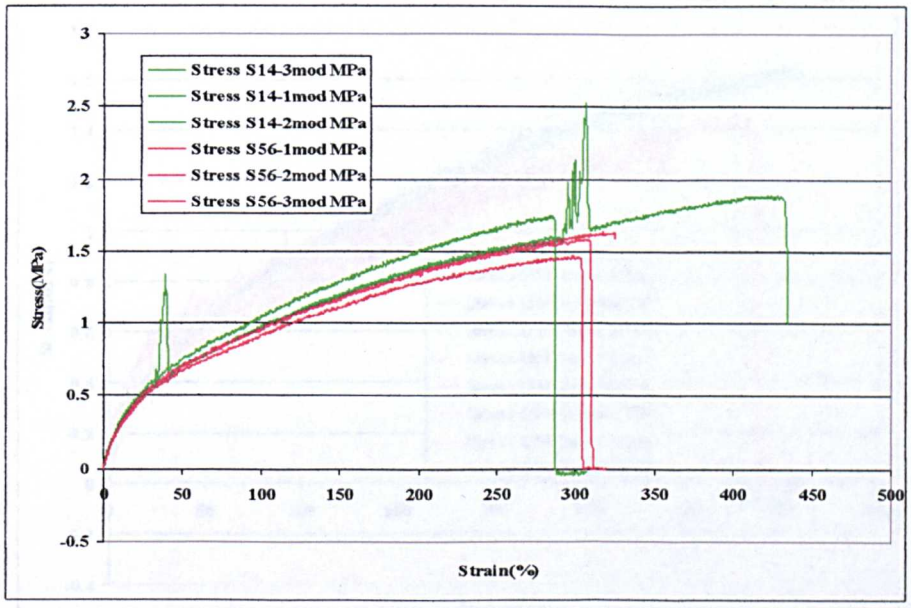

Figure 6.18 Combined results of saline solution with the constant removed from 14 day test results.

6.1.6. Combined results-Deionised water

It can be seen that on initial inspection the 14 and 28 day cure appears to alter the properties of the sealant **(Fig.6.19).** On closer inspection it can be seen that the load hadn't zeroed correctly giving an artificially high reading initially. If this is modified then the more realistic graph can be seen **(Fig. 6.20).**

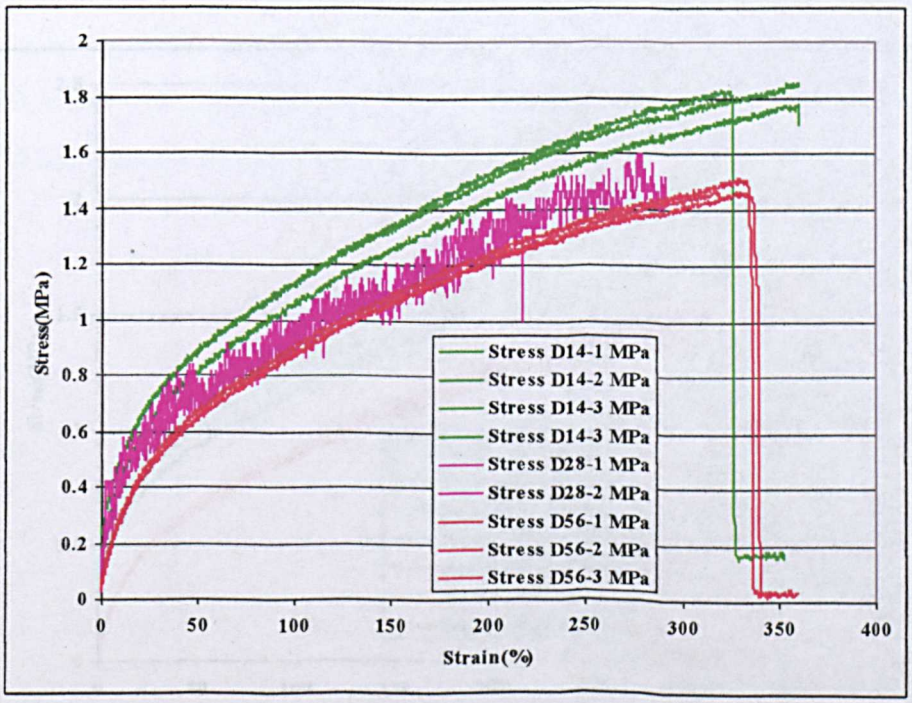

Figure 6.19 Combined results of deionised water.

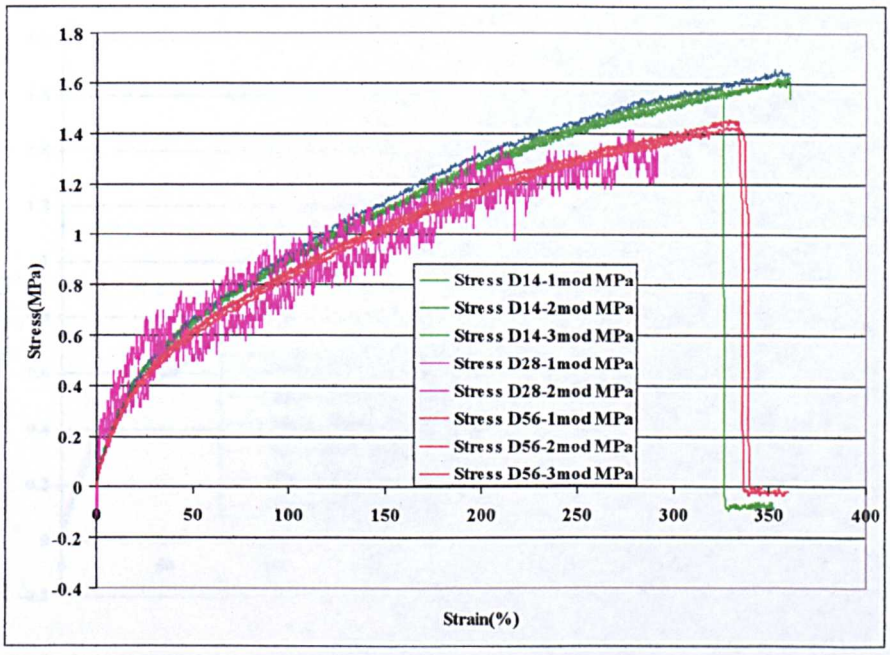

Figure 6.20 Combined results of air with the constants removed (stresses recalibrated to zero).

6.1.7. Combined results-JP8 jet fuel

It can be seen that on initial inspection the 14 day cure appears to alter the properties of the sealant **(Fig.6.17).** On closer inspection it can be seen that the load hadn't zeroed correctly giving an artificially high reading initially. If this is modified then the more realistic graph can be seen **(Fig. 6.18).**

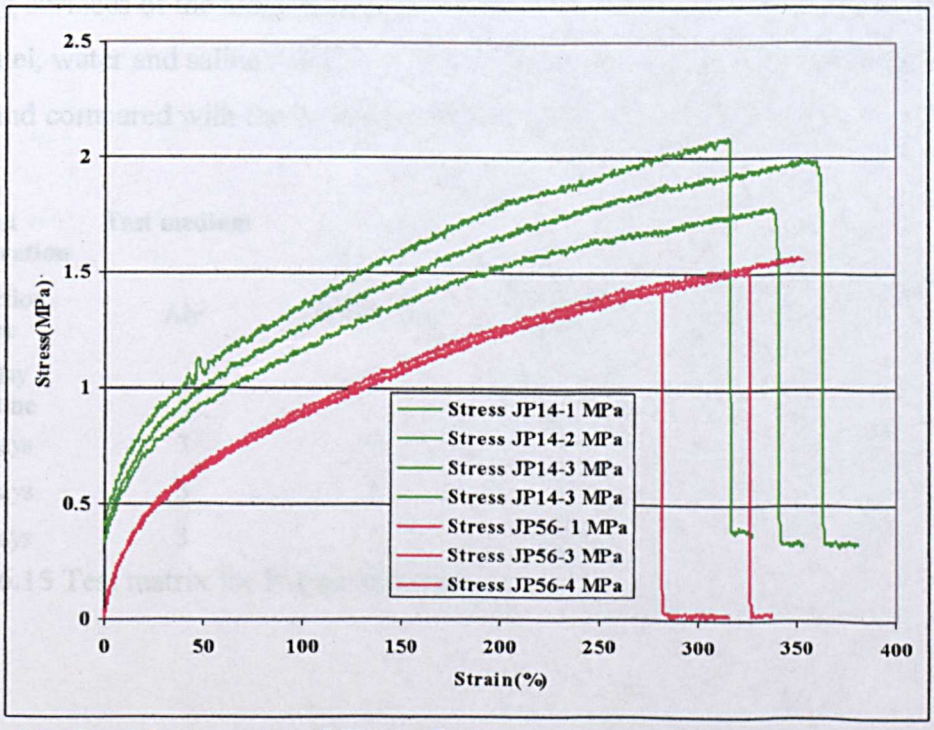

Figure 6.21 Combined results of JP8 jet fuel.

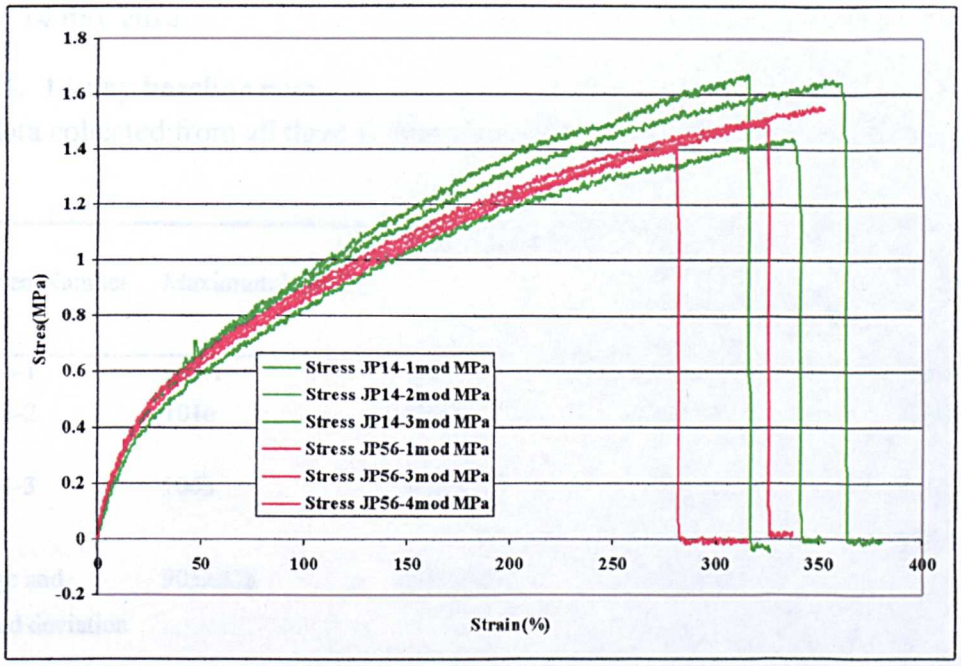

Figure 6.22 Combined results of JP8 with the constants removed (stresses recalibrated to zero).

6.2. H-Type specimen

H- Section type samples were used to investigate the influence of the various test fluids on the sealant. The adhesive qualities were not being checked because Airbus standard aluminium surface treatment was not used. However, in order to ensure adequate adhesion, fine grit blasting (180-220 mesh alumina) was used to prepare the bonding surfaces of the aluminium specimens. The H-section samples were immersed in jet fuel, water and saline solution over the different time periods (14, 28 and 56 days) and compared with the baseline test in air at 14 days **(Table 6.15).**

Test configuration	**Test medium**				
H-section type	**Air**	**JP8 jet fuel**	**Deionised Water**	**Saline solution 10% ww**	**Total**
14 day baseline	3				3
14 days	3	3	3	3	12
28 days	3	3	3	3	12
56 days	3	3	3	3	12

Table 6.15 Test matrix for H-type specimens.

6.2.1. 14 day cure

6.2.1.1. 14 day baseline cure

The data collected from all three H type specimens can be seen in Table 6.16.

Specimen Number	Maximum Load(N)	Peak Extension(%)	60 % Secant Modulus @ (MPa)	Failure Mode
HBL 14-1	631.1	302	0.46	Cohesive/10%
HBL 14-2	1016	299.3	0.80	Light cohesive
HBL 14-3	1068	301.3	0.77	Cohesive/10% adhesive
Average and Standard deviation	905±238	300.9±1.4	0.68±0.19	
Date samples made-22/05/2006	Age at test -14 days	Test date-05/06/2006	Test temperature-26°C RH 55%	Test speed 6 mm/min

Table 6.16 H-type test results 14 day baseline cure at 23°C 50%RH

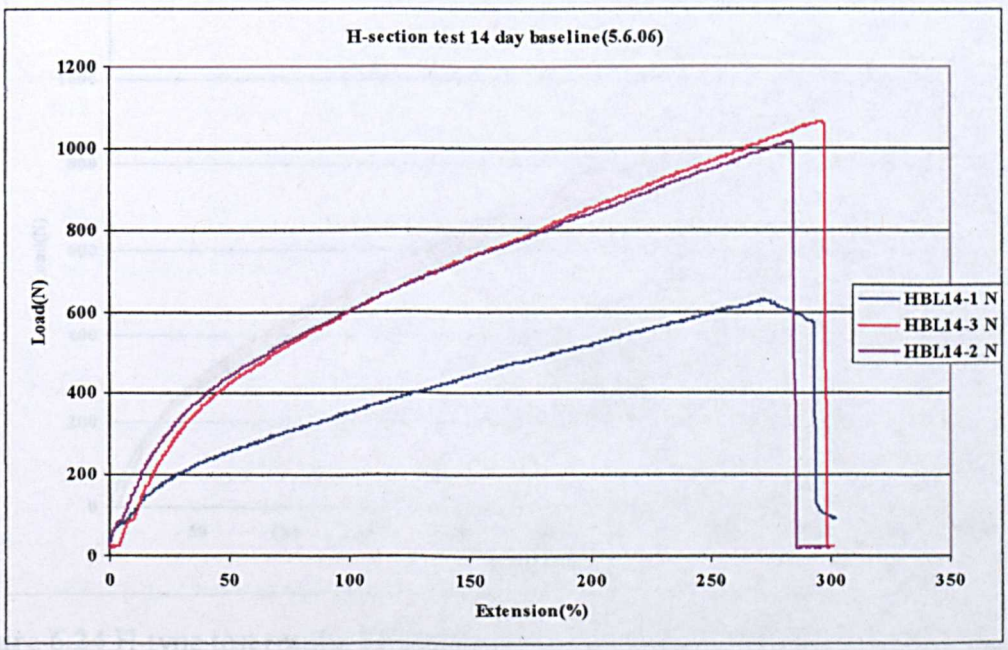

Figure 6.23 Results of 14 day baseline test.

6.2.1.2. 14 day baseline cure + 14 day cure in air@23°C and 50%RH

Specimen Number	Maximum Load(N)	Peak Extension(%)	60 % Secant Modulus @ (MPa)	Failure Mode
HA 14-1	976.9	450.3	0.5	Cohesive
HA 14-2	867.8	345.7	0.52	Adhesive/thin film cohesive
HA 14-3	787	285.3	0.55	Cohesive25% / adhesive75%
Average	877.2±95.3	360.4±83.5	0.52±0.03	
Standard deviation				
Date samples made-22/05/2006	Age at test -14 day baseline+ 14 days	Test date-19/06/2006	Test temperature-30°C R/H 31%	Test speed 6 mm/min

Table 6.17 H-type test results 14 day baseline cure at 23°C 50%RH+ 14 days air @23°C 50%RH

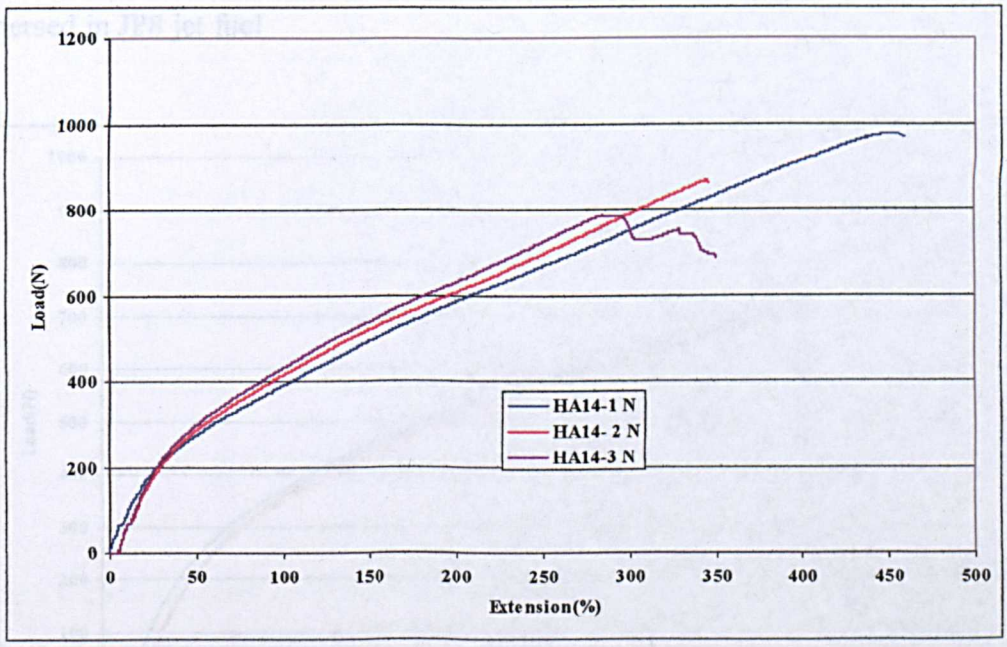

Figure 6.24 H-type test results 14 day baseline cure at 23°C 50%RH+ 14 days air @23°C 50%RH

6.2.1.3. 14 day baseline cure + 14 day immersed in JP8 jet fuel

Specimen Number	Maximum Load(N)	Peak Extension(%)	60 % Secant Modulus @ (MPa)	Failure Mode
HJ 14-1	726	245	0.6	Cohesive75%
HJ 14-2	714.4	251.7	0.56	Cohesive 90%
HJ 14-3	914.9	361.8	0.58	Cohesive75%
Average	785.1±112.6	286.2±65.6	0.58±0.02	
Standard deviation				
Date samples	Age at test -14 day	Test date-	Test temperature-	Test speed
made-22/05/2006	baseline + 14 days	19/06/2006	30°C R/H 31%	6 mm/min

Table 6.18 H-type test results 14 day baseline cure at 23°C 50%RH+ 14 days immersed in JP8 jet fuel

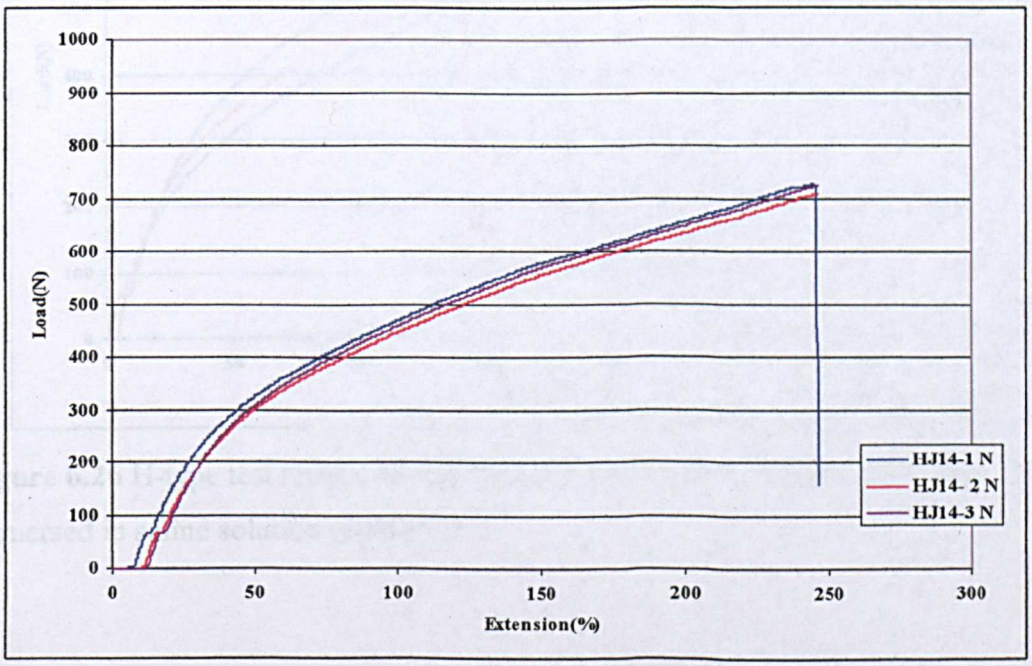

Figure 6.25 H-type test results 14 day baseline cure at 23°C 50%RH+ 14 days immersed in JP8 jet fuel

6.2.1.4. 14 day baseline cure + 14 day immersed in saline solution (10%ww)

Specimen Number	Maximum Load(N)	Peak Extension(%)	60 % Secant Modulus @ (MPa)	Failure Mode
HS 14-1	739.3	294	0.56	Adhesive/Thin film cohesive
HS 14-2	536.6	139.7	0.62	Cohesive
HS 14-3	658.9	179.3	0.69	Cohesive75%
Average	644.93±102.07	204.3±80.1	0.62±0.07	
Standard deviation				
Date samples made-22/05/2006	Age at test -14 day baseline +14days	Test date-19/06/2006	Test temperature-30°C R/H 31%	Test speed 6 mm/min

Table 6.19 H-type test results 14 day baseline cure at 23°C 50%RH+ 14 days immersed in saline solution (10%ww)

Figure 6.26 H-type test results 14 day baseline cure at 23°C 50%RH+ 14 days immersed in saline solution (10%ww)

6.2.1.5. 14 day baseline cure + 14 day immersed in deionised water

Specimen Number	Maximum Load(N)	Peak Extension(%)	60 % Secant Modulus @ (MPa)	Failure Mode
HD 14-1	830.5	305	0.67	Cohesive 50%
HD 14-2	826.7	289.7	0.69	Cohesive 75%
HD 14-3	818.8	482.3	0.43	Cohesive voids
Average	825.33±5.97	359.0±107.0	0.60±0.14	
Standard deviation Date samples made-22/05/2006	Age at test -14 day baseline + 14 days	Test date-19/06/2006	Test temperature-30°C R/H 31%	Test speed 6 mm/min

Table 6.20 H-type test results 14 day baseline cure at 23°C 50%RH+ 14 days immersed in deionised water

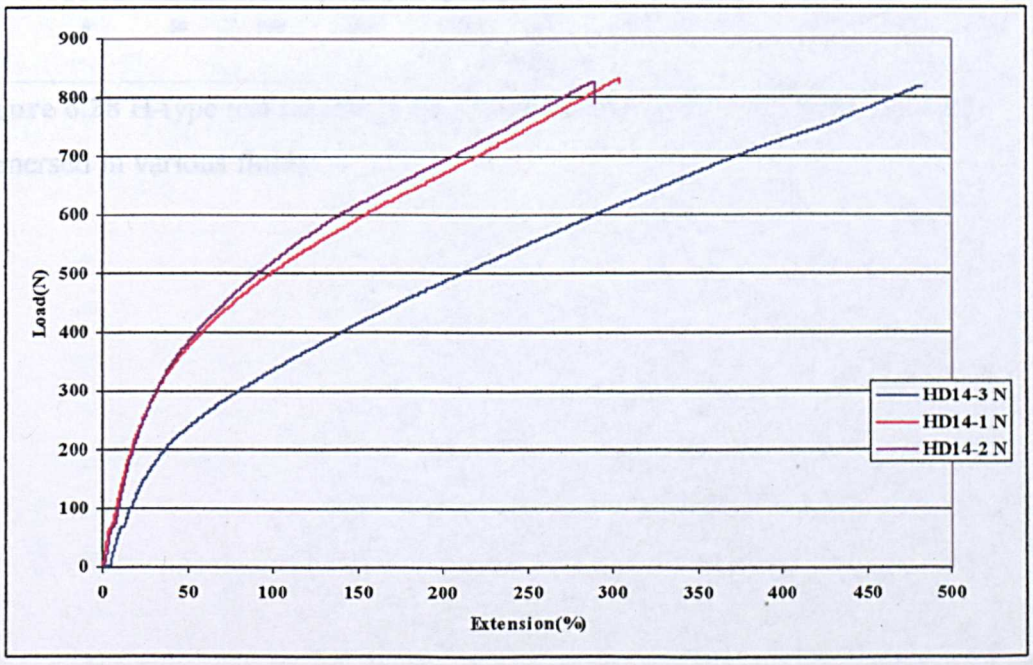

Figure 6.27 H-type test results 14 day baseline cure at 23°C 50%RH+ 14 days immersed in deionised water

6.2.1.6. Combined test results for 14 day baseline cure + 14 day immersed in various fluids

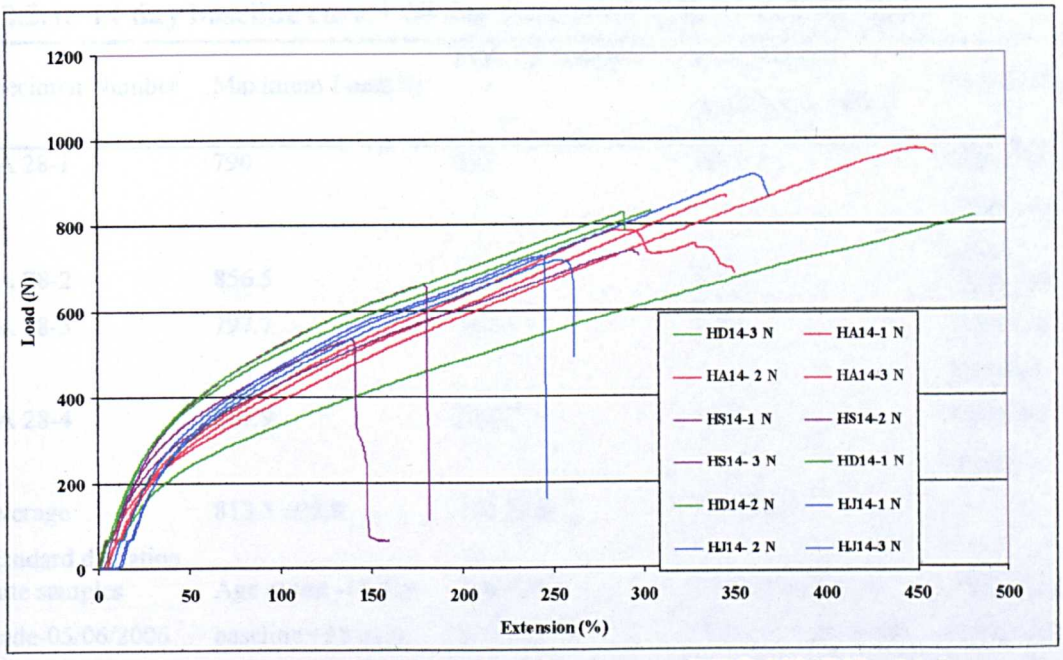

Figure 6.28 H-type test results 14 day baseline cure at 23°C 50%RH+ 14 days immersed in various fluids

6.2.2. 28 day cure

6.2.2.1. 14 day baseline cure + 28 day cure in air@23°C and 50%RH

Specimen Number	Maximum Load(N)	Peak Extension (%)	60 % Secant Modulus @ (MPa)	Failure Mode
HA 28-1	790	255	0.47	Thin film cohesive/small voids
HA 28-2	856.5	301	0.62	Large void
HA 28-3	797.7	262.3	0.63	Thin film cohesive
HA 28-4	809.9	263.7	0.63	Thin film cohesive
Average	813.5 ±29.8	270.5±20.7	0.59±0.1	
Standard deviation				
Date samples made-05/06/2006	Age at test -14 day baseline +28 days	Test date-17/07/2006	Test temperature-32°C R/H 26%	Test speed 6 mm/min

Table 6.21 H-type test results 14 day baseline cure at 23°C 50%RH+ 28 days air @23°C 50%RH

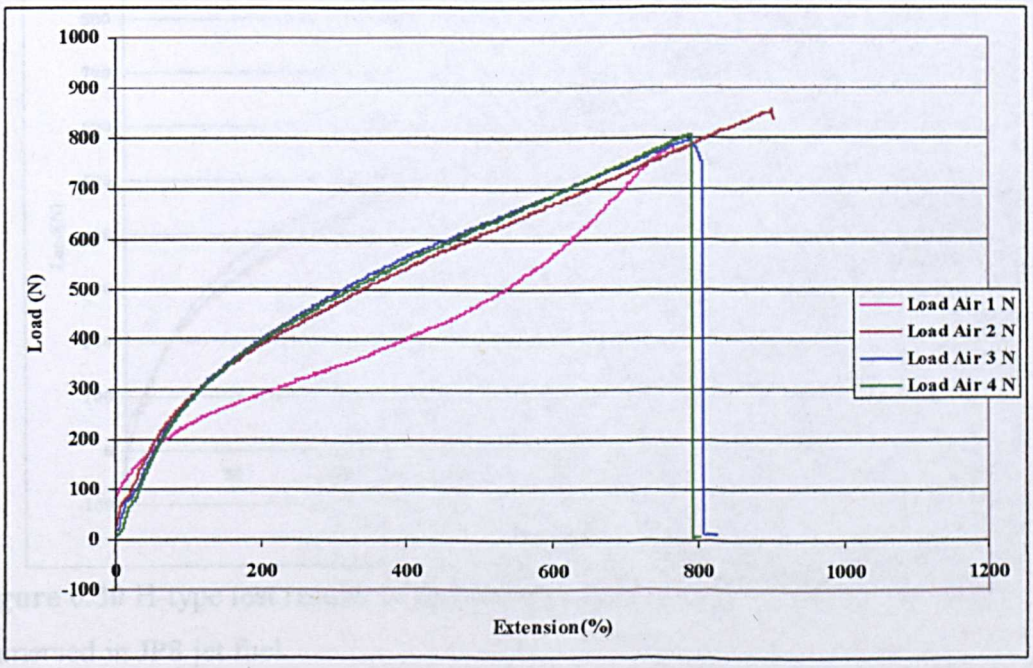

Figure 6.29 H-type test results 14 day baseline cure at 23°C 50%RH + 28 days in air at 23°C 50%RH.

6.2.2.2. 14 day baseline cure + 28 day cure immersed in JP8 jet fuel.

Specimen Number	Maximum Load(N)	Peak Extension (%)	60 % Secant Modulus @ (MPa)	Failure Mode
HJ 28-1	772.5	325.3	0.57	Thin film cohesive
HJ 28-2	819.1	348.7	0.56	Thin film cohesive
HJ 28-3	795.4	306	0.63	Thin film cohesive/small voids
Average	795.7±23.3	326.7±21.4	0.59±0.04	
Standard deviation				
Date samples made-05/06/2006	Age at test -14 day baseline +28 days	Test date-17/07/2006	Test temperature-32°C R/H 26%	Test speed 6 mm/min

Table 6.22H-type test results 14 day baseline cure at 23°C 50%RH+ 28 days immersed in JP8 jet fuel.

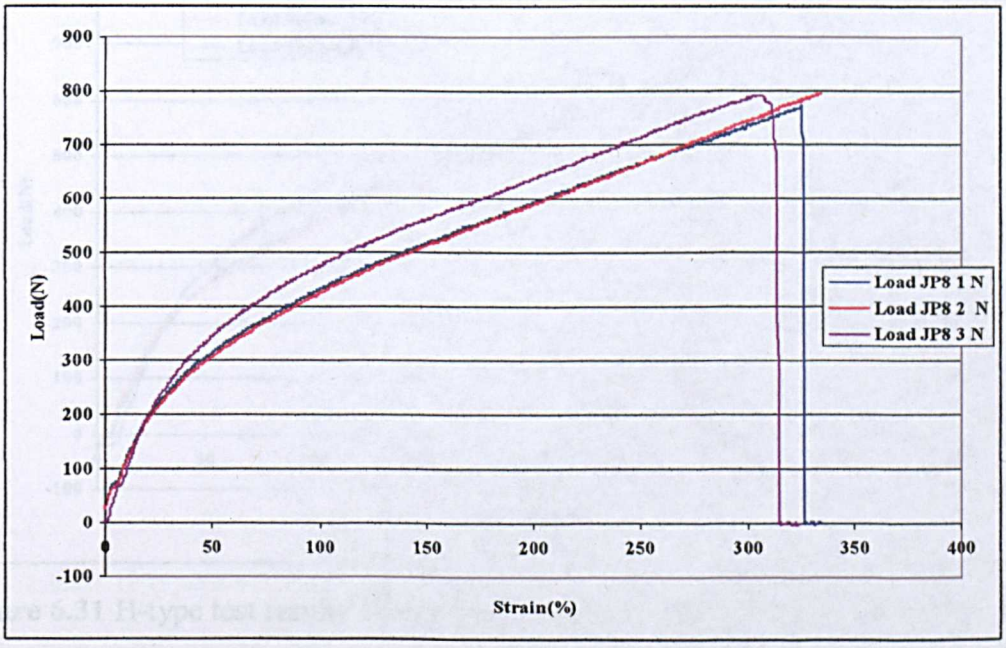

Figure 6.30 H-type test results 14 day baseline cure at 23°C 50%RH + 28 days immersed in JP8 jet fuel.

6.2.2.3. 14 day baseline cure + 28 day cure immersed in saline solution.

Specimen Number	Maximum Load(N)	Peak Extension (%)	60 % Secant Modulus @ (MPa)	Failure Mode
HS 28-1	618.1	271.3	0.48	50% cohesive
HS 28-2	782.4	372.3	0.49	Thin film cohesive
HS 28-3	705.2	266.3	0.55	Thin film cohesive
Average	701.9±82.2	303.3±59.8	0.51±0.04	
Standard deviation				
Date samples made-05/06/2006	Age at test -14 day baseline +28 days	Test date-17/07/2006	Test temperature-32°C R/H 26%	Test speed 6 mm/min

Table 6.23 H-type test results 14 day baseline cure at 23°C 50%RH+ 28 days immersed in saline solution.

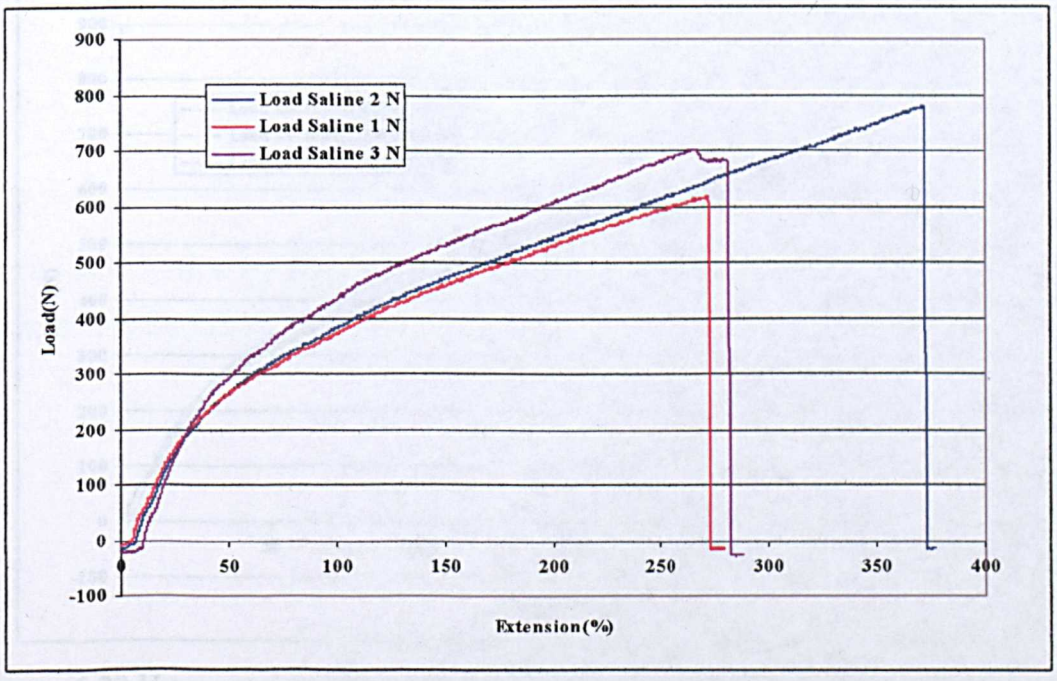

Figure 6.31 H-type test results 14 day baseline cure at 23°C 50%RH + 28 days immersed in saline solution.

6.2.2.4. 14 day baseline cure + 28 day cure immersed in de-ionised water.

Specimen Number	Maximum Load(N)	Peak Extension (%)	60 % Secant Modulus @ (MPa)	Failure Mode
HD 28-1	673.1	237.7	0.6	Thin film cohesive
HD 28-2	738.8	302.3	0.56	Thin film cohesive
HD 28-3	807.6	349	0.57	Thin film cohesive
Average	739.8±67.26	296.3±55.9	0.58±0.02	
Standard deviation				
Date samples made-05/06/2006	Age at test -14 day baseline +28 days	Test date-17/07/2006	Test temperature-32°C R/H 26%	Test speed 6 mm/min

Table 6.24 H-type test results 14 day baseline cure at 23°C 50%RH+ 28 days immersed in de-ionised water.

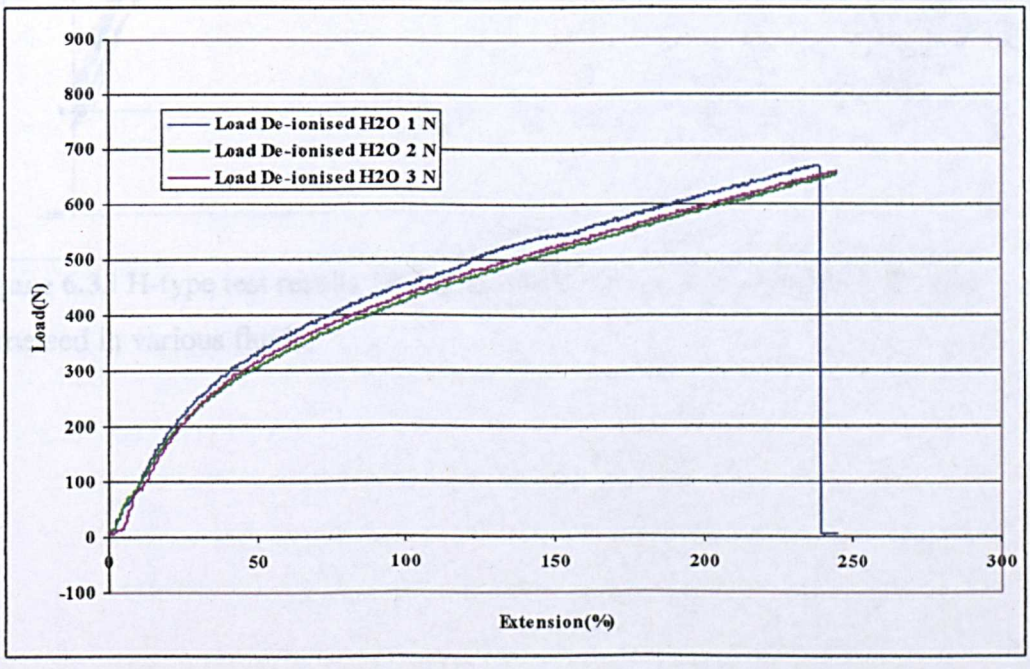

Figure 6.32 H-type test results 14 day baseline cure at 23°C 50%RH + 28 days immersed in de-ionised water.

6.2.2.5. Combined test result for 14 day baseline cure + 28 day cure immersed in various fluids.

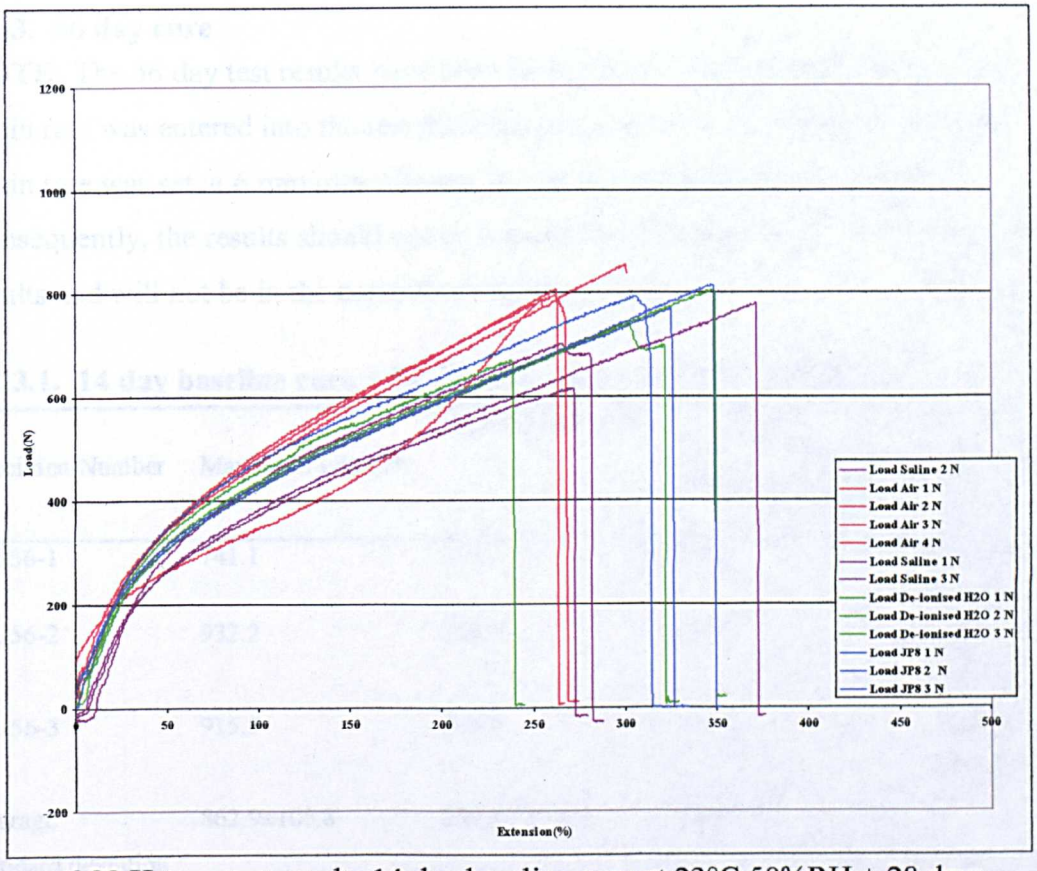

Figure 6.33 H-type test results 14 day baseline cure at 23°C 50%RH + 28 days immersed in various fluids.

6.2.3. 56 day cure

NOTE: The 56 day test results have been included but, unfortunately, the incorrect strain rate was entered into the test machine programme. The 14 and 28 day tests strain rate was set at 6 mm/min whereas the 56 day test was set at 12 mm/min. Consequently, the results should not be compared to those of the 14 and 28 day test results and will not be in the combined results sections.

6.2.3.1. 14 day baseline cure + 56 day cure in air at 23°C 50%RH.

Specimen Number	Maximum Load(N)	Peak Extension (%)	60 % Secant Modulus @ (MPa)	Failure Mode
HA 56-1	741.1	212.7	0.60	Thin film cohesive
HA 56-2	932.2	338.7	0.63	Thin film cohesive
HA 56-3	915.5	346.7	0.58	Thin film cohesive
Average	862.9±105.8	299.4±75.2	0.6±0.03	
Standard deviation				
Date samples made-22/05/2006	Age at test -14 day baseline +56 days	Test date-31/07/2006	Test temperature-32°C R/H 28%	Test speed 12 mm/min

Table 6.25 H-type test results 14 day baseline cure at 23°C 50%RH+ 56 days in air @23°C 50%RH.

Figure 6.34 H-type test results 14 day baseline cure at 23°C 50%RH + 56 days in air at 23°C 50%RH.

6.2.3.2. 14 day baseline cure + 56 day cure immersed in JP8 jet fuel.

Specimen Number	Maximum Load(N)	Peak Extension (%)	60 % Secant Modulus @ (MPa)	Failure Mode
HJ 56-1	700.9	351.3	0.49	Cohesive, 25% thin film cohesive
HJ 56-2	795.1	332.7	0.59	Cohesive
HJ56-3	687.7	255.3	0.6	Cohesive, 80% thin film cohesive
Average	727.9±58.57	313.1±50.9	0.56±0.06	
Standard deviation Date samples made-22/05/2006	Age at test -14 day baseline +56 days	Test date-31/07/2006	Test temperature-32°C R/H 28%	Test speed 12 mm/min

Table 6.26 H-type test results 14 day baseline cure at 23°C 50%RH+ 56 days immersed in JP8 jet fuel.

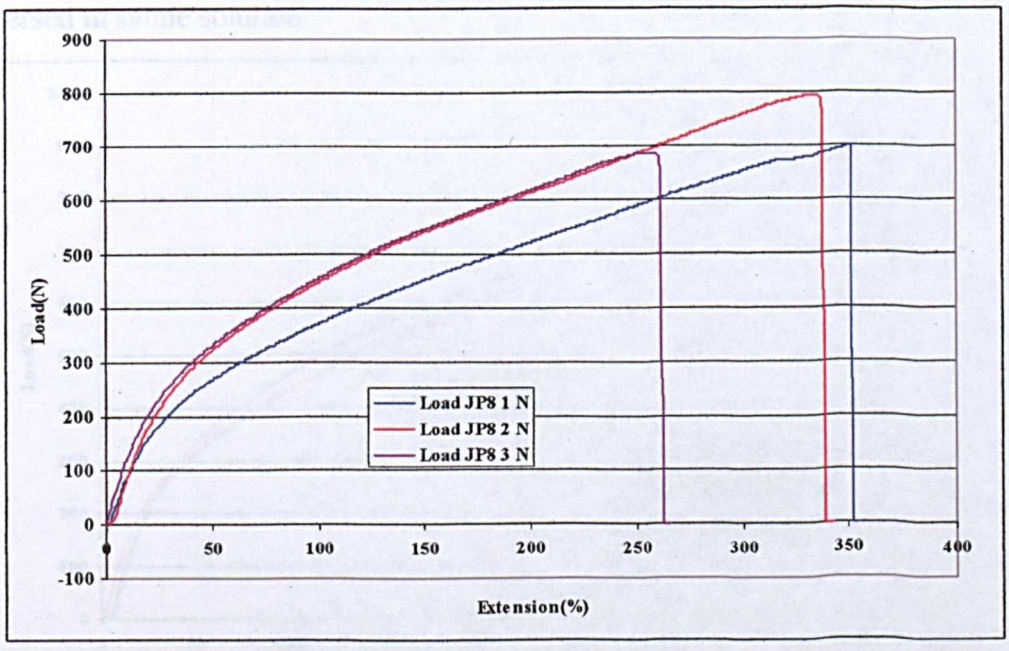

Figure 6.35 H-type test results 14 day baseline cure at 23°C 50%RH + 56 days immersed in JP8 jet fuel.

6.2.3.3. 14 day baseline cure + 56 day cure immersed in saline solution.

Specimen Number	Maximum Load(N)	Peak Extension (%)	60 % Secant Modulus @ (MPa)	Failure Mode
HS 56-1	589.4	204.7	0.58	Cohesive, 25% thin film cohesive
HS 56-2	898.7	416.7	0.57	Cohesive, 15% thin film cohesive
HS56-3	657.4	223.3	0.61	Cohesive, 40% thin film cohesive
Average	715.17±162.54	281.6±117.4	0.59±0.02	
Standard deviation				
Date samples made-22/05/2006	Age at test -14 day baseline +56 days	Test date-31/07/2006	Test temperature-32°C R/H 28%	Test speed 12 mm/min

Table 6.27 H-type test results 14 day baseline cure at 23°C 50%RH+ 56 days immersed in saline solution.

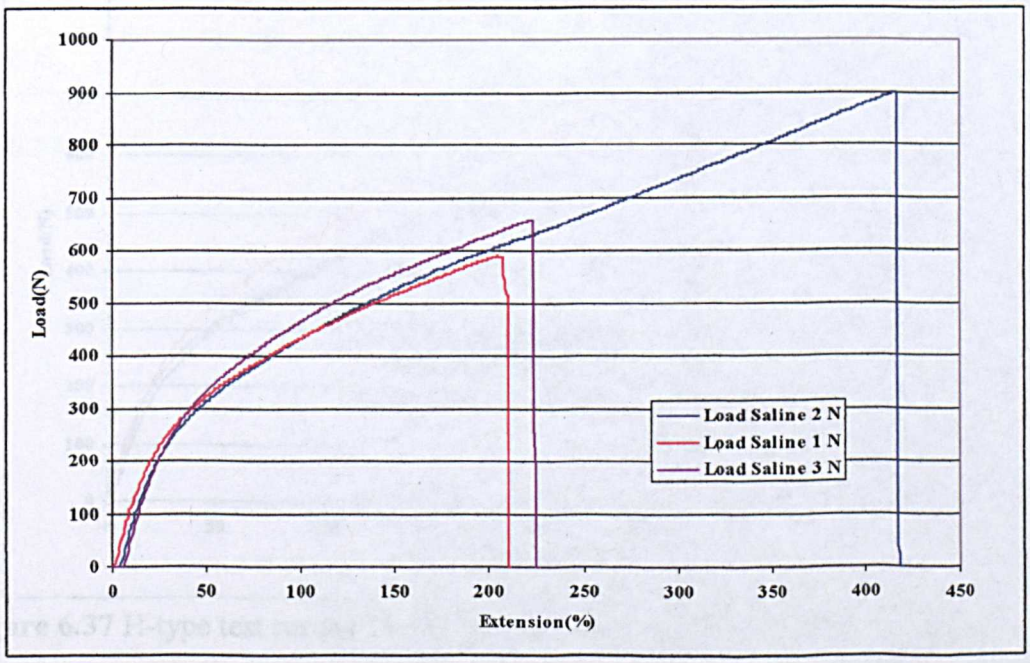

Figure 6.36 H-type test results 14 day baseline cure at 23°C 50%RH + 56 days immersed in saline solution.

6.2.3.4. 14 day baseline cure + 56 day cure immersed in de-ionised water.

Specimen Number	Maximum Load(N)	Peak Extension (%)	60 % Secant Modulus @ (MPa)	Failure Mode
HD 56-1	645.5	268.7	0.56	Cohesive, 10% thin film cohesive
HD 56-2	776.1	363.3	0.54	Cohesive
HD 56-3	734.6	275.3	0.62	Cohesive
Average	718.73±66.73	302.4±52.8	0.57±0.04	
Standard deviation				
Date samples made-22/05/2006	Age at test -14 day baseline +56 days	Test date-31/07/2006	Test temperature-32°C R/H 28%	Test speed 12 mm/min

Table 6.28 H-type test results 14 day baseline cure at 23°C 50%RH+ 56 days immersed in de-ionised water.

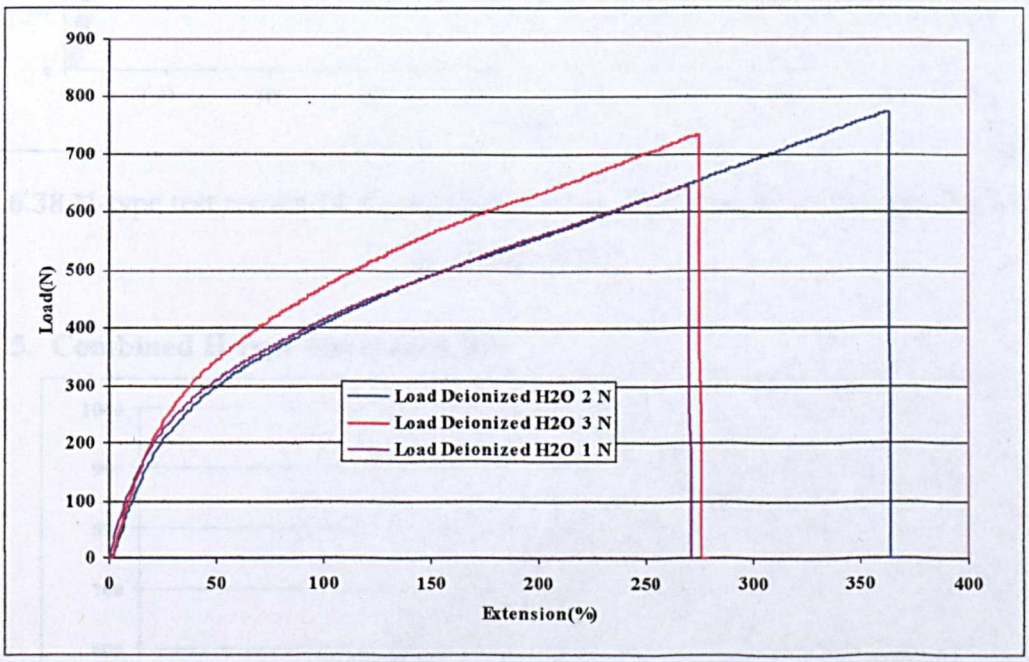

Figure 6.37 H-type test results 14 day baseline cure at 23°C 50%RH + 56 days immersed in de-ionised water.

6.2.4. Combined test result for 14 day baseline cure + 56 day cure immersed in various fluids

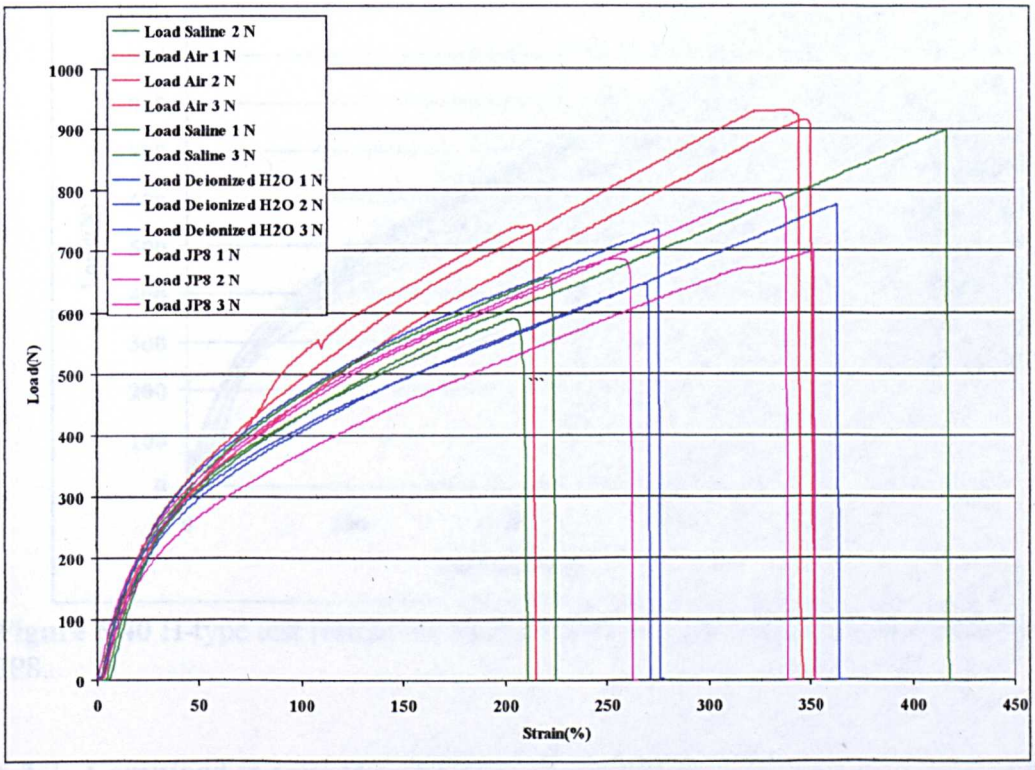

Figure 6.38 H-type test results 14 day baseline cure at 23°C 50%RH + 56 days immersed in various fluids.

6.2.5. Combined H-type test results-Air

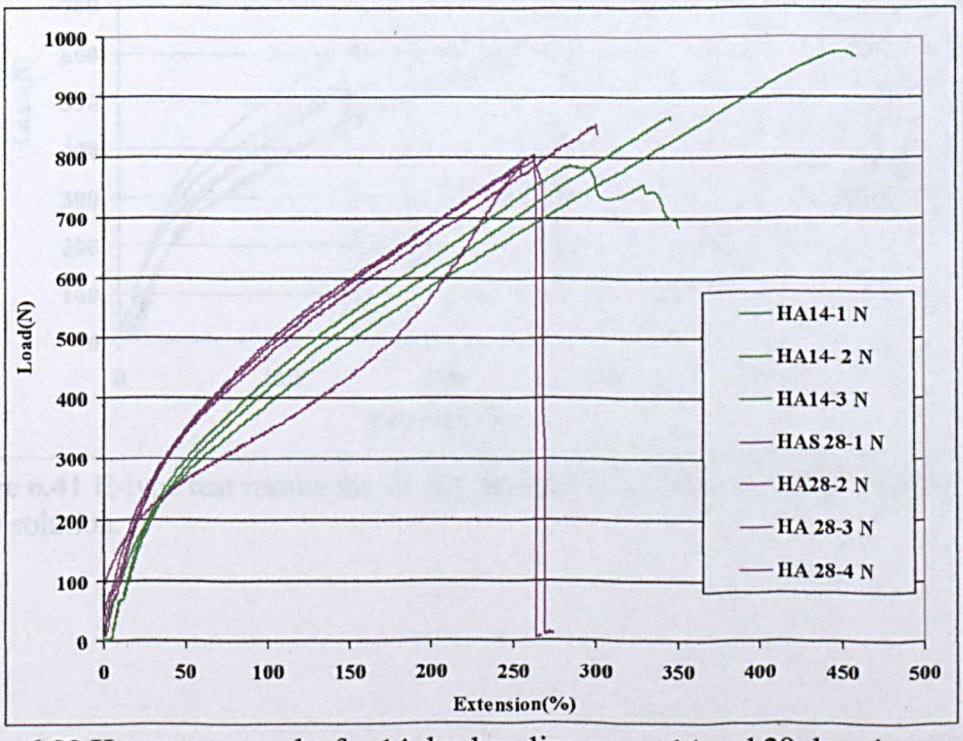

Figure 6.39 H-type test results for 14 day baseline cure +14 and 28 day air cure.

6.2.6. Combined H-type test results-JP8

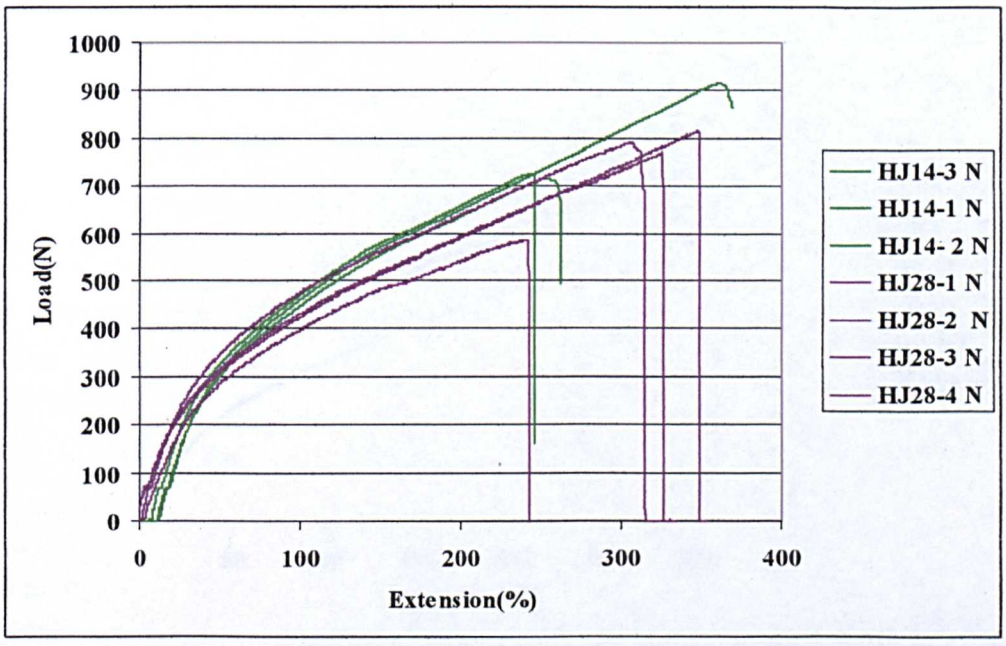

Figure 6.40 H-type test results for 14 day baseline cure +14 and 28 day immersed in JP8.

6.2.7. Combined H-type test results-Saline solution

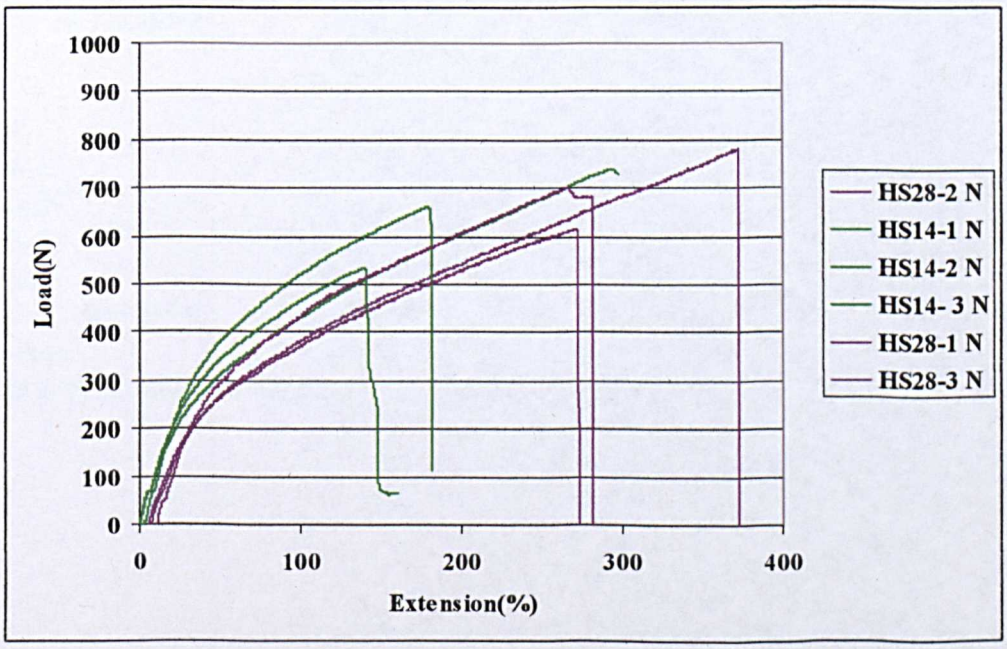

Figure 6.41 H-type test results for 14 day baseline cure +14 and 28 day immersed in saline solution.

6.2.8. Combined H-type test results-De-ionised water

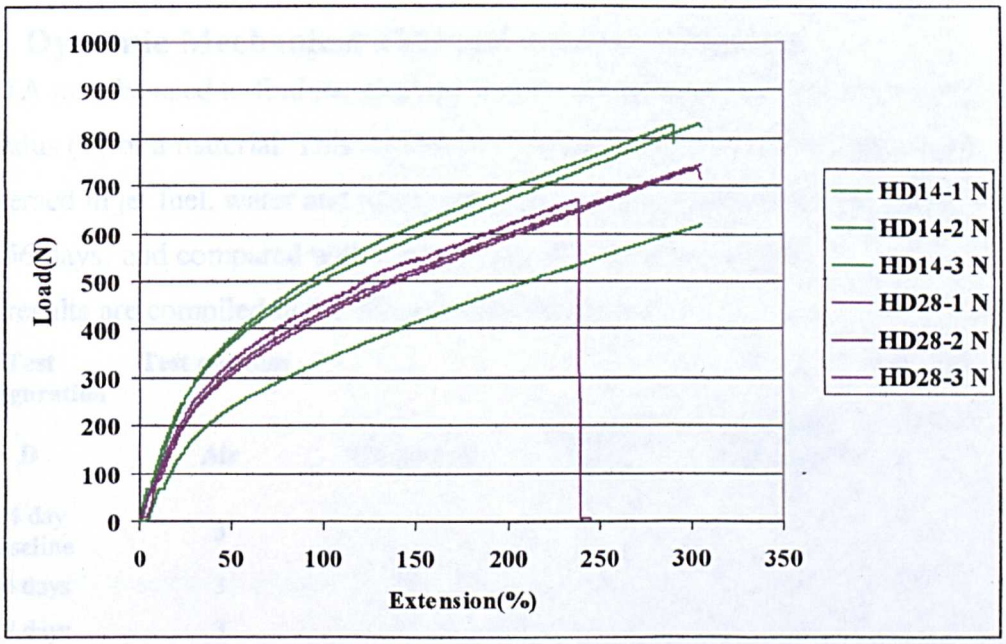

Figure 6.42 H-type test results for 14 day baseline cure +14 and 28 day immersed in de-ionised water.

6.3. Dynamic Mechanical Thermal Analysis (DMTA)

DMTA may be used to find the glass transition temperature (T_g) and the Young's modulus (E) of a material. This will involve several tests after the samples were immersed in jet fuel, water and saline solution over the different time periods(14, 28 and 56 days) and compared with the baseline test in air at 14 days.

The results are compiled in the following subsections.

Test configuration	Test medium				
D	**Air**	**JP8 jet fuel**	**Deionised Water**	**Saline solution 10% ww**	**Total**
14 day baseline	3				3
14 days	3	3	3	3	12
28 days	3	3	3	3	12
56 days	3	3	3	3	12

Table 6.29 Test matrix for DMTA tests

6.3.1. 14 day baseline cure @ 23°C and 50%RH

Specimen Number	Tan δ Peak (T_g)(° C)	Storage modulus (T_g)(° C)	Modulus @ approx -55°C (E) Gpa
BL14-1	-41.6	-49.9	1
BL14-2	-40.9	-49.3	1.374
BL14-3	-43.4	-50.6	0.75
Average	-41.97	-49.93	1.04
Standard deviation	±1.29	±0.65	±0.31
Test date	16.06.06		

Table 6.30 Results for baseline cure @ 23°C and 50%RH

6.3.2. 14 day baseline cure + 14 days cure in air(@ 23°C and 50%RH), JP8 Saline solution and deionoised water @ 23°C

Specimen Number	T_g @Tanδ Peak (° C)	T_g @ Storage modulus (° C)	Modulus @ approx -55°C (E) GPa
A14-1	-37.8	-47.2	1.3
A17-2	-39.9	-47.8	0.91
A18-3	-38.1	-47.5	1.6
Average	-38.6	-47.5	1.27
Standard deviation	±1.14	±0.3	±0.35
Test date	16,19 and 20.06.06		

Table 6.31 Results for baseline cure + **14 days in air @23°C and 50%RH**

Specimen Number	T_g @Tanδ Peak (° C)	T_g @ Storage modulus (° C)	Modulus @ approx -55°C (E) GPa
JP14-1	-46.7	-55.1	0.49
JP17-1	-39.9	-47.6	0.9
JP17-2	-42.8	-49.7	0.89
Average	-43.13	-50.8	0.76
Standard deviation	±3.41	±3.87	±0.23
Test date	16 and 19.06.06		

Table 6.32 Results for baseline cure + **14 days cure immersed in JP8 jet fuel @ 23°C**

Specimen Number	T_g @Tanδ Peak (° C)	T_g @ Storage modulus (° C)	Modulus @ approx -55°C (E) GPa
S14-1	-43.1	-50	0.86
S17-1	-39	-48.7	1.42
S18-1	-40.7	-48.3	1.24
Average	-40.93	-49	1.17
Standard deviation	±2.06	±0.89	±0.29
Test date 16,19 and 20.06.06			

Table 6.33 Results for baseline cure + **14 days cure immersed in saline solution @ 23°C**

Specimen Number	T_g @Tanδ Peak (° C)	T_g @ Storage modulus (° C)	Modulus @ approx -55°C (E) GPa
D14-1	-42	-48.9	0.46
D17-1	-42.6	-49.3	0.72
D18-1	-41.9	-49.3	0.67
Average	-42.17	-49.17	0.62
Standard deviation	±0.38	±0.23	±0.14
Test date	16,19 and 20.06.06		

Table 6.34 Results for baseline cure + **14 days cure immersed in deionised water @ 23°C**

6.3.3. 14 day baseline cure @ 23°C and 50%RH+ 28 days cure in air(@ 23°C and 50%RH), JP8 Saline solution and deionoised water @ 23°C

Specimen Number	T_g @Tanδ Peak (° C)	T_g @ Storage modulus (° C)	Modulus @ approx -55°C (E) GPa
A28-1	-39.9	-47.4	0.57
A28-2	-39.3	-48.4	1.012
A28-3	-39.7	-48.5	2.46
Average	-39.63	-48.1	1.35
Standard deviation	±0.31	±0.61	±0.99
Test date	18.07.2006		

Table 6.35 Results for baseline cure **@ 23°C and 50%RH + 28 days cure** days in air **@ 23°C and 50%RH**

Specimen Number	T_g @Tanδ Peak (° C)	T_g @ Storage modulus (° C)	Modulus @ approx -55°C (E) GPa
JP28-1	-41.5	-50.3	0.93
JP28-2	-43.2	-49.9	0.86
JP28-3	-41.2	-49.8	
Average	-41.97	-50	0.9
Standard deviation	±1.08	±0.26	±0.05
Test date	18.07.2006		

Table 6.36 Results for baseline cure + **28 days cure immersed in JP8 jet fuel @ 23°C**

Specimen Number	T_g @Tanδ Peak (° C)	T_g @ Storage modulus (° C)	Modulus @ approx -55°C (E) GPa
S28-1	-36	-48.2	0.86
S28-2	-38.9	-48.5	1.74
S28-3	-40.1	-49.3	1.89
Average	-38.33	-48.67	1.5
Standard deviation	±2.11	±0.57	±0.56
Test date	18.07.2006		

Table 6.37 Results for baseline cure + **28 days cure immersed in saline @ 23°C**

Specimen Number	T_g @Tanδ Peak (° C)	T_g @ Storage modulus (° C)	Modulus @ approx -55°C (E) GPa
D28-1	-39.4	-47.7	1.28
D28-2	-38.1	-47.6	1.47
D29-1	-37.3	-46.8	1.96
Average	-38.27	-47.37	1.57
Standard deviation	±1.06	±0.49	±0.35
Test date	18 and 19.07.2006		

Table 6.38 Results for baseline cure + **28 days cure immersed in deionised water @ 23°C**

6.3.4. 14 day baseline cure @ 23°C and 50%RH+ 56 days cure in air(@ 23°C and 50%RH), JP8 Saline solution and deionoised water @ 23°C

Specimen Number	T_g @Tanδ Peak (° C)	T_g @ Storage modulus (° C)	Modulus @ approx -55°C (E) GPa
A56-1	-39	-47.6	0.72
A56-2	-38.7	-47.4	1.13
A56-3	-38.5	-47.4	1.74
Average	-38.73	-47.47	1.2
Standard deviation	±0.25	±0.12	±0.51
Test date	28.07.2006		

Table 6.39 Results for baseline cure **@ 23°C and 50%RH + 56 days cure** days in air **@ 23°C and 50%RH**

Specimen Number	T_g @Tanδ Peak (° C)	T_g @ Storage modulus (° C)	Modulus @ approx -55°C (E) GPa
JP56-1	-40.3	-49.5	1.07
JP56-2	-44.5	-51.6	0.62
JP56-3	-43.2	-50.5	0.5
Average	-42.67	-50.53	0.73
Standard deviation	±2.15	±1.05	±0.3
Test date	28.07.2006		

Table 6.40 Results for baseline cure + **56 days cure immersed in JP8 jet fuel @ 23°C**

Specimen Number	T_g @Tanδ Peak (° C)	T_g @ Storage modulus (° C)	Modulus @ approx -55°C (E) GPa
S56-1	-36.7	-45.8	2.23
S56-2	-37	-46.7	1.99
S56-3	-39.8	-47.6	2.11
Average	-37.83	-46.70	2.11
Standard deviation	±1.71	±0.90	±0.12
Test date	28.07.2006		

Table 6.41 Results for baseline cure + **56 days cure immersed in saline @ 23°C**

Specimen Number	T_g @Tanδ Peak (° C)	T_g @ Storage modulus (° C)	Modulus @ approx -55°C (E) GPa
D56-1	-39.3	-48.3	2.043
D56-2	-37.6	-46.6	1.27
D56-3	-39.8	-48.7	1.77
Average	-38.9	-47.87	1.69
Standard deviation	±1.15	±1.12	±0.39
Test date	28.07.2006		

Table 6.42 Results for baseline cure + **56 days cure immersed in deionised water @ 23°C**

Appendix 7
Calculation of Stresses from Measured Strains

Strain Gauges

A strain gage rosette is, by definition, an arrangement of two or more closely positioned gage grids, separately oriented to measure the normal strains along different directions in the underlying surface of the test part. Rosettes are designed to perform a very practical and important function in experimental stress analysis. It can be shown that for the not-uncommon case of the general biaxial stress state, with the principal directions unknown, three independent strain measurements (in different directions) are required to determine the principal strains and stresses. And even when the principal directions are known in advance, two independent strain measurements are needed to obtain the principal strains and stresses.

Three-Element Rosettes

Where the directions of the principal strains are unknown, a three-element rectangular or delta rosette is always required; and the rosette can be installed without regard to orientation. The data-reduction relationships that follow yield not only the principal strains, but also the directions of the principal axes relative to the reference grid (Grid 1) of the rosette **(See Figure 7.1)**.

Gage Element Numbering

"Numbering", as used here, refers to the numeric (or alphabetic) sequence in which the gage elements in a rosette are identified during strain measurement, and for substitution of measured strains into data-reduction relationships. To obtain correct results, the grids in three-element rosettes must be numbered in a particular way. It is always necessary in a rectangular rosette, for instance, that grid numbers 1 and 3 be assigned to two mutually perpendicular grids. Any other arrangement will produce incorrect principal strains. Following are the general rules for proper rosette numbering. With a rectangular rosette, the axis of Grid 2 must be 45 degrees away from that of Grid 1; and Grid 3 must be 90 degrees away, in the same rotational direction.

In principal, the preceding rules could be implemented by numbering the grids in either the clockwise or counter clockwise direction, as long as the sequence is correct.

Calculations

The examples strain gauge readings are taken from the single coupon, joint in compression, Max load 4.5kN (**See Table 5.2**). The testing was carried out on 01/03/2005.

Grid Number	Direction	μStrain x10^{-6}
1	ε_x	318
2	$\varepsilon_{45°}$	-102
3	ε_y	314

Table 7.1. Strain gauge readings with their directions. (See **Figure 7.1**)

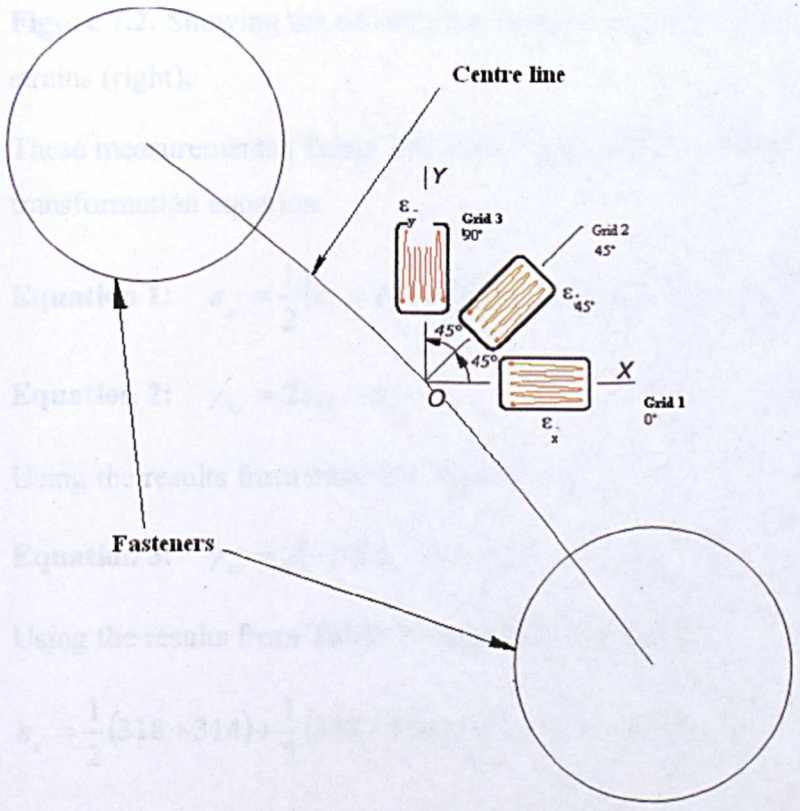

Figure 7.1. Rosette strain gauge layout as used on the test rig coupon **(See also Figure 5.13)**.

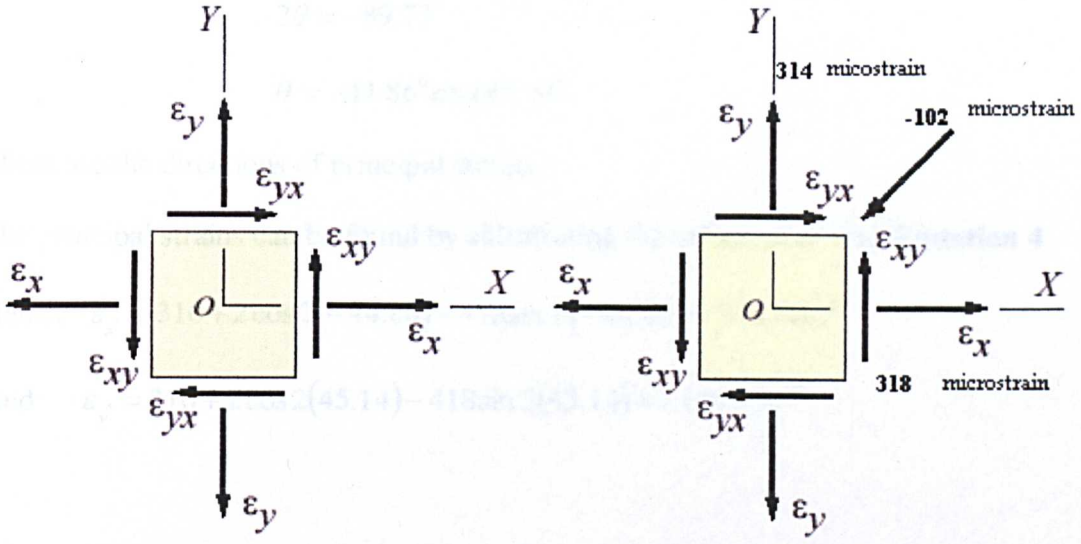

Figure 7.2. Showing the co-ordinate system for plane strain (left) and measured strains (right).

These measurements (**Table 7.1**) can be converted into the preferred set using the transformation equation.

Equation 1: $\varepsilon_{x'} = \frac{1}{2}(\varepsilon_x + \varepsilon_y) + \frac{1}{2}(\varepsilon_x - \varepsilon_y)\cos 2\theta + \frac{1}{2}\gamma_{xy}\sin 2\theta$

Equation 2: $\gamma_{xy} = 2\varepsilon_{45} - \varepsilon_x - \varepsilon_y$

Using the results from table 2 in **Eqn. 2:**

Equation 3: $\gamma_{xy} = 2(-102) - 318 - 314 = -836 \times 10^{-6}$

Using the results from **Table 7.1** and **Eqn. 2** in **Eqn.1**

$$\varepsilon_{x'} = \frac{1}{2}(318+314) + \frac{1}{2}(318-314)\cos 2\theta + \frac{1}{2}(-836)\sin 2\theta$$

Equation 4: $\varepsilon_{x'} = 316 + 2\cos 2\theta - 418\sin 2\theta$

Differentiate **Equation 4** to calculateθ : $\frac{d\varepsilon_{x'}}{d\theta} = 0 = -4\sin 2\theta - 836\cos 2\theta$

$$4\sin 2\theta = -836\cos 2\theta$$

$$\frac{\sin 2\theta}{\cos 2\theta} = \frac{-836}{4}$$

$$\tan 2\theta = -209$$

$$2\theta = -89.73^0$$

$$\theta = -44.86^0 \, and \, 45.14^0$$

These are the directions of principal strains.

The principal strains can be found by substituting the values of θ into **Equation 4**

Hence: $\varepsilon_{x'} = 316 + 2\cos 2(-44.86) - 418\sin 2(-44.86) = 734 \times 10^{-6}$

And: $\varepsilon_{y'} = 316 + 2\cos 2(45.14) - 418\sin 2(45.14) = -102 \times 10^{-6}$

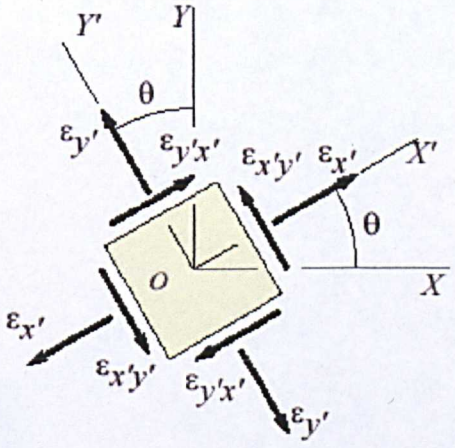

Figure 7.3 Showing the orientation of principal strains and (θ).

The principal stresses can be found from:

Equation 5 $$\sigma_{x'} = \frac{E}{1-\nu^2}\left(\varepsilon_{x'} + \nu\left(\varepsilon_{y'}\right)\right)$$

Using Aluminium 2024 T3, Young's Modulus (E) = 72.4 GPa and
Poisson's ratio (ν) = 0.33

Hence:

$$\sigma_{x'} = \frac{72.4 \times 10^9}{1-0.33^2}\left(734 \times 10^{-6} + 0.33\left(-102 \times 10^{-6}\right)\right) = 56.9 \times 10^6 = 56.9MPa$$

This equates to **Circumferential** or **Spanwise Stress.**

And: $\sigma_{y'} = \frac{72.4 \times 10^9}{1-0.33^2}\left(-102 \times 10^{-6} + 0.33\left(734 \times 10^{-6}\right)\right) = 11.39 \times 10^6 = 11.39MPa$

This equates to **Radial** or **Chordwise Stress.**

And **Maximum Shear Stress** $(\hat{\tau})$ can be found from:

Equation 6: $\hat{\tau} = \frac{1}{2}(\hat{\sigma} - \breve{\sigma})$

Hence: $\hat{\tau} = \frac{1}{2}(56.9\times10^{6} - 11.39\times10^{6}) = 22.75\times10^{6} = 22.75MPa$

Appendix 8
The results Finite Element Analysis (FEA) carried out at Oxford Brookes University

Model parameters

A 30° section (wedge) was enough to model the important features using boundary condition symmetry. The final model was constructed as a single object, revolved through 30° **(Fig. 1)**. This produced a $1/12^{th}$ slice of the complete coupon set that had all of the components within it, with the representative material properties assigned to the various regions within the model. This ensured a relatively short computation time to obtain reasonably accurate results. The main area in which the focus of the analysis concentrated on was in the position of the stacked rosette strain gauge. This position coincides with **Node 93 (Fig. 1)** used in the experimental testing.

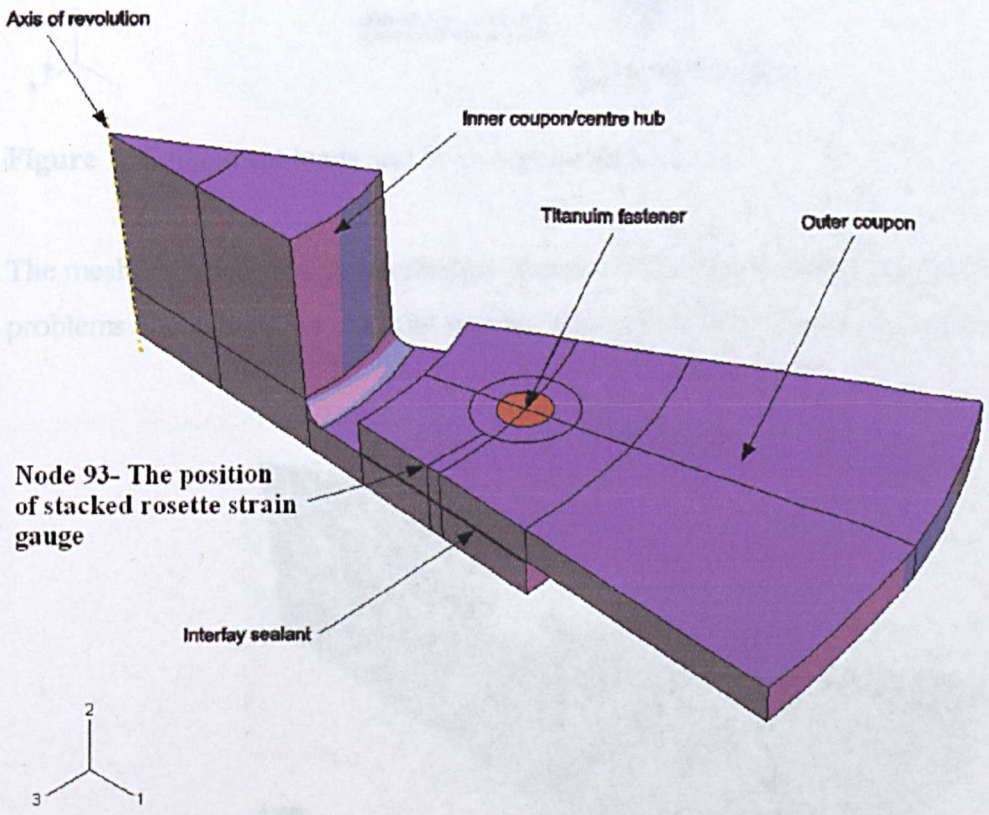

Figure 1 Coupon set components

The boundary condition around the outside perimeter was "clamped," allowing no translation or rotational movement. The other two sides of the wedge required the use of the two co-ordinate systems as shown in **Fig. 2**

The boundary conditions used in the model are also illustrated in **Fig. 2.**
Figure 2 also shows the placement of loads that were applied to the coupon set and the clamping forces from the fastener.

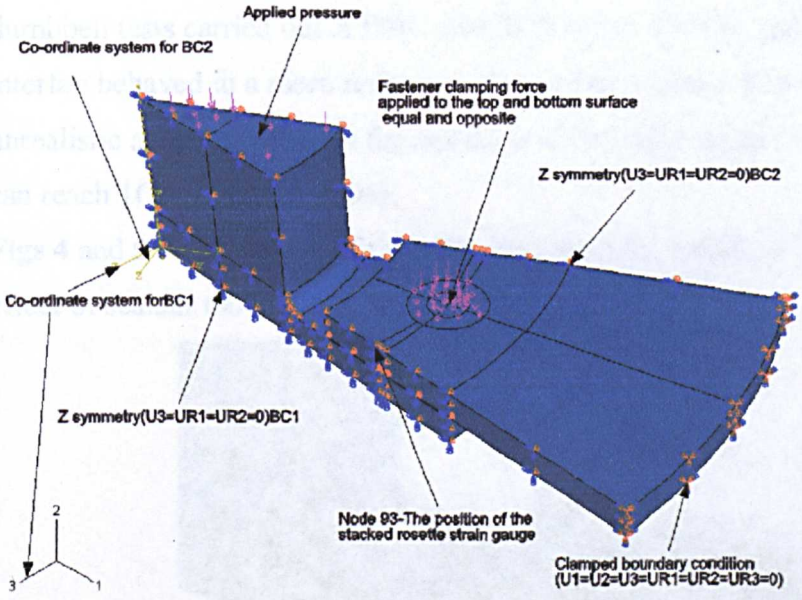

Figure 2. Coupon set loads and boundary conditions

The mesh included 4-node tetrahedral elements. This was selected because of problems encountered in the joint overlap area when using 8-node hexagonal

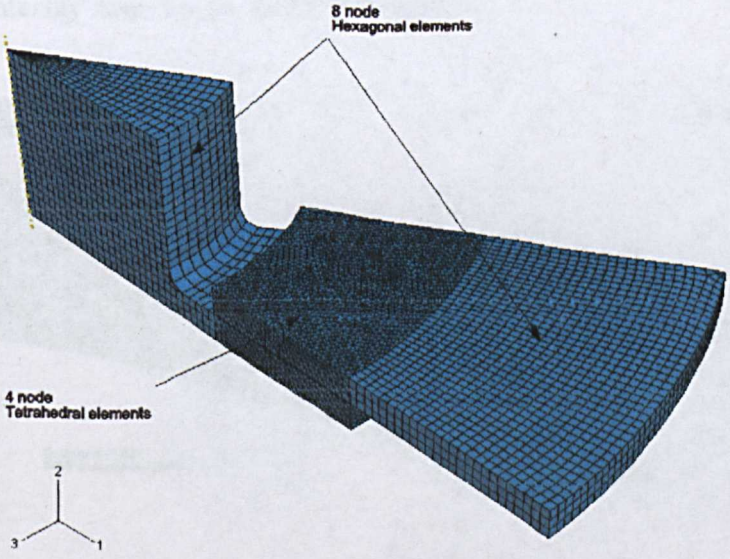

elements (**Fig. 3**).

Figure 3. Coupon set mesh

Similar problems were encountered with this model if the measured sealant properties were used directly, resulting in a gross distortion of the model elements. Due to the low stiffness of the sealant material's properties it was found that if the Modulus of the sealant was increased from 2.52 MPa (±0.92) (the average and SD of various dumbbell tests carried out at OBU during 2006) to 50 MPa, the modelled sealant interfay behaved in a more realistic and expected manner. This is not necessarily unrealistic as the modulus of the sealant at low temperatures (worse case scenario) can reach 1GPa (Healey, 1996).

Figs 4 and **5** are examples of the MSS FEA models results and these illustrate the effect of sealant modulus on the sealant interfay joint area.

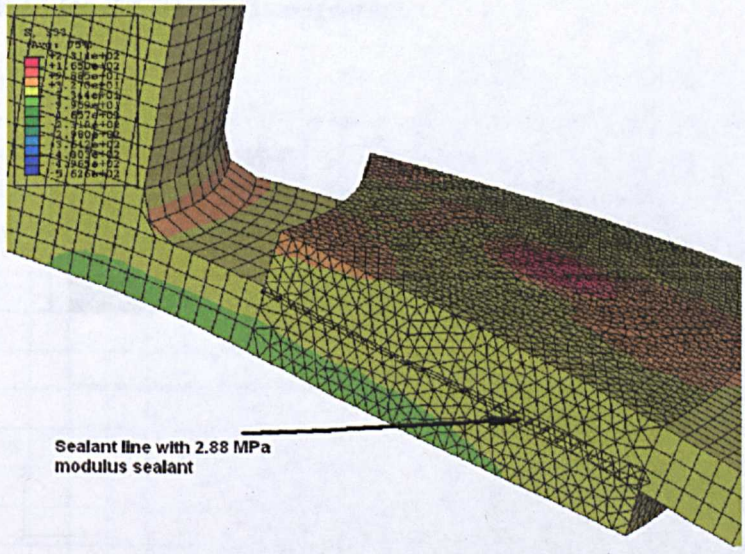

Figure 4 Sealant interfay zone for modulus of 2.88MPa

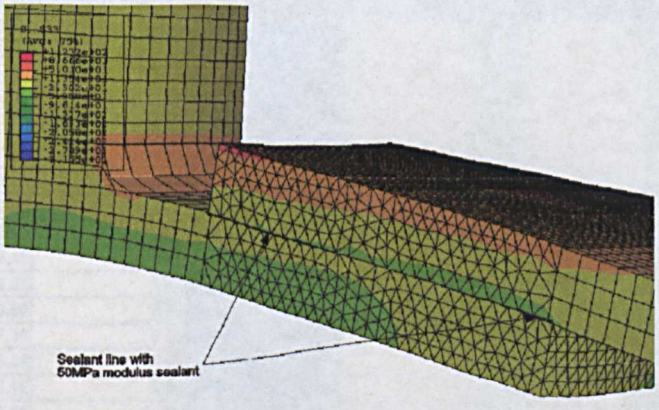

Figure 5 Sealant interfay zone for modulus of 50 MPa

Results for the standard coupon set (3.18mm thick)

This section covers the standard set of coupons with the inner and outer coupons having the same thickness (3.18mm). The models materials are listed along with the radial and circumferential stresses experienced using Finite Element Analysis (FEA) and these are compared with those gained from using strain gauges (SG). These stresses are then proportioned so that a comparison can be made between those gained from Buller (Buller, R.D. (b) (2002), the FEA and the strain gauges.

The FEA was carried out on the model shown in **Fig. 6.** A comparison result table is shown in **Table 1**, with proportioned stresses, for the standard coupon set. **Fig. 7** shows the stress against load for the standard coupon set. **Fig. 8** shows proportioned stress against load for the standard coupon set.

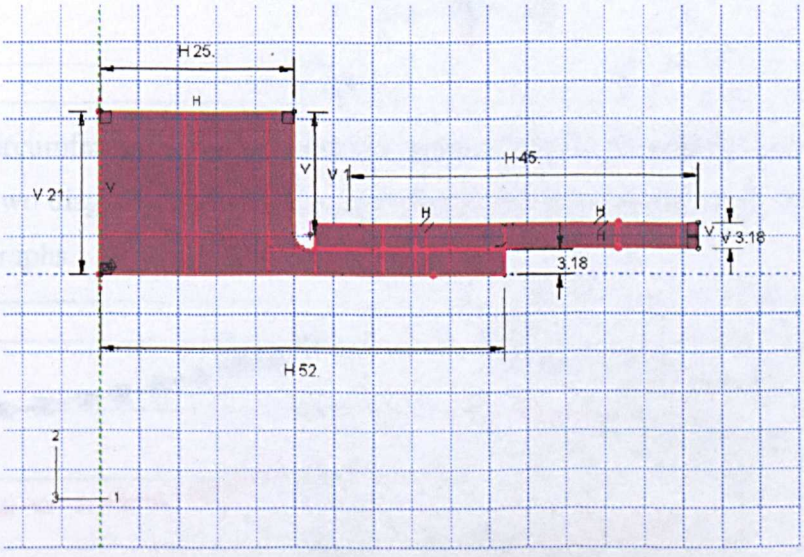

Figure 6. Section of revolved coupon set (dimensions in mm)

Load(KN)	SG circum σ(MPa)	SG radial σ(MPa)	Normalised sg σ	FEA circum σ(MPa)	FEA radial σ(MPa)	Normalised FEA σ
4.00	-49.85	-19.20	-2.60	-33.40	-10.40	-3.21
3.50	-45.00	-16.00	-2.81	-28.90	-9.01	-3.21
3.00	-39.20	-14.00	-2.80	-24.20	-7.70	-3.14
2.50	-33.40	-11.40	-2.93	-19.60	-6.40	-3.06
2.00	-27.20	-9.00	-3.02	-15.03	-5.03	-2.99
1.50	-21.30	-6.90	-3.09	-10.30	-3.65	-2.82
1.00	-15.00	-4.90	-3.06	-5.70	-2.30	-2.48
0.00	0.00	0.00	0.00	3.60	0.37	9.73
-1.00	12.60	2.20	5.73	12.85	3.10	4.15
-1.50	18.10	3.20	5.66	17.40	4.40	3.95
-2.00	24.30	4.40	5.52	22.14	5.80	3.82
-2.50	30.50	5.70	5.35	26.70	7.15	3.73
-3.00	37.10	7.10	5.23	31.25	8.50	3.68
-3.50	43.40	8.40	5.17	35.98	9.90	3.63
-4.00	50.10	9.90	5.06	40.54	11.20	3.62
-4.50	56.90	11.40	4.99	45.30	12.60	3.60

Note: + Load sealant in tension - Load sealant in compression

Table 1 Comparison results, with proportioned stresses, for the standard coupon set

Fig. 7 shows the circumferential and radial stress against load for the standard coupon set. **Fig. 8** shows proportioned stress against load for the standard coupon set.

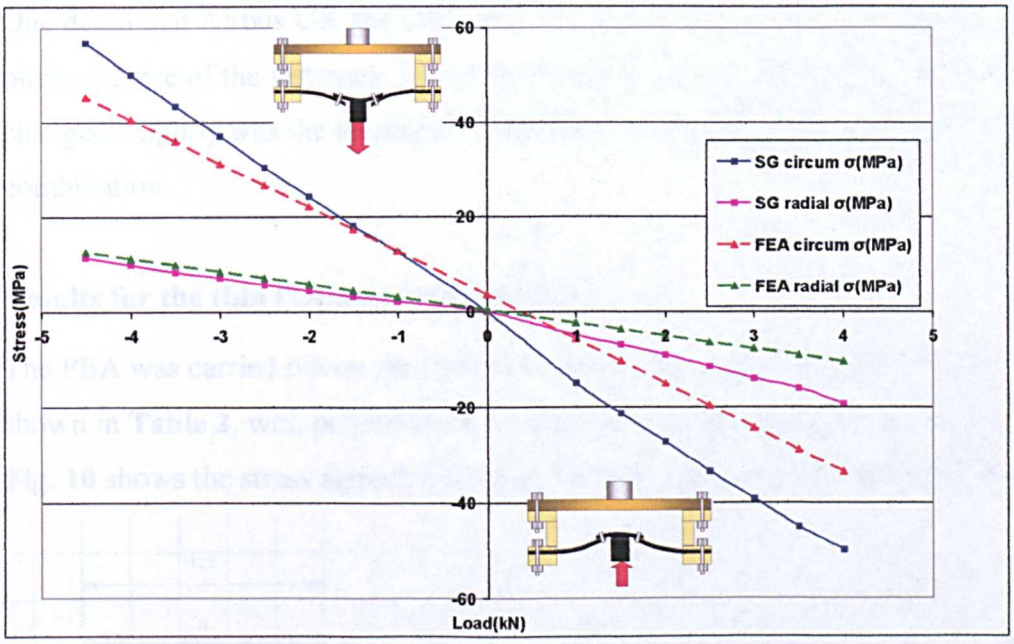

Figure 7 Circumferential and radial stress against load for the standard coupon set.

Note: The two diagrams showing the direction of the force apply to all of the following graphs.

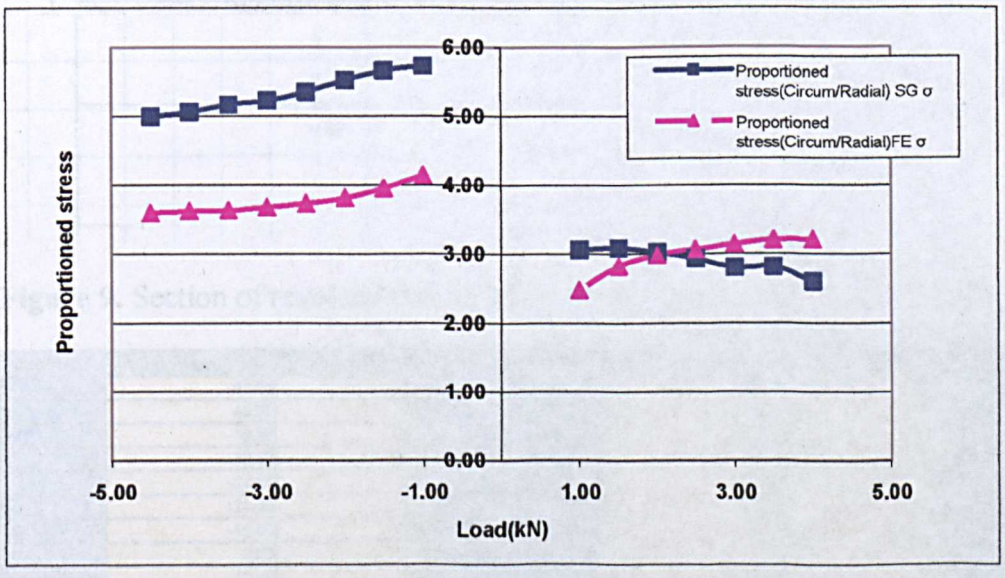

Figure 8 Proportioned stresses ($\sigma_{circum}/\sigma_{radial}$) against load for the standard coupon set

Parametric study to optimise the design

A limited parametric study was carried out to try and optimise the design. This section covers the different model geometries and material parameters inserted into top FEA

along with the results gained. These are set out in a similar manner to the previous section.

One detail that Airbus UK and OBU felt was inadvisable to alter at this stage was the pitch and size of the fasteners. It was decided that the component that could be changed, slightly was the thickness of the inner or outer coupon either both or in combination.

Results for the thin (2.4mm) outer coupon

The FEA was carried out on the model shown in **Fig. 9.** A comparison result table is shown in **Table 2**, with proportioned stresses, for the thin (2.4mm) outer coupon set. **Fig. 10** shows the stress against load. **Fig. 11** shows proportioned stress against load.

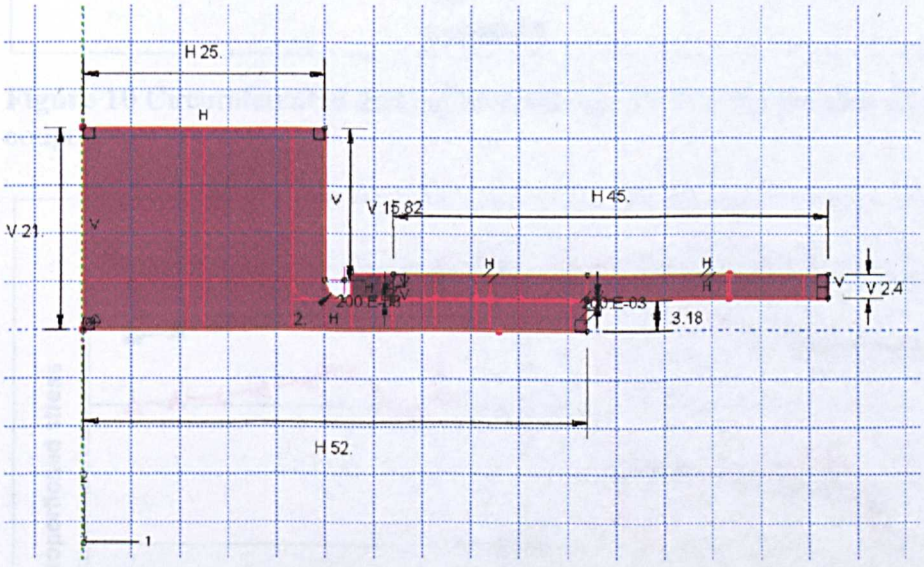

Figure 9. Section of revolved thin (2.4mm) outer coupon set (dimensions in mm)

Load(KN)	SG circum σ(MPa)	SG radial σ(MPa)	Proportioned SG σ	FEA circum σ(MPa)	FEA radial σ(MPa)	Proportioned FEA σ
4	-49.85	-19.20	-2.60	-33.40	-14.20	-2.35
3.5	-45.00	-16.00	-2.81	-28.90	-9.00	-3.21
3	-39.20	-14.00	-2.80	-24.10	-7.70	-3.13
2.5	-33.40	-11.40	-2.93	-19.60	-6.40	-3.06
2	-27.20	-9.00	-3.02	-15.00	-5.00	-3.00
1.5	-21.30	-6.90	-3.09	-9.20	-4.40	-2.09
1	-15.00	-4.90	-3.06	-5.70	-2.30	-2.48
0	0.00	0.00	0.00	7.30	0.25	29.20
-1	12.60	2.20	5.73	12.80	3.10	4.13
-1.5	18.10	3.20	5.66	17.40	4.40	3.95
-2	24.30	4.40	5.52	29.00	6.40	4.53
-2.5	30.50	5.70	5.35	34.50	7.90	4.37
-3	37.10	7.10	5.23	39.80	9.40	4.23
-3.5	43.40	8.40	5.17	45.40	11.00	4.13
-4	50.10	9.90	5.06	50.80	12.50	4.06
-4.5	56.90	11.40	4.99	56.40	14.10	4.00

Note: + Load sealant in tension - Load sealant in compression

Table 2 Comparison results, with proportioned stresses, for the thin (2.4mm) outer coupon

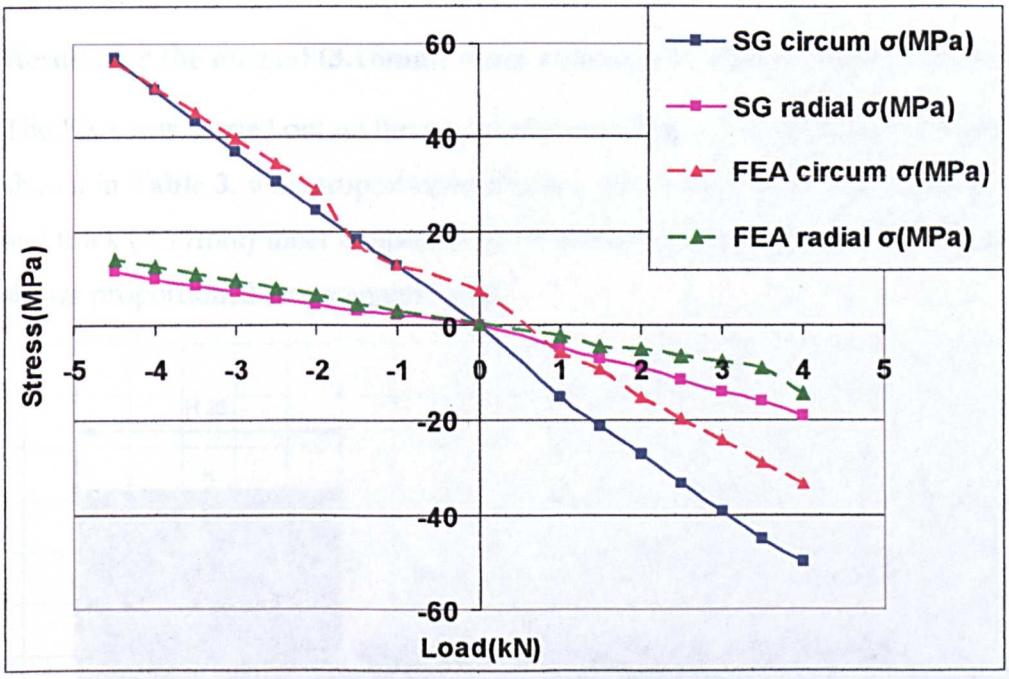

Figure 10 Circumferential and radial stress against load for the thin (2.4mm) outer coupon

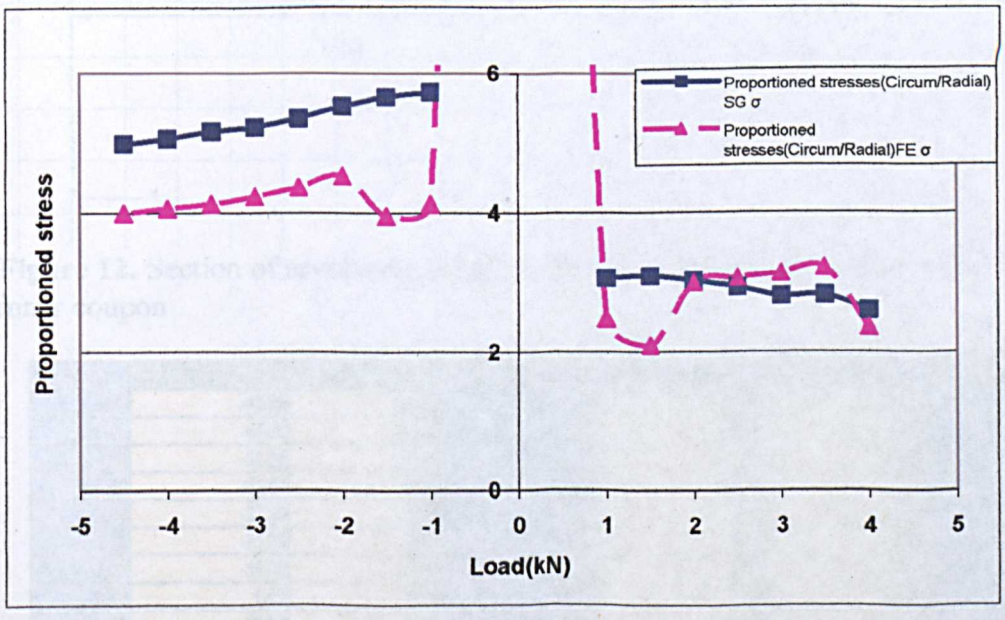

Figure 11 Proportioned stresses ($\sigma_{circum}/\sigma_{radial}$) against load for the thin (2.4mm) outer coupon

Results for the normal (3.18mm) outer coupon and thick (4.77mm) inner coupon

The FEA was carried out on the model shown in **Fig. 12.** A comparison result table is shown in **Table 3**, with proportioned stresses, for the normal (3.18mm) outer coupon and thick (4.77mm) inner coupon. **Fig. 13** shows the stress against load. **Fig. 14** shows proportioned stress against load.

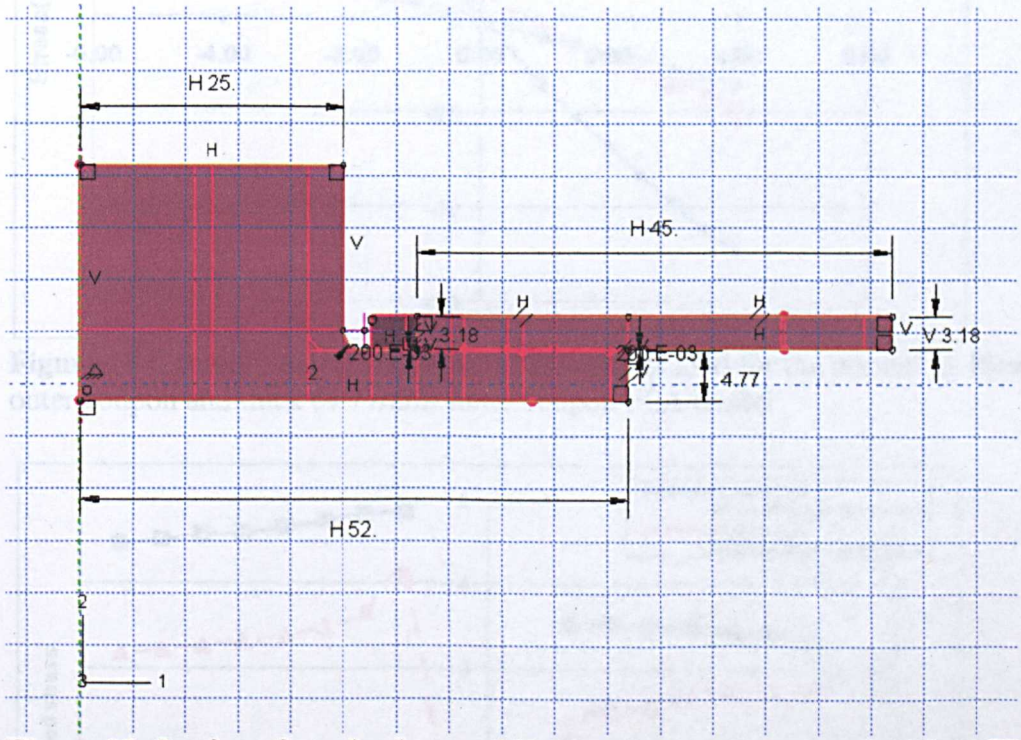

Figure 12. Section of revolved normal (3.18mm) outer coupon and thick (4.77mm) inner coupon

Load(KN)	SG circum σ(MPa)	SG radial σ(MPa)	ProportionedSG σ	FEA circum σ(MPa)	FEA radial σ(MPa)	Proportioned FEA σ
4.00	-49.85	-19.20	-2.60	-22.10	-14.30	-1.55
3.50	-45.00	-16.00	-2.81	-18.80	-12.60	-1.49
3.00	-39.20	-14.00	-2.80	-15.40	-10.90	-1.41
2.50	-33.40	-11.40	-2.93	-12.20	-9.20	-1.33
2.00	-27.20	-9.00	-3.02	-8.93	-7.57	-1.18
1.50	-21.30	-6.90	-3.09	-5.64	-5.85	-0.96
1.00	-15.00	-4.90	-3.06	-2.30	-4.20	-0.55
0.00	0.00	0.00	0.00	4.60	-0.80	-5.75
-1.00	12.60	2.20	5.73	11.00	2.60	4.23
-1.50	18.10	3.20	5.66	14.25	4.25	3.36
-2.00	24.30	4.40	5.52	17.60	5.97	2.95
-2.50	30.50	5.70	5.35	20.90	7.60	2.75
-3.00	37.10	7.10	5.23	24.10	9.30	2.59
-3.50	43.40	8.40	5.17	27.50	11.00	2.50
-4.00	50.10	9.90	5.06	30.80	12.70	2.43
-4.50	56.90	11.40	4.99	34.20	14.40	2.38

Note: + Load sealant in tension - Load sealant in compression

Table 3 Comparison results, with proportioned stresses, for the normal (3.18mm) outer coupon and thick (4.77mm) inner coupon FEA model

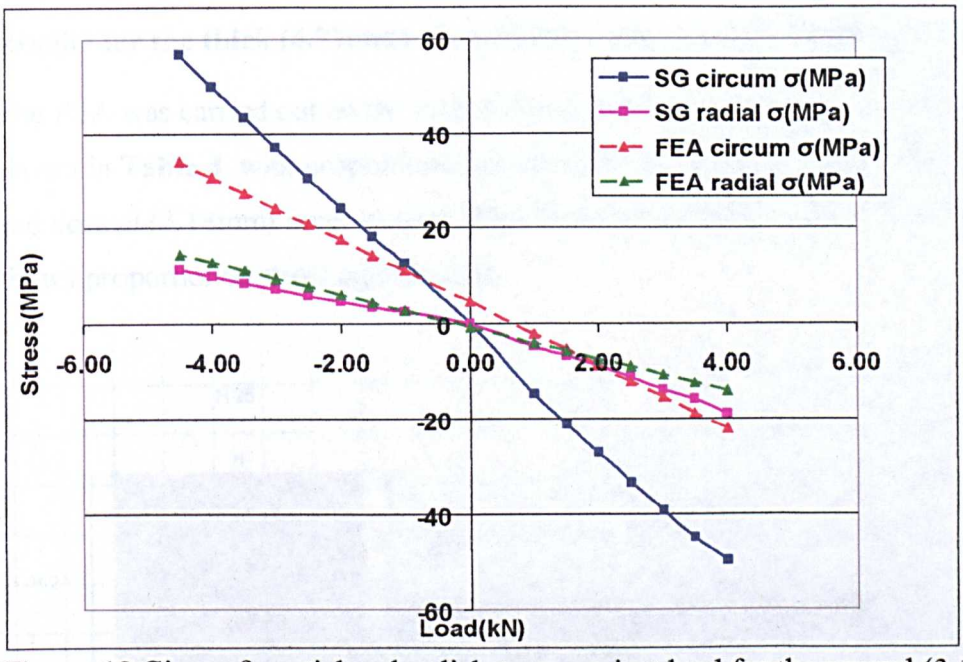

Figure 13 Circumferential and radial stress against load for the normal (3.18mm) outer coupon and thick (4.77mm) inner coupon FEA model

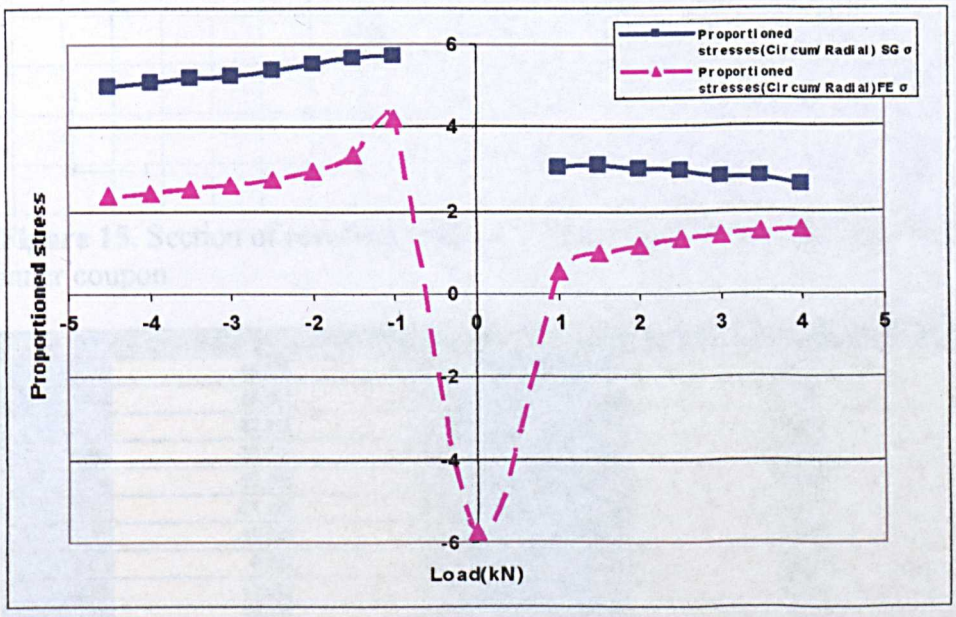

Figure 14 Proportioned stresses ($\sigma_{circum}/\sigma_{radial}$) stress against load for the normal (3.18mm) outer coupon and thick (4.77mm) inner coupon FEA model

Results for the thick (4.77mm) outer coupon and normal (3.18mm) inner coupon

The FEA was carried out on the model shown in **Fig. 15.** A comparison result table is shown in **Table 4**, with proportioned stresses, for the thick (4.77mm) outer coupon and normal (3.18mm) inner coupon. **Fig. 16** shows the stress against load. **Fig. 17** shows proportioned stress against load.

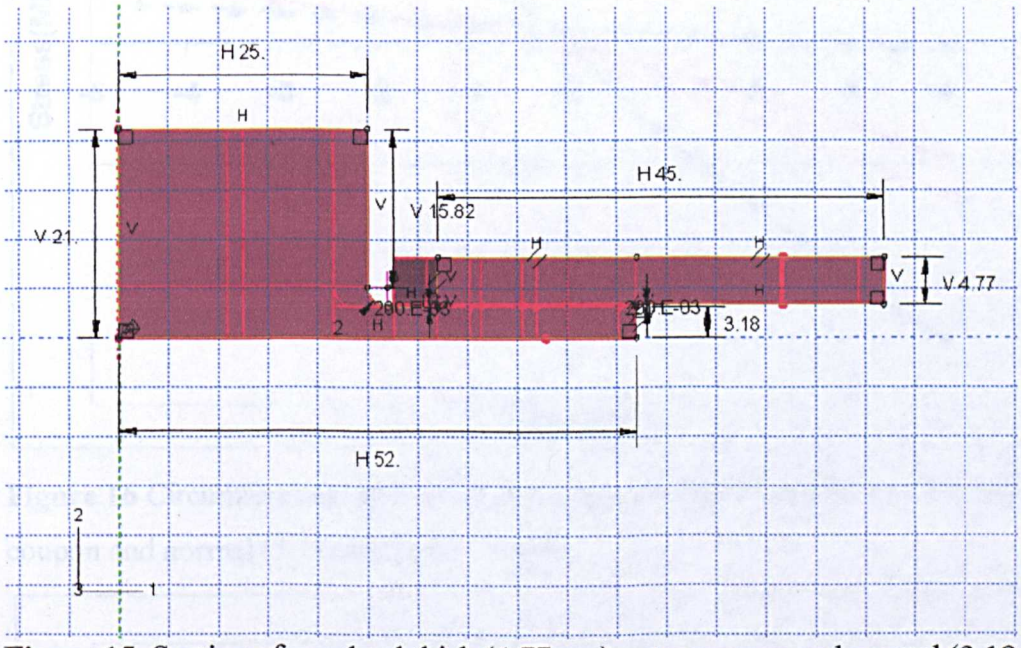

Figure 15. Section of revolved thick (4.77mm) outer coupon and normal (3.18mm) inner coupon

Load(KN)	SG circum σ(MPa)	SG radial σ(MPa)	Proportioned SG σ	FEA circum σ(MPa)	FEA radial σ(MPa)	Proportioned FEA σ
4.00	-49.85	-19.20	-2.60	-24.80	-1.40	-17.71
3.50	-45.00	-16.00	-2.81	-21.97	-0.90	-24.41
3.00	-39.20	-14.00	-2.80	-19.04	-0.50	-38.08
2.50	-33.40	-11.40	-2.93	-16.20	-0.02	-810.00
2.00	-27.20	-9.00	-3.02	-13.40	0.40	-33.50
1.50	-21.30	-6.90	-3.09	-10.50	0.90	-11.67
1.00	-15.00	-4.90	-3.06	-7.60	1.60	-4.75
0.00	0.00	0.00	0.00	-1.80	2.30	-0.78
-1.00	12.60	2.20	5.73	3.80	3.20	1.19
-1.50	18.10	3.20	5.66	6.60	3.70	1.78
-2.00	24.30	4.40	5.52	9.60	4.20	2.29
-2.50	30.50	5.70	5.35	12.40	4.60	2.70
-3.00	37.10	7.10	5.23	15.20	5.00	3.04
-3.50	43.40	8.40	5.17	18.10	5.50	3.29
-4.00	50.10	9.90	5.06	20.90	6.00	3.48
-4.50	56.90	11.40	4.99	23.90	6.50	3.68

Note: + Load sealant in tension - Load sealant in compression

Table 4 Comparison results, with proportioned stresses, for the thick (4.77mm) outer coupon and normal (3.18mm) inner coupon

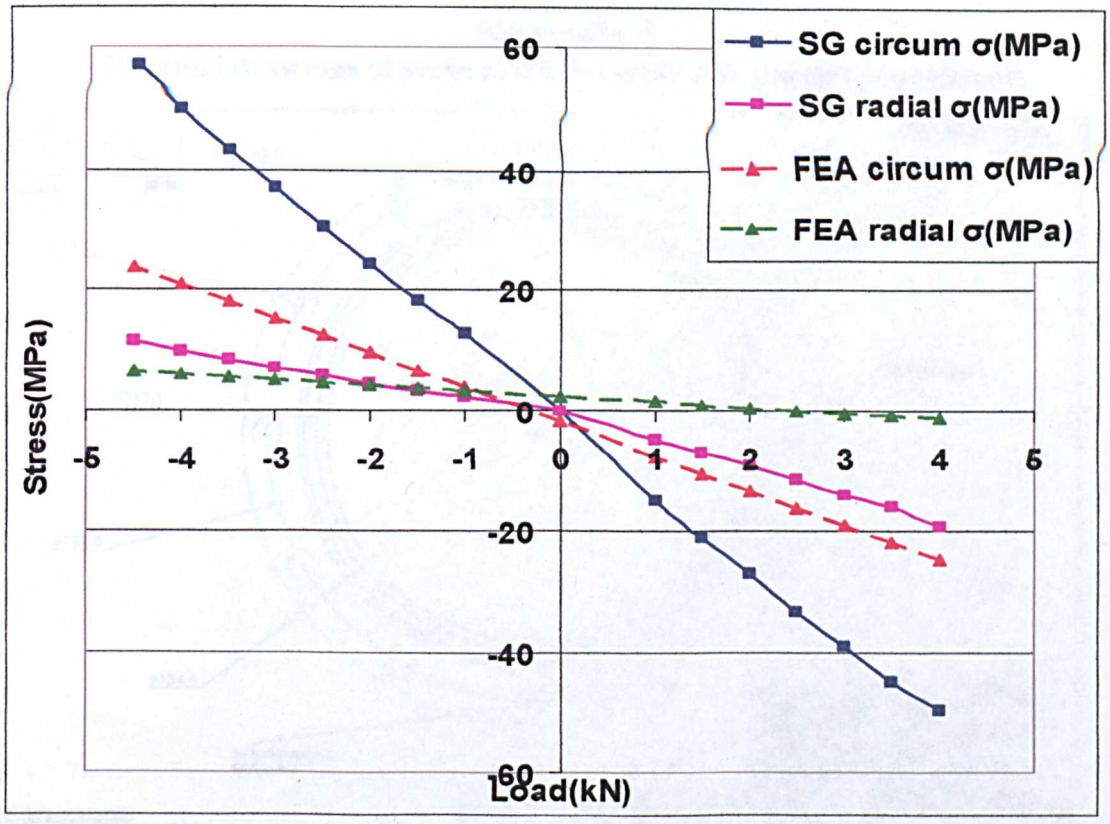

Figure 16 Circumferential and radial stress against load of the thick (4.77mm) outer coupon and normal (3.18mm) inner coupon

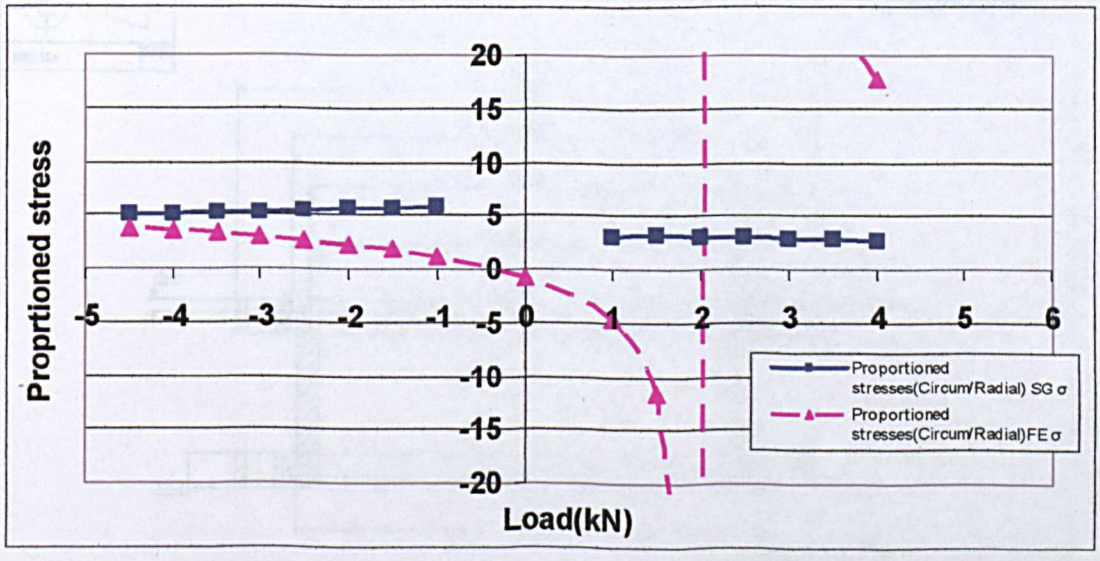

Figure 17 Proportioned stresses ($\sigma_{circum}/\sigma_{radial}$) stress against load of the thick (4.77mm) outer coupon and normal (3.18mm) inner coupon

Appendix 9

The final drawings of some of the Pressure Pot's major components

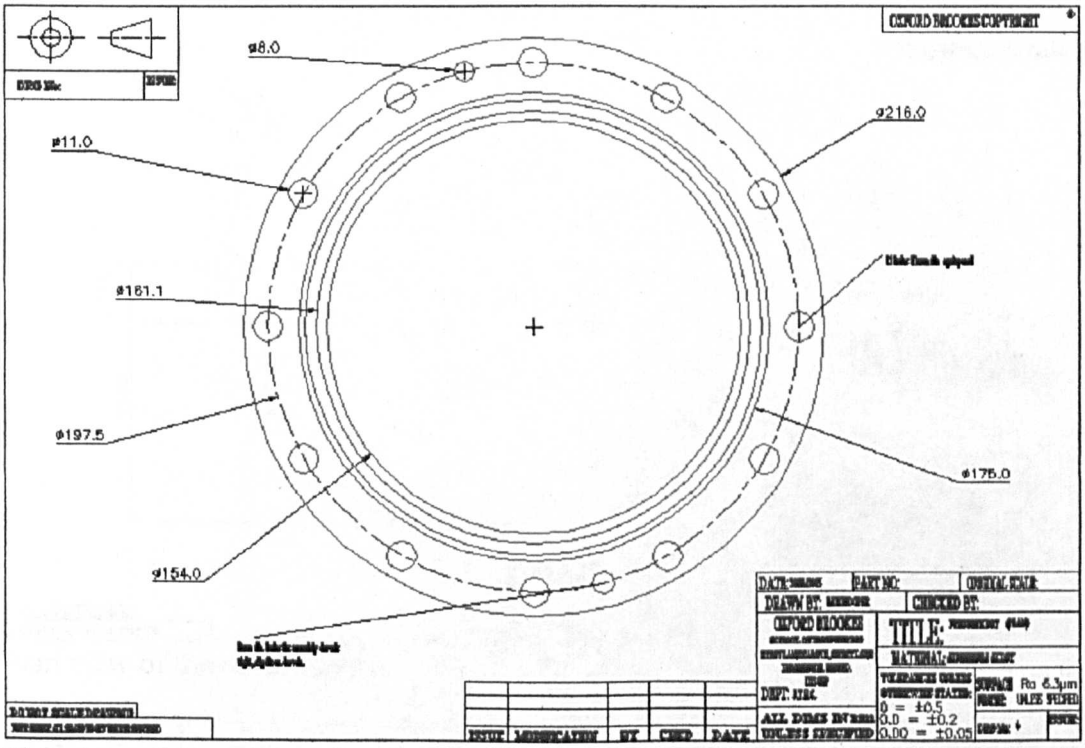

Plan view of the pressure pot

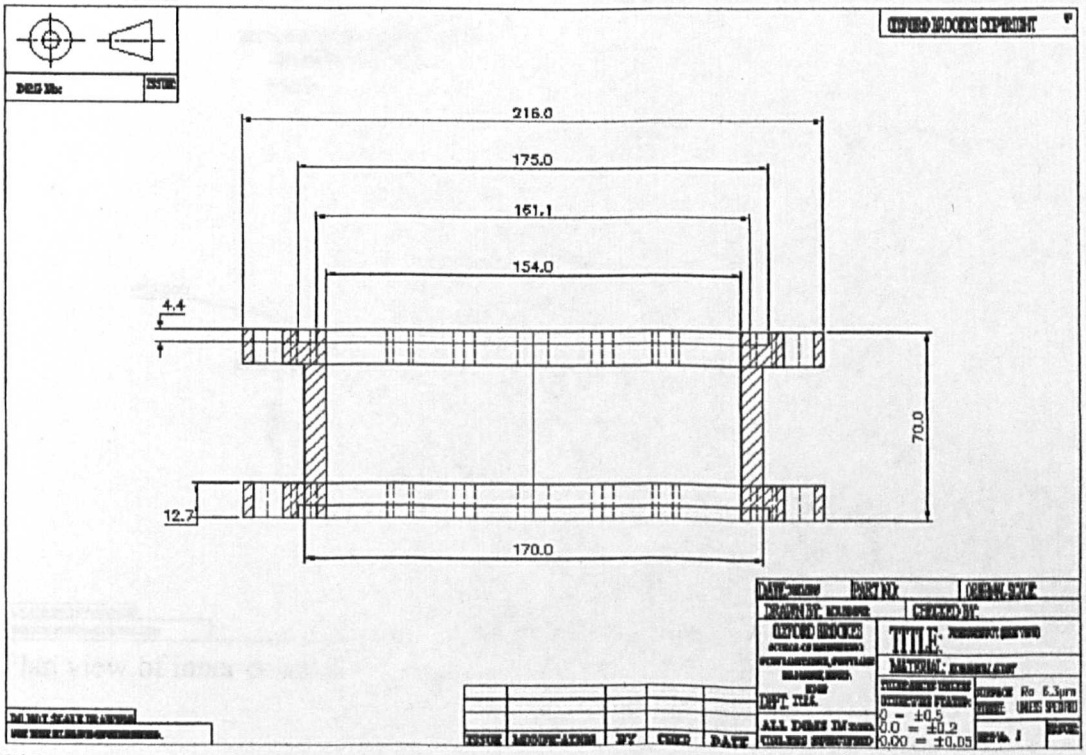

Side view of the pressure pot

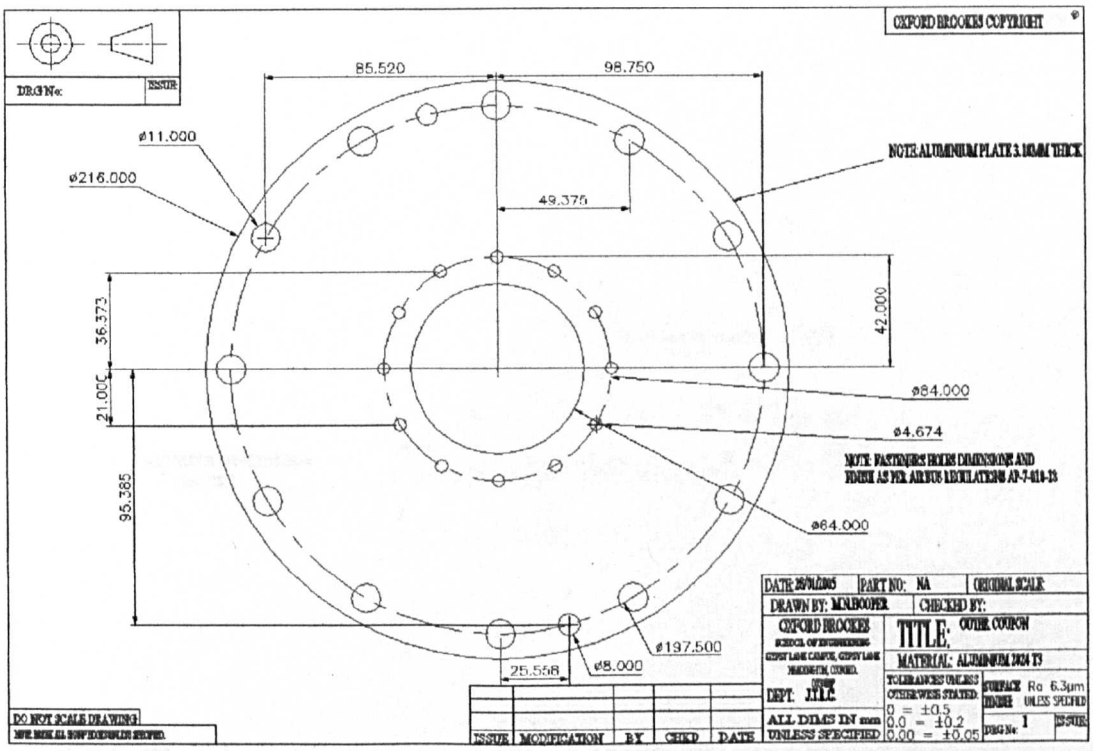

Plan view of the outer coupon

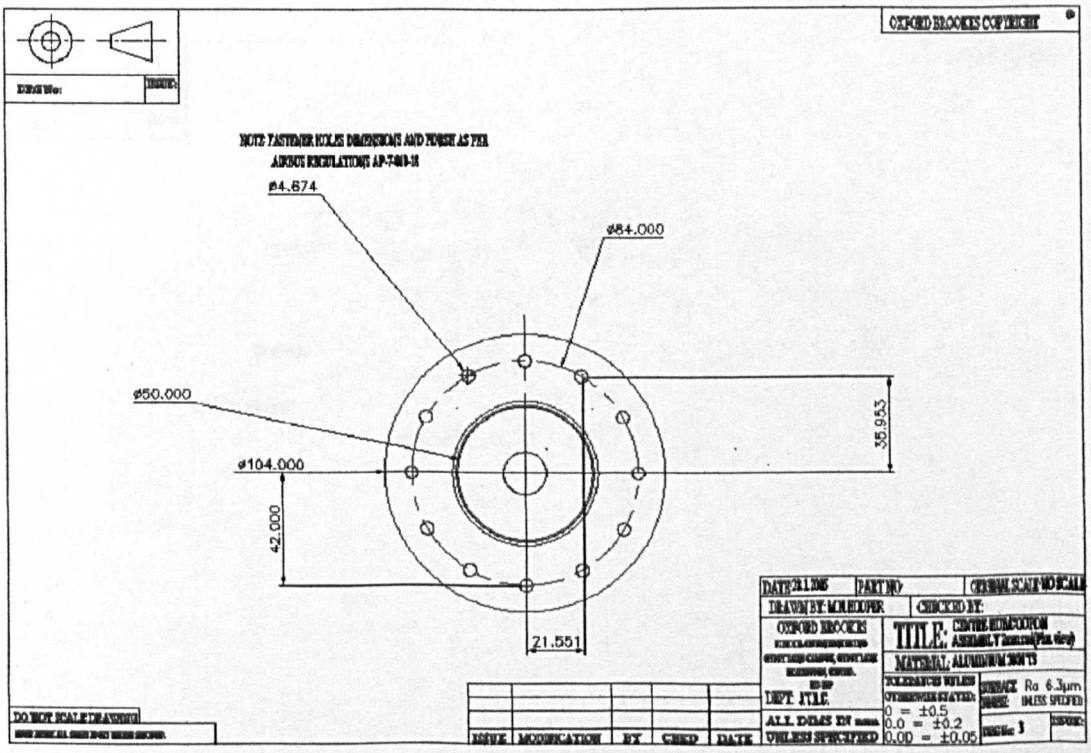

Plan view of inner coupon

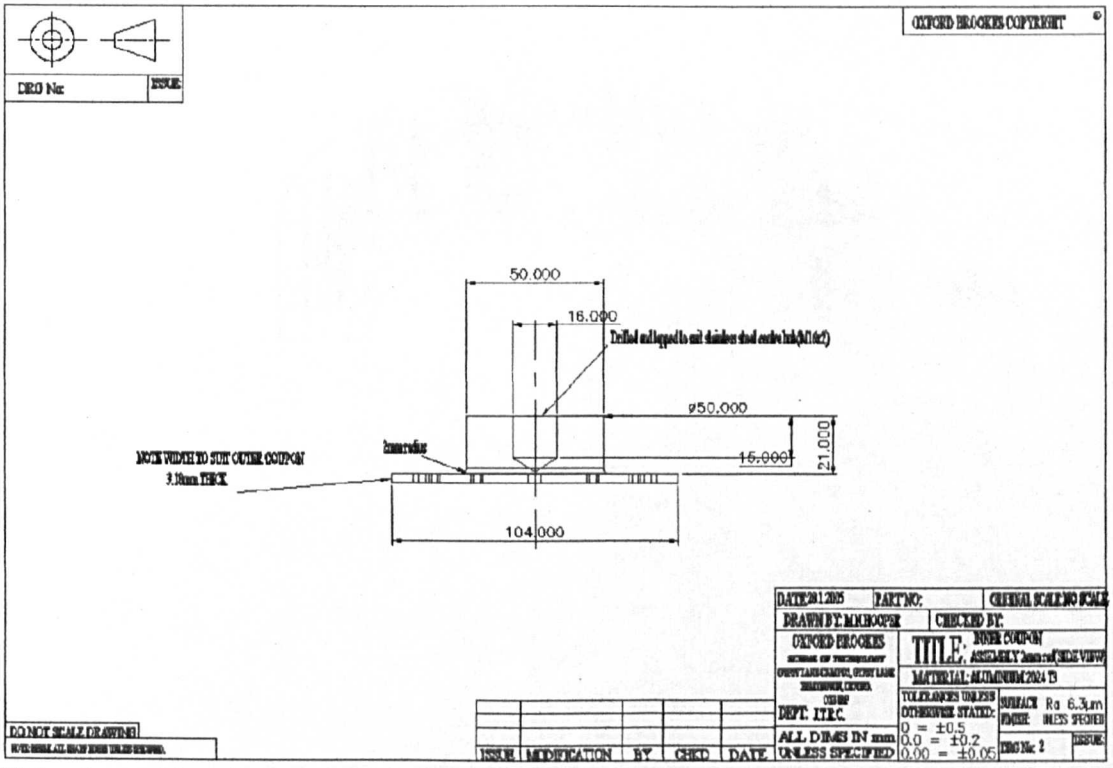

Side view of inner coupon

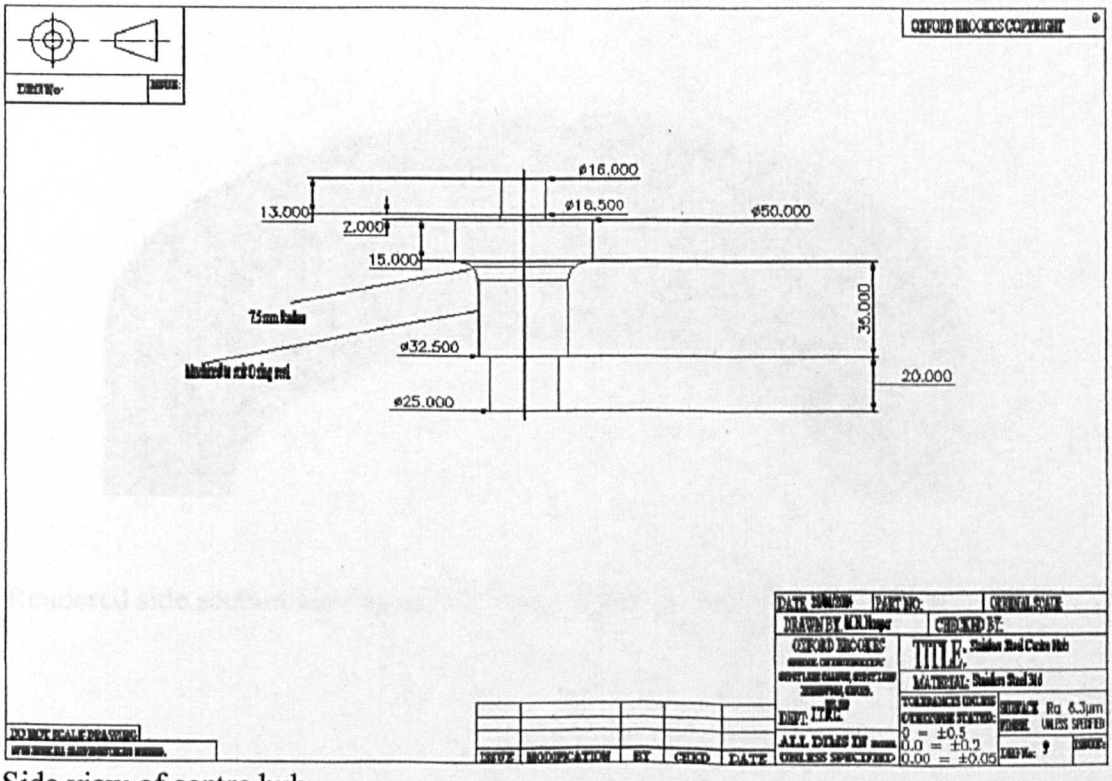

Side view of centre hub

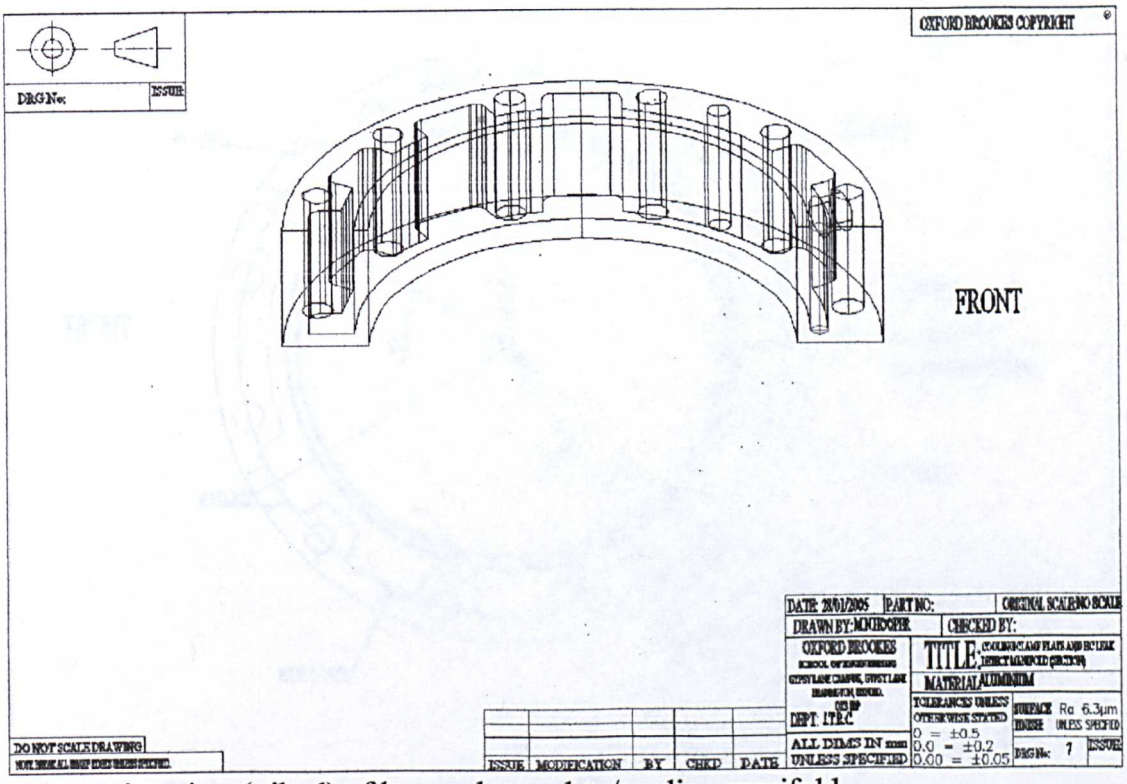

Side section view (tilted) of lower clamp plate/cooling manifold

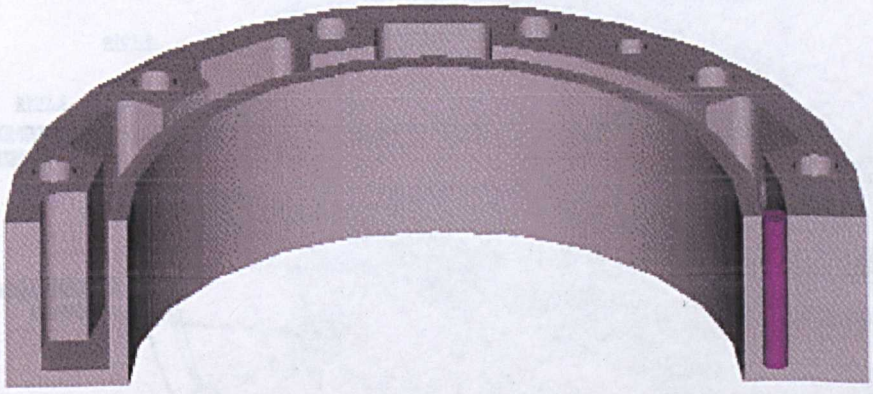

Rendered side section view (tilted) of lower clamp plate/cooling manifold

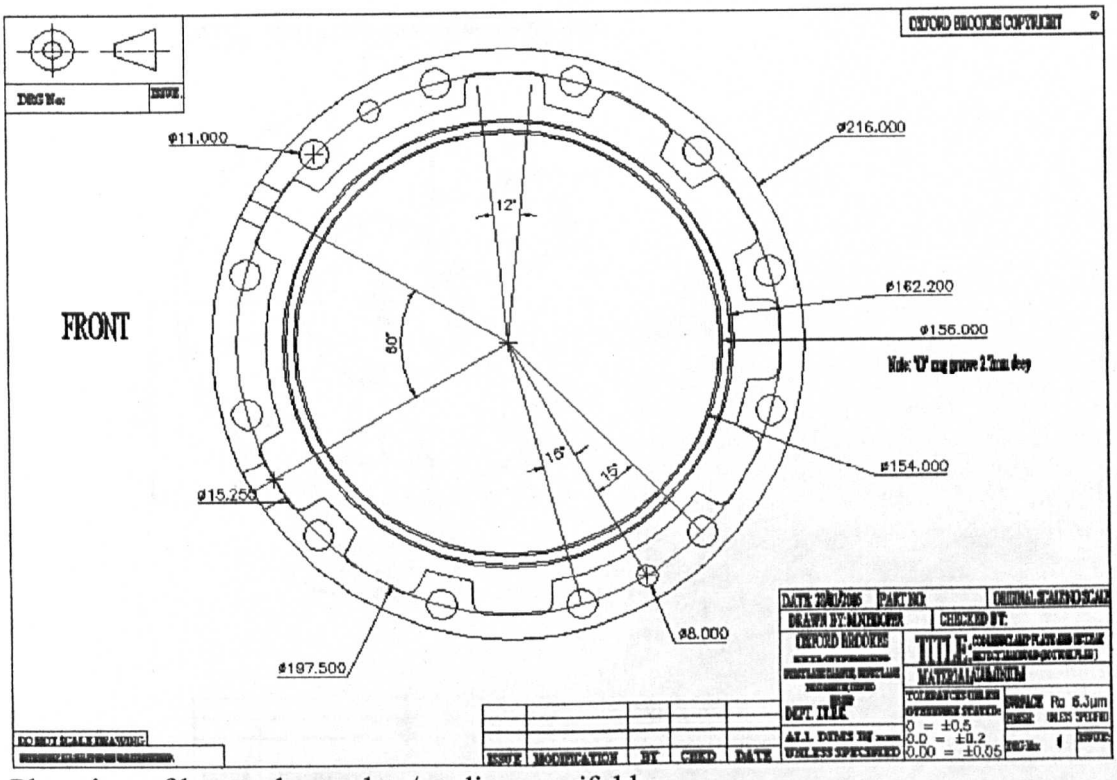

Plan view of lower clamp plate/cooling manifold

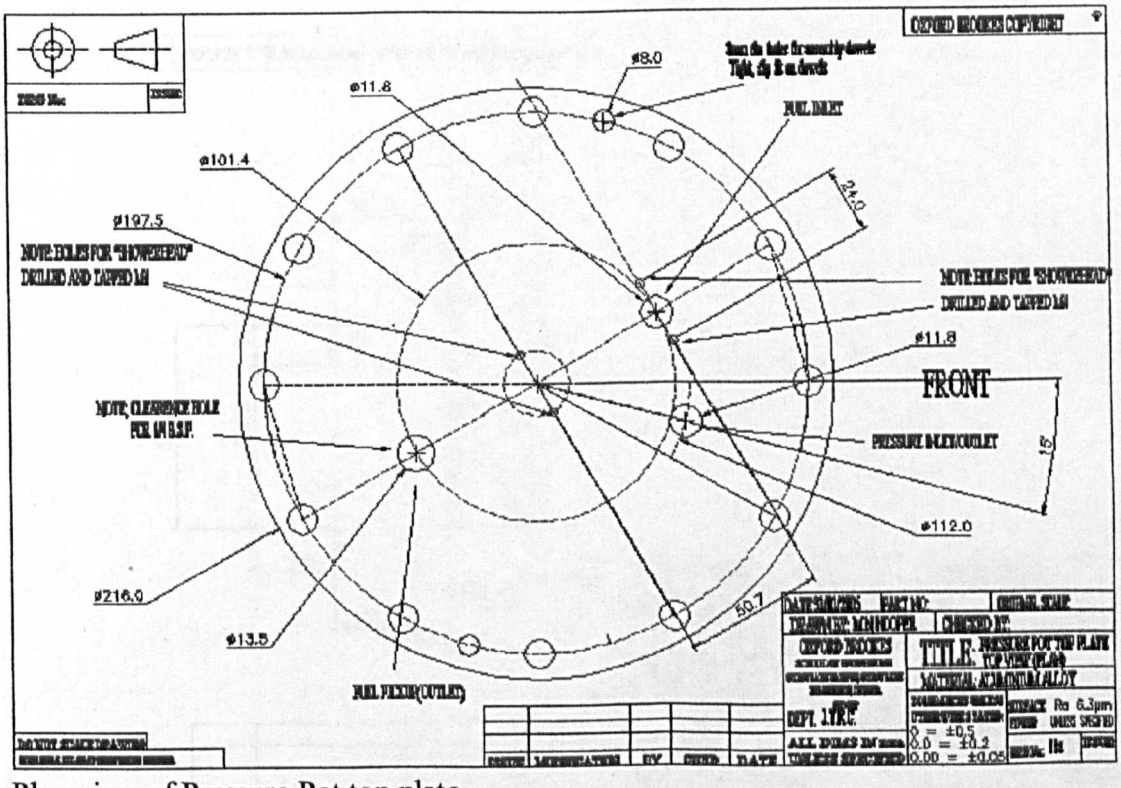

Plan view of Pressure Pot top plate

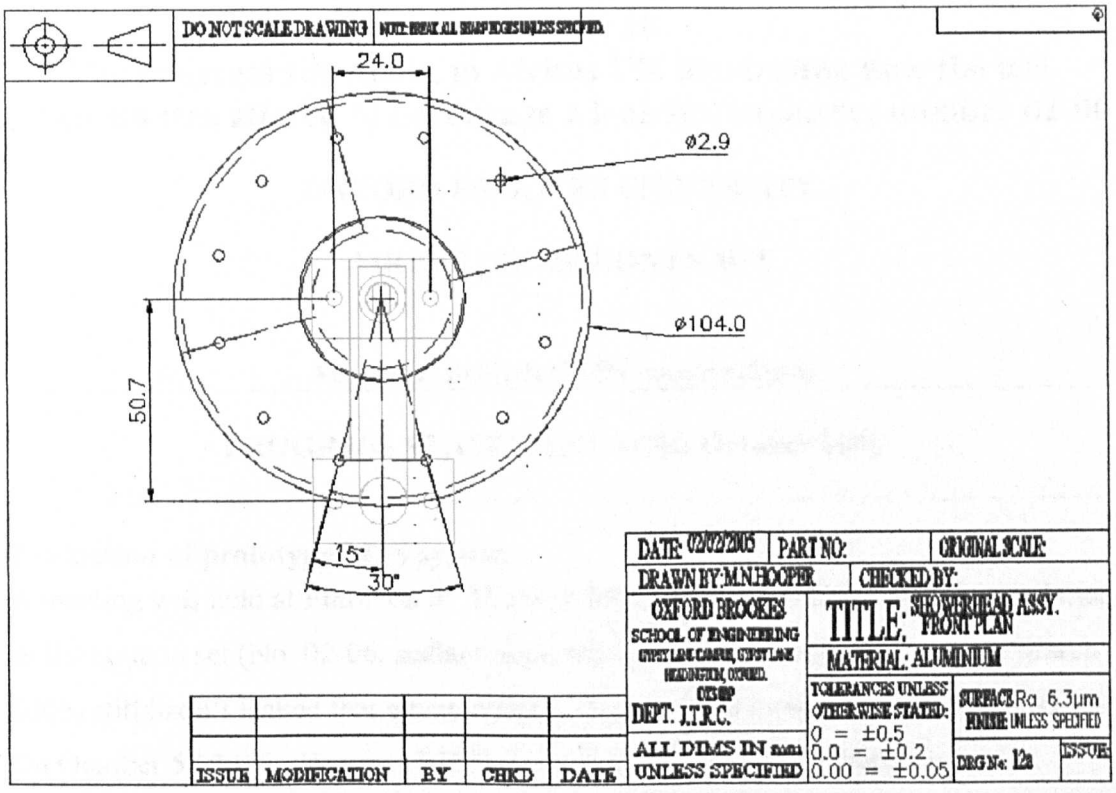

Plan view of showerhead assembly

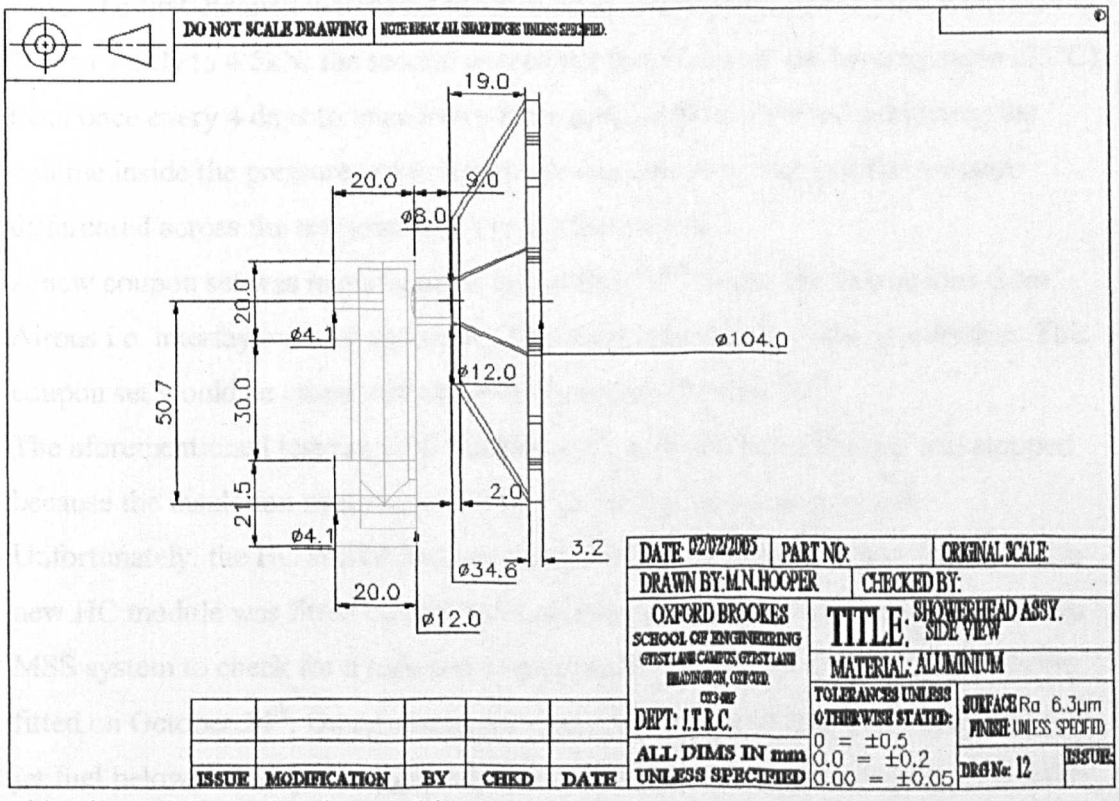

Side view of showerhead assembly

Appendix 10
The progress statement to Airbus UK illustrating how the test program was altered to encourage a leak in coupon set number 02-06

OXFORD BROOKES UNIVERSITY

AIRBUS UK Ltd CONTRACT

Aero-seal project (MSS construction)

PROGRESS STATEMENT FOR: October 2006

Evaluation of prototype MSS system

A meeting was held at Filton on 3rd October 2006. At this meeting it was decided that as the coupon set (No. 02-06, sealant application; fillet and overcoat, installed March 2006) still hadn't leaked that a new coupon set should be installed as soon as possible. On October 5th 2006, Hooper (OBU) decided to try a slightly updated test programme. This was very similar to the previous programme but was altered in three ways: the first entailed increasing the fatigue load compressing the joint from 2kN to 4kN to 1.5kN to 4.5kN; the second altered the frequency of the heating cycle (25°C) from once every 4 days to once every 8 hrs and the third involved subjecting the volume inside the pressure pot to a permanent pressure to increase the pressure differential across the test joint to try to instigate a leak.

A new coupon set was manufactured on October 10th as per the instructions from Airbus i.e. interfay and wet assembled fasteners only with no fillet or overcoat. This coupon set would be cured and ready for fitting by October 24th.

The aforementioned test ran until October 12th, at which point the test was stopped because the insulation material was wet with jet fuel, suggesting a leak.

Unfortunately, the HC sniffer had not detected the leak and so, suspecting a fault, a new HC module was fitted but still no leak was detected. It was decided to strip the MSS system to check for a leak and to prepare the PP for the new coupon set to be fitted on October 24th. On removing the coupon from the PP there was a quantity of jet fuel below the coupon suggesting that a leak had occurred at some point and that the leak had not been picked up by the HC sniffer. On further investigation it was found that the material used to seal the point at which the PT100 temperature sensor cable left the vacuum hose from beneath the test coupon had, over time, been forced

down the hose until it effectively blocked both the airflow from beneath the coupon set and with it any hydrocarbon fumes. This has now been modified on the current test by having the vacuum feed only through the hose and the PT100 temperature sensor cable coming through a separate, sealed, conduit.

The new coupon set (No. 03-06) was fitted on October 25th and the Pressure Pot assembly was refitted to the MSS on October 26th. A technician from Jencons had been scheduled to repair a fault, under warranty, on the front display panel of the Julabo on October 27th . This was carried out and the MSS (and Julabo) was checked to ensure correct operation, with no faults found and the new test was started on October 31st 2006.